MEDICAL UNIVERSITY OF VIENNA

Dissection of the hypusine-eIF5A axis by CRISPR/Cas9-aided functional genomics

Doctoral thesis at the Medical University of Vienna for obtaining the academic degree

Doctor of Philosophy

Submitted by

Dipl. – Ing. Patrick Eßletzbichler

Supervisor:

Univ.-Prof. Dr. Giulio Superti-Furga

CeMM Research Center for Molecular Medicine

Lazarettgasse 14, AKH BT 25.3, 1090 Vienna, Austria

Vienna 9/2023

Declaration

This doctoral thesis is presented in a cumulative format and contains two published research manuscripts as well as data intended to be submitted for publication. The author of this thesis (P.E.) is a co-author of manuscript #1 and the first author of manuscript #2. All chapters of this thesis have been written by the author Patrick Essletzbichler. Feedback on the writing of this work has been provided by Giulio Superti-Furga, Ann-Katrin Hopp, Fabian Frommelt and Evandro Ferrada. Most of the described experiments and analyses have been conducted in the Giulio Superti-Furga laboratory at the Research Center for Molecular Medicine of the Austrian Academy of Sciences (CeMM) in Vienna, Austria. In addition, the presented work was supported by other members of the Giulio Superti-Furga laboratory, as well as collaborators in the laboratories of Thijn Brummelkamp at the Netherlands Cancer Institute (NKI), Marko Jovanovic at Columbia University, and Didier Soulat at the University clinics Erlangen and Friedrich-Alexander-University Erlangen-Nürnberg. Individual author contributions are indicated in the respective prologue and interlude sections of the respective studies as well as in the author contribution statements therein.

The manuscript in Chapter 3.2 was published in **Cell Host & Microbe** under an open-access Creative Commons CC-BY License and has been reprinted with permission from the publisher Elsevier. **The Bicarbonate Transporter SLC4A7 Plays a Key Role in Macrophage Phagosome Acidification.** Sedlyarov V[*], Eichner R[*], Girardi E, Essletzbichler P, Goldmann U, Nunes-Hasler P, Srndic I, Moskovskich A, Heinz L, Kartnig F, Bigenzahn J, Rebsamen M, Kovarik P, Demaurex N and Superti-Furga G[#] (2018) Cell Host & Microbe 23, 766-774 [*]: equal contribution | [#]: corresponding author

The manuscript in Chapter 3.4 was published in **Life Science Alliance** under an open-access Creative Commons CC-BY 4.0 License and has been reprinted with permission from the publisher Life Science Alliance. **A genome-wide CRISPR functional survey of the human phagocytosis molecular machinery.**
Essletzbichler P, Sedlyarov V, Frommelt F, Soulat D, Heinz LX, Stefanovic A, Neumayer B, Superti Furga G[#] (2023) Life Science Alliance vol. 6 no.4 e202201715 [#]: corresponding author

Data presented in Chapter 3.6 is intended for publication.

Figure 2 of this thesis was reprinted with permission from Royal Society of Chemistry, Figure 3, 4, 10-17, 19 with permission from Springer Nature, Figure 5, 6, 9 with permission from Elsevier, Figure 7 with permission from Oxford University Press, Figure 7 with permission from Wiley and Sons and Figure 18, 20 with permission from Cold Spring Harbor Laboratory press.

Table of Contents

List of Figures

List of Tables

Abstract

Especially since the development of CRISPR/Cas9 as a potent genome-editing tool, functional genomics has matured into a scalable and powerful instrument for the generation of unbiased hypothesis-generating research. At the same time, innovations in mass spectrometry techniques and devices now allow the parallel assessment and comparison of whole proteomes from many cells and conditions. The combination of genetics and proteomics has therefore become a powerful approach to discover and functionally dissect complex molecular processes in high throughput, which is the unifying theme of my dissertation.

In this work, I make use of these advances, engineer tools, and optimize their use in genetic screening to identify new molecular regulators of phagocytosis and hypusination. In the first study, we focus on the regulation of phagocytosis in immune cells, which is crucial for their function. Leveraging a FACS-based pH-sensitive phagocytosis reporter, we searched for novel dependencies and metabolic bottlenecks in macrophages, by performing both, a transporter-focused, as well as a genome-wide genetic screen. In the transporter-focused CRISPRko screen, we found the bicarbonate transporter *SLC4A7* to be crucial for phagosome acidification. Intriguingly, SLC4A7 is located at the plasma membrane and not directly on the phagolysosome, thus suggesting the interaction to be indirect. In the genome-wide CRISPRko screen, we were able to identify 716 genes as phagocytic regulators. By assigning the hits to a comprehensive protein-protein interaction network, which we annotated for cellular processes, protein complexes that were scoring multiple times could be identified and missing phagocytosis regulators could be placed in a cellular context. In addition to known protein complexes, such as the Arp2/3 complex, the Wave-2 complex, and the vacuolar-ATPase-Rag machinery, we identified and validated interesting new phagocytosis-relevant regulators, such as the oligosaccharyltransferase complex (MAGT1/SLC58A1, DDOST, STT3B, and RPN2) and the hypusine pathway (eIF5A, DHPS, and DOHH).

Since the entire hypusine axis scored with high significance in our genetic screen and its mechanistic link to phagocytosis could not be easily explained with existing knowledge, I focused the rest of this work on the functional dissection of this pathway. Functionalizing a hypusine-specific antibody in a genome-wide CRISPRko screen for hypusine abundance and combining it with expression proteomics upon hypusine inhibition, we were able to observe a yet undescribed direct crosstalk between oxidative phosphorylation (OXPHOS) and hypusine levels. Specifically, we found that while a reduction in OXPHOS increases hypusine level, inversely, inhibition of hypusination decreases OXPHOS-related proteins and increases ATF4. With various pharmacological perturbations targeting

mitochondria, we confirmed that disruption of mitochondrial respiration or mitochondrial protein translation increases hypusine levels. Finally, we also examined eIF5A acetylation. In contrast to hypusination, this modification is reversible and our experiments revealed a positive correlation with glycolysis, while cells that require more OXPHOS have lower levels of acetylation at eIF5A.

Thus, using functional genomics and in particular reporter-based genetic screening, we mapped the genetic regulatory landscape of molecular processes and identified a crosstalk between the hypusine axis and OXPHOS within the cell.

Zusammenfassung

Vorallem seit der Entwicklung von CRISPR/Cas9 als leistungsfähiges Genomeditierungswerkzeug hat sich die funktionelle Genetik in ein skalierbares und mächtiges Instrument zur Aufstellung von Hypothesen-generierender und „unbiased“ Forschung etabliert. Gleichzeitig sind mittlerweile, dank Weiterentwicklungen von Massenspektrometrietechniken und -maschinen, ganze Proteome vieler Zellen und Konditionen parallel messbar und vergleichbar. Die Kombination aus Genetik und Proteomik hat sich deshalb in eine mächtige Methode entwickelt, welche die Entdeckung und funktionelle Zerlegung komplexer molekularer Prozesse im Hochdurchsatz ermöglicht, was das vereinende Thema meiner Dissertation ist.

In dieser Arbeit mache ich Nutzen dieser Fortschritte und entwickle Werkzeuge und optimiere diese für die Verwendung in genetischen Screens um neue molekulare Regulatoren der Phagozytose und Hypusinierung zu entdecken. In der ersten Studie, fokusieren wir uns auf die Regulierung der Phagozytose in Immunzellen, welche kritisch wichtig für deren Funktion ist. Mit Hilfe einer FACS-basierten pH-sensitiven Phagozytosereportermethode und Transporter-fokusierten als auch Genom-weiten genetischen Screenings, suchten wir nach neuen Abhängigkeiten und metabolischen Flaschenhälsen in Makrophagen. Im Transporter-fokusiertem CRISPRko Screenig fanden wir den Bicarbonattransporter *SLC4A7* als kritischen Regulator für die Ansäuerung des Phagolysosoms. Interessanterweise, ist SLC4A7 jedoch an die Plasmamembrane lokalisiert und nicht direkt am Phagolysosom, was deshalb eine indirekte Interaktion mit der Phagozytose nahelegt. Im Genom-weiten CRISPRko FACS Screening konnten wir 716 Gene identifizieren die Phagozytose regulieren. Durch die Anordnung dieser Gene in einem umfassenden auf Protein-Protein Interaktionen basierenden Netzwerk, annotiert für zelluläre Prozesse, konnten mehrmals gefundene Proteinkomplexe identifiziert werden und konnten noch unbekannte Regulatoren der Phagozytose in zellulären Kontext gestellt werden. Neben bekannten Proteinkomplexen wie zum Beispiel dem Arp2/3 Komplex, dem Wave-2 Komplex und der vakulären-ATPase Maschinerie, identifizierten und validierten wir interessante neue für die Phagozytose relevante Reugulatoren, wie den Oligosaccharyltransferase Komplex (MAGT1/SLC58A1, DDOST, STT3B, and RPN2) und die Hypusinache (eIF5A, DHPS, and DOHH).

Da die Hypusinachse komplett und mit hoher Signifikanz in unserem genetischen Screening gefunden wurde und deren mechanistische Involvierung in der Phagozytose nicht einfach mit existierendem Wissen zu erklären war, habe ich mich im Rest der Dissertation auf die funktionelle Zerlegung dieses Pathways konzentriert. Die Funtionalisierung eines Hypusinantikörpers in einem

Genom-weiten auf Hypusinlevel fokusierten CRISPRko Screenings in Kombination mit Expressionsproteomikmessungen in Hypusin inhibierten Konditionen, erlaubte es uns ein bis dahin noch unbekanntes beidseitiges Feedback zwischen oxidativer Phosphorylierung (OPXHOS) und Hypusinleveln zu beschreiben. Wir fanden, dass einerseits die Reduzierung von OXPHOS Hypusinlevel erhöht und umgekehrt, die Inhibierung von Hypusinierung die Level OXPHOS-verwandter Proteine verniedrigt und gleichzeitig das ATF4 Level erhöht. Mittels verschiedenster auf Mitochondrien abzielender pharmakologischer Perturbationen konnten wir bestätigen, dass die Störung mitochondrialer Atmung oder mitochondrialer Proteintranslation zur Erhöhung der Hypusinleveln führt. Schlussendlich untersuchten wir auch eine zweite Modifizierung am eIF5A, die Acetylierung am Lysin 47. Im Gegensatz zu Hypusinierung ist diese Modifizierung umkehrbar und unsere Experimente zeigten eine positive Korrelation mit der Glykolyse, während Zellen mit einem hohen Bedarf an OXPHOS niedrigere Level an acetyliertem eIF5A haben.

In Summe haben wir durch die Methoden der funktionellen Genetik, vorallem aber durch Reporter-basierte genetische Screenings, die genetische Regulierung von molekularen Prozessen abgebildet und weiters ein beidseitiges Feedback zwischen der Hypusinachse und der oxidativen Phosphorylierung in der Zelle identifiziert.

Abbreviations

A site	aminoacyl-site	**LC-MS**	liquid chromatography-mass spectrometry
aa-tRNA	aminoacyl-tRNA	**mtDNA**	mitochondrial DNA
aIF5a	archael translation initiation factor 5A	**mTORC1**	Mammalian target of rapamycin complex 1
AMPK	AMP-activated protein kinase	**NF-κB**	nuclear factor kappa-light-chain-enhancer of activated B cells
Cas9	CRISPR associated protein 9	**NHEJ**	non-homologous end joining
CHOP	C/EBP homologous protein	**NPC**	nuclear pore complex
CRISPR	clustered regular interspaced short palindromic repeats	**NTR**	nuclear transport receptors
crRNA	CRISPR RNA	**OAZ**	ornithine decarboxylase antizyme
DHPS	deoxyhypusine synthase	**ODC**	ornithine decarboxylase
DOHH	deoxyhypusine hydroxylase	**ORF**	open reading frame
eEF1A	eukaryotic translation elongation factor 1 alpha	**OXPHOS**	oxidative phosphorylation
eEF1B	eukaryotic translation elongation factor 1 beta	**P site**	peptidyl site
eEF2	eukaryotic translation elongation factor 2	**PRF**	programmed ribosomal frameshift
eEF2K	eEF2 kinase	**Pro-tRNA**	proline-tRNA
EF-P	elongation factor P	**PTC**	peptidyl transfer center
ER	endoplasmic reticulum	**sgRNA**	single guide RNA
eRF1	eukaryotic translation termination factor 1	**Sirt1**	NAD-dependent deacetylase sirtuin-1
eRF3	eukaryotic translation termination factor 3	**SNP**	single nucleotide polymorphism
ESI	electrospray ionization	**SSAT1**	spermidine/spermine-N1-acetyltransferase 1
FACS	Fluorescent-activated cell sorting	**TFEB**	transcription factor EB
GC7	N1-guanyl-1,7-diaminoheptane	**TMT**	tandem mass tags
GO	Gene Ontology	**tracRNA**	trans-acting CRISPR RNA
GWAS	genome-wide association studies	**tRNA**	transfer RNA
Hap1	heme-responsive zinc finger transcription factor Hap1	**Tsc2**	tuberous sclerosis complex 2
HDAC6	histone deacetylase 6	**uORF**	upstream open reading frame
HEAT	super helical structure with eight helical hairpins	**UTR**	untranslated region
IGF2BP1	insulin-like growth factor 2 mRNA-binding protein	**Xpo4**	exportin 4

Acknowledgments

This thesis marks the end of another chapter in my life. The long journey of acquiring a PhD is without doubt, one of the most unique but at the same time rewarding experiences. Clearly, none of this would have been possible without the support and contribution of several persons whom I would like to acknowledge.

First and foremost, I would like to thank my PhD supervisor Giulio Superti-Furga for putting his trust in me and letting me work independently on this project. I highly appreciate his constant support, the many interesting discussions we had, his enthusiasm, honest words, and the drive to think big. Especially on hypusine we had many lengthy discussions and brainstorming session where we learned a lot. I will always highly cherish this PhD time as a time of great experimental freedom and creativity.

I would also like to thank the GSF group members – students, postdocs, technicians, and lab management– for creating such a great lab atmosphere to work in. I am grateful for your kindness, professionality, and positive attitude that made working and the numerous events we spent together a more than pleasant experience. I hope I could also contribute to support some of your challenges. Special thanks to Stefania, Felix, Ania, and Leo for their warm welcome when I started in the lab. During my stay in the GSF lab, I saw it grow, go-through a pandemic, and turn over owing to many large projects, and I learned a lot during this time.

Thank also to the members of my PhD committee, Thijn Brummelkamp, Gaia Novarino, and Harald Sitte for their helpful input, guidance, and collaboration.

CeMM has been a unique place to conduct a PhD. I would like to thank Giulio and Anita for creating a place that feels like one big family that I am proud to have been part of. I am grateful to have met all the inspiring people that love to collaborate, share their knowledge and reagents, and are just pleasant to work with and learn new things. I would like to thank for the contribution of every person past and present at CeMM, spanning from facility support to administration and faculty whose commitment to go the extra mile impacted my traineeship tremendously.

I am grateful for the many people that directly contributed to this work and that I have been lucky enough to work with. That includes Vitaly, who mentored me in the beginning and laid the scientific basis for one of the projects. It also includes Fabian, Evandro, Ann-Kathrin, Yee-Kwan, Leo, Johannes, Adrijana, Felix, Ulrich, and Lukas who I was lucky enough to work with. My collaborators: Nicolaas, Thijn, Sohani, Marko, and Didier for all the meetings and scientific and experimental help. I

also feel lucky that I had the chance to mentor and work with Benedikt and Yee-Kwan for their master thesis and PhD work respectively. I learned a lot from that and hope I could also contribute a bit to your future paths.

A big gratitude also to Icíar my girlfriend, for inspiring conversations, continuous support and understanding for long workdays, as well as listening to my technical fantasies. I can't wait to see what the future holds for us.

I am grateful for my friends who always supported my journey while reminding me where I come from. A special shout out to Gerhard who already calls me "doctor" for many years, it took a while but looks like it is now coming to reality. Thanks, Mum and Dad, grandparents, and brother for providing me with support and trusting me fully on all the journeys I started. Knowing to have somewhere to put into harbor if ever needed is a liberating feeling. Thank you, this thesis is for all of you!

1 Introduction

In this thesis, we made use of a variety of functional genomics and in general omics techniques to systematically dissect molecular processes. The data presented in the results section encompasses two papers as well as still unpublished results. For the first two studies either focused or genome-wide genetic loss-of-function screening was employed to find regulators of phagocytosis. This effort led to the discovery of the hypusine axis as the most significant scoring gene family of the process. At the center of this gene family sits eIF5A, an enigmatic protein that binds and acts among other things on the ribosome and has been in recent years recognized as an important translational elongation factor. Therefore, we complemented our experimental setup for this part of the thesis with omics techniques suitable to capture effects on gene expression, such as ribosome profiling as well as expression proteomics. Since the activity of eIF5A is regulated by the post-translational modification hypusine, we could again employ a genetic screen to identify regulators of hypusine levels. The following introduction provides a comprehensive overview of the topics covered in the result section of this thesis and is divided into five largely different parts consisting of:

i. A broad overview of the history and application of functional genomics employed for human biology. This part serves as a common theme for this thesis work and is instrumental for the experimental design of all projects presented in the results section of this thesis.
ii. A description of how gene expression is regulated within cells, with a focus on protein synthesis and in particular the regulation for translational elongation especially by the translational elongation factor eIF5A, which is at the center of the third part of our result section.
iii. A review of the hypusine pathway, covering the three proteins that are involved in the pathway, where they localize in the cell, what metabolic roles they might have, diseases where the hypusine axis seems to be involved, and what kind of inhibitors are currently available to modulate this axis. This part is important for the third part of our result section, which focuses on the broad molecular dissection of the hypusine axis.
iv. An overview of loss-of-function genetic screening, focusing on CRISPR-based genetic screens employed in the first two parts of the presented results and haploid genetic screening which is instrumental for the third part of the thesis.
v. A brief description of the experimental approaches used in the thesis, comprising expression proteomics, ribosome profiling, and endogenous protein tagging, all techniques that we employed for the dissection of the hypusine axis in the third part.

1.1 Functional Genomics Employed for Human Biology

20 years have passed since the completion of the human genome project (International Human Genome Sequencing Consortium *et al.*, 2001; Venter *et al.*, 2001) that decoded the whole euchromatic fraction of the human genome and thereby started the post-genome era (International Human Genome Sequencing Consortium, 2004; Hood and Rowen, 2013). Recently, new developments in the ultralong-read sequencing developed by Oxford Nanopore and PacBio HiFi allowed to overcome previous technical limitations and allowed to complete also the last remaining 8% of the human genome including centromeric regions and the short arms of all chromosomes (Nurk *et al.*, 2022) adding to the ~20,000 known protein-coding genes, 140 new genes, being exclusive to the new released TST-CHM13 reference genome. But while sequencing technologies and genome information dramatically improved in the last 20 years, we still know fairly little about the function of the individual genes, especially in different disease contexts and different cellular tissues. Classical genetics, pioneered by Hermann Joseph Muller in 1927, which involves the introduction of mutations into genes, proved to be one of the most powerful unbiased approaches to investigate gene functions (Muller, 1927). Scientists over the year then made use of several different model organisms such as *Drosophila*, *Caenorhabditis elegans,* or yeast that were easier to genetically manipulate and allowed scientists to establish functions of numerous genes. Later, one of the first genetic screens ever conducted showed how certain genes regulate the segment number and polarity in *Drosophila* (Nüsslein-Volhard and Wieschaus, 1980). A major motive for research funding is the hope to ease human diseases. However, the inability at the time to construct strains of known genotypes, such as knock-out strains, limited the ability to systematically test hypotheses and therefore denied the use of many classical genetic approaches (White and Caskey, 1988).

This changed in 1959, when the conditions for cultivating mammalian cells were decoded and cultivating human cell lines under controlled conditions became possible (Eagle, 1959). First genetic screens still relied on Sanger sequencing, the dominating and powerful sequencing technique of the 1970s invented by Fred Sanger (Sanger *et al.*, 1977). This sequencing technique allowed scientists to determine the first-ever complete genome, namely the one of the bacteriophage PhiX174 (Sanger *et al.*, 1977). It was also honored with a Nobel prize shared with Walter Gilbert and Paul Berg in 1980 and was on top employed to produce the first human reference genome in the Human Genome Project (Venter *et al.*, 2001), which took 13 years and the immense costs of three billion USD. This enormous effort of decoding the human genome kickstarted the system biology field which has the task of unraveling the function of the around 20,000 proteins encoded in a cell (Nurse and Hayles, 2011; Mast *et al.*, 2014).

In 1998 a new DNA sequencing technique termed pyrosequencing was published by Mostafa Ronaghi, Mathias Uhlén, and Pål Nyrén which is considered as the birth hour of next-generation DNA sequencing techniques (Ronaghi *et al.*, 1998). Its "sequencing by synthesis" principle, which relies on the detection of light released during a chain reaction with pyrophosphate, allows for automation and miniaturization of the process, hence turning DNA sequencing into a high-throughput technique. In 2016 Veritas Genetics then was among the first who could sequence whole human-genomes at below 1,000 USD ("Veritas Genetics Launches $999 Whole Genome And Sets New Standard For Genetic Testing," 2016). This not only enabled the use of sequencing as a clinical tool but also allowed for the first-time large population sequencing efforts, which led to the discovery of many single nucleotide polymorphisms (SNP) linked to diseases collected in projects such as gnomAD or the 100,000 Genomes project (Turnbull *et al.*, 2018; Karczewski *et al.*, 2020; Chen *et al.*, 2022) and further boosted a large interest in personal genomics. For the first time in history, the human body became a direct model organism.

Functional genomics is defined as the process of investigating how genes and intergenic regions participate in different biological processes. Research employing functional genomics usually performs genome-wide investigation or studies of multiple genes simultaneously rather than employing a "candidate-gene" approach, with the goal of identifying a list of candidate genes that are most strongly associated with the process that can then be validate in detail. In response to the vastly increasing amount of sequencing data in the post-genomic era, functional genomics gained even more importance. Applied in functional genomic screening it can help to understand genome sequencing data in biological contexts and allows us to better understand how biological systems operate, how drugs function, and can unravel the mechanisms behind a disease (Przybyla and Gilbert, 2022). Next-generation sequencing was also crucial for functional genomics itself, as it made large-scale pooled sequencing-based genetic screens affordable and feasible (Goodwin *et al.*, 2016; Pervez *et al.*, 2022).

The development of RNAi (Chan *et al.*, 2006; Wilson and Doudna, 2013) and gene trap technology in haploid cells (Carette *et al.*, 2009) led then to the development of the first genome-wide genetic loss-of-function screens (Boutros and Ahringer, 2008; Carette *et al.*, 2009, 2011*a*; Brockmann *et al.*, 2017), being one of the most powerful methods to date to assign gene function. With the discovery of CRISPR/Cas9 (clustered regular interspaced short palindromic repeats/CRISPR-associated protein 9) the toolbox of genetic tools was then further expanded and allowed now loss-of-function screens in almost any cell type (Koike-Yusa *et al.*, 2014; Shalem *et al.*, 2015; Komor *et al.*, 2017; Bock *et al.*, 2022), but also allows for gene interference and gene activation screens which further makes targeting of non-coding sequences possible (Gilbert *et al.*, 2014; Przybyla and Gilbert, 2022; Morris *et al.*, 2023). Some of these techniques will be reviewed in detail in chapter 1.4. Considering that most

disease-associated genetic variants from genome-wide association studies (GWAS) are located in non-coding regions screening techniques that allow studying this “dark matter” of the genome will become increasingly important (Warren *et al.*, 2017).

Nevertheless, the key ingredients for every successful genetic screen remained the same since the very beginning. Every genetic screen requires a perturber, a model system, and a suitable readout for the biological process that needs to be studied (Grimm, 2004) (Figure 1). By following this scheme, complex biological processes can be dissected with genetics screens and genes can be assigned to phenotypes. By doing this in a large variety of cellular systems and different disease contexts and by sharing this information in public databases such as DepMap, CRISP-view, CRISPbrain, or the Open Repository for CRISPR Screens (ORCS) database (Meyers *et al.*, 2017; Oughtred *et al.*, 2019; Cui *et al.*, 2021; Tian *et al.*, 2021), powerful resources for deorphanizing genes are created.

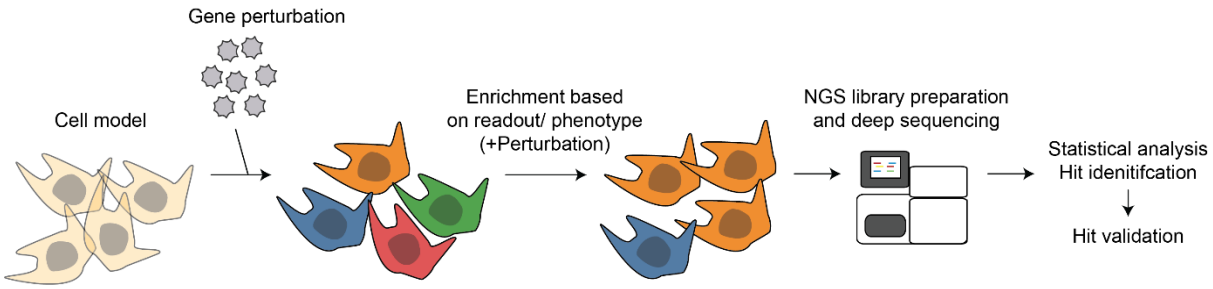

Figure 1. Schematic of a functional genomics screen.

Simplified overview of the key steps involved in a functional genomics screen.

A long-standing goal of system biology has been to use a multitude of omics-techniques such as expression analysis, proteomics, metabolomics, and ribosome profiling to better understand molecular processes in the cell. The addition of genetic screens has added yet another instrument to the toolbox of system biology. As genetic screening, proteomics, and ribosome profiling are key techniques for this thesis, these methodologies will be addressed in detail below.

1.2 Gene Expression

The findings of this thesis will concern genes that affect various types of regulation at different steps of the genetic information flow from gene to phenotype. Therefore, I would like to first review the basic principles of gene expression, which will help to put our findings in context and understand the choice of experimental system that I used for dissection of these genes.

The central dogma of molecular biology describes the flow of genetic information starting from DNA to RNA to protein and thereby closely interlinks these molecular species with each other (Figure 2). Gene expression is a term that summarizes the process of turning the information encoded in genes into functional products such as proteins or functional non-coding RNAs and thereby manifests a certain phenotype. Proteins are the essence of all cells and their levels are regulated by a series of connected processes starting with the transcription, processing, and degradation of mRNAs and finishing with the translation, modification, and coordinated destruction of proteins (Vogel and Marcotte, 2012) (Figure 2). These tasks are executed by a multitude of transcription and translation factors encoded in the human genome (McManus *et al.*, 2015). Of the ~20,000 proteins encoded in the genome, around 2,000 code for transcription factors (Vaquerizas *et al.*, 2009) and roughly 1,000 for RNA binding proteins with assumed roles on RNA stability and translation (Baltz *et al.*, 2012; Castello *et al.*, 2012) (Figure 2).

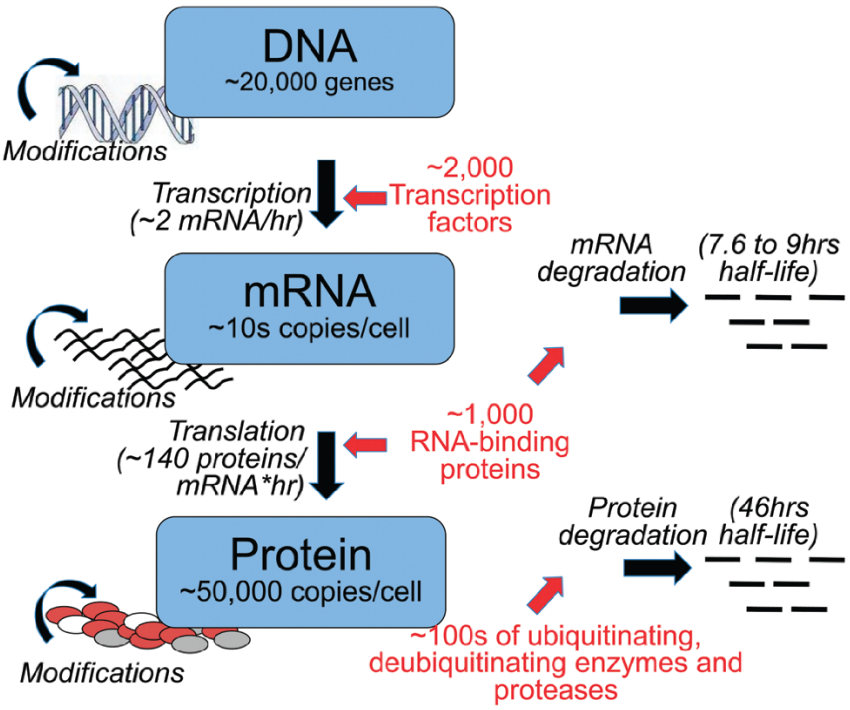

Figure 2. The central dogma of molecular biology in numbers.

Reprinted from Molecular BioSystems Issue 10, McManus, J., Cheng, Z., Vogel, C., Next-generation analysis of gene expression regulation – comparing the roles of synthesis and degradation, 2015, with permission from ROYAL SOCIETY OF CHEMISTRY

While it is still poorly understood how much each step precisely contributes to the final level of a protein, advances in RNA sequencing techniques and proteomics allow us nowadays to perform global systematic studies matching transcriptomic data with measured protein concentrations. It has been a long debate if mRNA levels or post-translational events have a stronger influence on protein levels in unperturbed mammalian cells (Schwanhäusser *et al.*, 2011, Li *et al.*, 2014*a*). With the help of the latest technology, newer studies now imply that changes in the steady-state protein concentrations in cells are primarily explained by changes in mRNA levels (Li and Biggin, 2015; Liu *et al.*, 2016). This was also confirmed in a study performed in mouse bone marrow dendritic cells analyzed at steady-state and upon stimulation with LPS (Jovanovic *et al.*, 2015). In steady-state 68% of alterations in protein expression could be explained by mRNA levels, and 26% and 8% by translation rate and protein degradation respectively; in stimulated cells mRNA even explained 90% (Jovanovic *et al.*, 2015; Li and Biggin, 2015). However the authors intriguingly also found that the translation and degradation rates in sum have the largest effect on absolute protein changes, affecting especially proteins that perform basic cellular functions, that exist often in way higher total numbers of protein units per cell (Jovanovic *et al.*, 2015). While for example the change in expression for a lower expressed *gene X* from 1,000 to 10,000 proteins accounts for a fold change of ten another much stronger expressed *gene Y* that changes its concentrations from 1,000,000 to 1,300,000 calculates a fold change of only 1.3. In a classical analysis, where typically the proteins with the strongest fold changes are prioritized *gene X* would appear to have much more importance than *gene Y*. However, if one considers that a typical mammalian cell expresses ~10^3-10^8 proteins per cell, the expression change of *gene Y* (fold change 1.3) would affect the total proteome in the most crowded cell ~30 times more than the expression change of *gene X* (fold change 10) (Li *et al.*, 2014*a*; Jovanovic *et al.*, 2015).

1.2.1 Protein Synthesis

Proteins make up the largest proportion of macromolecules in a cell and their production is modulated at several levels that we will describe in detail in this section (Tahmasebi *et al.*, 2019). Turning messenger RNA (mRNA) into proteins and folding them into their active form is the core of every biological process (Hershey *et al.*, 2019) and ultimately defines the biochemical constitution of a cell. Requiring four phosphate bonds for each amino acid added to a polypeptide chain (two for the charging of a tRNA and two for the formation of the peptide bond during the elongation), protein synthesis also represents the single largest investment of energy within a cell (Russell and Cook, 1995; Rolfe and Brown, 1997). Additionally, the protein levels are usually the molecularly relevant output of gene expression and regulatory finetuning or constraints happen rather on the protein level than on the mRNA level (Ingolia *et al.*, 2019). Therefore, it is not surprising that multiple pathways have

evolved that adjust the translation rate according to the availability of energy, nutrients, and external signals (Lindqvist *et al.*, 2018) but also based on the cell cycle state or differentiation of a cell (Teixeira and Lehmann, 2019; Wang and Amoyel, 2022; Leesch *et al.*, 2023). Additionally, protein production does not always follow transcriptional changes, but instead employs an armada of translation factors offering a universe of regulatory control over protein production (Pechmann *et al.*, 2013; Slobodin and Dikstein, 2020). Therefore, understanding the details of translational regulation is a key pillar in understanding biology.

In eukaryotes, protein translation is coordinated by the 40S and 60S ribosomal subunit, which together consists of over 80 proteins, 4 mRNAs, and aminoacyl-tRNAs, and energy provided by ATP and GTP hydrolysis (Hershey *et al.*, 2019) (Figure 3). The aminoacyl-tRNAs are specific for certain codons and are continuously regenerated and loaded with the specific amino acid by the corresponding aminoacyl-tRNA synthases (Hershey *et al.*, 2019). Protein translation consists of three steps: initiation, elongation, and termination (Figure 3).

During initiation, a complex consisting of the small ribosomal 40S subunit and the initiator methionyl-$tRNA_i$ is formed, which binds to the 5'-end of the mRNA and together with other initiation factors forms the preinitiation complex (PIC) (Merrick and Pavitt, 2018). PIC then scans the mRNA towards the 3'-end until the anticodon of methionyl-$tRNA_i$ pairs with a start codon, which is usually an AUG (Hinnebusch *et al.*, 2016). A successful pairing of PIC with the start codon then terminates PIC scanning, various initiation factors fall off, and the 40S subunit fuses with the 60S large ribosomal subunit, which now forms the 80S initiation complex (Merrick and Pavitt, 2018) (Figure 3).

The next translation phase, the elongation phase, begins right after the 80S initiation complex has formed next to the start codon. Briefly, aminoacyl-tRNAs (aa-tRNAs) that match upcoming codons on the mRNA continuously bind in the aminoacyl-site (A site) of the ribosome, and the ribosome catalyzes the attachment of the loaded amino acid to the amino acid located in the peptidyl site (P site) (Hershey *et al.*, 2019) (Figure 3). After successful peptide bond formation, the peptidyl-tRNA in the A site migrates together with the mRNA into the P site, a step called translocation (Dever *et al.*, 2018) (Figure 3). The elongation process is described in detail in the next chapter.

As soon as a so-called STOP codon (UAA, UGA, or UAG) binds to the A site of the ribosome, it is not recognized by any matching tRNA (Hershey *et al.*, 2019). Instead, eukaryotic peptide chain release factors (eRFs) will bind and catalyze the release of the nascent peptide from the peptidyl-tRNA of the P site and thereby terminate protein translation (Schuller and Green, 2018) (Figure 4). The translation is now finalized by other proteins that bind to the ribosome, which assist in the release of mRNA and tRNA, disassemble the ribosome, and aid in its recycling (Hellen, 2018). Depending on the protein,

after termination, the polypeptide still has to fold into the right shape (Dobson, 2003; Pechmann *et al.*, 2014), must be transported to the correct location in the cell (Bauer *et al.*, 2015), receive posttranslational modifications (Lin and Caroll, 2018) or form complexes with other proteins (Schwarz and Beck, 2019) before it can fulfill its task in the cell.

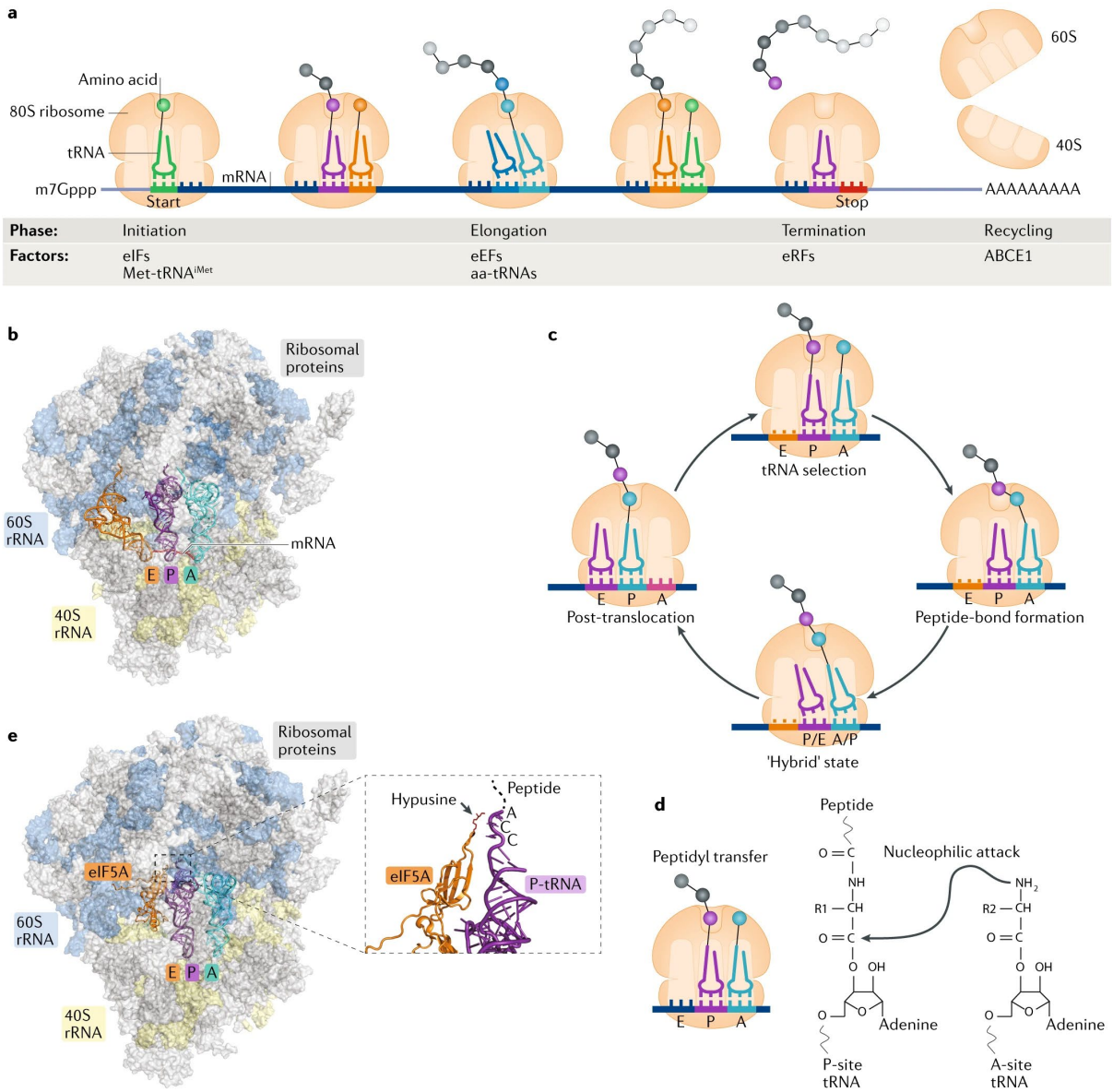

Figure 3. Summary of eukaryotic translation.

a. Overview of steps in eukaryotic translation starting with initiation, followed by elongation, termination, and ribosome recycling. **b.** Model of the yeast 80S ribosome structure with the three sites of tRNA binding mapped: E (exit; in orange), P (peptidyl; in purple), and A (aminoacyl; in cyan) (PDB 4V88, PDB 4V9I) **c.** Schematic of the elongation circle illustrating the different states and locations of tRNAs during translational elongation. **d.** Schematic of the peptidyl-transfer reaction taking place during translational elongation. **e.** Model of the yeast 80S ribosome structure as described in (b) with eIF5A bound in the ribosomal E site. On the right, the interaction of the hypusine modification with the CCA nucleotides at the 3' end of the peptidyl-tRNA is indicated. (PDB 4V88, PDB 5GAK)

1.2.2 Translational Elongation

As mentioned briefly above, translational elongation follows right after translational initiation and comprises the process of lengthening the polypeptide chain during protein synthesis. It starts with an 80S ribosome placed at an AUG start codon as well as a methionyl-$tRNA_i$ in the P site and delivers codon-matching aa-tRNAs to the A site of the ribosome until it reaches the STOP codon of the open reading frame (ORF) (Schuller and Green, 2018). Translation elongation consists of three steps: (i) tRNA selection (also called decoding), (ii) peptide bond formation, and (iii) translocation of the tRNAs and bound mRNA (Schuller and Green, 2018) (Figure 4). Similar as other steps of translation, elongation is a highly regulated process, that requires the interplay and help of multiple factors that I will now briefly review below.

tRNA Selection

During tRNA selection, the eukaryotic translation elongation factor eEF1A forms a complex with GTP and an aminoacyl-tRNA. This ternary complex binds to the A site, where base pairing between the A site codon and the anticodon of the aminoacyl-tRNA activates eEF1A, hydrolyses GTP and facilitates the positioning of the tRNA within the A site (Dever *et al.*, 2018).

Peptide Bond Formation

The next step in the elongation process is peptide bond formation and comprises an attack of the ribosomal A site amino acid on the ester linkage on the peptidyl-tRNA in the P site, as well as the transfer of the peptide chain onto the tRNA in the A site (Schuller and Green, 2018). The reaction takes place in the peptidyl transferase center (PTC), a place in the large ribosomal subunit that consists of rRNA elements (Ben-Shem *et al.*, 2011; Klinge *et al.*, 2011). It aids the peptide bond formation by positioning the peptidyl- and aa-tRNA into suitable positions for catalysis (Dever *et al.*, 2018). Eukaryotic translation initiation factor 5A (eIF5A) is an additional factor that binds to the exit site (E site) and helps with peptide bond formation (Schmidt *et al.*, 2016). Due to its relevance for this thesis, it will be described in greater detail below.

During peptide bond formation, the two ribosomal subunits rotate and the tRNAs position themselves into a hybrid state (Moazed and Noller, 1989). In this phase, the acceptor ends of the tRNAs are already in the E and P site of the large ribosomal subunit, while the anticodon of the tRNAs

remains still in the A and P site of the small subunit of the ribosome (Budkevich *et al.*, 2014; Schuller and Green, 2018) (Figure 4).

Translocation of the tRNA and bound mRNA

The GTPase eukaryotic translation elongation factor 2 (eEF2) then translocates the tRNA-mRNA complex relative to the ribosome and brings back the tRNAs to their canonical E and P sites (Schuller and Green, 2018). After translocation, the E site is loaded with a deacetylated tRNA and the P site harbors the peptidyl-tRNA (Dever *et al.*, 2018). All the above-described steps are repeated until the entire protein encoded on the mRNA has been produced.

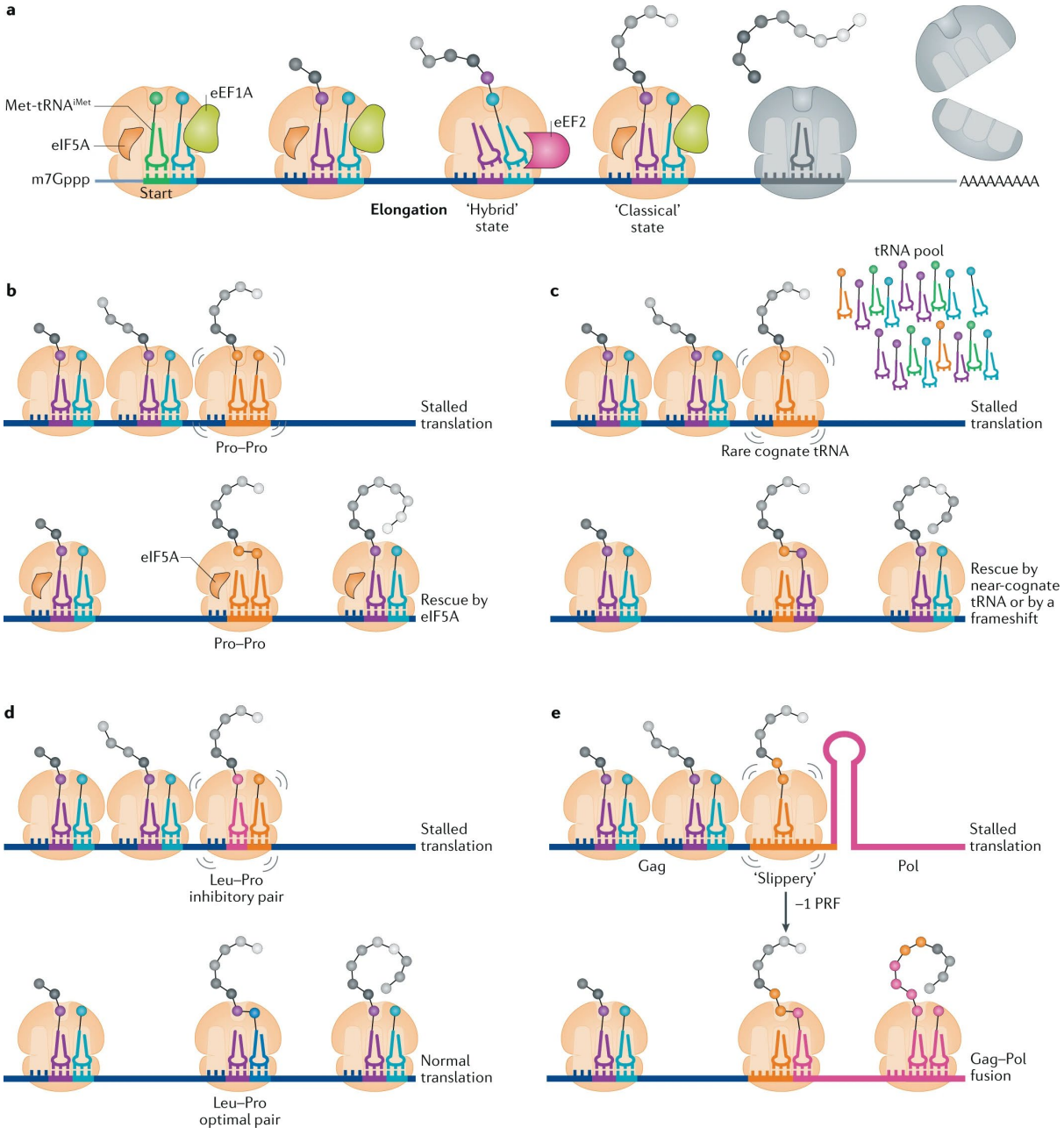

Figure 4. Summary of elongation, ribosome stalling and its resolution.

a. Overview of steps in eukaryotic translational elongation. **b.** Stalled translation induced by slow peptidyl-transfer kinetics (e.g. formation of Pro-Pro) is rescued by eIF5A. **c.** Ribosome stalling caused by poor A-site occupancy as a result of low availability of the respective tRNA can be rescued by misincorporation of near-cognate tRNAs or by frameshifting. **d.** Stalled translation by suboptimal consecutive tRNA-codon pair orders. **e.** mRNA secondary structures can lead to ribosome stalling, which can be resolved by programmed ribosomal frameshifting (PRF) at adjacent 'slippery' sequences.
Reprinted from Nature Reviews Molecular Cell Biology 19, 526-541, Schuller, AP., Green, R., Roadblocks and resolution in eukaryotic translation, 2018, with permission from Springer Nature

1.2.3 Regulation of Translational Elongation

While translational initiation is known to be highly regulated and the rate-limiting step for protein production (Jackson *et al.*, 2010), the much simpler process of translational elongation is also subject to a wide range of regulation (Schuller and Green, 2018) (Figure 4). Additionally, there can be direct feedback of elongation rate on initiation rate. The average elongation rate is about five amino acids per second (Ingolia *et al.*, 2011), while the time span for initiation is around five seconds (Palmiter, 1975) and can only take place if the ribosome is already five amino acids downstream of the start codon (Hershey *et al.*, 2019). Hence, if elongation is drastically slowed down it can directly influence the rate of initiation (Hershey *et al.*, 2019).

Regulation of Translational Elongation Factors

One of the main disadvantages of intervening at the translational elongation level is, that it is a very costly way of reducing protein production, which is because then more ribosomes are required to make the same amount of protein, and ribosomes are large molecular complexes that require large amounts of energy to produce (Fromont-Racine *et al.*, 2003). On the other hand, interfering with elongation offers an elegant way for rapid pausing of translation in situations where energy is needed spontaneously, like muscle contraction (Rose *et al.*, 2005). In this way the polysomes stay preserved, the mRNA is possibly better protected, and translation can resume swiftly once the demand for energy and nutrients is fulfilled again (Proud, 2019).

A significant part of the regulation during translational elongation occurs through direct regulation of the few elongation factors involved in the elongation process: (i) eEF1a, (ii) eEF2, (iii) eIF5A.

eEF1A

As mentioned earlier the ATP of the eEF1a ternary complex is hydrolyzed at the ribosome and released as a binary complex with GDP (Gromadski *et al.*, 2007). Fresh eEF1A•GTP is then regenerated by elongation factor 1-beta (eEF1B) to allow the formation of new eEF1A•GTP•aminoacyl-tRNA

ternary complexes (Gromadski *et al.*, 2007). eEF1A is post translationally modified by methylation of lysines through several characterized lysine methyltransferases and loss of its methylation is linked to changed translation (Dever *et al.*, 2018).

eEF2

The domain IV of eEF2 has a similar shape as the anticodon of a tRNA and binds deep in the A site of the ribosome (Dever *et al.*, 2018). The tip of domain IV on eEF2 harbors a conserved histidine residue that gets post translationally modified to diphthamide (2-[3-carboxyamido-3-(trimethylammonio)propyl]histidine) (Su *et al.*, 2013). Diphthamide is produced in a 4-step reaction using seven different proteins (DPH1-7) and the absence of this posttranslational modification causes developmental defects and death in mice; nevertheless, some cancer cell lines like CHO or MCF7 have been reported to be viable without functional diphthamide synthesis (Dever *et al.*, 2018). The absence of diphthamide has been linked to an increase in -1 ribosomal frameshifting, suggesting that this modification enables eEF2 to accurately translocate the ribosome (Liu *et al.*, 2012). In addition, eEF2 can also be phosphorylated by eEF2 kinase (eEF2K), which then blocks its binding to the ribosome and thereby stops translation (Ryazanov *et al.*, 1988; Carlberg *et al.*, 1990). The activity of eEF2K is regulated through the mammalian target of rapamycin complex I (mTORC1) and AMP-activated protein kinase (AMPK), linking translational regulation through eEF2 to nutrient and energy levels in the cell (Browne and Proud, 2004; Proud, 2015). Considering that elongation consumes almost all the energy of protein production (four to five ATP for each amino acid added to the polypeptide chain), this phosphorylation switch offers a rapid way to reduce energy and amino acid consumption in the cell by slowing translation rates (Redpath *et al.*, 1996). An example where this regulation mechanism seems to be exploited is muscle contraction, where eEF2 is rapidly phosphorylated and thereby quickly frees ATP that would usually be consumed by protein translation (Rose *et al.*, 2005).

eIF5A

The third factor supporting translational elongation is eIF5A (Saini *et al.*, 2009). Its activity is largely dependent on the unique post-translational modification hypusine (Park *et al.*, 1981). Due to the importance of hypusine for this work, we devote a separate chapter to it below.

Regulation through mRNA Encoded Obstacles

In addition to the direct regulation of elongation factors, the ribosome also encounters a variety of obstacles in the sequence code during the journey along the ORF of a gene, which can slow down its speed of translation (Schuller and Green, 2018) or can even lead to “recoding” which describes a situation where signals built into the mRNA sequences temporarily alter decoding of the mRNA

(Gesteland and Atkins, 1996). These obstacles can be: (i) certain amino acid sequence combinations, (ii) prolines, (iii) codons of low expressed cognate tRNAs, (iv) the order of codons, (v) secondary structures in the mRNA, and (vi) factors interacting with the mRNA (Figure 4).

Amino Acid Sequence Combinations

Using the 20 different protein-coding amino acids, 400 different amino acid combinations are possible during peptide bond formation. However, not all combinations react with the same efficiency and some amino acid combinations can lead to inhibitory confirmations of the nascent peptide chain in the ribosome exit tunnel (Schuller and Green, 2018).

Proline

An amino acid with particularly challenging properties is proline. Its reactive amine is part of the cyclic side chain known as imidazole ring, making Proline-tRNA (Pro-tRNA) a poor A site peptidyl acceptor due to reduced nucleophilicity (Wohlgemuth *et al.*, 2008; Pavlov *et al.*, 2009). In addition, entropic limitations make proline a poor substrate for the P site as well, which makes the synthesis of Pro-Pro stretches especially slow (Doerfel *et al.*, 2013; Gutierrez *et al.*, 2013; Ude *et al.*, 2013) (Figure 4).

Codons of Low Expressed Cognate tRNAs

If a mRNA is rich in codons of low-expressed cognate tRNAs or regeneration of fresh cognate aa-tRNAs for that codon is slow, it can lead to decreased elongation rates as well (Hanson and Coller, 2018) (Figure 4). This can further result in miscoding if the stalled ribosome is resolved by providing an alternative near-cognate tRNA or it can lead to noncanonical events such as frameshifting (Schuller and Green, 2018). A specific codon bias within an mRNA can therefore guide protein production and affect the translation efficiency of a transcript or the efficiency of protein folding (Hanson and Coller, 2018).

mRNA Structures

Lastly, *cis*- and *trans*-acting regulatory elements encoded on mRNA direct the ribosome to pause at specific locations on the transcript (Dever *et al.*, 2018). *Cis*-elements are encoded entirely in the mRNA itself and some of the best-characterized *cis*-factors are mRNA secondary structures like stem-loops or pseudoknots that are thought to induce ribosome stalling (Dever *et al.*, 2018). Often the ribosome stops in these cases on conserved “slippery” sequences that can cause ribosome frameshifting (Namy *et al.*, 2006; Belew *et al.*, 2014) (Figure 4). *Trans*-elements can consist of

proteins, nucleic acids, or small molecules that interact with a specific part of the mRNA transcript (Dever *et al.*, 2018).

The regulatory loop of *ornithine decarboxylase* (*ODC*), the enzyme that catalyzes the first step of polyamine synthesis, is one such case of a *trans*-acting regulatory element (Dever *et al.*, 2018). Its protein level is regulated by a +1-programmed ribosomal frameshift (PRF) on the mRNA encoding the *ornithine decarboxylase antizyme* (*OAZ*), which is stimulated by polyamines (Venkataramanan and Floor, 2018) (Figure 5). OAZ regulates ODC levels (Heller and Canellakis, 1981) by inducing its degradation in a ubiquitin-independent way by the 26S proteasome (Murakami *et al.*, 1992). When polyamine levels are low, little +1 PRF occurs on the *OAZ* mRNA, which downregulates OAZ and therefore increases polyamine synthesis (Ivanov *et al.*, 2018). Then as polyamine levels increase, +1 RF increases, OAZ levels rise, ODC levels fall, and polyamine synthesis is reduced again (Ivanov *et al.*, 2018) (Figure 5). In addition, several other proteins involved in the polyamine synthesis pathway are regulated translationally and will be addressed in the chapter below (Miller-Fleming *et al.*, 2015).

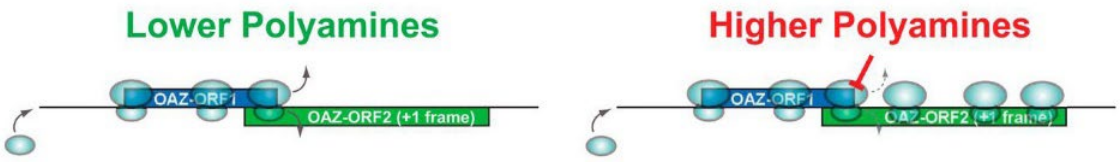

Figure 5. Schematic of regulation of *OAZ* translation via polyamines.

The expression of OAZ is coordinated via two partially overlapping ORFs that are linked through ribosomal +1 frameshifting. In case of low cellular polyamine levels translation is terminated at the STOP codon of ORF1. In case of high cellular polyamine levels, ribosomes shift at the ORF1 stop codon which leads to expression of full-length OAZ. *Adapted from J Biol Chem., 293(48):18719-18729, Dever, TE., Ivanov, IP., Roles of polyamines in translation, 2018, article from Elsevier under open access Creative Commons CC-BY license*

1.2.4 The Function of eIF5A in Translation

One of the few translation factors that is universally conserved from bacteria to humans is eIF5A (Kyrpides and Woese, 1998). It is 157 amino acids in size and its activity largely depends on the post-translational modification hypusine, a modification unique to eIF5A, which will be addressed in detail in the next chapter of this work (Park *et al.*, 1981; Gutierrez *et al.*, 2013). Early fractionation experiments and the use of an assay for Met-puromycin bond formation, suggested that eIF5A promotes translational initiation, which also explains its naming as an initiation factor (Kemper *et al.*, 1976; Schreier *et al.*, 1977; Benne *et al.*, 1978). Meanwhile, it is well understood that the Met-puromycin bond formation assay reports mainly on the rate of peptide bond formation, and the

effect on initiation is more of a feedback due to puromycin being suboptimal positioned in the PTC and therefore a poor substrate for the formation of peptide bonds (Dever *et al.*, 2018). This would suggest that eIF5A is more likely to support peptide bond formation, which fits well with recent studies showing that eIF5A supports the elongation step and rather mimics the action of cycloheximide (an inhibitor that blocks elongation by interfering with translocation) (Gregio *et al.*, 2009; Saini *et al.*, 2009; Henderson and Hershey, 2011; Gutierrez *et al.*, 2013; Dever *et al.*, 2018).

Nevertheless, a study by Manjunath and colleagues, for example, showed that eIF5A can have an indirect effect on translation initiation (Manjunath *et al.*, 2019). In this study, the absence of eIF5A leads to ribosome pausing, resulting in feedback to the translation initiation at an upstream start codon in the 5'-UTR leading to the production of an N-terminal extended form of Myc (Manjunath *et al.*, 2019). Similarly, eIF5A was found to be a sensor of polyamine levels by causing ribosome queuing in front of a Pro-Pro-Trp motif of scanning ribosomes, resulting in initiation at a near-cognate upstream start codon (AUU), which then leads to termination at an early stop codon (Ivanov *et al.*, 2018) (Figure 6B). Higher levels of polyamines, and therefore higher levels of hypusinated eIF5A instead lead to skipping of the weaker upstream start codon and initiation at the canonical AUG start codon and production of *AZIN1* (a negative regulator of cellular polyamine synthesis, by a mechanism described above) (Ivanov *et al.*, 2018) (Figure 6A).

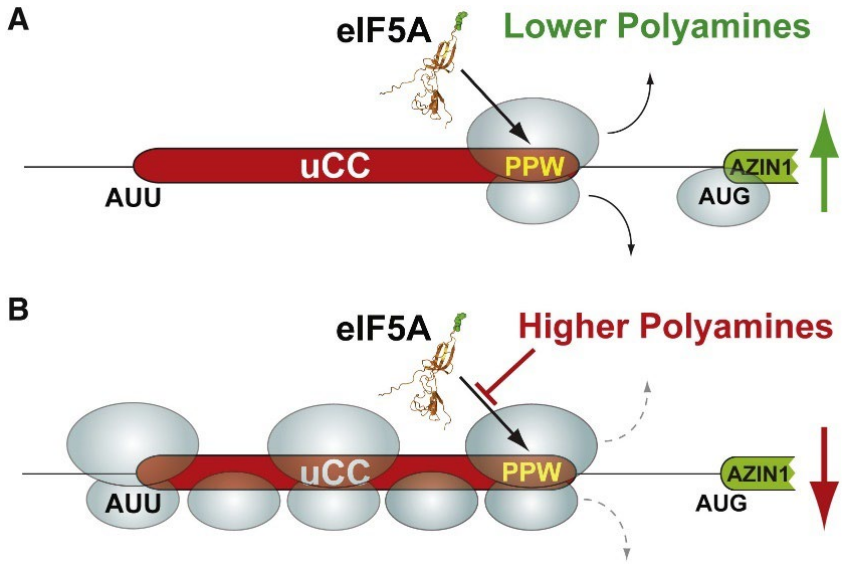

Figure 6. Model illustrating the polyamine-induced interference with eIF5A function, leading to ribosome queuing and increased initiation at an upstream AUU Start Codon on the *AZIN1* mRNA.

Reprinted from Molecular Cell, Volume 70, Issue 2, Pages 254-264.e6, Ivanov, IP., Shin, B., Loughran, G., Tzani, I., Young-Braid, S., Cao, C., Atkins, JF., Dever, TE., Polyamine Control of Translation Elongation Regulates Start Site Selection on Antizyme Inhibitor mRNA via Ribosome Queuing, 2018, with permission from Elsevier

Much of the early work was done on *elongation factor P* (*EF-P*), the bacterial ortholog of *eIF5A*, which has also been shown to be essential for resolving ribosome stalling on proline stretches in bacteria (Doerfel *et al.*, 2013; Ude *et al.*, 2013; Woolstenhulme *et al.*, 2015). And it has also been shown in yeast that eIF5A is required for the synthesis of the proline-rich protein *Bni1* (Li *et al.*, 2014*b*). Studies in human cell models revealed clear requirements of eIF5A for the translation of specific motifs within proteins, such as a specific motif in the *autophagy related 3 protein* (*ATG3*) (Lubas *et al.*, 2018). However, looking at global changes in the proteome of human HeLa cells after *eIF5A* knockdown could not identify an depletion in polyproline-rich proteins (Mandal *et al.*, 2016), indicating a broader significance of eIF5A in mammalian cells.

Structures of eIF5A bound to the ribosome highlighted the binding of eIF5A in the E site and revealed that simultaneous binding of eIF5A and a tRNA in the E site is sterically not possible, meaning that the tRNA release must precede eIF5A binding (Melnikov *et al.*, 2016; Schmidt *et al.*, 2016). A structural study that captured an eIF5A-80S complex with a tRNA in the P site, revealed further interactions between the hypusine residue of eIF5A and the acceptor (CCA-end) arm of the peptidyl-tRNA (Schmidt *et al.*, 2016) (Figure 7). This suggests that eIF5A promotes peptide-bond formation by stabilizing the conformation of peptidyl-tRNA for nucleophilic attack by the aminoacyl-tRNA in the A site (Schmidt *et al.*, 2016). Another structural study that employed X-ray and cryo-EM found a contribution of eIF5A in resolving stalled ribosomes (Pochopien *et al.*, 2021). The mechanistic role of eIF5A was found to be placed in the E site of the ribosome, helping with the positioning of the P-tRNA and assisting with the transfer of the nascent peptide chain from the P-tRNA to the A-tRNA (Pochopien *et al.*, 2021).

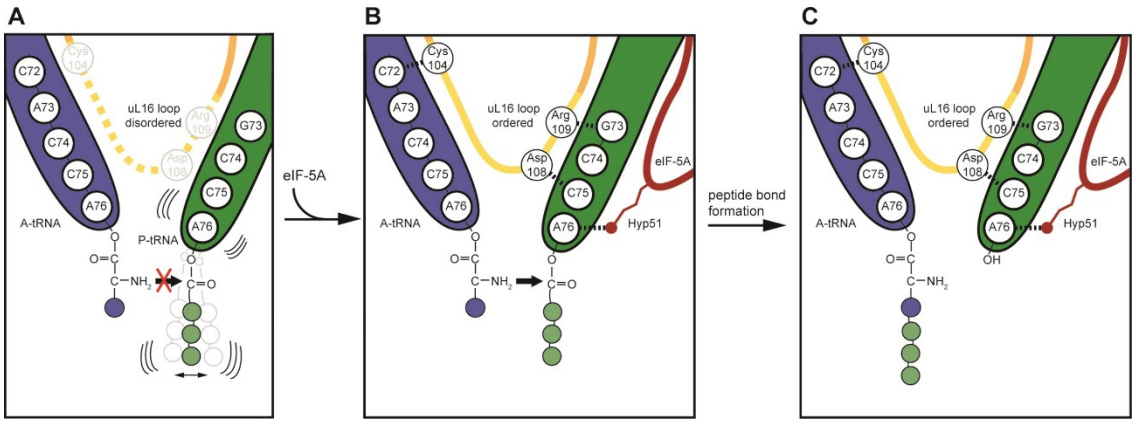

Figure 7. Model of the interaction of eIF5A with the ribosome.

Reprinted from Nucleic Acid Research, Vol. 44, No. 4, 1944-1951, Schmidt, C., Becker, T., Heuer, A., Braunger, K., Shanmuganathan, V., Pech, M., Berninghausen, O., Wilson, D., Beckmann, R., Structure of the hypusinylated eukaryotic translation factor eIF-5A bound to the ribosome, 2016, with permission from Oxford University Press

As described above, due to reduced nucleophilicity, proline is a poor A site peptidyl acceptor (Wohlgemuth *et al.*, 2008; Pavlov *et al.*, 2009) and eIF5A helps among others prolines during the catalysis of the peptide bond formation (Gutierrez *et al.*, 2013). By using misacylated Pro-tRNA^{Phe} and Phe-tRNA^{Pro} Shin and colleagues were able to show that the requirement for eIF5A stems from the structural rigidity of the imino acid proline and not from the tRNA^{Pro} (Shin *et al.*, 2017). In this context, the role of hypusinated eIF5A seems to be to functionally substitute polyamines, which is also the precursor from which hypusine is directly derived (Shin *et al.*, 2017).

With about three copies of eIF5A per ribosome in HeLa cells (Hershey, 1994), and with being one of the 20 most abundant proteins in proliferating cells (Hukelmann *et al.*, 2016) as well as its very high abundance in yeast (Kulak *et al.*, 2014), *eIF5A* is one of the most highly expressed genes in eukaryotic cells. It is also an essential protein in yeast (Schnier *et al.*, 1991) and its absence in human cancer cell lines has potent antiproliferative effects (DepMap, 2022). This enormous abundance of eIF5A indicates a broader significance within the cell (Gutierrez *et al.*, 2013). Considering that a *Saccharomyces cerevisiae* cell consists of >273,000 eIF5A molecules, compared to 630,000 eEF1A molecules and 181,000 eEF2 molecules as well as 187,000 ribosomes (Kulak *et al.*, 2014; Schuller and Green, 2018) and considering the high affinity of eIF5A for ribosomes, the numbers suggest a situation in the cell where eIF5A contributes to most peptidyl transfer events during translation (Schuller and Green, 2018). This would mean that eIF5A should be viewed as a core translation factor, acting during the formation of each peptide bond where it increases the processivity and efficiency of translational elongation (Schuller and Green, 2018).

And indeed, studies performed with ribosome profiling (Schuller *et al.*, 2017) and 5PSeq (Pelechano and Alepuz, 2017) show significant pausing across a wide spectrum of amino acid motifs, including those containing proline, aspartic acid, glycine, alanine, valine, and isoleucine. In addition, studies performed by Schuller and colleagues using an *in vitro* reconstituted translation system showed that eIF5A is critical in stimulating peptide-bond formation of seven out of eight combinations tested in the study; all except Phe-Phe (Schuller *et al.*, 2017). As mentioned above, simultaneous binding of eIF5A and a tRNA in the E site is sterically not possible (Melnikov *et al.*, 2016; Schmidt *et al.*, 2016) (Figure 7). However, in the case of slow peptide-bond formation (e.g. for Pro-Pro), the aminoacyl-tRNA remains unreacted longer than usual, while the tRNA, which is in the E site at that moment, still dissociates and makes room for binding and action of eIF5A (Schuller and Green, 2018).

Lastly, it has been shown that eIF5A also promotes eukaryotic translation termination factor 1 and 3 (eRF1 and eRF3)-dependent translational termination in an *in vitro* peptide release assay (Saini *et al.*, 2009; Schuller *et al.*, 2017). Additionally, cells lacking *eIF5A* showed increased accumulation of

ribosomes at stop codons as determined by ribosome profiling (Schuller *et al.*, 2017). Interestingly, eIF5A was also found to be involved in ribosome-associated quality control (RQC), by assisting in the peptidyl transfer reactions occurring during carboxy-terminal tails (CAT) tailing (Tesina *et al.*, 2023). These CAT tails serve as substrates for the ubiquitination via Ltn1/Listerin and subsequent proteasomal degradation of these nascent peptides (Tesina *et al.*, 2023). This is especially interesting in the light that absence or mutations in *eIF5A* or other genes of the hypusine pathway lead to neurodevelopmental disorders as described below (Ganapathi *et al.*, 2019; Faundes *et al.*, 2021; Ziegler *et al.*, 2022), a phenotype also observed when known RQC factors like *Ltn1/Listerin* or *Rqc2/NEMF* are mutated or dysfunctional (Chu *et al.*, 2009; Martin *et al.*, 2020; Udagawa *et al.*, 2021; Tesina *et al.*, 2023). The involvement of eIF5A in RQC could also explain the findings of a recent preprint, where eIF5A was found sequestered in the polysomes caused by ribosomal collision on mutant HTT mRNA causative for Huntington's disease (Aviner *et al.*, 2022).

1.3 The Hypusine Pathway

The name hypusine is constructed by the combination of the names of its two structural components hydroxyputrescine and lysine (Shiba *et al.*, 1971). It was first discovered and isolated from the bovine brain and structurally characterized with nuclear magnetic resonance (NMR), mass spectrometry, and biochemical assays; due to its properties, it was at the time categorized accidentally as amino acid (Shiba *et al.*, 1971). Shortly after its initial discovery, hypusine was then found to be present in all animal tissues as a protein component but also as free acid (Nakajima *et al.*, 1971; Imaoka and Nakajima, 1973). Finally, the radioactivity detected in hypusine fractions isolated from rats injected with radiolabeled lysine led to the assumption that hypusine derives from lysine (Imaoka and Nakajima, 1973).

Hypusine then stayed unstudied for a decade until only a single modified protein was identified during a search for proteins integrating radioactive polyamines (Park *et al.*, 1981). This protein was eIF5A and the radioactive part of it turned out to be hypusine, now proving that spermidine is the precursor of hypusine and that hypusine is not a free amino acid (Park *et al.*, 1981). The free hypusine in the soluble part of animal tissues that was discovered in earlier studies therefore must have stemmed from breakdown products of hypusinated eIF5A. Soon the hypusine modification on eIF5A was confirmed by a variety of other studies (Folk *et al.*, 1980; Park *et al.*, 1981, 1982; Cooper *et al.*, 1983), it became clear that the hypusine modification is not reversible (Duncan and Hershey, 1986; Gordon *et al.*, 1987; Dever *et al.*, 2014) and that hypusine represents the most specific post-translational modification known to date (Wolff *et al.*, 2007). Hypusine appears soon after production of eIF5A as the posttranslational reaction catalyzed by deoxyhypusine synthase (DHPS) and deoxyhypusine hydroxylase (DOHH), two enzymes that are described in detail below (Murphey and Gerner, 1987; Park, 1987, 2006). Hypusine is also essential for the activity of eIF5A and its role in cell proliferation (Park *et al.*, 1991, 1993; Pällmann *et al.*, 2015; Park and Wolff, 2018). Recently, a study showed that also free hypusine applied to cells can exhibit biological activity (Tamborlin *et al.*, 2023).

Lastly, hypusinated eIF5A has also been suggested as a shuttle for transcripts involved in the replication of retroviruses (Hauber *et al.*, 2005) and *inducible nitric oxide synthase*, which is critically related to islet ß-cell dysfunction (Maier *et al.*, 2010).

1.3.1 eIF5A

eIF5A is a 154 amino acid large, ~17 kDa heavy protein that was previously also called eIF4D or IF-M2Bα (Kemper *et al.*, 1976; Smit-McBride *et al.*, 1989; Tong *et al.*, 2009) and as mentioned before is one of the 20 most abundant protein in proliferating cells, presenting for example around one

percent of the whole cellular protein pool of cytotoxic T lymphocytes (Hukelmann *et al.*, 2016). It is an essential gene and the knock-out of *eIF5A* is embryonically lethal in mice (Nishimura *et al.*, 2012). It is the only known protein that undergoes the posttranslational modification hypusination, a modification that is described in detail above, which largely influences the activity of eIF5A (Park *et al.*, 1981; Gutierrez *et al.*, 2013). The X-ray structure of eIF5A revealed that it consists of two domains: a basic N-terminal domain and an acidic C-terminal domain containing an oligonucleotide-binding fold (Tong *et al.*, 2009) (Figure 8). The hypusine modification is integrated on lysine 50 (K50) which sits on the tip of an exposed loop on the N-terminal domain and is strictly conserved in eukaryotes (Wolff *et al.*, 2007). Attempts to create a homozygous K50R mutant for the canonical isoform of *eIF5A* (*eIF5A-1*) proved to be embryonically lethal in mice (Schultz *et al.*, 2023).

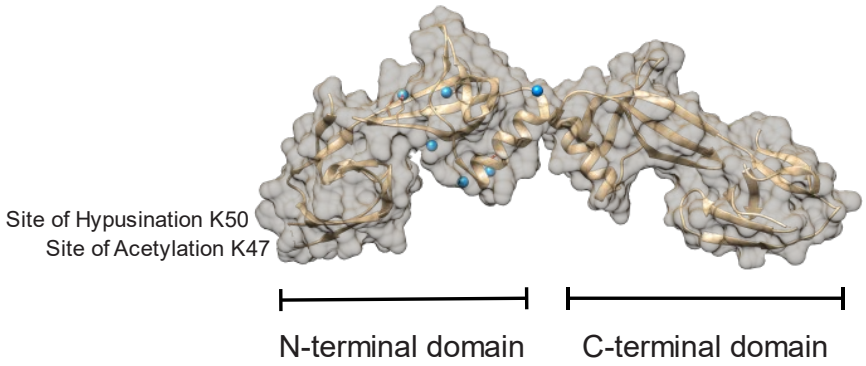

Figure 8. Crystal structure of the truncated human eIF5A.

Adapted from PDB: 3CPF, Proteins, 75(4):1040-5, Tong, Y., Park, I., Hong, B-S., Nedyalkova, L., Tempel, W., Park, H-W., Crystal structure of human eIF5A1: insight into functional similarity of human eIF5A1 and eIF5A2, 2009, with permission form John Wiley and Sons; created with UCSF Chimera, J Comput Chem, 25(13):1605-12, Petterson, EF., Goddard, TD., Huang, CC., Couch, GS., Greenblatt, DM., Meng, EC., Ferrin, TE., UCSF Chimera--a visualization system for exploratory research and analysis, 2004

eIF5A is important for translation (Cooper *et al.*, 1983) and contrary to its annotation as an initiation factor, it plays an important role during elongation and peptide bond formation (Saini *et al.*, 2009; Lassak *et al.*, 2016) but also has a described role during termination (Pelechano and Alepuz, 2017). It is an important factor in the synthesis of proline repeat-rich proteins (Mandal *et al.*, 2014) where it helps to overcome ribosome stalling at proline-rich regions (Gutierrez *et al.*, 2013; Pelechano and Alepuz, 2017). Interestingly, a recent study revealed that eIF5A is also among four factors that bind to functionally relevant sites in dormant ribosomes isolated from zebrafish and *Xenopus* eggs and embryos (Leesch *et al.*, 2023). These factors help to stabilize ribosomes, repress translation, and allow the cells to turn on translation during the correct developmental program (Leesch *et al.*, 2023).

Since eIF5A is among the top conserved proteins between the two kingdoms of eukaryotes and archaebacteria it is no surprise that many structural and functional analogies exist between different eIF5A homologs (Gordon *et al.*, 1987; Bartig *et al.*, 1992; Kyrpides and Woese, 1998). eIF5A has a structural and functional analogy with the homolog archaeal translation initiation factor 5A (aIF5a) and both share the conserved lysine residue that is the target of hypusination (Bartig *et al.*, 1992). The bacterial ortholog EF-P also shares many similarities with eIF5A but carries a ß-lysine modification catalyzed by elongation factor P--(R)-beta-lysine ligase (YjeA) and elongation factor P hydroxylase (YfcM) instead of hypusine, at the same lysine residue that is otherwise hypusinated (Navarre *et al.*, 2010; Yanagisawa *et al.*, 2010). However, similar to hypusine, the ß-lysylation only occurs on EF-P and is also crucial for the activity of EF-P, which also has an important role in overcoming ribosome stalling at polyproline stretches (Park *et al.*, 2012; Bullwinkle *et al.*, 2013; Doerfel *et al.*, 2013; Ude *et al.*, 2013).

In humans two isoforms of *eIF5A* (*eIF5A-1* and *eIF5A-2*) are known, both are hypusinated and while *eIF5A-1* is constitutively expressed in mammalian cells and overexpressed in cancer, the *eIF5A-2* isoform is expressed only in testis, the brain and certain cancer types (Clement *et al.*, 2003; Caraglia *et al.*, 2013; Mathews and Hershey, 2015).

Another *eIF5A* isoform has been described by Pereira and colleagues and derives from the extension of *eIF5A-1* by an upstream start codon in its 5'-UTR that is less favorably picked as the start site by the ribosome (Pereira *et al.*, 2016). It produces an eIF5A protein with additional 30 amino acids on the N-terminal peptide sequence and can undergo hypusination as well (Pereira *et al.*, 2016). Its potential link to mitochondria is addressed below.

There are multiple indications for the involvement of *eIF5A* in a variety of diseases, that will be discussed in a later chapter of this thesis (Kaiser, 2012). Interestingly, hypusinated eIF5A has also DNA and RNA binding properties whose sequence-specific binding was shown by using systematic evolution of ligands by exponential enrichment (SELEX) and affinity co-purification and PCR differential display (Xu and Chen, 2001; Xu *et al.*, 2004).

Besides hypusination, eIF5A can also be phosphorylated and acetylated (Kang *et al.*, 1993; Klier *et al.*, 1993; Ishfaq *et al.*, 2012). The significance of the phosphorylation, that happens on serine 102 is however currently not understood (Kang *et al.*, 1993; Klier *et al.*, 1993).

Acetylation of eIF5A

Considering the irreversibility of the hypusine modification combined with the high abundance and very long half-life of eIF5A, which is reported to be 3-7 days, other reversible modifications might

offer a solution for a more rapid way of regulating eIF5A activity, without the necessity to change the actual protein level (Torrelio *et al.*, 1987; Nishimura *et al.*, 2005). eIF5A has been reported to be acetylated on the lysine residues K47 and K68 (Klier *et al.*, 1995, Kim *et al.*, 2006*a*). Furthermore, Lee *et al*. showed experimentally, that exogenously expressed eIF5A gets strongly acetylated at K47 and they also showed that K47 is in general the main side of acetylation (Lee *et al.*, 2009). An antibody specific for K47-acetylated-eIF5A ($_{eIF5A^{AcK47}}$) allowed to identify P300/CBP-associated factor (PCAF) as a main acetylase of eIF5A (Ishfaq *et al.*, 2012). The same team also found the deacetylases for K47 acetylation of eIF5A which are the histone deacetylase 6 (HDAC6) and the NAD^+-dependent deacetylase sirtuin-2 (SIRT2) (Ishfaq *et al.*, 2012). However, as discussed below, additional transferases and hydrolases might be involved in the turnover of acetylated eIF5A, too.

In addition to eIF5A itself, the protein-bound hypusine residue seems to be also targetable by acetylation by the polyamine catabolic enzyme spermidine/spermine-*N1*-acetyltransferase 1 (SSAT1) (Lee *et al.*, 2011). SSAT1 targets the terminal amino group of hypusine or deoxyhypusine (Lee *et al.*, 2011). As free hypusine or deoxyhypusine alone could not act as a substrate for SSAT1 in *in vitro* assays, at least partial interaction of eIF5A with SSAT1 seems to be required (Lee *et al.*, 2011). Acetylated eIF5A further eliminates the activity of eIF5A in methionyl-puromycin assay, indicating that acetylation on eIF5A has a deactivating function for its role as elongation factor (Lee *et al.*, 2011). Causative for this could be the change in charge induced by the acetylation. The strong basic charge of hypusine gets reduced by acetylation, which could perturb the binding of eIF5A in the acidic pocket of binding partners such as the ribosome (Lee *et al.*, 2011). Since SSAT1 expression levels are low and eIF5A is a very abundant protein, it remains to be investigated how relevant this regulation is in live cells (Lee *et al.*, 2011).

While the specific role of the acetylated form of eIF5A is still largely unknown, it is interesting to note that the acetylated form of eIF5A is found mainly in the nucleus, while the unacetylated form is primarily found in the cytoplasm (Ishfaq *et al.*, 2012). Although the nuclear role of eIF5A remains to be investigated, a recent study demonstrated one case where eIF5A acts as an important translatome remodeler in cells under acidosis, with the acetylation on eIF5A acting as an activating switch (Balukoff *et al.*, 2020). The team of Balukoff *et al*. demonstrated in their model that the NAD^+-dependent deacetylase sirtuin-1 (Sirt1) senses pH and deacetylates nuclear eIF5A during anaerobiosis. eIF5A then serves as a shuttle for *tuberous sclerosis complex 2* (*Tsc2*) mRNA out of the nucleus facilitating its translation (Balukoff *et al.*, 2020). Since Tsc2 acts as an inhibitor for the mammalian target of rapamycin complex 1 (mTORC1), cellular metabolism is downregulated, preventing DNA damage that would otherwise be caused by acidosis (Balukoff *et al.*, 2020).

1.3.2 Enzymes of the Hypusine Pathway: DHPS

The first step in the synthesis of hypusine is the formation of deoxyhypusine. This enzymatic reaction happens through deoxyhypusine synthase (DHPS), which cleaves spermidine and transfers a 4-aminobutyl moiety to the ε-amino group of the lysine 50, forming deoxyhypusine (N^{ε}-4-aminobutyl(lysine)) on eIF5A (eIF5A(Dhp)) (Wolff *et al.*, 1995, 1997; Lee *et al.*, 1999; Wątor *et al.*, 2020). The DHPS reaction uses NAD^+ as a coenzyme and encompasses four reaction steps, with two imine intermediates and a transient hybrid (Chen and Dou, 1988; Wolff *et al.*, 1990, 1997, 2000) (Figure 9).

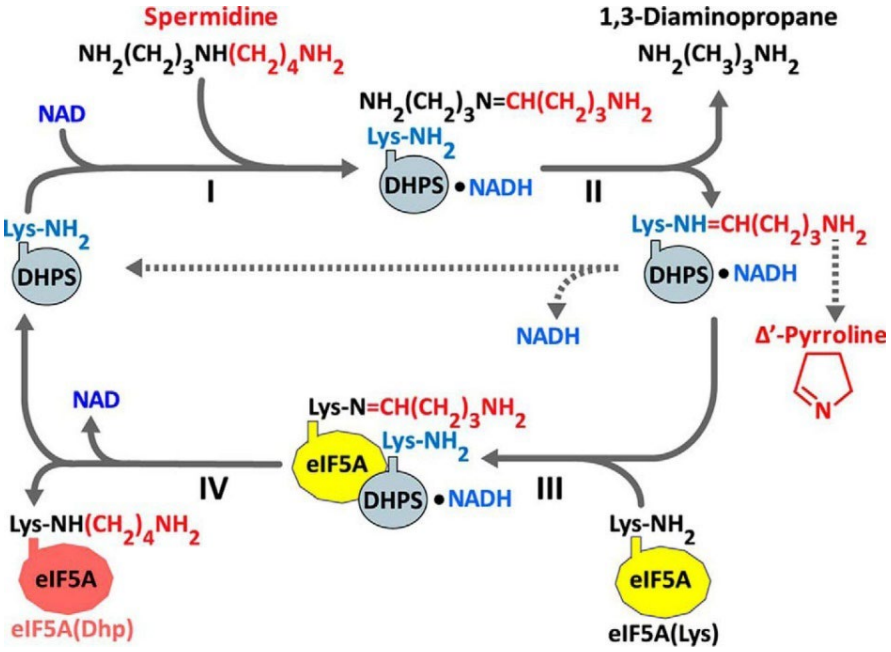

Figure 9. Reaction mechanism of hypusine reaction.

Reprinted from Journal of Biological Chemistry, Volume 293, Issue 48, Pages 18710-18718, Park, MH., Wolff, EC., Hypusine, a polyamine-derived amino acid critical for eukaryotic translation, 2018, article from Elsevier under open access Creative Commons CC-BY license.

Not only is the lysine 50 highly specific for this posttranslational modification but also the motif flanking the hypusine modification site is conserved across all aIF5A and eIF5A proteins (Park *et al.*, 1991; Cano *et al.*, 2008). The highly conserved motif KxG-K(Hyp)-HGxAK is located at the tip of a loop linking two strands (β3 and β4) of the N-terminal domain and substitutions in the sequence abolish deoxyhypusination (Cano *et al.*, 2008). The minimal substrate of eIF5A that is required for the deoxyhypusination reaction by DHPS was assessed *in vitro* with purified DHPS and encompasses Phe30-Asp80 of eIF5A, a highly conserved region on this protein throughout the eukaryotic kingdom (Joe and Park, 1994).

Structures of enzymes, especially when they are solved in complex with their co-factors or substrates are crucial to understand the mode of action of the catalytic reaction. Thanks to an early X-ray structure of human DHPS bound with its co-factor NAD^+ it became clear that DHPS forms a tetramer, consisting of four identical subunits (Liao *et al.*, 1998). The tetramer consists of two dimers with a total of four active sites, two per dimer interface; one subunit of each active site harbors the catalytic site, and the other matching subunit contains the NAD^+-binding portion (Liao *et al.*, 1998).

The first structure of DHPS looked like a so-called "ball-and-chain" mechanism consisting of two-turn α helices, that block access to the active site of DHPS (Liao *et al.*, 1998). Later, the same lab managed to crystalize the human DHPS:NAD holoenzyme also under low ionic strength and a pH of 8.0, which is close to the optimal pH for the enzymatic reaction, and now could not detect the "ball-and-chain" mechanism anymore suggesting that this part of the protein swings freely and doesn't block the active site (Umland *et al.*, 2004). Meanwhile, yet more structural work revealed that the "ball-and-chain" motif is crucial for the assembly of the DHPS tetramer (Wątor *et al.*, 2020). A recent structure of the substrate-bound complex captured during the hypusination reaction shows that DHPS binds only the N-terminus of eIF5A containing the ß-sheet structure and gives insights into interactions and residues that are key for the catalytic reaction (Wątor *et al.*, 2023) (Figure 10a-b). The first step of the enzymatic reaction is coupled to the reduction of NAD^+ to NADH during which spermidine is oxidized and cleaved into 1,3-diaminopropane and a 4-aminobutyl moiety, which forms then an imine bound to Nε of $K329^{DHPS}$ (Figure 10c-d). During this reaction, $W327^{DHPS}$ is an important gating residue for $K50^{eIF5A}$ and positions it for hypusination (Wątor *et al.*, 2023) (Figure 10c-d). Additionally, it may also shift the $K329^{DHPS}$ in a way optimal to transfer the 4-aminobutyl group to then form an imine intermediate with $K50^{eIF5A}$ (Wątor *et al.*, 2023). This, in turn, makes the imine bound accessible to the hydride ion transfer from NADH and therewith the formation of deoxyhypusine (Wątor *et al.*, 2023).

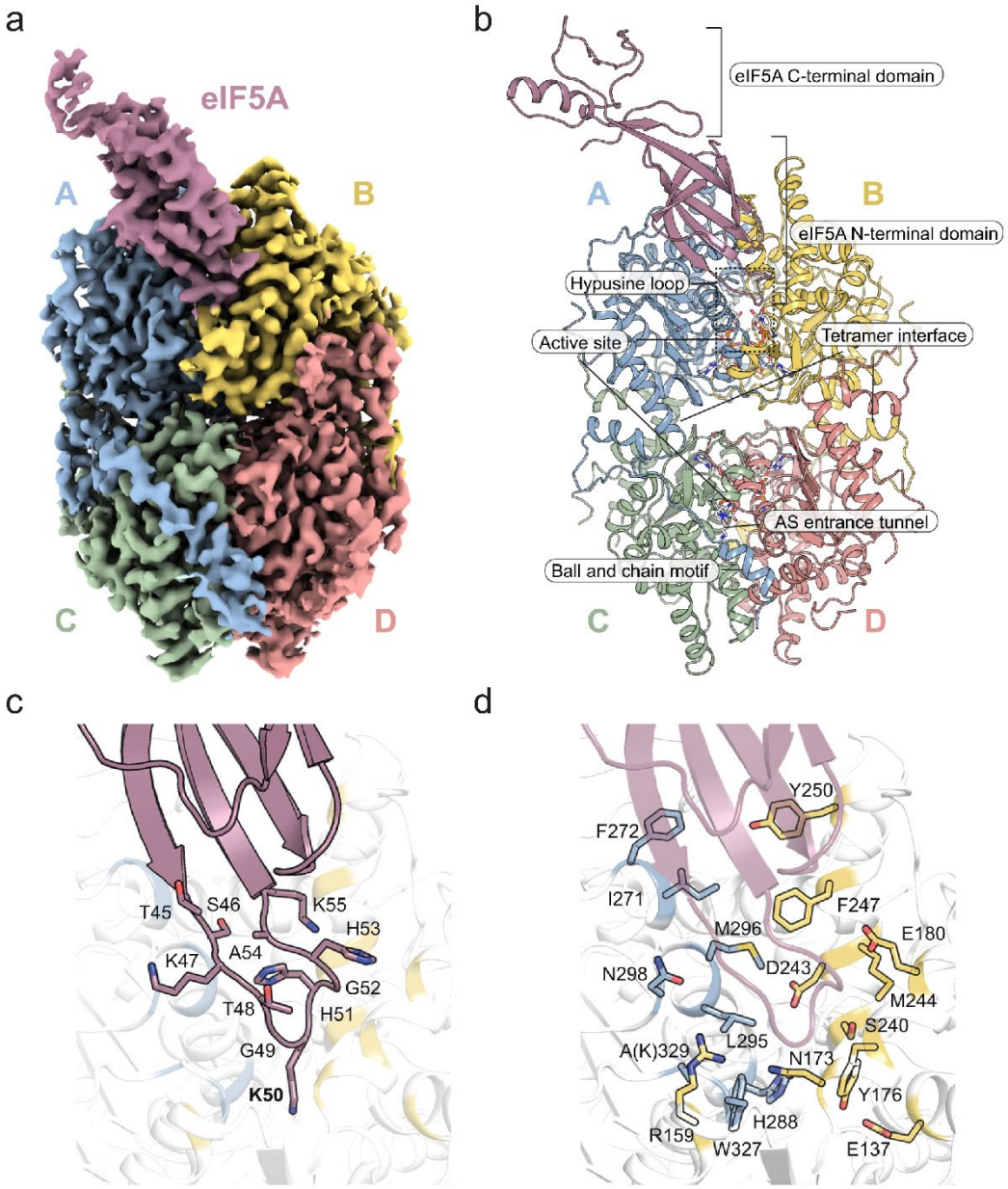

Figure 10. The eIF5A-DHPS complex.

Reprinted from Nature Communications, 14, Article number 1698, Wator, E., Wilk, P., Biela, A., Rawski, M., Zak, KM., Steinchen, W., Bange, G., Glatt, S., Grudnik. P., Cryo-EM structure of human eIF5A-DHS complex reveals the molecular basis of hypusination-associated neurodegenerative disorders, 2023, article from Springer Nature under open access Creative Commons CC-BY license

1.3.3 Enzymes of the Hypusine Pathway: DOHH

The second and final catalytic step of hypusine formation involves the hydroxylation of deoxyhypusine to hypusine (N^{ε}-4-amino-(2-hydroxybutyl)lysine) by deoxyhypusine hydroxylase (DOHH) (Kim *et al.*, 2006*b*). DOHH was first identified in a yeast two-hybrid screen as an interaction partner of eIF5A with unknown function and therefore named Lia1 (ligand of eIF5A) (Thompson *et al.*, 2003*b*). In 2006 the enzyme was then cloned and expressed which allowed studying *DOHH* in detail and assigning it the first time a function (Park *et al.*, 2006). DOHH has a symmetrical superhelical structure with eight helical hairpins (also named HEAT repeats) (Park *et al.*, 2006). HEAT repeat-containing proteins got their name for their occurrence in human huntingtin (H), elongation factor 3 (E), a subunit of protein phosphatase 2a (A) and the target of rapamycin (TOR) (Andrade *et al.*, 2001). Each particle of DOHH contains two molecules of iron that are coordinated by four essential His-Glu pairs, forming part of the diiron active site (Kim *et al.*, 2006*b*; Kang *et al.*, 2007). The reaction of the reduced form of DOHH with oxygen forms a peroxo-diiron(III) intermediate in the diiron center of DOHH (Han *et al.*, 2015). Similar to DHPS, also DOHH interacts and recognizes the N-terminus of eIF5A, however preferentially the deoxyhypusinated form (Wolff *et al.*, 2007). Although truncation of eIF5A leads to reduced hypusination of the protein, amino acid 20-90 are in principle sufficient for binding and hydroxylation of eI5A (Wolff *et al.*, 2007), a finding that is also in agreement with the docking of eIF5A(Dhp) onto a DOHH structure derived by X-ray crystallography (Han *et al.*, 2015). Interestingly, DOHH is only essential in higher eukaryotes such as *Caenorhabditis elegans*, *Drosophila*, and mammals (Sugimoto, 2004; Patel *et al.*, 2009; Sievert *et al.*, 2014) but not in yeast (Park *et al.*, 2006).

1.3.4 Subcellular Localization of eIF5A and Nuclear Translocation by Xpo4

Fully hypusinated eIF5A is a cytoplasmic protein (Lee *et al.*, 2009). However, eIF5A can also be found in the nucleus of the cell (Lipowsky *et al.*, 2000). Although the nuclear pore complex (NPC) permeability barrier prevents the mixing of cytoplasmic and nuclear matter it is only tight for molecules larger than ~5 nm in diameter or ~30 kDa in mass (Schmidt and Görlich, 2016). The small size of eIF5A of just 17 kDa suggests that it can enter the nucleus effortlessly solely by passive diffusion, which was experimentally demonstrated by an experiment proving eIF5As insensitivity to reagents blocking facilitated NPC passage (Lipowsky *et al.*, 2000). Nevertheless, there is also a study that proposes that the N-terminus of eIF5A signals additionally for nuclear localization (Parreiras-E-Silva *et al.*, 2007; Lee *et al.*, 2009). Despite this large tendency of eIF5A to enter the nucleus, the by-far largest fraction of eIF5A is, as mentioned above, in the cytoplasm. This suggests that there must be a cellular active nuclear export system for eIF5A in place.

So-called nuclear transport receptors (NTRs) can carry a load through the permeability barrier of nuclear pore complexes (NPCs) using the RanGTPase system as a source of energy for this active transport (Lipowsky *et al.*, 2000). The best characterized NTR is Xpo1/CRM1/Exportin 1, a protein that can be inhibited specifically thanks to the availability of inhibitors such as leptomycin B; it detects the 9-15 amino acids long linear nuclear export signal (NES) sequence and exports proteins (Dong *et al.*, 2009; Monecke *et al.*, 2009). Adding such NES sequences to artificially expressed proteins can be exploited to force their localization to the cytoplasm (Zetsche *et al.*, 2015; Koraïchi *et al.*, 2018). But export signals can also be more complex and interact with the NTRs in a three-dimensional interface, in which case the NTRs often have additionally some kind of chaperone function (Kutay *et al.*, 1997). This is for example the case for Xpo2/CAS/Cse1, which detects a special conformation of importin α (Kutay *et al.*, 1997), but also for the export of eIF5A by the exportin Xpo4 (Aksu *et al.*, 2016).

Xpo4 is a member of the importin ß family, built of HEAT repeats in the shape of an α-helical protein (Aksu *et al.*, 2016) (Figure 12). Intra-repeat loops on the HEAT repeats 8-16 on Xpo4 form a binding pocket that allows both domains (the N-terminal SH3-like domain and the C-terminal oligonucleotide-binding (OB)-fold domain) of eIF5A to interact with it (Aksu *et al.*, 2016) (Figure 12). In total, the interaction surface entails 2169 A^2 and shields most of the highly conserved positively charged residues of eIF5A that are responsible for eIF5As 25S RNA – and tRNA-binding properties (Melnikov *et al.*, 2016; Schmidt *et al.*, 2016). Interestingly, Xpo4 also contacts hypusine (Hpu50) with its two positive charges and its neighboring histidine (H51), by docking it in a deep, acidic pocket of Xpo4, which makes hypusine part of the eIF5A export signature (Aksu *et al.*, 2016) (Figure 11). While Xpo4 seems to still be capable of exporting unmodified eIF5A, although it binds ~35 times more weakly (Lipowsky *et al.*, 2000), the nuclear accumulation of acetylated eIF5A suggests that the acetylated form is not or only very inefficiently exported (Ishfaq *et al.*, 2012).

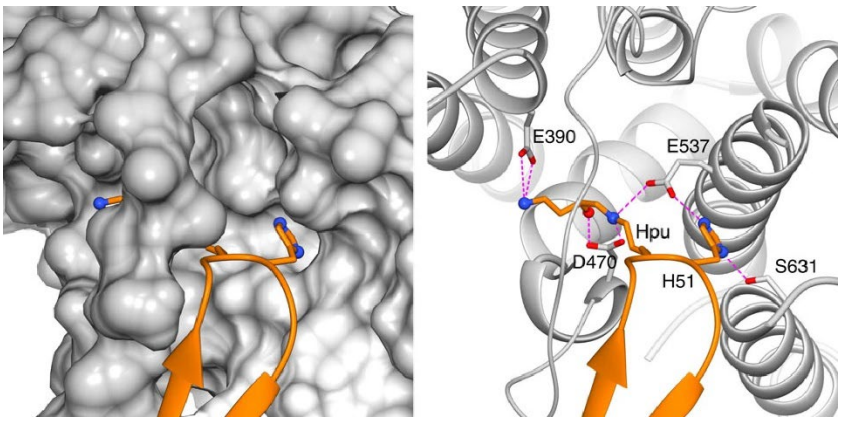

Figure 11. Docking of hypusinated loop of eIF5A into the acidic pocket of Xpo4.

Reprinted from Nature Communications, 7, Article number 11952, Aksu, M., Trakhanov, S., Görlich, D., Structure of the exportin Xpo4 in complex with RanGTP and the hypusine-containing translation factor eIF5A, 2016, article from Springer Nature under open access Creative Commons CC-BY license.

Xpo4 therefore not only acts as an exportin by shuttling mislocalized eIF5A out of the nucleus but also acts as a chaperone-like and compartment-specific antagonist of eIF5A, preventing possible off-target interactions in the nucleus (Aksu *et al.*, 2016). This could be of particular importance since it has been shown that eIF5A accumulates in the nucleoli or interacts with the ribosomal export adapter Nmd3, both of which could have detrimental effects on ribosome assembly or by its interaction with the ribosome export adapter Nmd3, which was recently described (Malyutin *et al.*, 2017). In addition, by the large surface interface, Xpo4 ensures clean extraction of eIF5A out of the nucleus and prevents carrying cargo bound to eIF5A out of the nucleus (Aksu *et al.*, 2016). Despite the very optimal binding of Xpo4 to eIF5A it also serves as a shuttle for other cargos, such as Sox-type transcription factors (Gontan *et al.*, 2009) and many other proteins (Mackmull *et al.*, 2017).

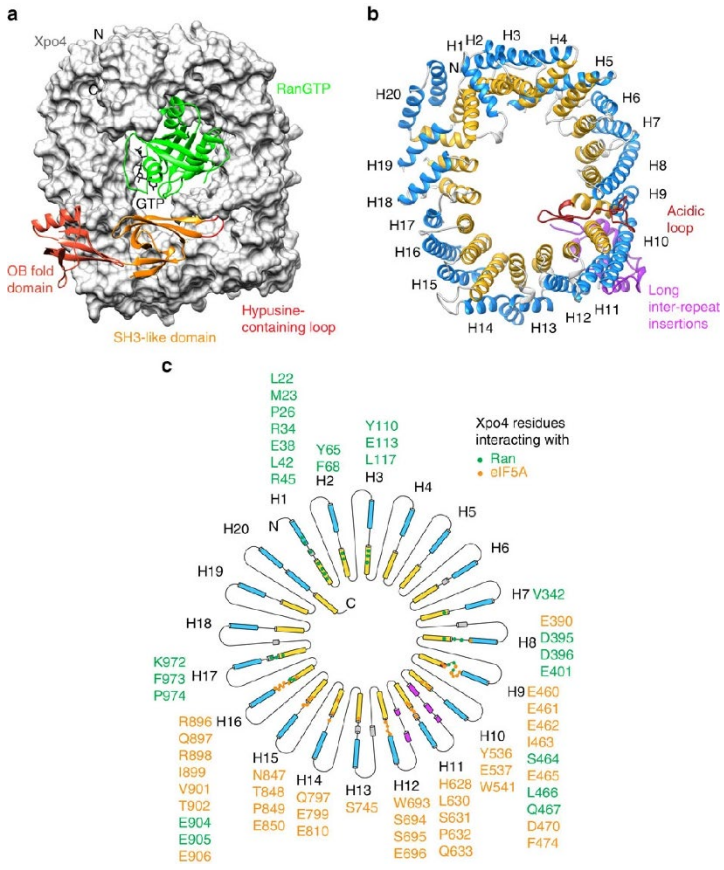

Figure 12. Structure of the RanGTP•Xpo4•eIF5A export complex with HEAT repeat organized Xpo4.

Reprinted from Nature Communications, 7, Article number 11952, Aksu, M., Trakhanov, S., Görlich, D., Structure of the exportin Xpo4 in complex with RanGTP and the hypusine-containing translation factor eIF5A, 2016, article from Springer Nature under open access Creative Commons CC-BY license.

It was also discovered that eIF5A interacts with the insulin-like growth factor 2 mRNA-binding protein (IGF2BP1) in the cytoplasm and that absence of IGF2BP1 leads to the accumulation of eIF5A in the mitochondria, further inducing apoptosis (Miyake *et al.*, 2015). Since IGF2BP1 is exported from the nucleus by Xpo1, inhibition of Xpo1-mediated nuclear export induces mitochondrial accumulation of eIF5A (Miyake *et al.*, 2015).

Additionally, eIF5A has been reported to be able to localize to the endoplasmatic reticulum (ER) membrane where it assists with the co-translational translocation of proteins into the ER (Shi *et al.*, 1996; Rossi *et al.*, 2014).

1.3.5 Metabolic Role of the Hypusine Axis

Besides eIF5A's known role in translational elongation, it has been implicated over the last years in a whole array of diseases and physiological processes such as diabetes, autophagy, tolerance to ischemia, aging, and immune cell differentiation (Tauc *et al.*, 2021).

Diabetes

Diabetes is a metabolic disease that involves the dysregulation of glucose levels related to the malfunction of beta cells in the pancreas (Olokoba *et al.*, 2012). Since pro-inflammatory cytokines from immune cells are known to activate signaling cascades that drive beta cell dysfunction and since inactivation of *eIF5A* reduced the levels of inflammatory cytokines in a mouse sepsis model it was investigated if eIF5A is involved in diabetes progression (Moore *et al.*, 2008). And indeed, when hypusination was blocked with N1-guanyl-1,7-diaminoheptane (GC7) in a mouse model of streptozotocin-induced diabetes, loss of beta cell mass was reduced and mice thereby protected from hyperglycemia (Maier *et al.*, 2010). As a mechanism, the authors of the study could show that eIF5A is required for shuttling *nitric oxide synthase 2* (*NOS2*) mRNA out of the nucleus (Maier *et al.*, 2010). Furthermore, another group showed in a diabetes model of obese mice that GC7 treatment improved glucose tolerance which in addition correlated with the reduced production of C/EBP homologous protein (CHOP), a key part of the ER stress response that can induce apoptosis (Robbins *et al.*, 2010). They found, that despite mRNA levels of *Chop* being elevated 30-fold, the protein levels stayed low, which indicates a block in translation (Robbins *et al.*, 2010). Interestingly, Anderson-Baucum and colleagues saw the hypusinated form of eIF5A increased in adipose tissue resident M1 macrophages, which are known to be involved in the proinflammatory status of these tissues (Anderson-Baucum *et al.*, 2021). They further found that DHPS aids with the production of proteins that activate nuclear factor kappa-light-chain-enhancer of activated B cells (NF-κB) signaling in macrophages and showcased that specific deletion of the *Dhps* gene in macrophages blunted their proinflammatory

characteristics and improved insulin sensitivity as well as glucose homeostasis (Anderson-Baucum *et al.*, 2021). In summary, blocking hypusination has been applied in different models for diabetes, where it improved glucose tolerance and reduced inflammation (Maier *et al.*, 2010; Robbins *et al.*, 2010; Tersey *et al.*, 2014; Levasseur *et al.*, 2019; Cougnon *et al.*, 2021).

Autophagy and Mitophagy

Another recurring link of hypusine is its implication with autophagy, a process known to prevent aging, where hypusinated eIF5A was shown to be required for translation of *ATG3* and *transcription factor EB* (*TFEB*) in separate studies (Lubas *et al.*, 2018; Zhang *et al.*, 2019). Lubas *et al.* found initially that treatment with the hypusine inhibitor GC7 had similar effects as the depletion of the autophagy protein ATG3 (Lubas *et al.*, 2018). They then further showed that depletion of *eIF5A* in cell lines or *Caenorhabditis elegans* reduced autophagy, indicated by a decrease in lipidation of LC3 (Lubas *et al.*, 2018). Interestingly, *Drosophila* that were fed with spermidine, the substrate of hypusination, showed an *ATG3*-dependent increase in autophagy (Liang *et al.*, 2021).

The second autophagy protein linked to hypusine is TFEB; it regulates autophagy by activating the expression of genes with CLEAR (coordinated lysosome and regulation) elements (Zhang *et al.*, 2019). *TFEB* contains a triple proline motif and its translation is modulated by hypusinated eIF5A (Zhang *et al.*, 2019). *TFEB* expression is lowered in immune cells of older adults and spermidine was successfully used to restore B cell response in old mice and humans (Zhang *et al.*, 2019) as well as in T cells from old human donors (Alsaleh *et al.*, 2020) in both cases via eIF5A. Additionally, TFEB and its ortholog transcription factor binding to IGHM Enhancer 3 (TFE3) are important facilitators of mitochondrial quality control, a topic that will be discussed in the next chapter (Wang *et al.*, 2020).

eIF5A Isoforms Correlate with the Cellular Metabolic State

As introduced above, most eukaryotes carry two paralogous genes encoding two *eIF5A* isoforms that in humans are 84% identical (Clement *et al.*, 2006). Despite having significantly different expression patterns in both, humans and yeast, the precise functional roles are still not known (Barba-Aliaga and Alepuz, 2022*a*). However, Barba-Aliaga and Alepuz demonstrated the role of *eIF5A* in respiration in yeast and showed that the expression of the two *eIF5A* isoforms (translation initiation factor 51A (*TIF51A*) and *TIF51B*) correlate with the metabolic and respiratory state of yeast cells (Barba-Aliaga and Alepuz, 2022*b*). In short, when respiration is high, the heme activator protein 1 (Hap1) binds constitutively to the *TIF51A* promoter to stimulate its expression as well as to the promoter of the *TIF51B* repressor genes *ROX1* and *MOT3*; when respiration is low, or in anaerobe conditions, Hap1 recruits the corepressor Tup1 to repress *TIF51A* expression and represses *ROX1* and

MOT3, allowing then for the expression of *TIF51B* (Barba-Aliaga and Alepuz, 2022*b*). In summary, *TIF51A* seems to promote respiration while *TIF51B* promotes anaerobic glycolysis (Barba-Aliaga and Alepuz, 2022*b*). Although so far a homolog for *Hap1* in mammalian systems has not been identified, it is worth noting that the *eIF5A-2* isoform is frequently expressed in cancer cells, which are known to commonly upregulate glycolytic enzymes (Meng *et al.*, 2015; Cao *et al.*, 2017).

1.3.6 eIF5A and Mitochondria

Mitochondria are double layered organelles and the main generators of ATP, the energy currency of the cell that is generated through a process called oxidative phosphorylation (OXPHOS) (Walsh *et al.*, 2018). According to the endosymbiotic theory, mitochondria are derived from the endosymbiosis between a α-proteobacteria and an early ancestor of a eukaryotic cell. This symbiosis allowed the host cells to survive in the arising highly oxidized atmosphere in early Earth development that triggered a selective pressure on organisms with respiratory capacity (Castresana and Saraste, 1995; Lyons *et al.*, 2014). Mitochondria are maintaining their own genome, which is encoded in the so-called mitochondrial DNA (mtDNA) and is expressed by a mitochondria-specific transcription and translation machinery (Kummer and Ban, 2021). The human mtDNA contains 13 protein-coding genes which are all critical components of the OXPHOS machinery (Kummer and Ban, 2021). All other mitochondrial proteins (around 1500 known proteins) are encoded in the nucleus and need to be imported by a sophisticated importing, processing, and assembly machinery (Song *et al.*, 2021). Besides OXPHOS, mitochondria are involved in a multitude of other biochemical functions, have cell- and tissue-specific phenotypes, and undergo constant dynamic physiological recalibrations (Spinelli and Haigis, 2018; Monzel *et al.*, 2023). When electrons escape the electron transport chain, mitochondria generate reactive oxygen species (ROS) (Murphy, 2009). While a certain amount of ROS was shown to be crucial for cell signaling, increased ROS levels can severely damage multiple parts of the cell, including mitochondria (Shadel and Horvath, 2015). Damage to mitochondria can lead to increased electron leakage causing excess ROS generation, uncoupled OXPHOS, and perturbed Ca^{2+} uptake (Liu and O'Rourke, 2008; Mailloux, 2020). To avoid the accumulation of damaged mitochondria, cells and these organelles themselves, employ several pathways that remove damaged mitochondria and keep mitochondrial stress low, such as mitophagy, dynamic fusion and fission processes or the mitochondrial unfolded protein response (Youle and Narendra, 2011; Youle and van der Bliek, 2012; Quirós *et al.*, 2017; Fessler *et al.*, 2020; Guo *et al.*, 2020). Mitochondrial functions decline with age and mitochondrial stress in return can contribute to age-related diseases (Sun *et al.*, 2016; Lima *et al.*, 2022). Hypusinated eIF5A helps keep mitochondrial functionality intact (Barba-Aliaga and Alepuz, 2022*a*). Blocking hypusination therefore should increase the tolerance to

hypoxia by downregulation of oxygen-consuming OXPHOS, which can be indeed observed in the case of ischemia-induced damage, stroke, and malaria (Melis *et al.*, 2017; Kaiser *et al.*, 2020; Bourourou *et al.*, 2021). Even though there are multiple reported links between the hypusine axis as well as the hypusination substrate spermidine and mitochondrial function, looking at the summary of all these reports, the mechanistic interplay of these pathways and metabolites with mitochondria remain unclear (Barba-Aliaga and Alepuz, 2022*a*). The next section of the thesis will therefore collect known and possible links between hypusine and mitochondria.

Blocking Hypusination in Limiting Oxygen Environment

One of the first investigations to establish associations between *eIF5A* and respiration was a study that found that inhibition of hypusination with GC7 in *Drosophila* under hypoxia, was sufficient to mediate tolerance to these hypoxic conditions (Vigne and Frelin, 2008). Meanwhile, similar findings were made in renal cells, where treatment with GC7 again led to tolerance towards anoxia by shifting respiration towards glycolysis by downregulation of respiratory chain complexes and thereby reduced mitochondrial oxygen consumption (Melis *et al.*, 2017). This effect and application of GC7 could further be used to protect kidneys from ischemia-induced damage in rat and preclinical pig kidney transplant models, indicating that the hypusine pathway could offer an innovative target for preventing hypoxic-ischemia induced damage (Melis *et al.*, 2017). The administration of GC7 was also beneficial when given prior to the transplantation of kidneys derived from preclinical porcine brain death donation models and led to reduced ROS markers and increased expression of mitochondrial protective peroxisome proliferator-activated receptor-gamma coactivator-1-alpha (*PGC-1α*) as well as of the antioxidant proteins: *superoxide-dismutase-2*, *heme oxygenase-1*, *nuclear factor [erythroid-derived 2]-like 2* (*NRF2*), and *Sirtuin 3* (Giraud *et al.*, 2020). In another study, a mouse cerebral ischemia model was used where GC7 treatment prevented toxic ROS generation by mitochondria upon treatment with depolarization agents and thereby protected neurons from neuronal cell death (Bourourou *et al.*, 2021). Administrating GC7 in *in vivo* mice models reduced the infarct volume and the functional deficits post-stroke events (Bourourou *et al.*, 2021). Lastly, a study on small infants with complicated *Plasmodium falciparum* malaria infections showed that during this disease, hypoxia leads to apoptosis of cardiac ventricular myocytes (Kaiser *et al.*, 2020). Blocking hypusination in human cultured cardiomyocytes infected with malaria proved beneficial as marked by reduced secretion of cytochrome c and lactate from mitochondria thereby reducing pro-apoptotic myocardial caspase-1 activity (Kaiser *et al.*, 2020).

In summary, all the above-mentioned studies show a positive role of eIF5A in promoting mitochondrial function and performance of OXPHOS, while inhibiting hypusination leads to the downregulation of OXPHOS (Barba-Aliaga and Alepuz, 2022*a*).

eIF5A and Apoptosis

Nevertheless, excess of eIF5A, both in its hypusinated but also in its unhypusinated form seems to have the opposite effect and therefore a detrimental effect on mitochondria and cells. In rat cardiac muscle cells, doxorubicin treatment led to an overexpression of *eIF5A* and an increase in ROS and Ca^{2+} influx into mitochondria which correlate with apoptosis in cells (Tan *et al.*, 2010). Knock-down of *eIF5A* could successfully reduce the induction of apoptosis (Tan *et al.*, 2010). These findings agree with the findings of a study that expressed *eIF5A* in human HT-29 cells and observed induction of apoptosis through the mitochondrial pathway (Sun *et al.*, 2010). This effect could also be observed when a hypusination site mutated form of *eIF5A* was overexpressed, indicating that high levels of unhypusinated eIF5A1 promote apoptosis (Sun *et al.*, 2010). As expected, the knock-down of *eIF5A-1* consequently made cells resistant to a variety of different apoptosis stimuli (Sun *et al.*, 2010).

Mitochondrial Isoform

Another potential link between *eIF5A* and mitochondria was discovered by Pereira and colleagues (Pereira *et al.*, 2016). They found that *eIF5A-1* harbors a second start codon in its 5'-UTR that is less favorably translated by the ribosome, but nevertheless produces a fraction of eIF5A in the cell with an extended 30 amino acid on the N-terminal peptide sequence (Pereira *et al.*, 2016). Just as the canonical *eIF5A-1*, this longer isoform also undergoes hypusination at the same lysine residue and the extra 30 amino acids at the N-terminus are predicted to be a putative mitochondrial localization signal (Pereira *et al.*, 2016). An experiment further strengthening this prediction was the co-isolation of this longer isoform with mitochondria from HeLa cells overexpressing the longer isoform (Pereira *et al.*, 2016). More recently, the same group knocked down this longer isoform with a specific siRNA in HeLa cells and saw downregulation of mitochondrial biogenesis related genes, causing modulation of oxidative metabolism (Pereira *et al.*, 2021). Except for higher oxygen consumption, the knock-down of the longer isoform alone resembles many phenotypes observed after total inhibition of hypusination, raising the question if many of the mitochondrial links to *eIF5A* actually stem from the inhibition of this longer isoform (Pereira *et al.*, 2021). This however still requires further investigation, with more cellular systems and mechanistic understanding of the role of this longer *eIF5A* isoform in mitochondria.

Reprogramming Respiration

The blockage of hypusination that was used to protect tissues and cells from hypoxia by downregulating mitochondrial OXPHOS at the same time shifted cellular metabolism towards increased anaerobe glycolysis.

In a 2019 study, this effect was demonstrated by blocking hypusination with different inhibitors for the hypusine axis (GC7, CPX) or polyamine synthesis (DFMO) in an OXPHOS -dependent mouse macrophage activation model (Puleston *et al.*, 2019). The authors showed, that hypusine is required in situations where glycolysis is limited and further showed that blocking hypusine leads to downregulation of mitochondrial proteins while leaving proteins involved in glycolysis unaffected (Puleston *et al.*, 2019). While they could show that the mRNA levels of the downregulated mitochondrial proteins are unaffected it is still unclear why only certain OXPHOS proteins are affected (Puleston *et al.*, 2019). Some of the downregulated proteins contained a mitochondrial targeting sequence (MTS) and the authors showed in a reporter assay that these MTS sequences are sensitive to hypusine deficiency (Puleston *et al.*, 2019). While those MTS sequences are often enriched in stretches of charged amino acids it is not clear how hypusine would specifically help with the translation of these stretches specifically in OXPHOS proteins while not assisting with such stretches in other proteins across the proteome (Puleston *et al.*, 2019). It, therefore, remains puzzling how hypusine mechanistically regulates OXPHOS.

In the context of T cells, another recent study shows that polyamines direct the T cell epigenome through the synthesis of hypusine. Loss of either polyamines or hypusine disturbs the tricarboxylic acid cycle (TCA cycle) and thereby interferes with histone acetylation (Puleston *et al.*, 2021).

While it is known that the *krüppel-like factor 5* (*Klf5*) transcription factor is essential for cardiovascular remodeling, Ma *et al*. investigated how it mediates the link between mitochondrial dynamics and vascular smooth muscle cell (VSMC) senescence (Ma *et al.*, 2020). They found that *Klf5* knock-down enhances mitochondrial fission, while overexpression of *Klf5* suppresses it (Ma *et al.*, 2020). Interestingly, they further found that Klf5 acts on *eIF5A* by binding to its promoter, where it activates its expression (Ma *et al.*, 2020). They further showed that eIF5A physically interacts with mitofusin 1 (Mfn1), a transmembrane protein of the outer mitochondrial membrane that is a key regulator of mitochondrial fusion (Ma *et al.*, 2020). Fittingly, lowering the expression of *eIF5A* led to more mitochondrial fission and ROS production in their cell model (Ma *et al.*, 2020). While it remains unsolved how the interaction of eIF5A with Mfn1 leads to changes in mitochondrial integrity, it is clear that correct coordination of mitochondrial fusion and fission is elementary to maintaining the

performance of mitochondria but also is involved in the regulation of energy metabolism, cell cycle, and apoptosis (Youle and van der Bliek, 2012, Barba-Aliaga and Alepuz, 2022*a*).

Mitophagy

As mentioned above the translation of the *autophagy regulator TFEB* is modulated by eIF5A. In addition to autophagy, *TFEB* and its ortholog *TFE3* are important facilitators of mitochondrial quality control (Wang *et al.*, 2020). TFEB acts on mitochondria by being critically involved in the expression of genes involved in mitochondrial biogenesis, OXPHOS, and fatty acid oxidation as well as for autophagy genes required for mitophagy (Wang *et al.*, 2020). These roles in the biogenesis and degradation of mitochondria make *TFEB* an important coordinator for metabolic flexibility where the formation and destruction of mitochondria are of essence (Mansueto *et al.*, 2017; Sass *et al.*, 2021).

Rejuvenation and Life Extension through Spermidine Supplementation

Positive effects of spermidine supplementation on life extension have been shown in cells and multiple organisms such as yeast, worms, and flies (Eisenberg *et al.*, 2009; Zhang *et al.*, 2019; Schroeder *et al.*, 2021) as well as in the population-based Bruneck study, where higher spermidine intake was associated with lower mortality in humans (Kiechl *et al.*, 2018; Kiechl and Willeit, 2019). Many of the effects of spermidine in the context of aging are mediated by spermidine-induced eIF5A hypusination and its subsequent role in preserving mitochondrial integrity (Zhang *et al.*, 2019; Schroeder *et al.*, 2021). Polyamines decrease during aging, a process that has been documented for mammalian cell culture but also human organs (Hofer *et al.*, 2022). Fittingly, the depletion of spermidine on the other hand decreases the life span of yeast and increases ROS production and necrosis (Eisenberg *et al.*, 2009).

One of the first life extension experiments with spermidine was done with human immune cells, yeast, worms, and flies in 2009 by Eisenberg and colleagues, observing a mechanism that acts through autophagy (Eisenberg *et al.*, 2009). As mentioned above, induction of autophagy through spermidine-promoted hypusination of eIF5A was also the mechanism behind a work focused on the rejuvenation of B cells (Zhang *et al.*, 2019). In another study conducted by Schroeder *et al*., aged mice were fed spermidine, which was found to successfully pass the blood-brain barrier, leading there to an increase in hippocampal eIF5A hypusination and mitochondrial function (Schroeder *et al.*, 2021). In the same study they showed that in a *Drosophila* aging model, spermidine feeding increases mitochondrial activity and further demonstrated that this effect depends on the *autophagy regulator Atg7* and the *mitophagy-associated PTEN-induced putative kinase 1* (*Pink1*) as well as the *homolog of human E3 ubiquitin ligase Parkin* (*PARK*) (Schroeder *et al.*, 2021). These findings are also in line with recent

studies that show that impaired autophagy of mitochondria (impaired mitophagy) can be a driver of a variety of neurodegenerative disorders (Kumar *et al.*, 2018).

Interestingly, when Liang and colleagues reduced hypusination genetically in *Drosophila* they observed defects in mitochondrial respiration and ATP synthesis and a general reduction of the mitochondrial protein machinery in the brain (Liang *et al.*, 2021). Concordantly, they also observed a drop in brain hypusination levels correlating with age and could demonstrate that spermidine supplementation can restore and boost hypusine levels (Liang *et al.*, 2021). In short, they could demonstrate that efficient hypusination is critical for spermidine-mediated protection of mitochondrial functionality and show its protective roles on locomotion and memory in premature aging brains (Liang *et al.*, 2021).

In summary, all the studies discussed in this chapter have in common that hypusine and eIF5A have a crucial role in the integrity of mitochondria. Nevertheless, the mechanistic involvement is largely unclear, and adding a new perspective on this question is a key goal of this thesis.

1.3.7 Pathophysiological Roles of eIF5A and the Hypusine Axis

Being such an essential protein, eIF5A has been implicated over the years in a whole array of physiological processes and diseases such as retrovirus production, diabetes, ischemic tolerance, cancer, aging, development, and immune cell differentiation (Kaiser, 2012; Turpaev, 2018; Tauc *et al.*, 2021, Barba-Aliaga and Alepuz, 2022*a*) that are listed Table 1 below. Pathologies related to respiration and mitochondria, which are of special relevance for this work, are described additionally in detail in the previous chapter. Excitingly, in the last years, progressively more large datasets containing genome sequencing data of patients became available. This now allows us to perform genome-wide association studies (GWAS) and identify patients with mutations in the hypusine pathway. Therefore, for the first time in history, we are in a position where we can understand and observe the effects of a perturbed hypusination pathway in humans instead of model organisms. These new insights are discussed below.

Table 1: Hypusine-Axis-Associated Diseases

Role in process	Disease/ Pathogen / Model Organism	(References)	Associated with
Retroviral infection	Human immunodeficiency virus type 1	(Ruhl *et al.*, 1993; Bevec *et al.*, 1996)	*eIF5A*

		contradicting findings: (Henderson and Percipalle, 1997; Lipowsky *et al.*, 2000)	
	Human immunodeficiency virus type 1	(Hoque *et al.*, 2009)	*DOHH*
	Retroviral Therapy	(Hauber *et al.*, 2005)	*DHPS*
	Ebola	(Olsen *et al.*, 2016, 2018)	Hypusinated-eIF5A, Polyamines
Diabetes	Glucose homeostasis	(Tersey *et al.*, 2014; Levasseur *et al.*, 2019)	Hypusine, Polyamines, *DHPS*, DFMO
	Translation of *iNOS*-encoding mRNA (mouse)	(Maier *et al.*, 2010)	*eIF5A*
Ischemia	Tolerance to hypoxia/ Antioxidative effect (Drosophila, Rat, Porcine)	(Vigne and Frelin, 2008; Melis *et al.*, 2017; Giraud *et al.*, 2020)	Hypusine/ *DHPS* (GC7)
Cancer	Polyamine-hypusine circuit as a target for cancer and cancer progression	Reviewed in (Mathews and Hershey, 2015; Nakanishi and Cleveland, 2016; Wu *et al.*, 2020; Puleston, 2023)	Polyamine, Hypusine
	Differential expression of *eIF5A-1* and *eIF5A-2* in cancer	(Clement *et al.*, 2006)	*eIF5A*
	Prostate and Gastric cancer	(Meng *et al.*, 2015; Lu *et al.*, 2019)	*eIF5A-2*
	Expression level of *eIF5A* related to aggressiveness of cancer	(Scuoppo *et al.*, 2012)	*eIF5A*
Mendelian Disorders	Developmental delays, neurological disabilities (human and mouse)	(Ganapathi *et al.*, 2019; Kar *et al.*, 2021)	*DHPS*

	Developmental delays, neurological disabilities (human and mouse)	(Faundes *et al.*, 2021; Kar *et al.*, 2021)	*eIF5A*
	Developmental delays, neurological disabilities	(Ziegler *et al.*, 2022)	*DOHH*
Aging	Autophagy	Reviewed in (Hofer *et al.*, 2022)	Spermidine, *eIF5A*
Huntington	Mutant huntington protein induced ribotoxicity by sequestering eIF5A	Preprint (Aviner *et al.*, 2022)	*eIF5A*

Human Patient Mutations in the Hypusine Pathway

In the last years, individuals with mutations in proteins of the hypusine axis could be identified and studied. Interestingly, all, patients with some variants of *DHPS* (Ganapathi *et al.*, 2019; Padgett *et al.*, 2023) and individuals with certain mutations in *eIF5A* (Faundes *et al.*, 2021) or *DOHH* (Ziegler *et al.*, 2022) show similar developmental delays and neurological disabilities. These findings are in line with phenotypes observed in patients with mutations in other translation factors such as *EEF2*, the *eukaryotic elongation factor 1a2* (*EEF1A2*), the *elongator acetyltransferase complex subunit 1* (*ELP1*), and the *ribosomal protein 23* (*RPS23*) that have been linked to neurological diseases as well (Kapur and Ackerman, 2018; Kojic *et al.*, 2023).

An eIF5A-zebrafish knock-down model recapitulated the phenotype observed in human patients with *eIF5A* mutations (Faundes *et al.*, 2021). Remarkably, spermidine supplementation decreased the pathogenicity, suggesting a future avenue for the treatment of patients with *eIF5A*-induced pathologies (Faundes *et al.*, 2021). A neurodevelopmental role of hypusine was also observed in mouse models in which *eIF5A* or *DHPS* were removed specifically from neurons, which caused impaired neurodevelopmental and cognitive functions in these mice (Kar *et al.*, 2021).

The disease-causing mutations discovered in the human *DHPS* encoding gene (*dhps*) lead to a genetic syndrome that was termed DHPS deficiency (Ganapathi *et al.*, 2019; Padgett *et al.*, 2023). Symptoms of this syndrome encompass global developmental delay and seizures and as mentioned above the disease is characterized as a neurodevelopmental disorder (Ganapathi *et al.*, 2019). Effects of these mutations on the hypusination reaction have been structurally investigated recently (Wątor *et al.*, 2023). Interestingly, all five patients described in the report have always a single copy of the *DHPS* N173S variant ($DHPS^{N173S}$), which according to recent structural work still ensures structural

integrity and some enzymatic activity (Ganapathi *et al.*, 2019; Wątor *et al.*, 2023). However, Wator and colleagues suggest that the mutation could affect the stability and mobility of the "ball-and-chain" motif of DHPS, leading to decreased access of spermidine and eIF5A to the active site of DHPS (Wątor *et al.*, 2023). These findings are in line with our data showing that overexpression of *DHPS*^{N173S} in inducible *DHPS* knock-out cell lines can still rescue its absence (Essletzbichler *et al.*, 2023).

Of the clinical variants of *eIF5A* only one of the mutation maps to the shared interface with DHPS (T48N substitution), while the others are on the interface responsible for ribosome binding (Faundes *et al.*, 2021; Wątor *et al.*, 2023).

Why liabilities in the polyamine pathway have such severe impacts on neuronal tissue still needs to be experimentally investigated, but the particular high energy consumption in those tissues and the recently emerging role of *eIF5A* in the regulation of mitochondria and respiration could be an explanation (Hofer *et al.*, 2022).

Retrovirus and HIV generation

One of the earliest observations around eIF5A was that this protein somehow helps with the production of the human immunodeficiency virus type 1 (HIV-1) and other viruses. Additionally, several of the molecules that were identified in searches for HIV-1 inhibitors later turned out to act through inhibition of the hypusine axis. However, some early findings are under debate and the question of how hypusine assists with the production of viruses still needs further research. In one of the earliest reports, eIF5A was found to help with the translocation of unspliced viral mRNA out of the nucleus by engaging with the viral Rev transport factor of HIV-1 (Ruhl *et al.*, 1993; Bevec *et al.*, 1996). Despite this finding was contradicted already in 1997 in an experiment showing that purified eIF5A is unable to bind Rev specifically (Henderson and Percipalle, 1997) and again in 2000 with an investigation involving immobilized Rev that failed to bind eIF5A while binding known other binders such as CRM1 (Lipowsky *et al.*, 2000), the association of *eIF5A* with HIV-1 still gets mentioned frequently until today. Possibly this is because newer studies show again links between the hypusine axis and HIV-1 production. The DOHH inhibitors Ciclopirox and Deferiprone, for example, showed inhibitory effects on HIV-1 gene expression, at the level of transcriptional initiation (Hoque *et al.*, 2009). Additionally, DHPS has been identified as a target for retroviral therapy (Hauber *et al.*, 2005), and derivatives of the DHPS inhibitors CNI-1493 were found to suppress HIV-1 replication in a dose-dependent manner without toxic side effects (Schröder *et al.*, 2016). Lastly, hypusinated eIF5A and polyamines seemed to also be involved in the expression of the VP30 Ebola protein, another viral protein (Olsen *et al.*, 2016, 2018)**.** How exactly hypusine and eIF5A affect the expression of these viruses however still needs further investigations.

1.3.8 Inhibitors for eIF5A Inactivation

The important metabolic role and involvement in a large variety of diseases that were described in the previous chapters make the hypusine axis an attractive target for molecular interventions. Therefore, there is a constant drive to develop new inhibitors for key enzymes of the hypusine axis that are leading to the stop of hypusination and thereby inactivation of eIF5A. These published inhibitors for the hypusine axis will be described in this chapter of the thesis.

N1-guanyl-1,7-diaminoheptane: GC7

One of the widest-used inhibitors for blocking DHPS and therefore for blocking hypusination of eIF5A is N1-guanyl-1,7-diaminoheptane (GC7). It was identified in 1993 in a study that compared different compounds similar in structure to spermidine (Jakus *et al.*, 1993). The authors found that mono-guanyl derivatives are much more potent inhibitors than the parent amines or their bis-guanylated forms of them (Jakus *et al.*, 1993). Of all the tested compounds, GC7 was the most effective and had a K_i of 10 nM, which is around 400-fold lower than the Km of spermidine (Jakus *et al.*, 1993; Tauc *et al.*, 2021). Since GC7 is a synthetic polyamine there is naturally the fear that this drug also influences total polyamine levels. However, cellular and structural studies indicate that thanks to the enormous abundance of polyamines combined with GC7's high affinity for DHPS with a 400-fold lower Km compared to that of spermidine, this might be less of a problem than initially assumed (Jakus *et al.*, 1993; Pegg, 2009). In one such study, Chinese hamster ovary cells were treated with GC7 and while doses ranging from 1 to 10 µM GC7 led to an almost complete abrogation of hypusination, cellular levels of polyamines stayed largely unaffected (Joe and Park, 1994). At the same time, specific binding of GC7 in the active site of DHPS could be shown in a variety of structural studies (Umland *et al.*, 2004, Tanaka *et al.*, 2020*a*; Wątor *et al.*, 2020). Nevertheless, applying GC7 to cells at higher concentrations of around 200 µM does indeed lead to an off-target effect indicated by the induction of autophagy (Oliverio *et al.*, 2014).

Even though 30 years have passed since the discovery of GC7, and since alternative inhibitors for DHPS are lacking, it is still the widest-used inhibitor for DHPS and was an essential tool for a number of recent studies investigating the role of the hypusine axis (Puleston *et al.*, 2019, 2021; Giraud *et al.*, 2020; Tan *et al.*, 2022; Wątor *et al.*, 2023).

Inhibitors for Novel Allosteric Sites: 11g/8m/26d

Recently, multiple screening campaigns with the goal to find new inhibitors for DHPS were published. One such effort by Tanaka and colleagues identified in high-throughput screens inhibitors for DHPS (Tanaka *et al.*, 2020*a*). Synthetic studies with the top candidate hit and further optimization

led to the development of bromobenzothiophene (11g), which proved to be a potent inhibitor against DHPS in an *in vitro* enzyme assay, binding DHPS with a K_i around 60 nM (Tanaka *et al.*, 2020*a*). Attachment of 11g to DHPS leads to a conformational change which suggests that it binds to a novel allosteric site (Tanaka *et al.*, 2020*a*).

Shortly after, the same group published 5,6-dihydrothieno[2,3-*c*]pyridine derivative (26d) and used X-ray crystallography to find out that 26d binds to yet another allosteric site on DHPS with an K_i of around 9 nM (Tanaka *et al.*, 2020*b*).

Despite promising *in vitro* data for 11g and 26d the inhibitors or analogs of them remain to be tested in cells or organisms. However, 11g already served as the basis for the development of a compound called 8m, which not only proved to be an inhibitor of DHPS but was also already applied as an anti-malignant melanoma drug and verified on A375 xenograft models (Liu *et al.*, 2021).

CNI-1493

The inhibitor semapimod tetrahydrochloride (CNI-1493), also called AXD455 or CPSI-2364, was originally developed and tested in RAW 264.7 cells and thought to be an inhibitor for macrophage arginine transport and nitride oxide production (Bianchi *et al.*, 1995). Only later it turned out to be actually a potent inhibitor for DHPS (Bianchi *et al.*, 1995; Sommer *et al.*, 2004). Interestingly, it was administered in a different context already in past clinical trials as an inhibitor for mitogen-activated protein kinases, like in a clinical trial focused on Crohn's disease (Hommes *et al.*, 2002). Additionally, derivatives of CNI-1493 showed suppression of HIV replication in a dose-dependent manner (Schröder *et al.*, 2016). Considering that it only became clear later that CNI-1493 is an inhibitor of DHPS it will be interesting to see if the effects that were seen in macrophages or clinical trials can be linked rather to the inhibition of DHPS and eIF5A (Sommer *et al.*, 2004).

Metal Chelating Drugs, Inhibitors of DOHH

Ciclopirox (CPX) is a broad-spectrum Food and Drug Administration (FDA)-approved antifungal drug (Gupta and Plott, 2004) and acts as a metal-binding hydroxypyridinones as an inhibitor for DOHH (Csonga *et al.*, 1996; Clement *et al.*, 2002). Besides its function as an inhibitor for DOHH it has been used for the treatment of cardiac disorders, diabetes, inflammation, cancer, and HIV infections (Gupta and Plott, 2004; Hoque *et al.*, 2009; Zhou *et al.*, 2010; Ko *et al.*, 2011; Subbaiah *et al.*, 2023).

Similar to CPX, Deferiprone (3-hydroxy-1,2-dimethylpyridin-4-one) is an FDA- and EMA-approved metal chelating drug and is mainly used to relieve iron overload (Chan *et al.*, 2006). It inhibits the function of DOHH and therefore the hydroxylation step of the eIF5A modification (Andrus *et al.*, 1998) and through that inhibits HIV-1 replication in cell culture (Hoque *et al.*, 2009).

Lastly, Mimosine (α-amino-β-(3-hydroxy-4-oxo-1,4,dihydropyridine-1-yl)propanoic acid) is a compound that arrests the cell cycle at the G1-S border and thereby locks the cell cycle (Watson *et al.*, 1991). Similar to CPX and Deferiprone, Mimosine is also a metal chelator and blocks the hydroxylation reaction of DOHH during the synthesis of hypusine, and in addition also the hydroxylation step that is important for collagen synthesis (Hanauske-Abel *et al.*, 1994; McCaffrey *et al.*, 1995; Clement *et al.*, 2002). Mimosine is very similar to leucenol, a toxic non-protein amino acid initially found in seeds of Leucaena (Adams *et al.*, 1945).

While inhibitors for DHPS and DOHH are available, there are currently no molecules known that directly inhibit eIF5A or specifically one of the isoforms of eIF5A (eIF5A-1 or eIF5A-2). However, the availability of high-resolution structures for DHPS (Liao *et al.*, 1998; Umland *et al.*, 2004; Wątor *et al.*, 2023), DOHH (Han *et al.*, 2015), and eIF5A (Schmidt *et al.*, 2016) will hopefully make the identification of novel inhibitors easier and faster in the future.

1.4 Loss-of-Function Genetic Screening in Human Cells

The fundamental idea of any genetic screen is to connect a genotype with a certain cellular phenotype and thereby ascribe functions to genes. To do this, a gene is modified in an experimental setting and then the experimenter observes what happens to a specific readout. Functional genomics is doing the same, but at a larger scale, modifying many or even all genes and then mapping the changes in phenotype back to the individual gene at a large scale. Genetic screens are especially useful for the discovery of previously unknown molecular mechanisms, offering the chance to generate fundamentally new knowledge and thereby generate totally novel hypotheses.

Following these principles and applying them for screens in model organisms like *Saccharomyces cerevisiae* or *Schizosaccharomyces pombe* fundamental processes in eukaryotic biology such as cell cycle regulation, ubiquitin-mediated protein degradation, vesicle trafficking, and DNA replication and repair could be illuminated (Spellman *et al.*, 1998; Winzeler *et al.*, 1999; Forsburg, 2001; Giaever *et al.*, 2002; Jazayeri and Jackson, 2002). Other eukaryotic processes like the immune system, neuronal development, and tissue differentiation can however only be studied in more complex model systems or human cells. This led to the development of human cell cultivation techniques, novel gene manipulation techniques that allow their manipulation, and new approaches for genetic screening with these systems.

The Ideal Functional Genomic Screen

The ideal functional genomic screen identifies no false positive hits while discovering all true positive hits (Hart *et al.*, 2014). To get as close as possible to this scenario, potent, specific, and reliable genomic perturbers that can be applied experimentally are needed.

1.4.1 Longstanding Ways of Gene Manipulation

Before the development of CRISPR/Cas9 as a gene editing tool in human cells, a technology described later in detail, gene modulation could be induced either by random mutagenesis, via transposons and retrovirus, with zinc finger (ZF), transcription activator-like effector nucleases (TALEN) or with RNA interference (RNAi). The application of chemical mutagenesis with agents such as N-ethyl-N-nitrosourea (ENU) (Russell *et al.*, 1979; Acevedo-Arozena *et al.*, 2008) or screens based on transposons (Spradling *et al.*, 1995; Keng *et al.*, 2009) allowed researchers to perform the first unbiased cellular genetic studies. However, the lack of specific programmability of these tools made it difficult to mutate at saturation or identify easily the respective mutated alleles and therefore limited their application for broad screening campaigns.

Most modern gene editing technologies are based on the specific induction of double strand breaks in the DNA of cells that are then repaired by the cell either via error-prone non-homologous end joining (NHEJ) or by homologous recombination (HR). In order to develop specific and controllable gene editing tools it became key to understand how these repair pathways function and how they can be controlled and exploited (Jasin and Haber, 2016; Yeh *et al.*, 2019; Hussmann *et al.*, 2021), which is done by inducing double-strand breaks in DNA with e.g. the rare-cutting endonuclease I-SceI (Rouet *et al.*, 1994) and study their repair outcomes under different settings (Jasin and Haber, 2016; Yeh *et al.*, 2019; Hussmann *et al.*, 2021).

With the discovery and understanding of ZF and their fusion to a Fok I cleavage domain, programmable sequence-specific DNA cuts became possible for the first time (Kim *et al.*, 1996; Urnov *et al.*, 2010; Carroll, 2011) and their power was showcased for gene silencing in human embryonic stem cells (ESC) and induced pluripotent stem cells (iPSC) (Hockemeyer *et al.*, 2009). Similar applications became possible with the development of TALEN, consisting of an array of DNA-binding protein elements combined with a Fok I cleavage domain (Boch *et al.*, 2009; Moscou and Bogdanove, 2009; Joung and Sander, 2013). Again, their remarkable potential to specifically cleave DNA was demonstrated by applying them for gene editing in pluripotent stem cells (Hockemeyer *et al.*, 2011). Additionally, these TALEN constructs allowed now to fuse and recruit gene activation technologies to a gene location of choice (Konermann *et al.*, 2013). Meanwhile, these technologies were applied for gene editing in patients to edit *CCR5* in CD4-positive T cells (Tebas *et al.*, 2014) as well as correct sickle cell anemia (Hoban *et al.*, 2015). Since for both systems, the specific DNA recognition is encoded in a protein sequence, a whole new protein has to be designed, tested, and cloned which makes the creation of new ZF and TALEN binder labor-intense and expensive and therefore still hindered genome-wide functional genomics (Carroll, 2011; Gaj *et al.*, 2013).

RNA Interference

This changed with the development of RNAi, a technology that was awarded the Nobel Prize to Andrew Z. Fire and Craig C. Melo in 2006. This tool is based on the evolutionary conserved machinery that regulated gene expression via small RNAs (Wilson and Doudna, 2013). Thanks to the conservation of this pathway, it is present in just about any mammalian somatic cell. This allows easy loss-of-function experiments by only introducing a siRNA, without large genetic manipulations for the expression of additional proteins (Boettcher and McManus, 2015). This opened the door for the design and cloning of large-scale loss of function libraries and made programmed genome-wide editing affordable and possible for the first time (Bernards *et al.*, 2006; Mohr *et al.*, 2010). In both cases, RNAi and shRNA, an RNA is introduced that is loaded into the RNA-induced silencing complex

(RISC), which then binds to complementary RNA in the cell and induces its degradation (Carthew and Sontheimer, 2009). This leads subsequently to the reduction of target mRNA levels and consequently to lowered target protein levels. The drawbacks of this technology are however that the RNAi machinery is mostly active in the cytoplasm, which makes targeting nuclear transcripts, such as long non-coding RNAs more difficult (Boettcher and McManus, 2015). Alternative systems that can be recruited to different locations within the cells are type VI CRISPR systems, they are RNA-guided and allow to knock-down or edit RNA, when fused to base editors (Abudayyeh *et al.*, 2016, 2017). RNAi experiments additionally often turned out to struggle from large off-target effects (Jackson *et al.*, 2003; Jackson and Linsley, 2010) and the nature of the approach only allows to reduce transcript levels but fails in total abrogation of expression of the targeted gene.

1.4.2 Haploid Genetic Screening

Two approaches that offer full gene knock-out are transposon and gene-trap methods. However, since they do not offer an efficient way to generate bi-allelic mutants in diploid cell lines, these techniques are limited to haploid model organisms and cell lines. The identification of a human leukemia cell line, that was haploid for all chromosomes except chromosome 8, termed KBM-7 (Kotecki *et al.*, 1999), allowed the lab of Thijn Brummelkamp to develop a screening method that allowed to generate null alleles in human cells at large scale (Carette *et al.*, 2009). This made screens that were until then only possible in yeast (Forsburg, 2001), that have a natural haploid life stage, finally possible in human cells.

Overexpression of (*sex determining region Y)-Box 2* (*SOX2*), *krueppel-like factor 4* (*KLF4*), *POU class 5 homeobox 1* (*POU5F1*), and *MYC* allows reprogramming of KBM-7 to induced pluripotent stem cells (Takahashi and Yamanaka, 2006; Carette *et al.*, 2010). These experiments also led to the generation and isolation of the near-haploid cell line HAP1, which possesses fibroblast-like morphology (Carette *et al.*, 2011*b*) and is contrary to KBM-7 adherently growing and lacks the second copy of Chromosome 8. However, HAP1 cells still possess two copies of a piece of Chromosome 15, one of which forms a fusion with Chromosome 19. But we removed this last diploid 30-megabase fragment, which encompasses 330 genes, by using CRISPR/Cas9-based genome engineering and proved that deriving a stable fully haploid human cell line (eHAP) is possible (Essletzbichler *et al.*, 2014). Our approach also demonstrated the feasibility of excising megabase-sized fragments from the genome employing CRISPR/Cas9 (Essletzbichler *et al.*, 2014). Meanwhile, other haploid human cell lines were discovered and established such as murine haploid cells (Elling *et al.*, 2011; Leeb and Wutz, 2011) and also human haploid embryonic stem cell (Sagi *et al.*, 2016), which now allow a wider variety of haploscreen in different cell models.

Haploid genetic screening is based on the insertion of a gene-trap cassette-containing vector into a haploid cell. The gene-trap construct consists of a splice acceptor site, a marker gene (antibiotic resistance marker or fluorescent protein), and an mRNA polyadenylation signal. Applying viral infection of the gene-trap and subsequent random integration throughout the genome at high enough coverage leads to saturating mutagenesis; with the mild constraint that retroviruses have the tendency to integrate mostly into actively expressed genes (Carette *et al.*, 2011*a*; Bürckstümmer *et al.*, 2013). The inserted gene-trap cassette leads to aberrant splicing within the specific gene and induces premature termination of the mRNA transcript, causing the generation of a null allele. However, depending on the orientation of the insertion of the cassette the gene-trap either leads to mRNA truncation (sense orientation) or does not interfere with transcript expression at all, providing then however an additional control for interpretation of the screening results.

Inverse PCR or linear amplification mediated-PCR (LAM-PCR), followed by single-stranded (ss)DNA linker ligation and NGS, allows to identify and map the integration sites to the respective gene (Schmidt *et al.*, 2007, Carette *et al.*, 2011*a*). Haploscreens have in the meanwhile been employed in many settings and led to many discoveries such as host factors essential for virus infection (Carette *et al.*, 2009, 2011*b*; Jae *et al.*, 2013), biosynthetic factors for the synthesis of diphthamide (Carette *et al.*, 2009), and drug sensitivity targets (Carette *et al.*, 2009; Birsoy *et al.*, 2013; Winter *et al.*, 2014; Bigenzahn *et al.*, 2018). Additionally, they have also been successfully applied to generate one of the first human synthetic lethality papers (Blomen *et al.*, 2015). Lastly, gene-traps were used to assemble a big library of human isogenic cell lines (Bürckstümmer *et al.*, 2013).

Finally, in 2017, coupling haploscreens with antibody-based reporter sorting allowed a whole new class of genetic screens (Brockmann *et al.*, 2017). Using protein levels or levels of post-translational modification as a reporter allows the generation of genetic wiring maps, without depending on a readout or perturbation that leads to a change in cellular fitness (Brockmann *et al.*, 2017). Additionally, reporter constructs such as the *interferon-regulatory factor 1* (*IRF1*) reporter, which is induced by interferon-γ and is known to be under strong genetic control, can be used as readout for genetic screens (Brockmann *et al.*, 2017). Meanwhile, the same concept has been applied to find among many other studies factors of mitochondrial stress response (Fessler *et al.*, 2020), regulators of actin maturation (Haahr *et al.*, 2022), pathways involved in DNA interstrand crosslink repair (Mazouzi *et al.*, 2023) and was also used in this work to screen for modulators of the post-translational modification hypusine, described below in detail. In case no antibodies are available for the protein of interest, endogenous tagging of this protein can offer a solution. This solution is discussed in a later chapter and was also employed in the experimental part of this work.

1.4.3 CRISPR Screening

The discovery of clustered regular interspaced short palindromic repeats (CRISPR) starts in the year 1987 when these repetitive DNA sequences with defined features in bacterial genomes were discovered (Ishino *et al.*, 1987). Since these sequences matched the ones of bacteriophages other groups hypothesized correctly that the CRISPR pathway functions as an adaptive immune system (Mojica *et al.*, 2005; Pourcel *et al.*, 2005). A group that studied the genome of *Streptococcus thermophilus* then found yet another CRISPR array, which consists of CRISPR and CRISPR-associated proteins (Cas), containing a novel cas enzyme that is now known as Cas9 and the workhorse for all CRISPR technologies used in this study (Bolotin *et al.*, 2005). Additionally, they recognized that all spacer sequences share a common end, a sequence that is now termed protospacer adjacent motif (PAM) and is crucial for target recognition (Bolotin *et al.*, 2005). A problem in the dairy industry, where phages that infect *Streptococcus thermophilus* frequently lead to problems with yogurt production then led to the first experimental demonstration of CRISPR by scientists at Danisco; the bacteria indeed integrated the DNA of the attacking phage into a CRISPR array and thereby could counteract the next phage attack (Barrangou *et al.*, 2007). Shortly after, the group of John van der Oost could show that these acquired spacer sequences are transcribed into small RNAs (CRISPR RNAs/crRNAs) that then guide the Cas enzymes to target DNA (Brouns *et al.*, 2008). Next, it could be shown that contrary to RNAi, CRISPR acts on DNA and cleaves it, requiring only the protein Cas9 to do so (Marraffini and Sontheimer, 2008; Garneau *et al.*, 2010). Finally, scientists led by Emmanuelle Charpentier at Umea University Sweden and University Vienna Austria performed small RNA sequencing and discovered a second small RNA needed for Cas9-guiding (Deltcheva *et al.*, 2011). They called it trans-acting CRISPR RNA (tracrRNA) and showed that this small RNA forms a duplex with the crRNA (Deltcheva *et al.*, 2011). Next different groups showed that CRISPR could be programmed to cut any sequence in bacterial genomes (Gasiunas *et al.*, 2012; Jinek *et al.*, 2012).

In summary, clustered regular interspaced short palindromic repeats (CRISPR) form together with CRISPR-associated proteins (Cas) an RNA-guided adaptive immune system. It is now known that these systems can be found in about half of the bacteria and most archaea. Its purpose is a defense against invading nucleic acids from parasites or viruses using a three-step process. In the first step, the adaption phase, pieces of invading DNA or RNA (spacers) are inserted in between pairs of direct repeats (DR), thereby creating a record of the invader. In the expression and processing step, the CRISPR array gets transcribed into a long pre-CRISPR RNA (pre-crRNA), which is then processed into shorter mature CRISPR RNAs (crRNAs). The last and final step is interference, where the crRNAs bind and guide a complex of Cas enzymes to specifically cleave a target DNA or RNA (Adli, 2018).

CRISPR as Functional Genomics Tool

The real breakthrough for CRISPR as a functional genomics tool came when CRISPR was successfully adapted for genome editing in eukaryotic cells (Cong *et al.*, 2013; Mali *et al.*, 2013). Key to the success of CRISPR as a functional genomic tool was the relative ease of introducing the CRISPR enzyme and a whole library of guide-RNAs into human cells. These gRNAs can be designed to target any loci in the human genome, where they induce then double-strand breaks at the specific location, causing gene disruption by error-prone NHEJ-mediated repair or other DNA repair mechanisms and then leading in most cases to out-of-frame mutations (Hsu *et al.*, 2014; Ferreira da Silva *et al.*, 2019). In certain cases, DNA repair can also lead to in-frame editing. This is an important limitation to keep in mind when working with CRISPR, which means that the presence of a gRNA in a single cell is not always a guarantee for a full knock-out (Bock *et al.*, 2022). Nevertheless, the much higher specificity of CRISPR compared to RNAi was demonstrated in a study that identified the targets of many cancer drugs that were at the time in different stages of clinical testing (Lin *et al.*, 2019). Contrary to the targets identified mostly by using RNAi or small-molecule inhibitors, the CRISPR studies showed that these drugs act on cancer by targeting previously unknown off-target proteins, that are not essential for cancer cell proliferation (Lin *et al.*, 2019).

The ease of delivery of CRISPR systems also allowed scientists to work with a whole palette of different cell types, therefore allowing them to pick the perfect model system for the corresponding research question (Wang and Doudna, 2023). In addition, the convenience of programming Cas9 with just a short guide RNA led to the production of many pooled genome-wide knock-out libraries such as the GeCKO, the Brunello, or the TKOv3 library (Sanjana *et al.*, 2014; Hart *et al.*, 2017; Sanson *et al.*, 2018) as well as focused libraries targeting a small set of genes such as metabolic genes or all solute-carriers (Birsoy *et al.*, 2015; Morgens *et al.*, 2017; Girardi *et al.*, 2020), making CRISPR the ideal functional genomics tool for genetic screens.

Pooled Genetic Screening

Genetic screening is the systematic and specific genetic alteration of a set of genes in parallel. A very common type of genetic screen is a pooled genetic screen, which beauty lies in the relative ease of design and conduction of the screen itself (Bock *et al.*, 2022; Przybyla and Gilbert, 2022).

Pooled genetic screens start with the introduction of a CRISPR guide RNA (gRNA) library into a bulk of cells (Bock *et al.*, 2022) (Figure 13a). Individual cells receive different gRNAs, which is typically achieved by transducing cells lentivirally at a low multiplicity of infection (MOI); an MOI of around 0.3-0.5 ensures that cells only receive one single guide RNA (sgRNA) at a time (Doench, 2018) (Figure

13b). The gRNA integrates into the genome and fulfills a dual function: it perturbs the individual cell and serves as an identifier for the induced perturbation (Doench, 2018). The Cas9 enzyme is either already stable expressed in the receiving cells or can be co-delivered on the same vector as the sgRNA, introduced as protein, mRNA, separate virus, or plasmid (Bock *et al.*, 2022).

The next step of a pooled genetic screen is the application of a challenge to the engineered cell pool. In short, a selection pressure is applied that puts the modified cells in competition with each other; such a pressure can be cell proliferation, drug treatment, or viral infection (Bock *et al.*, 2022). Surviving cells are afterward harvested, lysed and their genomic DNA isolated; using high-throughput sequencing the distribution of gRNAs in the collected samples is compared (Doench, 2018) (Figure 13a). Guide RNAs that are enriched in the populations represent genes that when disturbed gave cells a selection advantage to the challenge, while gRNAs that are depleted in the population represent genes that when disturbed led to sensitization to the challenge (Bock *et al.*, 2022). By assessing the abundance of sgRNAs in multiple experimental conditions, genes that were targeted by these guides can be identified that lead to certain phenotypes (Przybyla and Gilbert, 2022).

The possibility to create a CRISPR library that targets only a subset of genes, something not possible with haploid genetic screening, allows to screen also in more difficult cell models where cultivation of large cell numbers required for genome-wide screens is not feasible.

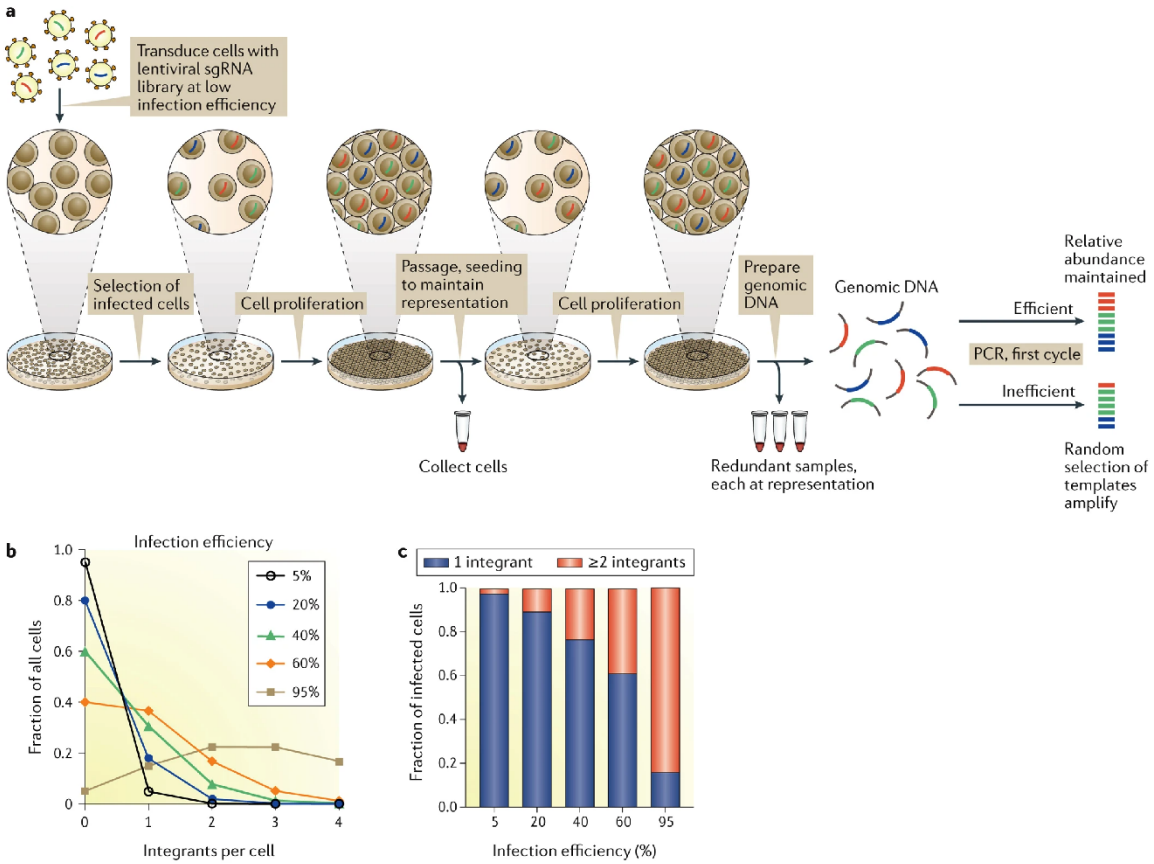

Figure 13. Pooled CRISPR genetic screening.

a. Overview of the steps of a genome wide pooled CRISPR screen. **b.** The number of viral integrations per cell can be modelled with a Poisson distribution and depends on the infection efficiency of the experiment. **c.** An infection efficiency of around 20-60% ensures that a reasonable coverage can be achieved, without discarding too man uninfected cells, while keeping the number of cells with more than one viral integration low.

Reprinted from Nat. Rev. Genet., 19, 67-80, Doench, JG., Am I ready for CRISPR? A user's guide to genetic screens, 2018, with permission from Springer Nature

1.4.4 Applying Loss-of-Function CRISPR Genetic Screening to Dissect Biological Pathways and Diseases

Two seminal first genome-scale CRISPR/Cas9 genetic screens demonstrated the enormous power of pooled genetic CRISPR screens (Shalem *et al.*, 2014, 2015; Wang *et al.*, 2014). However, while these initial screens mostly were proof-of-concept experiments and very important for library optimization, pooled CRISPR screens in the meanwhile have been extensively used to decipher complex biological pathways.

Viability Based Screens

The easiest and most common pooled genetic screens typically use viability and proliferation-based assays as challenges for the engineered cell population (Doench, 2018) (Figure 14). Such screens have been meanwhile successfully applied to identify cancer drivers and regulators (Hart *et al.*, 2015; Wang *et al.*, 2015; Dong *et al.*, 2022; Katti *et al.*, 2022). They also were used to find genes affecting pluripotency or differentiation, modulating viral or bacterial pathogenesis, causing synthetic lethality with drugs or other genes or in more sophisticated screens to understand processes such as proliferation, senescence, and apoptosis (Przybyla and Gilbert, 2022; Wang and Doudna, 2023).

As mentioned earlier, copious amounts of genetic screens are collected in large databases. This not only allows to assess essentiality of individual genes in a certain cell type but also allows the comparison of essentiality profiles across different datasets, which can, for example, help to identify new partner proteins in metabolism or protein complexes (Meyers *et al.*, 2017; Bayraktar *et al.*, 2020; Wainberg *et al.*, 2021).

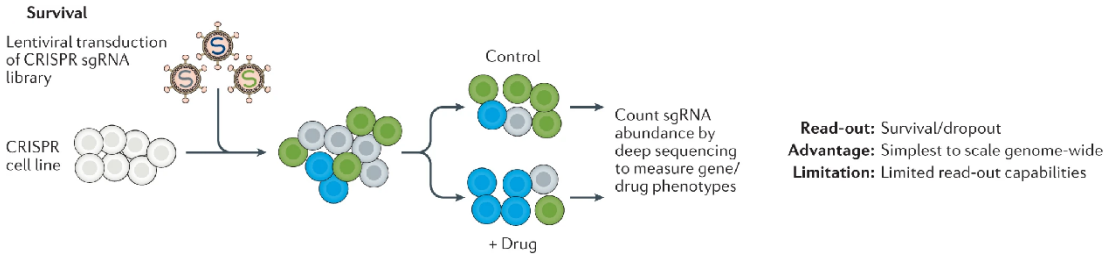

Figure 14. Pooled CRISPR genetic survival screening.

Adapted from Nat Rev Genet., 23(2):89-103, Przybyla, L., Gilbert, LA., A new era in functional genomics screens, 2022, with permission from Springer Nature

Fluorescent-Activated Cell Sorting (FACS) Based Screens

The limiting factor for systematic genetic screens is to have a good readout. Fluorescent-activated cell sorting (FACS) based screens can offer a solution by offering the possibility to read out a multitude of cellular reporters (Figure 15). While these screens are versatile, they come with the disadvantage of way higher cell processing times, compared to classical viability screens. The core principle of using FACS for genetic screens is, that cells are sorted based on high and low marker expression; this can for example be the top and bottom 5% of cells, which are then processed and analyzed for gRNA distribution as described above (Bock *et al.*, 2022).

A method that requires the least investment of time in reporter generation but comes with the requirement of having a specific antibody available, is to use antibody staining for proteins or

secondary modifications. In this case, the level of a specific protein serves as a readout for the genetic screen (Bock *et al.*, 2022). This method was also applied in a genetic screen that is part of this work. Similarly, fluorescent dyes that stain compartments of cells offer a quick readout (Bock *et al.*, 2022). Other readouts that have been employed for FACS-based screens are fluorescent transcriptional reporters for cell state or signaling pathways, uptake of labeled fluorescent proteins, fluorescent viruses, fluorescent bacteria, protein interactions, or abundance of metabolites of small molecules via fluorescence resonance energy transfer (FRET)-based readouts (Przybyla and Gilbert, 2022). Another example that has been applied for genetic screening is cells that induce the expression of a fluorescent protein dependent on their chromatin state in a specific region (Li *et al.*, 2021). In cases where no specific antibody for a protein is available, proteins can also be tagged endogenously and used as reporters. This approach is described in detail below and was employed also for this thesis (Serebrenik *et al.*, 2019; Reicher *et al.*, 2020). Lastly, complex reporters that change properties after uptake, such as beads coated with a pH-sensitive dye in phagocytosis assays can give multiple information simultaneously (Colas *et al.*, 2014). We used such an assay and coupled it to focused and genome-wide screens that are described in the attached publications below (Sedlyarov *et al.*, 2018; Essletzbichler *et al.*, 2023).

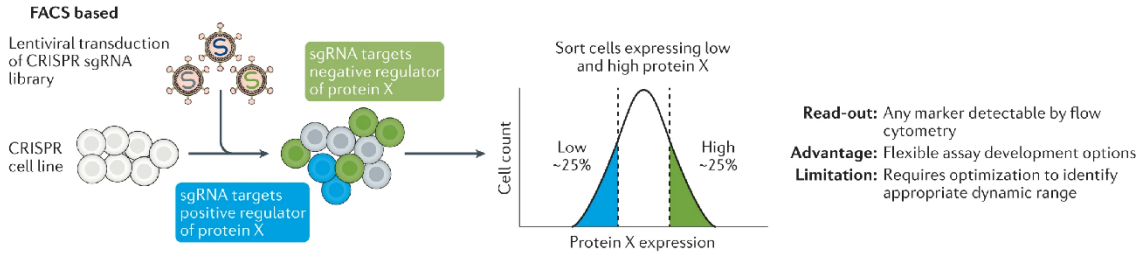

Figure 15. Pooled FACS-based CRISPR genetic screening.

Adapted from Nat Rev Genet., 23(2):89-103, Przybyla, L., Gilbert, LA., A new era in functional genomics screens, 2022, with permission from Springer Nature

1.5 Experimental Approaches complementing Functional Genomics

1.5.1 Global Expression Proteomics

While mass spectrometry (MS) was routinely used in analytical chemistry in the twentieth century the difficulty of ionizing proteins made it barely usable for molecular biology (Mann, 2016). This changed with the development of electrospray ionization (ESI) in 1989 (Fenn *et al.*, 1989), which was also acknowledged with the 2002 Nobel Prize in Chemistry (Mann, 2016) and allowed for the first time to efficiently analyze proteins with mass spectrometry. Nowadays, ESI combined with liquid chromatography-mass spectrometry (LC-MS) is one of the most common setups to analyze complex peptide mixtures, a common task in modern proteomics where whole proteomes often need to be compared (Ardrey, 2003; Aebersold and Mann, 2016; Pappireddi *et al.*, 2019) (Figure 16). Another commonly used technique for ionization, but one that works better for simple peptide mixtures, is matrix-assisted laser desorption/ionization (MALDI) (Karas and Hillenkamp, 1988; Pappireddi *et al.*, 2019).

While so-called top-down proteomics approaches are studying proteins as intact entities, which has the advantage that all modifications can be traced back to the same molecule (Tran *et al.*, 2011), bottom-up proteomics approaches are nonetheless far more widespread, because they are several orders of magnitude more sensitive and thus allow to profile entire proteomes. As with all bottom-up proteomics approaches proteins are isolated from a cell or tissue-derived sample and then proteolytically cleaved into peptides using a protease with defined cleavage preferences such as trypsin (Aebersold and Mann, 2016). The resulting peptides are then separated using liquid chromatography (LC) and eluted at the end of the column, the so-called emitter, which is located directly in front of the mass spectrometer (Pappireddi *et al.*, 2019).

After ESI, the ionized peptides can now be filtered and detected based on their mass-to-charge (*m/z*) ratio in a first mass analyzer typically referred to as MS1 (Pappireddi *et al.*, 2019). For the analysis of proteins, several mass analyzers are commonly coupled together and ions of certain *m/z* ratios from MS1 can be selected, further fragmented, and then sent to a second mass spectrometer (MS2) for detection and optionally even further fragmented and sent to a third mass analyzer (MS3) (Pappireddi *et al.*, 2019) (Figure 16). Recording multiple spectrums in different mass analyzers improves the identification and discriminability of peptides, especially when they have very similar *m/z* ratios (Gstaiger and Aebersold, 2009).

Figure 16. Protein identification with mass spectrometry.

Reprinted from Nat. Rev. Genet., 10, 617-627, Gstaiger, M., Aebersold, R., Applying mass spectrometry-based proteomics to genetics, genomics and network biology, 2009, with permission from Springer Nature

One limitation of MS lies in the difficulty to derive accurate quantities, which is due to the efficiency of digestion, the variety of peptide solubility, and the efficiency of peptide ionization, all dependent on the sequence and biochemical properties of individual peptides. Nevertheless, compared to traditional methods of protein quantification such as immunoblotting or ELISA it has clear advantages such as that it doesn't require specific antibody of detecting the protein of choice and instead detects specific peptides, has lower limits of quantification and higher reproducibility. However, advancements in acquisition speed, completeness of chromatogram databases, and speed of identification by MS machines now allow whole proteomes to be quantitatively assessed in a few hours, similar to transcriptomics-based cellular characterizations (Bekker-Jensen *et al.*, 2017; Nusinow *et al.*, 2020; Gonçalves *et al.*, 2022; Bennett *et al.*, 2023). These technological advances make proteomics a powerful tool to accurately quantify the spatiotemporal dynamics of protein signaling networks, reveal protein-protein interactions as well as abundance, stability, post-translational modifications, and subcellular localizations for thousands of proteins (Larance and Lamond, 2015).

A classic task in biology is to identify differentially expressed proteins in different samples at a large scale. For these large-scale proteomics studies and in order to ask hypothesis-driven questions, reliable high-throughput setups for the quantitative assessment of whole proteomes were needed and led to the development of modern label-free or labelled multiplexed proteomics (Aebersold and Mann, 2016; Pappireddi *et al.*, 2019).

Multiplexed Proteomics with Isobaric TMT Labels

In particular, the development of the label based isobaric-tag-centered proteomics, which relies on tandem mass tags (TMT) has expanded the possibilities of MS-based analysis by enabling proteome-wide relative quantification for multiple samples within a single experiment (Thompson *et al.*, 2003*a*; Rauniyar and Yates, 2014). TMT labels consist of three main elements: an amine-reactive group, a mass normalization group, and a reporter ion group (Thompson *et al.*, 2003*a*). The amine-

reactive group is responsible for the N-terminal labeling of peptides (Li *et al.*, 2020). The labels are isobaric, but differ in their altered configuration of five heavy isotopes within the normalization and reporter ion group (Li *et al.*, 2020). Since all TMT tags have identical structures and nominal mass, labeled peptides still co-elute simultaneously regardless of the heavy isotope distribution, and have the same *m/z* values in an MS1 scan (Thompson *et al.*, 2019). However, further fragmentation of labeled peptides in MS2 or MS3 produces reporter ion peaks, which now have different masses and can be used to quantify the different samples (Rauniyar and Yates, 2014). Due to the recent technological development of TMTpro, 16 different samples can now be labeled with individual tags (Thompson *et al.*, 2019). It has been demonstrated that they have similar performance as the heavily used tandem mass tag reagents such as the TMT11plex (Li *et al.*, 2020) (Figure 17a-b). More individual labels enable more complicated experimental setups, as multiplexing of samples can be expanded. This allows to include more replicates, treatments, or more samples within a single experiment and within the identical measurement (Figure 17c). This is important because splitting samples across different TMT-labelled MS experiments is suboptimal owing to variation in the peptide quantification, labelling efficiency, and the semi-stochastic sampling during shotgun proteomics, which makes the comparison of different TMT-experiments challenging (O'Connell *et al.*, 2018). This can be circumvented by utilizing a so-called reference channel in each experiment (Rauniyar and Yates, 2014; Thompson *et al.*, 2019). TMT-experiments however also come with a whole array of disadvantages which range from the high costs of reagents, the requirement for offline fractionation and the frequently occurring issue of ratio compression (Ting *et al.*, 2011; McAlister *et al.*, 2014; Weiner *et al.*, 2022).

Additional advantages of comparing samples within a single experiment are: (i) that isotope labeling allows for sample multiplexing and precise quantification, (ii) comparing samples within the same experiment allows statistical interference to be performed with more statistical power and (iii) the more complex experiment design allowing comparison of more replicates and treatments within the same experiment (Li *et al.*, 2020).

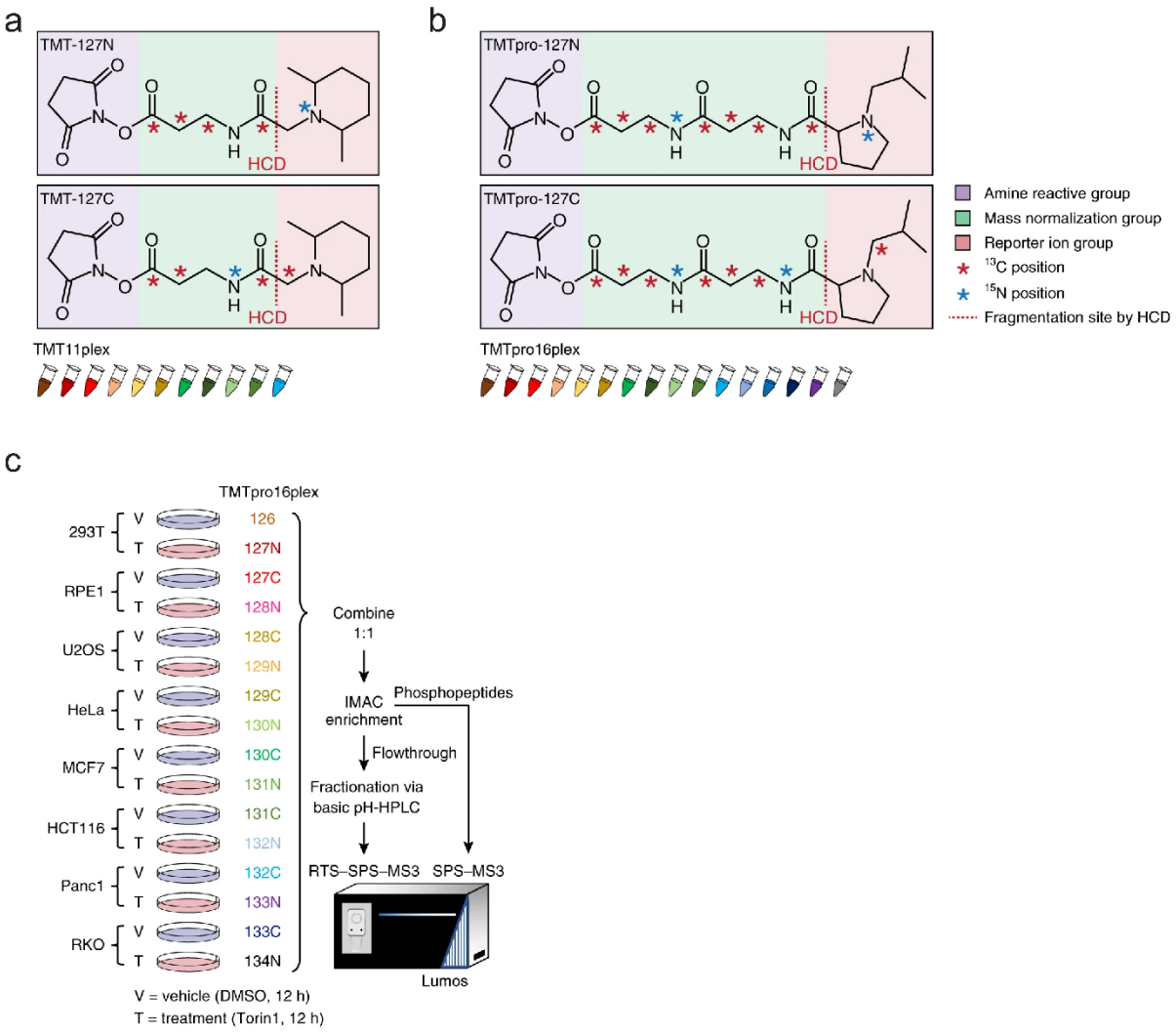

Figure 17. Structure, overview, and use of TMT labels.

Reprinted from Nat Methods, 17(4):399-404, Li, J., Van Vranken, JG., Vaites, LP., Schweppe, DK., Huttlin, EL., Etienne, C., Nandhikonda, P., Viner, R., Robitaille, AM., Thompson, AH., Kuhn, K., Pike, I., Bomgarden, RD., Rogers, JC., Gygi, SP., Paulo, JA., TMTpro reagents: a set of isobaric labeling mass tags enables simultaneous proteome-wide measurements across 16 samples, 2020, with permission from Springer Nature

Applications of TMT Expression Proteomics

TMT labels are applied to a whole range of methods based on multiplexed quantitative proteomics, such as protein turnover studies, single-cell proteomics (Bennett *et al.*, 2023), drug target identification (Savitski *et al.*, 2014; Franken *et al.*, 2015; Gaetani *et al.*, 2019; Li *et al.*, 2020), protein correlation profiling (Doron-Mandel *et al.*, 2023), clinical proteomics (Ruckhäberle *et al.*, 2010; Keshishian *et al.*, 2017), protein dynamics (Murphy *et al.*, 2015), subcellular protein localization (Dunkley *et al.*, 2004), and many more. Some of these applications are described in more detail in the following section.

The characterization of single cells rather than lysates of a mixture of cells is a key practice in modern system biology. Single-cell transcriptomics in particular has been a great success but suffers however from the fact that the majority of transcripts do not correlate well with protein expression (Ctortecka *et al.*, 2022*a*). Therefore, it is important to supplement transcriptomic data with single-cell proteomics datasets. While TMT-multiplexing has proven to be very useful to acquire and compare multiple full proteomes derived from larger numbers of cells in parallel, a remaining challenge is that whenever multiple quantitative shotgun proteomics experiments are merged, that a significant number of peptides are not quantified in all TMT-channels. This leads to an decrease of the overall number of proteins that can be compared between experiments (Brenes *et al.*, 2019). However, the combination of data-independent acquisition (DIA), a method in which all ions within a selected *m/z* range are analyzed in MS2, and TMT multiplexing seem to offer a solution to this challenge by providing complete proteome signatures independently of peptide identification (Ctortecka *et al.*, 2022*b*). While the label-free analysis of single cells requires at least 35 min per cell and thus enables the analysis of about 40 cells per day, the multiplex analysis with 16 labels can measure about 256 cells per day (90 min for 16 cells) (Bennett *et al.*, 2023).

Cellular Thermal Shift Assay (CETSA) exploits the principle of ligand-induced thermal stabilization of target proteins (Martinez Molina *et al.*, 2013). Combining this assay with multiplexed quantitative mass spectrometry, based on TMT labeling, led to the development of thermal protein profiling (TPP). TPP assesses differences in the aggregation behavior of proteins across multiple temperature points by fitting melting curves for all quantified proteins (Savitski *et al.*, 2014; Franken *et al.*, 2015; Huber *et al.*, 2015). TPP is a powerful approach to identify targets and off-targets of drugs, to study interactions of proteins with metabolites and even to investigate protein stabilization caused by post translational modifications such as phosphorylation (Mateus *et al.*, 2020). One disadvantage is that TPP requires large quantities of compound and sample and in addition for each biological replicate a batch of TMT reagents is needed (Zhang *et al.*, 2022). Thus, the Proteome Integral Solubility Alteration (PISA) assay was developed. PISA enables a higher throughput that also assesses protein stability under different conditions (Gaetani *et al.*, 2019). The main concept of PISA is to use the integral under the curve instead of individually fitted curves for each temperature (Gaetani *et al.*, 2019). While the initial PISA assays used only a temperature gradient to challenge protein stability (Gaetani *et al.*, 2019), in the meanwhile other challenges such as kosmotropic salts (Beusch *et al.*, 2022) and organic solvents (Van Vranken *et al.*, 2021) have been successfully used. Whilst TPP uses an individual TMT label for each temperature condition, in PISA assays all samples treated with different temperatures are mixed together and are labeled with a single TMT label, thus making the approach cheaper and allowing more replicates within the same TMT experiment (Li *et al.*, 2020).

Large Protein-Protein Interaction Datasets

A systems biology task where the introduction of TMT labeling has also proved beneficial is the global mapping of protein-protein interactions (PPI) within a cell. Typical and powerful approaches to study these interactions are affinity purification (AP) or proximity biotinylation (BioID) of bait proteins, requiring either antibodies for the proteins of interest or a fused tag on each individual bait protein (Liu *et al.*, 2018; Go *et al.*, 2021; Huttlin *et al.*, 2021).

So-called protein correlation profiling allows for the construction of PPI networks based on the concept that proteins that are fractioned together due to similar biophysical properties are more likely to also interact in complexes within a cell (Havugimana *et al.*, 2012; Kirkwood *et al.*, 2013). Previously, SILAC labeling techniques were used to additionally measure temporal changes of proteins within protein complexes (Kristensen *et al.*, 2012). Lately, combination of native separation or size exclusion chromatography (SEC) with TMT labeling showcased the possibility to measure protein fractions in a multiplex workflow, thereby reducing the overall LC-MS/MS machine time needed (Guerrero-Castillo *et al.*, 2021; Havugimana *et al.*, 2022; Doron-Mandel *et al.*, 2023). These high-throughput measurements of PPI now open the possibility to ask more interesting questions about the dynamics of PPI across different time dimensions or physiological conditions.

The cell is a collection of protein machinery that consists of modules and organelles formed through a myriad of interactions between proteins that adapt dynamically to external and internal cues (Alberts, 1998; Huttlin *et al.*, 2021; Tsitsiridis *et al.*, 2023). Therefore, global mapping of protein-protein interactions (PPIs) is a suitable and interesting approach to understanding what is happening within a cell (Gavin *et al.*, 2002). Pioneering work on characterizing protein interactions globally has been made initially in yeast (Gavin *et al.*, 2002, 2006). This was followed by studies in human cells, focusing on distinct protein families such as kinases (Gavin *et al.*, 2006; Varjosalo *et al.*, 2013) or human deubiquitinating enzymes (Sowa *et al.*, 2009). AP-MS is the most sensitive method to study protein interactions, and was also shown to be highly reproducible across different laboratories (Gavin *et al.*, 2006; Varjosalo *et al.*, 2013). AP-MS is also employed in an ongoing effort to probe the entire human proteome for proteins interactions, which is called BioPlex project (Huttlin *et al.*, 2015, 2017). BioPlex is performed by one laboratory employing one cellular system (293T), a standardized protocol and stable MS-set ups, thereby ensuring high-quality data for thousands of human proteins. The latest release of Bioplex encompasses data for 10,128 proteins, almost half of the expressed proteome of human cells (Huttlin *et al.*, 2021). It reports close to 120,000 interactions among 14,586 proteins (Huttlin *et al.*, 2021). Since proteins act mostly in complexes for their regulatory and catalytic functions it is of high relevance to also understand the composition of these complexes (Tsitsiridis *et*

al., 2023). A particularly powerful resource that collects this information is the comprehensive resource of mammalian protein complexes (CORUM), a collection of manually collected experimentally characterized protein complexes (Giurgiu *et al.*, 2019; Tsitsiridis *et al.*, 2023). Both resources BioPlex and CORUM have been elementary for the work presented in this thesis. An alternative to affinity purification for protein complex discovery within the cell is an approach that exploits the fact that proteins with similar biological properties that are often part of larger modules tend to co-elute on size exclusion chromatography (Heusel *et al.*, 2019; Doron-Mandel *et al.*, 2023). In addition, interacting proteins also co-localize within cells and therefore show up together in subcellular fractionation profiles (Mulvey *et al.*, 2017; Orre *et al.*, 2019).

1.5.2 Ribosome Profiling

The ribosome is the machinery responsible for synthesizing the proteins guided by the mRNA template in a cell, thereby defining the biochemical makeup and the role and function of a cell (Ingolia *et al.*, 2019) and serves additionally as hub for protein quality control (Pechmann *et al.*, 2013). (Figure 18). As described in detail above, during protein synthesis the speed of elongation varies across different transcripts (Gingold and Pilpel, 2011) and can be slowed down by a variety of mRNA-encoded features (Figure 4). Slowing the elongation speed can aid co-translational (i) protein folding (Pechmann and Frydman, 2013; Yu *et al.*, 2015), (ii) assembly of protein complexes, and (iii) protein targeting to the right organelle (Pechmann *et al.*, 2014; Chartron *et al.*, 2016). One of the best-studied systems involves the signal recognition particle (SRP) complex that co-translationally targets proteins to their proper membrane destination (Mandon *et al.*, 2013).

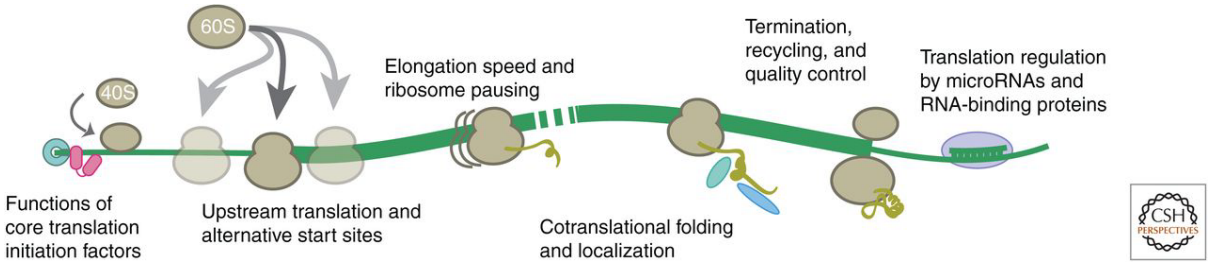

Figure 18. Insights in regulation of protein synthesis gained by ribosome profiling.

Overview of different steps of translational regulation and protein synthesis that can be quantified with the help of ribosome profiling.

Reprinted from Cold Spring Harb Perspect Biol., 11(5):a032698, Ingolia, NT., Hussmann, JA., Weissman, JS., Ribosome Profiling: Global Views of Translation, 2019, with permission from Cold Spring Harbor Laboratory press.

The study of such translation events has been very challenging until the development of ribosome profiling in 2009 (Ingolia *et al.*, 2009) a technique that informs about the position of the

ribosome at codon or nucleotide precision, revealing information about codon usage and novel means of translational regulation (Figure 19). Thanks to this technique completely new insights in translation, such as the development of computational models that can predict the translation initiation rate for all yeast genes and understand the factors that lead to variation in initiation could be suddenly understood and modeled (Shah *et al.*, 2013; Weinberg *et al.*, 2016). The first steps of ribosome profiling involve the sample collection and cell lysis which involves blocking translating ribosomes. It exploits the biological phenomena that during translation, the ribosome covers a fragment of approximately 30 nucleotides (Ingolia *et al.*, 2009). The core of the ribosome profiling strategy is based on halting the translating ribosomes and thereby protecting the mRNA they are bound to at this moment from nuclease that is applied in the protocol to digest away exposed and unprotected mRNA (Steitz, 1969; Wolin and Walter, 1988). The next step of ribosome profiling consists of the recovery of the ribosomes and the isolation and purification of the bound ribosome footprints (Ingolia *et al.*, 2009). Considering that the average mammalian cell encodes over 20,000 proteins with an average of 500 codons per coding region, digestion of all ribosome-protected mRNA footprints yields around ten million RNA fragments (Brar and Weissman, 2015). The fundamental innovation brought about by the contemporary ribosome profiling technique was to couple ribosome profiling to next generation short read sequencing which allows sequencing of these protected mRNA sections (termed Ribosome Protected Fragments, RPFs, or ribosome footprints) (Brar and Weissman, 2015), which is the next step of the procedure. Following sequencing, reads are mapped to a reference transcriptome or genome, revealing where the ribosome was located at the transcript at this very specific moment of harvest (Brar and Weissman, 2015). Similarly, the density of protected fragments on the transcript provides an estimate of the rate of protein synthesis (Brar and Weissman, 2015). In addition, doing parallel total RNA sequencing allows to compare the ribosome footprint density with the density of mRNA and thereby estimating the fraction of translated transcripts, or "translation efficiency" (Ingolia *et al.*, 2009). RPFs provide information about the dynamics of translation of a transcript. For instance, a high average abundance of RPFs across a transcript suggests high levels of translation; while a local over-abundance of RPFs within a sequence is frequently interpreted as ribosome pausing, or a region of slow translation (Ingolia *et al.*, 2009; Ingolia, 2014; Brar and Weissman, 2015).

In summary, the ribosome profiling procedure consists of (i) sample collection and cell lysis which involves blocking translating ribosomes, (ii) digestion of half of the cell lysate with nuclease to produce ribosome-protected RNA footprints, (iii) recovery of ribosomes, (iv) isolation and purification of ribosome footprints, (v) converting ribosome footprints into next-generation sequencing compatible libraries, (vi) deep sequencing of those libraries and alignment of the reads to a reference genome and optionally (vii) isolation and sequencing of RNA allowing to determine translational

efficiency for each mRNA (Ingolia *et al.*, 2009, 2012) (Figure 19). Among the main strengths of ribosome profiling are the sensitivity of the method, the precision of quantification, the accuracy of positional information, and the possibility of instant measurements (Ingolia *et al.*, 2014).

While protein-coding regions in the human genome had to be initially annotated based on simple rules such as a minimal length of ORFs, starting at the first AUG of a transcript or a bias in the codon usage (Brent, 2005); with the use of ribosome profiling, annotation of protein-coding regions became easier and more precise, and in addition, multiple new upstream open reading frames (uORFs), which are frequently involved in translational regulation, were characterized, such as the uORF for *activating transcription factor 4* (*ATF4*), *activating transcription factor 5* (*ATF5*), *Myc* or *Nanog* (Ingolia *et al.*, 2011). Since ribosome profiling further does not require any genetic manipulation it can be applied to any tissue or organism (Brar and Weissman, 2015) and the development of a ribo-seq genome browser makes many of these datasets publicly available and comparable (Michel *et al.*, 2014).

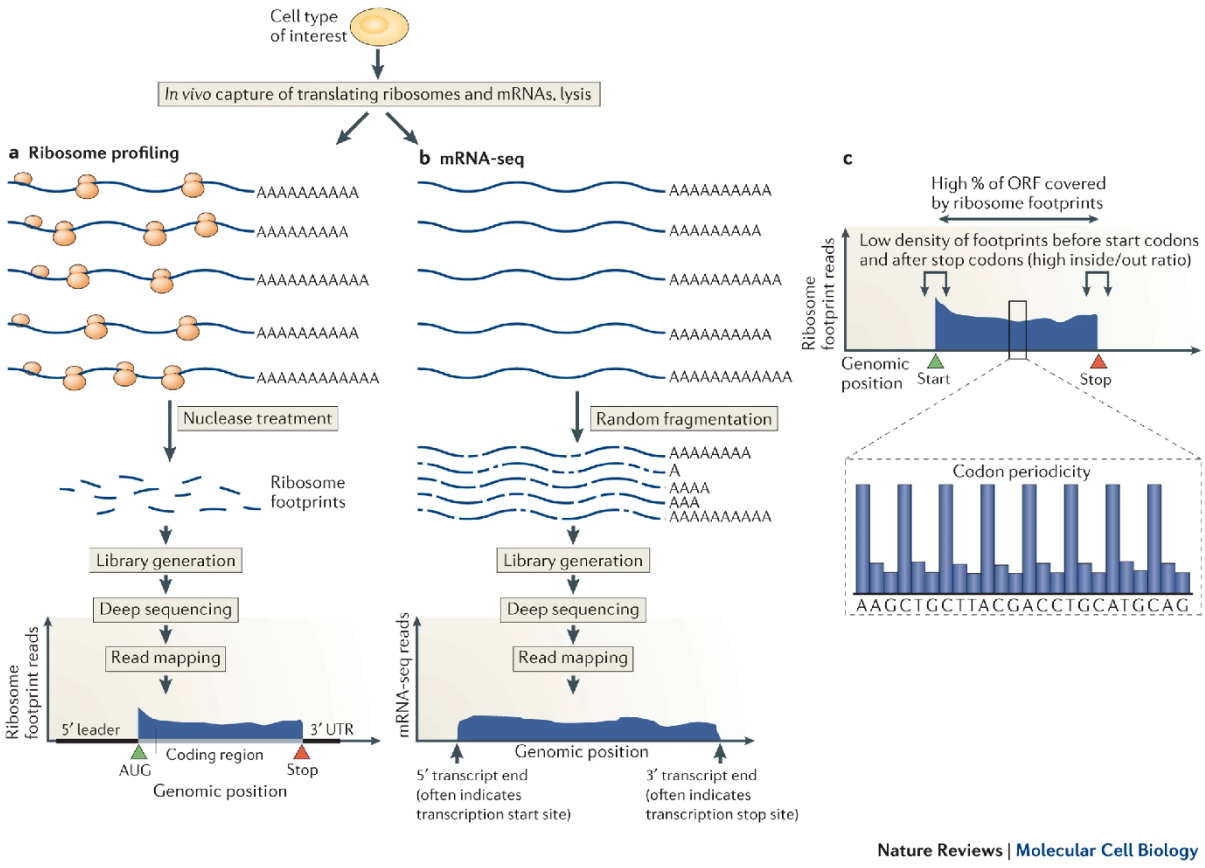

Figure 19. Schematic illustrating the process of ribosome profiling.

a. For ribosome profiling mRNAs bound to ribosome are isolated and treated with nonspecific nucleases. Fragments protected by the ribosome are isolated. These so-called ribosome footprints are converted in to NGS compatible libraries. NGS reads are then mapped to a reference genome. **b.** For classical mRNA sequencing, the complete mRNA transcripts are fragmented, converted to NGS libraries and NGS reads again mapped to a reference genome. **c.** Translated ORFs have a

stereotypic distribution of ribosome footprints across the coding region. Ribosome footprint density begins sharply at the start codon and ends sharply at the stop codon and shows indications of codon periodicity. *Reprinted from Nat Rev Mol Cell Biol, 16(11):651-64, Brar, GA., Weissman, JS., Ribosome profiling reveals the what, when, where and how of protein synthesis, 2015, with permission from Springer Nature*

1.5.3 Endogenous Protein Tagging in Human Cells

The standard approach for studying protein localization and also the method of choice for large protein localization collections such as the Cell Atlas, a subproject of the Human Protein Atlas, is to stain fixed cell samples with a protein-specific antibody and analyze its localization (Thul *et al.*, 2017). This approach is typically limited to fixed cell samples and requires the availability of specific antibodies. Fusing fluorescent proteins or other tags on endogenous proteins is an alternative approach that allows to study protein abundance and localization in live cells and also in their natural context (Bukhari and Müller, 2019). Due to the lower homologous recombination rate of mammalian cells, endogenous tagging was in the past mainly used in yeast models, where homologous recombination can be achieved naturally very efficiently (Baudin *et al.*, 1993; Ghaemmaghami *et al.*, 2003).

Thanks to the development of CRISPR/Cas9 as a genome-editing tool (Ran *et al.*, 2013; Doudna and Charpentier, 2014; Hsu *et al.*, 2014) endogenous tagging in mammalian cell model systems became easier to use (Roberts *et al.*, 2017; Bukhari and Müller, 2019) and even made the generation of large collections of endogenously tagged cell lines possible, such as the CeMM vpCells, or the OpenCell collection (Cho *et al.*, 2022).

For homology-directed repair (HDR) for programmed insertion of protein tags, gene-specific reagents for each position and gene have to be designed and synthesized. Since tags are inserted directly into the coding region of genes, it is important to consider in the design that inserted tags are in-frame with the encoded gene and to validate that insertions at the corresponding position do not disrupt endogenous protein function.

Using split proteins allows the insertion of a small tag into the endogenous protein while expressing the larger subunit of the tag somewhere else in the cell, which disrupts the target protein less and makes the synthesis and cloning of reagents more efficient (Serebrenik *et al.*, 2019; Reicher *et al.*, 2020; Cho *et al.*, 2022). The variety of split proteins encompasses, for example, fluorescent proteins such as the commonly used split-mNeonGreen2 system (Feng *et al.*, 2017) or the split-luciferase system that divides NanoLuc luciferase into a small 1.3 kDa subunit (Small BiT) and a large 18 kDa part (Large BiT) (Dixon *et al.*, 2016).

As the synthesis of individual homology templates for each position to be tagged is costly, generic exon tagging methods, acting independent of homology-directed repair, have been developed. They allow the use of the same donor template for all endogenous-tagging reactions and only need sgRNAs specific for the different positions to tag (Lackner *et al.*, 2015; Sakuma *et al.*, 2016; Schmid-Burgk *et al.*, 2016). Since with this method insertions happen within exons, all integrations must be in-frame with the coding sequence, which restricts the positions that can be targeted.

Another way of tagging proteins endogenously is the delivery of synthetic exons by retroviruses or transposons, that integrate randomly into the genome, an approach that is also termed "gene trapping" or "CD trapping" (Trinh and Fraser, 2013). Since these approaches rely on the random integration of viruses or transposons and those systems typically have integration site biases (Lewinski *et al.*, 2006), tagging a specific protein requires the isolation and screening of many individual clones. Through the addition of flanking splice acceptor and donor sites around the synthetic exons and by making the whole cassette excisable with a generic sgRNA, Serebrenik and colleagues created a synthetic exon system that can be integrated into introns and is, therefore, frame independent. By co-expression of this system with a site-specific sgRNA it allows specific tagging of proteins (Serebrenik *et al.*, 2019), an approach that can be combined with whole libraries of sgRNAs and is therefore high-throughput compatible (Reicher *et al.*, 2020) (Figure 20). This approach was employed for this thesis work to generate tagged mitochondrial proteins, that serve as reporters and are described in the results section below.

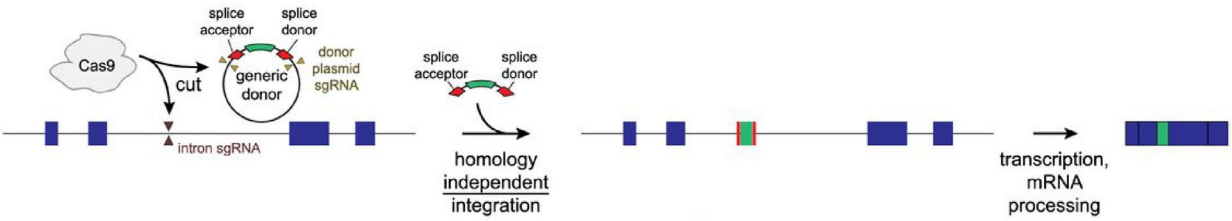

Figure 20. Homology-independent intron tagging of endogenous gene locus.

Schematic of the endogenous tagging approach based on the induction of double-strand breaks via Cas9 in intronic regions of the gene and subsequent integration of a synthetic exon which leads to fusion of a tag to the coding sequence. *Reprinted from Genome Res., 29: 1322-1328, Serebrenik, YV., Sansbury, SE., Kumar, SS., Henao-Mejia, J, Shalem, O., Efficient and flexible tagging of endogenous genes by homology-independent intron targeting, 2019, article from Cold Spring Harbor Laboratory press under Creative Commons License (Attribution-NonCommercial 4.0 International)*

2 Aims of this Thesis

A long-standing goal of systems biology has been to use a variety of omics techniques such as RNA expression analysis, expression proteomics, and ribosome profiling to dissect molecular processes in the cell. Genetic screens offer a useful additional tool to discover unknown molecular pathways and create hypothesis-generating studies.

Therefore, for the first aim of this thesis, we engineered a reporter-based genome-wide approach for the cell line THP-1 that allows us to characterize the molecular landscape involved in phagocytosis. This effort led then to the discovery of the entire hypusine axis as the most significantly scoring gene family for this process. At the center of the hypusine axis is eIF5A, an enigmatic protein that binds and acts among other things on the ribosome and has been reported to cause a myriad of cellular actions that remain to be finalized. Given that the knowledge about translational control is in its infancy we decided to gain a better understanding of the role of hypusine by engineering a toolbox specific for hypusine and making use of the omics readouts expression proteomics and ribosome profiling in cells perturbed for hypusination. In addition, our toolbox allowed us to perform a genome-wide survey for regulators of hypusination, which allowed us in summary to generate a global molecular survey of hypusination.

Overall, the aim was to address the following points:

i. What is the molecular regulation network of phagocytosis, and can we engineer methods to genome-wide screen for it?
ii. Why did we identify the hypusine axis as top-regulated machinery and how is it regulated?
iii. Can we engineer a toolbox specific for hypusine that allows its dissection?
iv. What are the proteins, transcripts, and genes affected by hypusination or vice versa?
v. Can we mechanistically dissection the role and regulation of hypusination?

3 Results

3.1 Prologue

Cellular metabolism is crucial for the function of immune cells. Functional genomics in combination with informative reporters offers a powerful approach to deciphering novel metabolic dependencies and bottlenecks. As it is known that macrophages undergo substantial metabolic reprogramming during differentiation and during processes such as phagocytosis, we set out to genetically screen for these dependencies in a macrophage cell line (Artyomov *et al.*, 2016; O'Neill and Pearce, 2016).

Using a CRISPR knock-out library that focuses on all solute carriers (SLCs), the largest group of facilitative and concentrative transporters in the human genome, we identify a transporter required for the efficient execution of phagocytosis (César-Razquin *et al.*, 2015). This was done by introducing this knock-out library into the monocytic cell line U937 which can be turned into a more macrophage-like state using a differentiation protocol (Liu and Wu, 1992). Using then a phagocytosis reporter that can be measured on FACS, transporters could be identified that modulate phagocytosis (Colas *et al.*, 2014). The transporter *SLC4A7* stands out as the most significant modulator of phagocytosis. Considering, that the cytoplasmic SLC4A7 is a known electroneutral sodium bicarbonate co-transporter we investigate next if acidification of the phagolysosome is influenced by this solute carrier protein (Romero *et al.*, 2013). And indeed, in the absence of *SLC4A7*, the acidification rate of the phagolysosome is slowed down.

3.2 Manuscript #1

Results section 3.2 contains the full reprint of the manuscript listed below. The author of this thesis is a co-author of the article. The article is from Elsevier and under open access Creative Commons CC-BY License.

Sedlyarov V[*], Eichner R[*], Girardi E, Essletzbichler P, Goldmann U, Nunes-Hasler P, Srndic I, Moskovskich A, Heinz L, Kartnig F, Bigenzahn J, Rebsamen M, Kovarik P, Demaurex N and Superti-Furga G[#] (2018) The Bicarbonate Transporter SLC4A7 Plays a Key Role in Macrophage Phagosome Acidification. Cell Host & Microbe 23, 766-774

[*]: equal contribution | [#]: corresponding author

Detailed information on the contribution of all authors is listed on page 8 (772) under “Author Contributions” of the article

Brief Report

Cell Host & Microbe

The Bicarbonate Transporter SLC4A7 Plays a Key Role in Macrophage Phagosome Acidification

Graphical Abstract

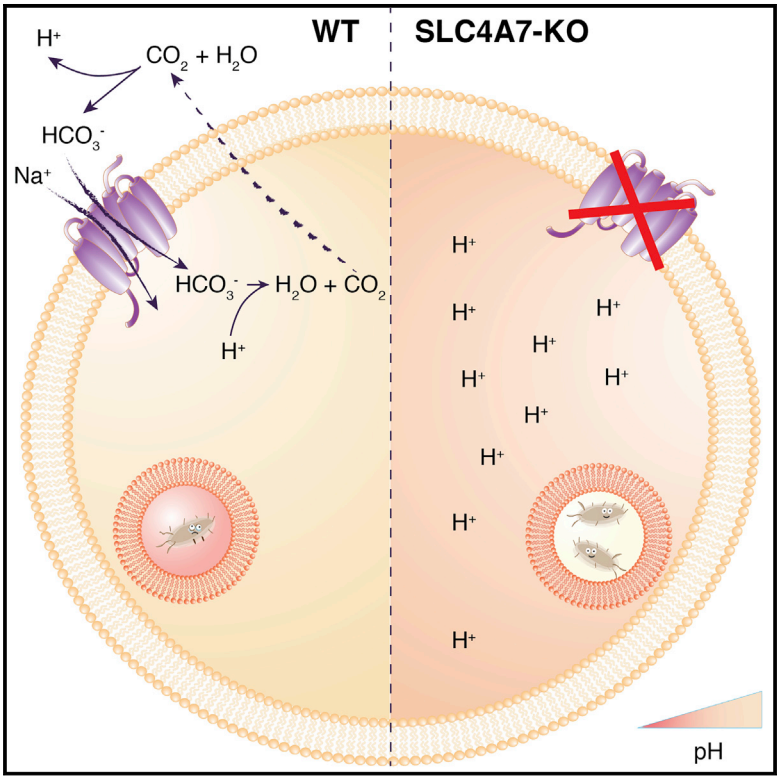

Authors

Vitaly Sedlyarov, Ruth Eichner, Enrico Girardi, ..., Pavel Kovarik, Nicolas Demaurex, Giulio Superti-Furga

Correspondence

gsuperti@cemm.oeaw.ac.at

In Brief

Phagosome acidification is a necessary step in pathogen clearance by macrophages. Sedlyarov et al. identify the bicarbonate transporter SLC4A7 as essential for phagosome acidification. SLC4A7-mediated bicarbonate import ensures homeostatic regulation of cytoplasmic pH. In the absence of SLC4A7, the macrophage cytoplasm acidifies, which perturbs phagosome maturation and impairs bacterial killing by macrophages.

Highlights

- CRISPR screen identifies SLC4A7 to be required for phagosome acidification
- Intracellular bacterial killing by macrophages is impaired in absence of SLC4A7
- Bicarbonate transport activity of SLC4A7 is required for phagosome acidification
- SLC4A7 regulates phagosome acidification via homeostatic control of cytoplasmic pH

Sedlyarov et al., 2018, Cell Host & Microbe *23*, 766–774
June 13, 2018
https://doi.org/10.1016/j.chom.2018.04.013

CellPress

CellPress

Cell Host & Microbe
Brief Report

The Bicarbonate Transporter SLC4A7 Plays a Key Role in Macrophage Phagosome Acidification

Vitaly Sedlyarov,[1,5] Ruth Eichner,[1,5] Enrico Girardi,[1] Patrick Essletzbichler,[1] Ulrich Goldmann,[1] Paula Nunes-Hasler,[2] Ismet Srndic,[1] Anna Moskovskich,[1] Leonhard X. Heinz,[1] Felix Kartnig,[1] Johannes W. Bigenzahn,[1] Manuele Rebsamen,[1] Pavel Kovarik,[3] Nicolas Demaurex,[2] and Giulio Superti-Furga[1,4,6,*]

[1]CeMM Research Center for Molecular Medicine of the Austrian Academy of Sciences, Vienna 1090, Austria
[2]Department of Cell Physiology and Metabolism, University of Geneva, Geneva 1211, Switzerland
[3]Max F. Perutz Laboratories, University of Vienna, Vienna Biocenter (VBC), Vienna 1030, Austria
[4]Center for Physiology and Pharmacology, Medical University of Vienna, Vienna 1090, Austria
[5]These authors contributed equally
[6]Lead Contact
*Correspondence: gsuperti@cemm.oeaw.ac.at
https://doi.org/10.1016/j.chom.2018.04.013

SUMMARY

Macrophages represent the first line of immune defense against pathogens, and phagosome acidification is a necessary step in pathogen clearance. Here, we identified the bicarbonate transporter SLC4A7, which is strongly induced upon macrophage differentiation, as critical for phagosome acidification. Loss of SLC4A7 reduced acidification of phagocytosed beads or bacteria and impaired the intracellular microbicidal capacity in human macrophage cell lines. The phenotype was rescued by wild-type SLC4A7, but not by SLC4A7 mutants, affecting transport capacity or cell surface localization. Loss of SLC4A7 resulted in increased cytoplasmic acidification during phagocytosis, suggesting that SLC4A7-mediated, bicarbonate-driven maintenance of cytoplasmic pH is necessary for phagosome acidification. Altogether, we identify SLC4A7 and bicarbonate-driven cytoplasmic pH homeostasis as an important element of phagocytosis and the associated microbicidal functions in macrophages.

Cellular metabolism is central to many specific functions of immune cells. Accordingly, the interplay between metabolism and specific functions of immune cells has emerged as key focus in immunological research (Buck et al., 2017). Macrophages represent the first line of immune defense against pathogens. Upon activation, they undergo massive metabolic reprogramming to allow execution of specialized programs such as phagocytosis (Artyomov et al., 2016; O'Neill and Pearce, 2016; Shapiro et al., 2011). An appropriate metabolic response requires the cell to rapidly interact with its environment for nutrient uptake and ion transport (Lin et al., 2015; Sahoo et al., 2014). Movement of metabolites and molecules across cellular membranes is mainly achieved by transporter proteins, such as solute carriers (SLCs), which represent the largest group of facilitative and concentrative transporters in the human genome (César-Razquin et al., 2015).

We hypothesized that SLCs could be essential for macrophages to undergo the metabolic changes associated with phagocytosis, and aimed for an appropriate model system suitable for CRISPR/Cas9-based genetic screens (Figure 1A).

Phagocytosis and phagosome maturation eventually lead to progressive acidification of phagolysosomes (Kinchen and Ravichandran, 2008). Phagosome acidification, detected by pH-dependent fluorophores is a valid surrogate endpoint to measure phagocytosis (Colas et al., 2014; Fine et al., 2017; Nunes et al., 2015; Surewaard and Kubes, 2017; Takahashi et al., 2017). We chose phorbol myristate acetate (PMA)-differentiated human myeloid U937 cells as a macrophage model system to detect and quantify phagosome acidification (Liu and Wu, 1992). We subjected differentiated U937 cells to phagocytosis assays with opsonized latex beads, which were coupled to a pH-sensitive (pHrodo) and a pH-insensitive dye (YG, yellow green) (Figure 1B) (Colas et al., 2014). The dual-colored beads allowed discrimination between cells that underwent phagocytosis and phagosome acidification (PhagoLate, YG and pHrodo-positive), cells that have bound and/or phagocytosed, but not acidified the cargo (PhagoEarly, only YG-positive), and cells that have neither bound nor incorporated any beads (PhagoNeg) (Figure 1B).

To validate our experimental strategy, we tested a range of pharmacological and genetic perturbations targeting different stages of the phagocytic process (Figure S1A). Disruption of phagocytic uptake using the actin polymerization inhibitor cytochalasin D led to ablation of the PhagoLate fraction with simultaneous increase of the PhagoNeg, but not the PhagoEarly fraction. By contrast, inhibition of phagosome acidification using the vacuolar-ATPase inhibitor bafilomycin A1 resulted in a strong decrease of the PhagoLate fraction, accompanied by an elevation of the PhagoEarly and, to lesser extent, of the PhagoNeg fraction. CRISPR-mediated knockout of nicotinamide adenine dinucleotide phosphate (NADPH) oxidase 2 (NOX2 or CYBB), a major producer of reactive oxygen species during phagocytosis, and of Lamp1 or Lamp2, important lysosomal structural proteins, resulted in a slight decrease of the PhagoLate and minor increases in the PhagoEarly and PhagoNeg fractions, corresponding to a slight decrease in phagosome acidification (Figure S1A). Finally, knockout of RAB7A, a small guanosine

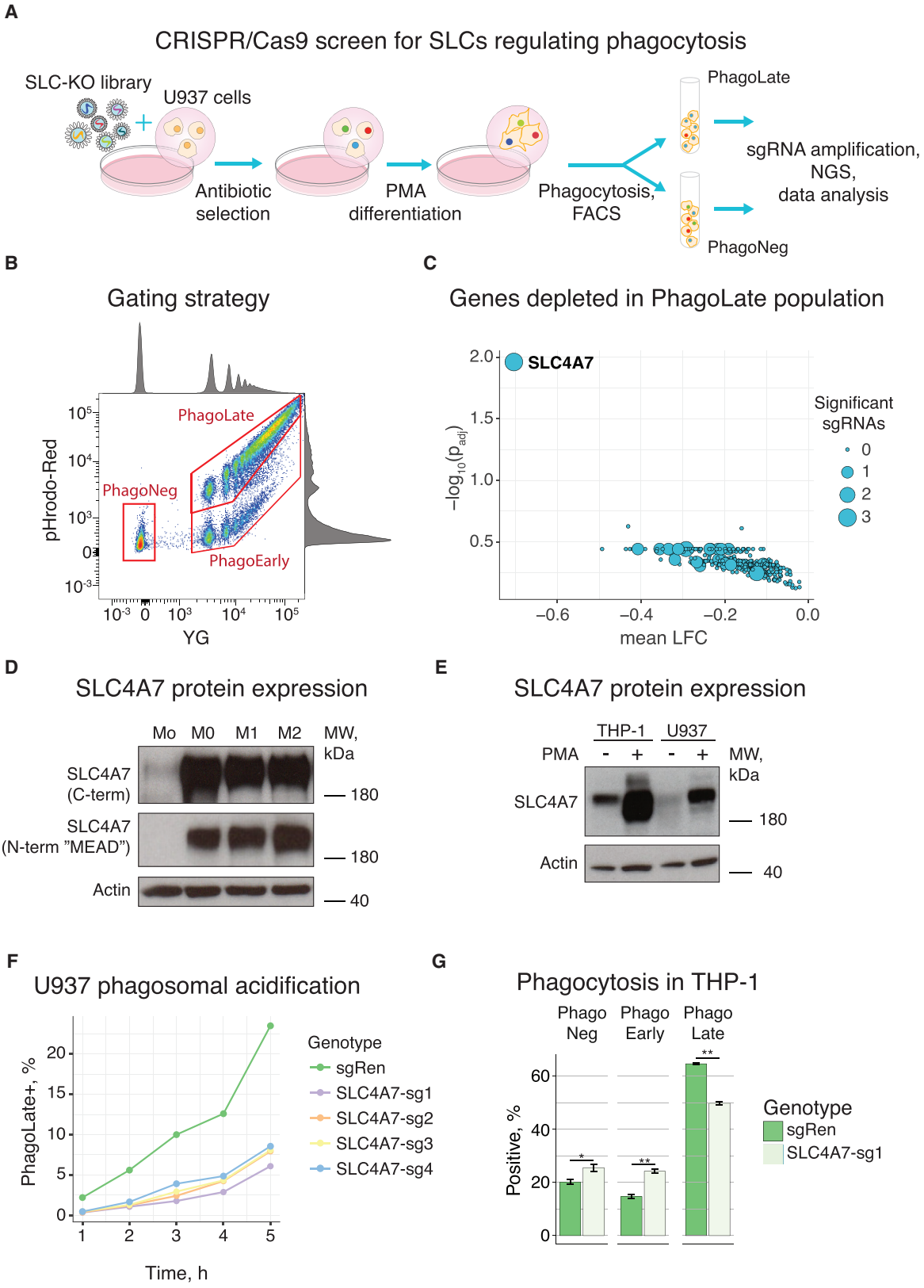

(legend on next page)

triphosphatase required for phagosome maturation and phagosome-to-lysosome fusion, strongly reduced the PhagoLate fractions, while strongly increasing the PhagoEarly, but not the PhagoNeg fractions, corresponding to a strong inhibition of phagosome maturation (Soldati et al., 1995; Via et al., 1997) (Figure S1A).

Having validated the experimental strategy, we set out to systematically identify SLCs involved in the regulation of phagocytosis. We established a CRISPR/Cas9-based loss-of-function screen using an SLC-wide knockout library, designed in our laboratory, and a fluorescence-activated cell sorting (FACS)-based readout. The pooled library targets 391 human SLC genes with six single guide RNAs (sgRNAs) per gene and additionally comprises sgRNAs targeting essential genes and non-targeting sgRNAs as controls. We infected U937 cells with lentiviral particles carrying the SLC knockout library and differentiated them with PMA to establish a macrophage-like phenotype (Figure 1A). To identify SLCs essential for phagocytosis, we isolated two populations via FACS: the phagocytosis- and acidification-positive fraction (PhagoLate) and the phagocytosis-negative population (PhagoNeg) (Figure 1B). After amplification and sequencing of the sgRNAs from each population, the reads were mapped and quantified using a two-step differential abundance analysis. After identifying differentially enriched sgRNAs using DESeq2 (Figure S1B; Data S1) (Love et al., 2014), we aggregated sgRNAs to genes using the gene set enrichment algorithm (Figure 1C) (Sergushichev, 2016; Subramanian et al., 2005). Strikingly, among all SLCs, SLC4A7 was the only gene significantly depleted from the PhagoLate fraction (Figures 1C and S1B).

SLC4A7, also known as NBCn1 and NBC3, is an electroneutral sodium bicarbonate co-transporter involved in maintenance of cytosolic pH by extruding acid equivalents (Lee et al., 2014; Romero et al., 2013). SLC4A7 has a high number of different isoforms, which show tissue-specific expression and differ in surface abundance and transport activity. They arise from two alternative promotors, three optional structural elements (cassettes I-III), and respective alternative splicing (Figure S1C) (Liu et al., 2013; Parker and Boron, 2013; Pushkin et al., 1999). SLC4A7 is expressed in several cell types and tissues including brain, heart, and kidney (Damkier et al., 2007; Liu et al., 2015; Pushkin et al., 1999; Romero et al., 2013). Although data on SLC4A7 expression in the immune system are scarce, there is evidence for a specific role in macrophages. SLC4A7 was shown to be strongly upregulated upon macrophage colony-stimulating factor (M-CSF)- and receptor activator of nuclear factor-κB ligand-induced osteoclast differentiation (Riihonen et al., 2010). Moreover, a transcriptional study identified SLC4A7 among the genes differentially expressed during the monocyte-to-macrophage differentiation and polarization (Martinez et al., 2006). To further investigate the potential specific role of SLC4A7 in macrophages, we treated primary human monocytes with M-CSF and observed a strong upregulation of SLC4A7 upon macrophage differentiation, suggesting a particular function in macrophage biology (Figure 1D). Polarization of macrophages to the M1 phenotype or the M2 phenotype did not further modulate SLC4A7 protein abundance (Figure 1D). Consistently, the expression levels of SLC4A7 in human U937 and THP-1 cells strongly increased upon PMA-induced differentiation toward macrophages (Figure 1E).

To validate the findings of the CRISPR screen, we generated SLC4A7-deficient U937 cells using four different sgRNAs targeting different exons common to all SLC4A7 isoforms (Figures S1C and S1D). After confirming SLC4A7 knockout efficiency by immunoblot (Figure S1D), we performed phagocytosis assays with the respective U937 cells at different time points. Importantly, at each time point, all four sgRNAs resulted in strongly decreased numbers of PhagoLate cells as compared with control cells infected with a non-targeting sgRNA (sgRen, directed toward *Renilla* luciferase) (Figure 1F).

If SLC4A7 plays a fundamental role in phagocytosis, it should do so also in other human macrophage model cell lines. We CRISPR/Cas9-inactivated SLC4A7 in human THP-1 myeloid cells and differentiated them with PMA. Phagocytosis assays showed a significant reduction in the PhagoLate fraction upon SLC4A7 knockout, which was accompanied by an increase in

Figure 1. SLC-Focused CRISPR/Cas9 Genetic Loss-of-Function Screens Identify SLC4A7 to Be Important for Phagosome Acidification

(A) Schematic representation of the major steps of the SLC-focused CRISPR/Cas9 screen to identify SLCs involved in phagocytosis.

(B) Representative flow cytometry scatterplot of phagocytosis assays. PMA-differentiated U937 cells were incubated with dual-colored opsonized beads. Each dot represents one cell: intensity of the pH-insensitive dye (YG) is displayed on the x axis, intensity of pH-sensitive dye (pHrodo-Red), whose signal intensity increases with decrease in pH, is shown on the y axis. Double-negative cells were classified as phagocytosis-negative (PhagoNeg), double-positive cells (YG and high pHrodo-Red signal) were classified as cells having undergone phagocytosis and phagosome acidification (PhagoLate), and single positive cells (YG and low pHrodo-Red signal) were classified as cells at early stages of phagocytosis (PhagoEarly). The marginal intensity distributions are shown on the sides of the plot.

(C) Volcano plot showing the statistical significance of genes depleted in the PhagoLate population on the y axis as $-\log_{10}(p_{adj})$ against average $\log_2$ fold-change (mean LFC) on the x axis calculated for all sgRNAs per gene. The size of the dots represents the number of significant changes in sgRNAs counts. See Figure S1B for differential abundance of individual sgRNAs.

(D) Immunoblot analysis of primary human monocytes (Mo) derived from peripheral blood and M-CSF-differentiated monocyte-derived human macrophages, which were unpolarized (M0), or polarized toward M1 phenotype with interferon-γ and lipopolysaccharide, or to M2 phenotype with interleukin-4. Respective lysates were probed with an anti-SLC4A7 antibody detecting all isoforms (C-terminal epitope) and an anti-SLC4A7 antibody detecting an N-terminal epitope present only in isoforms starting with the amino acids "MEAD." Actin was used as loading control. MW, molecular weight. See Figure S1C for isoforms.

(E) Representative immunoblot analysis of SLC4A7 expression in undifferentiated and PMA-differentiated THP-1 and U937 cells. Actin was used as loading control. MW, molecular weight.

(F) Representative kinetics of phagosome acidification in four independent SLC4A7 knockout (sg1-sg4) and control (sgRen) U937 cells. After PMA differentiation, U937 cells were incubated with dual-colored beads and analyzed at the indicated time points using flow cytometry. The fraction of PhagoLate cells is displayed against the incubation time with beads. See Figure S1D for confirmation of SLC4A7 knockdown.

(G) Phagocytosis assays with PMA-differentiated SLC4A7 knockout (sg1) or control (sgRen) THP-1 cells, which were incubated with dual-colored beads as described in (B). Bar graphs show the fraction of PhagoLate, PhagoEarly, and PhagoNeg cells as assessed by pHrodo and YG fluorescence in flow cytometry. Data are mean ± 95% confidence interval from four replicates. *$p < 0.05$, **$p < 0.001$; by Welsh's t test.

the PhagoEarly and, to a minor extent, of the PhagoNeg fraction (Figure 1G). This pattern was comparable with the phenotype of hampered phagosome acidification (Figure S1A). Therefore, the reduced number of PhagoLate cells was assumed to be the main effect, with the changes in the other fractions being secondary phenomena.

Together, the data demonstrate the general importance of SLC4A7 for phagosome acidification. To test the relevance of these findings for host-pathogen interactions, we subjected SLC4A7 knockout and control U937 cells to phagocytosis assays with pHrodo-labeled heat-inactivated *Staphylococcus aureus*. In analogy to labeled beads, we witnessed a strong decrease in the capacity of SLC4A7 knockout cells for acidification of phagocytosed bacteria (Figure S1E), suggesting that SLC4A7 is important for phagosome acidification of pathogens.

To test the specificity of the phenotype, we undertook reconstitution experiments. Among the different isoforms of SLC4A7, we chose two representative forms: isoform 1 (NBCn1-A), the canonical form, which is mainly expressed in cardiac and skeletal muscle, and isoform 6 (NBCn1-G), the most common form, which is expressed in various tissues and differs from isoform 1 in both N terminus and two splicing cassettes (Figure S1C) (Cooper et al., 2006; Liu et al., 2013). U937 sgRen and sgSLC4A7 cells were successfully reconstituted with lentiviral overexpression constructs coding for isoform 1 or 6 of SLC4A7, as confirmed by immunoblotting (Figure S1F). Overexpression of both isoforms increased the PhagoLate cell fraction beyond the mere rescue of deficient phagosome acidification (Figure 2A). Markedly, in U937, isoform 6 appeared to be more potent in increasing phagosome acidification than isoform 1, which could result from its reported higher bicarbonate transport and pH-buffering capacity (Liu et al., 2013). Interestingly, an antibody directed against the N-terminal sequence containing the amino acids "MEAD," present in isoform 6, but not 1 (Figure S1C), confirmed that MEAD-forms of SLC4A7 were induced in macrophages, and hence are of physiological relevance (Figure 1D). In THP-1 cells, overexpression of both SLC4A7 isoforms also increased the degree of phagosome acidification beyond the mere rescue of the sgSLC4A7 phenotype (Figures 2B and S1G). In this cellular context, however, there was no difference between isoform 1 and 6, which may result from the higher baseline phagocytic rate and saturation of the system (Figure 2B).

The microbicidal activity of phagosomes results from direct bacterial killing in an acidic environment and activation of pH-sensitive antimicrobial enzymes (Flannagan et al., 2015). To test if impaired phagosome acidification upon SLC4A7 loss decreased the intracellular bacterial killing capacity, we performed intracellular bacterial killing assays and infected PMA-differentiated THP-1 cells with Gram-negative (*Escherichia coli* K12) and Gram-positive (*Streptococcus pyogenes* ΔSLO strain and *Staphylococcus carnosus*) bacteria. Importantly, THP-1 cells deficient for SLC4A7 showed a significantly reduced intracellular killing capacity toward *E. coli*, *S. pyogenes*, and *S. carnosus*, compared with control cells (Figure 2C, left panel). Upon reconstitution of knockout cells with SLC4A7 isoform 6, the phenotype was rescued and normal intracellular bactericidal capacity restored (Figure 2C, left panel). Next, we performed intracellular killing assays with the *S. aureus* strains Newman and USA300, which both stem from clinical isolates. While Newman is pH sensitive, USA300 depends on phagosome acidification for intracellular survival and proliferation within macrophages (Tranchemontagne et al., 2016). In line with previous results, SLC4A7-deficient THP-1 cells displayed a reduced killing capacity toward the *S. aureus* Newman strain. In contrast, killing of the *S. aureus* USA300 strain was increased in the knockout cells compared with control (Figure 2C, right panel), suggesting impaired intracellular survival due to reduced acidification. Taken together, these data provide strong evidence for the importance of SLC4A7 in efficient phagosome acidification and microbicidal potency of the cells.

Given its role in bicarbonate transport and pH regulation, and the evidence that SLC4A7 isoforms with distinct bicarbonate transport capacity differentially affected phagosome acidification (Figure 2B), it can be concluded that SLC4A7-mediated bicarbonate transport is essential for proper phagosome acidification. If located at phagosomal membranes, SLC4A7 could theoretically affect phagosomal pH directly. By contrast, if localized exclusively at the plasma membrane, the mechanism would likely be indirect via regulation of cytoplasmic pH. Visualization of endogenous SLC4A7 in PMA-differentiated THP-1 cells using indirect immunofluorescence revealed a predominant localization of SLC4A7 at the plasma membrane (Figure 2D), which is in line with previous reports (Loiselle et al., 2003; Wang et al., 2015a). To investigate the dynamic localization of SLC4A7 during phagocytosis, we expressed GFP-tagged SLC4A7 isoform 6 in THP-1 cells and exposed them to pHrodo-labeled heat-inactivated *S. aureus* or dual-colored (pHrodo and bright blue) beads. Live-cell microscopy including time-lapse imaging confirmed the cell surface localization of SLC4A7 (Figure 2E; Video S1). Importantly, no association of SLC4A7 with the phagosomal cargo could be observed during the phagocytic process (Figure 2E; Video S1).

To test the hypothesis that SLC4A7 regulates phagosome acidification indirectly via dynamic cytoplasmic pH regulation, we undertook live-cell microscopy-based experiments. Using the ratiometric cytoplasmic pH indicator, BCECF-AM, and pHrodo-coated bacteria and beads, we simultaneously measured cytosolic and phagosomal pH at different time points during the phagocytic process (Figures S2A and S2B). At 1 hr after onset of phagocytosis of beads, neither average pHrodo intensity nor cytoplasmic pH differed between SLC4A7 knockout and control THP-1 cells (Figure 2F). At 6 hr, however, with increasing phagosome acidification, differences became apparent: while the phagosomal cargos were less acidified in SLC4A7 knockout cells, the cytoplasm was significantly more acidic (Figures 2F and S2C). Reduced phagosome acidification accompanied by more acidic cytoplasmic pH upon SLC4A7 knockout was consistently observed across different cell lines (THP-1 and U937) and phagosomal cargos (beads and heat-killed *S.aureus*) (Figures 2F and S2C).

Together with its specific upregulation upon macrophage differentiation, these findings argue against a general housekeeping role of SLC4A7 in cytosolic pH homeostasis. Instead, SLC4A7 seems to be of particular relevance for counteracting cytoplasmic acidification during the phagocytic process.

We next wanted to investigate whether bicarbonate transport was essential for SLC4A7-mediated pH regulation. As the 3D

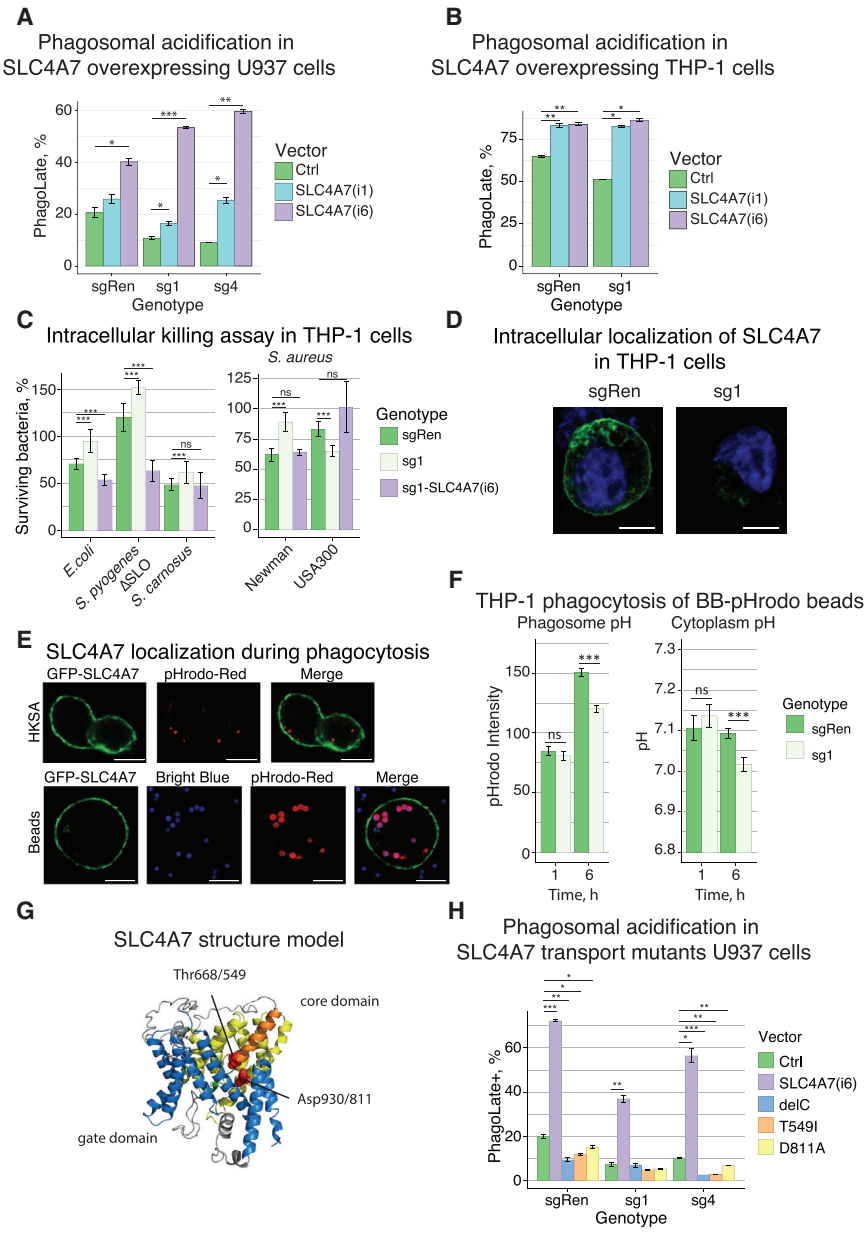

Figure 2. Functional Consequences of SLC4A7 Knockout and Overexpression

(A) Phagocytosis assays with control (sgRen) and SLC4A7 knockout (sg1, sg4) U937 cells, which were lentivirally infected to exogenously express HA-tagged SLC4A7 isoform 1, isoform 6, or empty vector control (Ctrl), respectively. Cells were incubated with dual-colored beads as described in Figure 1B. Bar graphs show the fraction of PhagoLate, PhagoEarly, and PhagoNeg cells as assessed by flow cytometry. Data are mean ± 95% confidence interval from three replicates. *p < 0.05, **p < 0.01, ***p < 0.001; by Welsh's t test. See Figure S1F for immunoblot confirmation of SLC4A7 knockout and exogenous expression.

(B) Phagocytosis assays with control (sgRen) and SLC4A7 knockout (sg1) THP-1 cells, which were lentivirally infected to exogenously express HA-tagged SLC4A7 isoform 1, isoform 6, or empty vector control (Ctrl), respectively. Cells were incubated with dual-colored beads as in Figures 1B and 2A. Bar graphs show the fraction of PhagoLate, PhagoEarly, and PhagoNeg cells as assessed by flow cytometry. Data are mean ± SD from two replicates. *p < 0.05, **p < 0.01; by Welsh's t test. See Figure S1G for immunoblot confirmation of SLC4A7 knockdown and exogenous expression.

(C) Intracellular killing assay with viable Gram-negative (*E. coli*) and Gram-positive (*Streptococcus pyogenes* ΔSLO, *Staphylococcus carnosus* Schleifer and Fischer, and *Staphylococcus aureus* Newman and USA300) bacteria in control (sgRen), SLC4A7 knockout (sg1), and SLC4A7 knockout reconstituted with SLC4A7 isoform 6 (sg1-SLC4A7(i6)) THP-1 cells. Bar graphs depict the percentage of surviving intracellular bacteria in relation to time point zero. Data are median and interquartile range from three replicates. ns, not significant, ***p < 0.001; by Wilcoxon-Mann-Whitney test.

(D) Representative confocal immunofluorescence images of endogenous SLC4A7 in control (sgRen) or SLC4A7 knockout (sg1) THP-1 cells. PMA-differentiated cells were fixed and stained with anti-SLC4A7 antibody (green). DNA was counterstained with DAPI (blue). The overlay of both signals is depicted. Scale bars, 5 μm.

(E) Representative confocal live-cell immunofluorescence images of THP-1 cells expressing GFP-tagged SLC4A7 isoform 6. After PMA-induced differentiation, cells were incubated with pHrodo-labeled heat-killed *S. aureus* (HKSA, upper panel) or dual-colored beads (pHrodo and bright blue; lower panel). Single channel images and respective overlays are shown. Scale bars, 10 μm. For time-lapse acquisitions, see Video S1.

(F) Simultaneous measurement of cytoplasmic and phagosomal pH during phagocytosis using live-cell microscopy. PMA-differentiated control (sgRen) and SLC4A7 knockout (sg1) THP-1 cells were loaded with BCECF-AM, incubated with dual-colored beads (pHrodo and bright blue), and imaged at the indicated time points. Incubation and imaging were done in Hank's balanced salt solution with 10% FCS at 37°C in 5% CO_2. At each time point, z stacks of five different fields were acquired per replicate. Bar charts represent pHrodo intensities of phagocytosed beads or cytoplasmic pH as calculated based on the BCECF calibration curve. Data are mean and 95% confidence interval from three replicates. ***p < 0.001; by Welch's t test. For *in situ* calibration of the BCECF 490/440 ratio, see Figure S2A; for example images, see Figure S2B. For simultaneous cytoplasmic and phagosomal pH measurements in THP-1 cells phagocyting heat-killed *S. aureus*, see Figure S2C (left panel), and for U937 cells phagocytosing beads, see Figure S2C (right panel).

(G) Schematic representation of the SLC4A7 model with the transmembrane domains (TMDs) of the core domain in yellow and the TMDs of the gate domain in blue. Helix 3 and helix 10, which align to form a continuous helix near the putative substrate binding site, are shown in orange and green, respectively. The residues mutated in the functional studies are shown in red with the isoform1/isoform6 numbering scheme.

(H) Phagocytosis assays with two independent U937 clones with SLC4A7 knockout (sg1, sg4) or control (sgRen), which were infected with lentiviral expression constructs coding for Strep-HA-tagged SLC4A7 isoform 6 (SLC4A7(i6)), an isoform 6 mutant lacking amino acids 1,008–1,131 (delC), two different predicted transport mutants (T549I and D811A), or empty vector control (Ctrl). PMA-differentiated cells were incubated with dual-colored beads as in Figure 1B and analyzed by flow cytometry. Bar graphs show the fraction of PhagoLate cells as assessed by pHrodo fluorescence intensity. Data are mean and 95% confidence interval from two replicates. *p < 0.05, **p < 0.01, ***p < 0.001; by Welsh's t test. For subcellular localization of the different proteins, see immunofluorescence analysis in Figure S2E.

structure of SLC4A7 is unknown, we generated a model of the transmembrane region of SLC4A7 with the I-Tasser Suite (Yang et al., 2015), using the available SLC4A1 structure as a template (PDB: 4YZF; Arakawa et al., 2015). The C-terminal domain of SLC4A7 shares 42% sequence identity with the corresponding domain of SLC4A1, and the model closely resembles the overall SLC4A1 architecture (Figure 2G). Mapping of functionally important residues on our model identified Asp930 (Asp811 in isoform 6) and Thr668 (Thr549 in isoform 6) as positions likely to be required for transporter activity (Figure 2G). Asp930 corresponds to SLC4A1 Glu681, a residue critical for anion exchange, while Thr668 corresponds to Ser465 in SLC4A1, a position tolerating only conservative mutations (Chernova et al., 1997; Barneaud-Rocca et al., 2013; Bonar et al., 2013). We generated mutant versions of SLC4A7 isoform 6 carrying the Asp811Ala (D811A) or the Thr549Ile (T549I) point mutation (Figure 2G). In addition, we generated a deletion mutant lacking the cytoplasmic C-terminal domain of SLC4A7, which contains a PDZ domain and is essential for membrane localization and function of SLC4A7 (Loiselle et al., 2003). We used all three mutants to reconstitute U937 cells lacking endogenous SLC4A7. Importantly, both the D811A and T549I transport mutants showed expression levels and subcellular localization comparable with the wild-type protein, whereas the C-terminal deletion mutant failed to localize to the plasma membrane (Figures S2D and S2E) (Loiselle et al., 2003). Notably, neither wild-type nor mutated SLC4A7 co-localized with the lysosomal marker Lamp1 (Figure S2E). In contrast to the wild-type protein, none of the three SLC4A7 mutants was able to rescue the phenotype of SLC4A7 knockout (Figure 2H). Whereas failure of the deletion mutant to rescue could be explained by its mislocalization (Figure S2E), the inability of both point mutants to rescue phagosome acidification suggested that transporter activity is essential for the biological function of SLC4A7. This supports the assumption that bicarbonate import into the cytosol is essential for cytosolic pH homeostasis and efficient phagosome acidification.

How Do We Envisage the Role of SLC4A7 in the Regulation of Phagocytosis?

The process of phagocytosis is associated with a rapid and transient acidification of the cytoplasm, which is believed to result from both respiratory burst and increased metabolic acid production (Coakley et al., 2002; Grinstein et al., 1991; Morgan et al., 2009; Swallow et al., 1991). Failure to counterbalance the cytoplasmic acidification results in cytoplasmic hyper-acidification, which, among others, inhibits the NADPH oxidase and reduces phagosome acidification (Coakley et al., 2002; Morgan et al., 2009). So far, it was assumed that Na^+/H^+ exchangers, passive proton conductance channels, and voltage-gated proton channels are the main players responsible for counteracting the initial cytoplasmic acidification (Coakley et al., 2002; Morgan et al., 2009). However, many studies were undertaken in nominally bicarbonate-free buffers, suggesting that the impact of bicarbonate transporters might have been overlooked.

The strong induction of SLC4A7 during macrophage differentiation, and the failure to maintain cytoplasmic pH during phagocytosis upon genetic inactivation, suggest SLC4A7 to be of key importance for pH homeostasis in phagocyting macrophages. Cell surface localization of SLC4A7 and the inability of transport mutants to maintain the biological function of SLC4A7 support a model in which SLC4A7-mediated bicarbonate import into the cytoplasm is crucial for net acid extrusion and maintenance of cytoplasmic pH during phagocytosis. Acidification of the cytoplasm, observed upon SLC4A7 loss, results in impaired acidification of phagosomes and reduced bactericidal capacity (Coakley et al., 2002; Grinstein et al., 1991; Morgan et al., 2009; Hackam et al., 1999).

Phagocytosis, a defining function of macrophages, is a fundamental process throughout macrophage-mediated immunity, starting from the first-line host defense against invading pathogens to removal of apoptotic cell debris associated with tissue remodeling and homeostasis. Given that SLC4A7 affected intracellular bacterial killing or intracellular survival of acid-sensitive and acid-dependent bacteria, respectively, we assume that a wide range of pathogens, including also viruses or parasites, may be affected by SLC4A7 function. This opens the possibility of modulating the activity of this transporter as anti-infective strategy (Huynh and Grinstein, 2007; Ip et al., 2010; Tranchemontagne et al., 2016; Wieland et al., 2004). Failure to remove dead cells and debris in SLC4A7 deficiency may lead to prolonged inflammatory conditions, which in turn may be associated with different pathologies, including cancer, extending the relevance of SLC4A7 function beyond infectious diseases (Novak and Thorp, 2013; Szondy et al., 2014).

Irrespectively, the unequivocal role of SLC4A7 in phagosome acidification of macrophages is surprising, as the protein had not been previously associated with any immune function (Boedtkjer et al., 2011a; Chen et al., 2012; Lopez et al., 2005).

This initial study will clearly have to be followed by animal studies, empowered, for example, by available knockout mice illuminating the role of SLC4A7 in animal physiology (Boedtkjer et al., 2011b; Lee et al., 2016). Nonetheless, the fundamental contribution of SLC4A7 to phagosome acidification is another case where a member of the SLC family is discovered to regulate fundamental biological processes (Rebsamen et al., 2015; Rusu et al., 2017; Wang et al., 2015b). The approach described here, employing a CRISPR/Cas9 library focusing on the entire SLC family allowing for analyses with high coverage and great statistical power, is likely to be instrumental in the uncovering of more roles for this still poorly characterized class of drug targets (César-Razquin et al., 2015; Lin et al., 2015).

STAR★METHODS

Detailed methods are provided in the online version of this paper and include the following:

- KEY RESOURCES TABLE
- CONTACT FOR REAGENT AND RESOURCE SHARING
- EXPERIMENTAL MODEL AND SUBJECT DETAILS
  - Cell Culture
  - Primary Cells and Monocyte to Macrophage Differentiation
  - Culture and Preparation of Bacteria
- METHOD DETAILS
  - SLC-Focused CRISPR/Cas9 Screen
  - Analysis of CRISPR Screens

SUPPLEMENTAL INFORMATION

Supplemental Information includes two figures, one table, one video, and one data file and can be found with this article online at https://doi.org/10.1016/j.chom.2018.04.013.

ACKNOWLEDGMENTS

We thank J. Praetorius (Aarhus University, Denmark) and J. Casey (University of Alberta, Canada) for providing serum from anti-SLC4A7 immunized mice. We thank N. Sedlyarova, G.I. Vladimer, T. Pemovska, and D. Lackner for assistance, scientific discussion, and critical reading of the manuscript. CeMM and the Superti-Furga laboratory are supported by the Austrian Academy of Sciences (G.S.-F. and I.S.). We acknowledge receipt of third-party funds from the Austrian Science Fund (FWF I2192-B22 ERASE, V.S.; FWF F4711-B20 Myeloid Neoplasms, J.W.B. and F.K.; FWF P29250-B30 VITRA, E.G.; FWF W1205 DK CCHD, A.M.), the European Research Council (ERC AdG 695214 GameofGates, P.E., U.G., and M.R.), the European Commission (Marie Skłodowska-Curie Action Fellowship 661491, E.G.), the European Molecular Biology Organization (EMBO Long-Term Fellowship ALTF245–2017, R.E.), and Boehringer Ingelheim (Research Collaboration Agreement BI-CeMM 238114, L.X.H. and M.R.).

AUTHOR CONTRIBUTIONS

Conceptualization, G.S.-F., V.S., and R.E.; Methodology, G.S.-F., V.S., R.E., P.K., P.N.-H., and N.D.; Investigation, V.S., R.E., E.G., P.E., I.S., A.M., F.K., J.W.B., L.X.H., P.K., P.N.-H., and M.R.; Formal Analysis, V.S. and U.G.; Data Curation, V.S. and U.G.; Writing – Original Draft, R.E., V.S., and G.S.-F.; Writing – Review & Editing, R.E., V.S., and G.S.-F.; Visualization, R.E. and V.S.; Project Administration, V.S. and G.S.-F.; Funding Acquisition, G.S.-F.; Supervision, G.S.-F.

DECLARATION OF INTERESTS

The Superti-Furga laboratory at CeMM has an active research collaboration with Boehringer Ingelheim (Research Collaboration Agreement BICeMM 238114).

Received: October 25, 2017
Revised: March 14, 2018
Accepted: April 19, 2018
Published: May 17, 2018

REFERENCES

Arakawa, T., Kobayashi-Yurugi, T., Alguel, Y., Iwanari, H., Hatae, H., Iwata, M., Abe, Y., Hino, T., Ikeda-Suno, C., Kuma, H., et al. (2015). Crystal structure of the anion exchanger domain of human erythrocyte band 3. Science *350*, 680–684.

Artyomov, M.N., Sergushichev, A., and Schilling, J.D. (2016). Integrating immunometabolism and macrophage diversity. Semin. Immunol. *28*, 417–424.

Barneaud-Rocca, D., Etchebest, C., and Guizouarn, H. (2013). Structural model of the anion exchanger 1 (SLC4A1) and identification of transmembrane segments forming the transport site. J. Biol. Chem. *288*, 26372–26384.

Blomen, V.A., Majek, P., Jae, L.T., Bigenzahn, J.W., Nieuwenhuis, J., Staring, J., Sacco, R., van Diemen, F.R., Olk, N., Stukalov, A., et al. (2015). Gene essentiality and synthetic lethality in haploid human cells. Science *350*, 1092–1096.

Boedtkjer, E., Praetorius, J., Matchkov, V.V., Stankevicius, E., Mogensen, S., Füchtbauer, A.C., Simonsen, U., Füchtbauer, E.-M., and Aalkjaer, C. (2011a). Disruption of Na^+,HCO_3^- cotransporter NBCn1 (slc4a7) inhibits no-mediated vasorelaxation, smooth muscle Ca^{2+} sensitivity, and hypertension development in miceclinical perspective. Circulation *124*, 1819–1829.

Boedtkjer, E., Praetorius, J., Matchkov, V.V., Stankevicius, E., Mogensen, S., Füchtbauer, A.C., Simonsen, U., Füchtbauer, E.-M., and Aalkjaer, C. (2011b). Disruption of Na^+,HCO_3^- cotransporter NBCn1 (slc4a7) inhibits NO-mediated vasorelaxation, smooth muscle Ca^{2+} sensitivity, and hypertension development in mice. Circulation *124*, 1819–1829.

Bonar, P., Schneider, H.-P., Becker, H.M., Deitmer, J.W., and Casey, J.R. (2013). Three-dimensional model for the human Cl^-/HCO_3^- exchanger, AE1, by homology to the *E. coli* ClC protein. J. Mol. Biol. *425*, 2591–2608.

Buck, M.D., Sowell, R.T., Kaech, S.M., and Pearce, E.L. (2017). Metabolic instruction of immunity. Cell *169*, 570–586.

César-Razquin, A., Snijder, B., Frappier-Brinton, T., Isserlin, R., Gyimesi, G., Bai, X., Reithmeier, R.A., Hepworth, D., Hediger, M.A., Edwards, A.M., et al. (2015). A call for systematic research on solute carriers. Cell *162*, 478–487.

Chen, M., Praetorius, J., Zheng, W., Xiao, F., Riederer, B., Singh, A.K., Stieger, N., Wang, J., Shull, G.E., Aalkjaer, C., et al. (2012). The electroneutral Na^+:HCO_3^- cotransporter NBCn1 is a major pH_i regulator in murine duodenum. J. Physiol. *590*, 3317–3333.

Chernova, M.N., Jiang, L., Crest, M., Hand, M., Vandorpe, D.H., Strange, K., and Alper, S.L. (1997). Electrogenic sulfate/chloride exchange in *Xenopus* oocytes mediated by murine AE1 E699Q. J. Gen. Physiol. *109*, 345–360.

Coakley, R.J., Taggart, C., McElvaney, N.G., and O'Neill, S.J. (2002). Cytosolic pH and the inflammatory microenvironment modulate cell death in human neutrophils after phagocytosis. Blood *100*, 3383–3391.

Colas, C., Menezes, S., Gutiérrez-Martínez, E., Péan, C.B., Dionne, M.S., and Guermonprez, P. (2014). An improved flow cytometry assay to monitor phagosome acidification. J. Immunol. Methods *412*, 1–13.

Cooper, D.S., Lee, H.J., Yang, H.S., Kippen, J., Yun, C.C., and Choi, I. (2006). The electroneutral sodium/bicarbonate cotransporter containing an amino terminal 123-amino-acid cassette is expressed predominantly in the heart. J. Biomed. Sci. *13*, 593–595.

Damkier, H.H., Nielsen, S., and Praetorius, J. (2005). An anti-NH2-terminal antibody localizes NBCn1 to heart endothelia and skeletal and vascular smooth muscle cells. Am. J. Physiol. Heart Circ. Physiol. *290*, H172–H180.

Damkier, H.H., Nielsen, S., and Praetorius, J. (2007). Molecular expression of SLC4-derived Na^+-dependent anion transporters in selected human tissues. Am. J. Physiol. Regul. Integr. Comp. Physiol. *293*, R2136–R2146.

Elsinghorst, E.A. (1994). Measurement of invasion by gentamicin resistance. Methods Enzymol. *236*, 405–420.

Fine, N., Barzilay, O., and Glogauer, M. (2017). Analysis of human and mouse neutrophil phagocytosis by flow cytometry. In Methods in Molecular Biology (Clifton), pp. 17–24.

Flannagan, R., Heit, B., and Heinrichs, D. (2015). Antimicrobial mechanisms of macrophages and the immune evasion strategies of *Staphylococcus aureus*. Pathogens *4*, 826–868.

Gratz, N., Siller, M., Schaljo, B., Pirzada, Z.A., Gattermeier, I., Vojtek, I., Kirschning, C.J., Wagner, H., Akira, S., Charpentier, E., et al. (2008). Group A *Streptococcus* activates type I interferon production and MyD88-dependent signaling without involvement of TLR2, TLR4, and TLR9. J. Biol. Chem. *283*, 19879–19887.

Grinstein, S., Swallow, C.J., and Rotstein, O.D. (1991). Regulation of cytoplasmic pH in phagocytic cell function and dysfunction. Clin. Biochem. *24*, 241–247.

Hackam, D., Rotstein, O., and Grinstein, S. (1999). Phagosomal acidification mechanisms and functional significance. In Phagocytosis: The Host (JAI), pp. 299–319.

Huynh, K.K., and Grinstein, S. (2007). Regulation of vacuolar pH and its modulation by some microbial species. Microbiol. Mol. Biol. Rev. *71*, 452–462.

Ip, W.K.E., Sokolovska, A., Charriere, G.M., Boyer, L., Dejardin, S., Cappillino, M.P., Yantosca, L.M., Takahashi, K., Moore, K.J., Lacy-Hulbert, A., et al. (2010). Phagocytosis and phagosome acidification are required for pathogen processing and MyD88-dependent responses to *Staphylococcus aureus*. J. Immunol. *184*, 7071–7081.

Joung, J., Konermann, S., Gootenberg, J.S., Abudayyeh, O.O., Platt, R.J., Brigham, M.D., Sanjana, N.E., and Zhang, F. (2017). Genome-scale CRISPR-Cas9 knockout and transcriptional activation screening. Nat. Protoc. *12*, 828–863.

Kinchen, J.M., and Ravichandran, K.S. (2008). Phagosome maturation: going through the acid test. Nat. Rev. Mol. Cell Biol. *9*, 781–795.

Lee, H.J., Kwon, M.H., Lee, S., Hall, R.A., Yun, C.C., and Choi, I. (2014). Systematic family-wide analysis of sodium bicarbonate cotransporter NBCn1/SLC4A7 interactions with PDZ scaffold proteins. Physiol. Rep. *2*, e12016.

Lee, S., Axelsen, T.V., Andersen, A.P., Vahl, P., Pedersen, S.F., and Boedtkjer, E. (2016). Disrupting Na^+,HCO_3^--cotransporter NBCn1 (Slc4a7) delays murine breast cancer development. Oncogene *35*, 2112–2122.

Lin, L., Yee, S.W., Kim, R.B., and Giacomini, K.M. (2015). SLC transporters as therapeutic targets: emerging opportunities. Nat. Rev. Drug Discov. *14*, 543–560.

Liu, M.Y., and Wu, M.C. (1992). Induction of human monocyte cell line U937 differentiation and CSF-1 production by phorbol ester. Exp. Hematol. *20*, 974–979.

Liu, Y., Qin, X., Wang, D.-K., Guo, Y.-M., Gill, H.S., Morris, N., Parker, M.D., Chen, L.-M., and Boron, W.F. (2013). Effects of optional structural elements, including two alternative amino termini and a new splicing cassette IV, on the function of the sodium-bicarbonate cotransporter NBCn1 (SLC4A7). J. Physiol. *591*, 4983–5004.

Liu, Y., Yang, J., and Chen, L.-M. (2015). Structure and function of SLC4 family HCO_3^- transporters. Front. Physiol. *6*, 355.

Loiselle, F.B., Jaschke, P., and Casey, J.R. (2003). Structural and functional characterization of the human NBC3 sodium/bicarbonate co-transporter carboxyl-terminal cytoplasmic domain. Mol. Membr. Biol. *20*, 307–317.

Lopez, I.A., Acuna, D., Galbraith, G., Bok, D., Ishiyama, A., Liu, W., and Kurtz, I. (2005). Time course of auditory impairment in mice lacking the electroneutral sodium bicarbonate cotransporter NBC3 (slc4a7). Dev. Brain Res. *160*, 63–77.

Love, M.I., Huber, W., and Anders, S. (2014). Moderated estimation of fold change and dispersion for RNA-seq data with DESeq2. Genome Biol. *15*, 550.

Martinez, F.O., Gordon, S., Locati, M., and Mantovani, A. (2006). Transcriptional profiling of the human monocyte-to-macrophage differentiation and polarization: new molecules and patterns of gene expression. J. Immunol. *177*, 7303–7311.

Morgan, D., Capasso, M., Musset, B., Cherny, V.V., Ríos, E., Dyer, M.J.S., and DeCoursey, T.E. (2009). Voltage-gated proton channels maintain pH in human neutrophils during phagocytosis. Proc. Natl. Acad. Sci. USA *106*, 18022–18027.

Novak, M.L., and Thorp, E.B. (2013). Shedding light on impaired efferocytosis and nonresolving inflammation. Circ. Res. *113*, 9–12.

Nunes, P., Guido, D., and Demaurex, N. (2015). Measuring phagosome pH by ratiometric fluorescence microscopy. J. Vis. Exp. https://doi.org/10.3791/53402.

O'Neill, L.A.J., and Pearce, E.J. (2016). Immunometabolism governs dendritic cell and macrophage function. J. Exp. Med. *213*, 15–23.

Parker, M.D., and Boron, W.F. (2013). The divergence, actions, roles, and relatives of sodium-coupled bicarbonate transporters. Physiol. Rev. *93*, 803–959.

Pushkin, A., Abuladze, N., Lee, I., Newman, D., Hwang, J., and Kurtz, I. (1999). Cloning, tissue distribution, genomic organization, and functional characterization of NBC3, a new member of the sodium bicarbonate cotransporter family. J. Biol. Chem. *274*, 16569–16575.

Rebsamen, M., Pochini, L., Stasyk, T., de Araújo, M.E.G., Galluccio, M., Kandasamy, R.K., Snijder, B., Fauster, A., Rudashevskaya, E.L., Bruckner, M., et al. (2015). SLC38A9 is a component of the lysosomal amino acid sensing machinery that controls mTORC1. Nature *519*, 477–481.

Richter, E., Ventz, K., Harms, M., Mostertz, J., and Hochgräfe, F. (2016). Induction of macrophage function in human THP-1 cells is associated with rewiring of MAPK signaling and activation of MAP3K7 (TAK1) protein kinase. Front. Cell Dev. Biol. *4*, 21.

Riihonen, R., Nielsen, S., Väänänen, H.K., Laitala-Leinonen, T., and Kwon, T.-H. (2010). Degradation of hydroxyapatite in vivo and in vitro requires osteoclastic sodium-bicarbonate co-transporter NBCn1. Matrix Biol. *29*, 287–294.

Romero, M.F., Chen, A.P., Parker, M.D., and Boron, W.F. (2013). The SLC4 family of bicarbonate (HCO_3^-) transporters. Mol. Aspects Med. *34*, 159–182.

Rusu, V., Hoch, E., Mercader, J.M., Tenen, D.E., Gymrek, M., Hartigan, C.R., DeRan, M., von Grotthuss, M., Fontanillas, P., Spooner, A., et al. (2017). Type 2 diabetes variants disrupt function of SLC16A11 through two distinct mechanisms. Cell *170*, 199–212.e20.

Sahoo, S., Aurich, M., Jonsson, J., and Thiele, I. (2014). Membrane transporters in a human genome-scale metabolic knowledgebase and their implications for disease. Front. Physiol. *5*, 91.

Sanjana, N.E., Shalem, O., and Zhang, F. (2014). Improved vectors and genome-wide libraries for CRISPR screening. Nat. Methods *11*, 783–784.

Sergushichev, A. (2016). An algorithm for fast preranked gene set enrichment analysis using cumulative statistic calculation. bioRxiv. https://doi.org/10.1101/060012.

Shapiro, H., Lutaty, A., and Ariel, A. (2011). Macrophages, meta-inflammation, and immuno-metabolism. ScientificWorldJournal *11*, 2509–2529.

Soldati, T., Rancano, C., Geissler, H., and Pfeffer, S.R. (1995). Rab7 and Rab9 are recruited onto late endosomes by biochemically distinguishable processes. J. Biol. Chem. *270*, 25541–25548.

Subramanian, A., Tamayo, P., Mootha, V.K., Mukherjee, S., Ebert, B.L., Gillette, M.A., Paulovich, A., Pomeroy, S.L., Golub, T.R., Lander, E.S., et al. (2005). Gene set enrichment analysis: a knowledge-based approach for interpreting genome-wide expression profiles. Proc. Natl. Acad. Sci. USA *102*, 15545–15550.

Surewaard, B.G.J., and Kubes, P. (2017). Measurement of bacterial capture and phagosome maturation of Kupffer cells by intravital microscopy. Methods *128*, 12–19.

Swallow, C.J., Grinstein, S., Sudsbury, R.A., and Rotstein, O.D. (1991). Cytoplasmic pH regulation in monocytes and macrophages: mechanisms and functional implications. Clin. Invest. Med. *14*, 367–378.

Szondy, Z., Garabuczi, É., Joós, G., Tsay, G.J., and Sarang, Z. (2014). Impaired clearance of apoptotic cells in chronic inflammatory diseases: therapeutic implications. Front. Immunol. *5*, 354.

Takahashi, D., Fujihara, M., Miyazaki, T., Matsubayashi, K., Sato, S., Azuma, H., Kato, T., Kino, S., Ikeda, H., Takamoto, S., et al. (2017). Flow cytometric quantitation of platelet phagocytosis by monocytes using a pH-sensitive dye, pHrodo-SE. J. Immunol. Methods *447*, 57–64.

Tranchemontagne, Z.R., Camire, R.B., O'Donnell, V.J., Baugh, J., and Burkholder, K.M. (2016). *Staphylococcus aureus* strain USA300 perturbs acquisition of lysosomal enzymes and requires phagosomal acidification for survival inside macrophages. Infect. Immun. *84*, 241–253.

Via, L.E., Deretic, D., Ulmer, R.J., Hibler, N.S., Huber, L.A., and Deretic, V. (1997). Arrest of mycobacterial phagosome maturation is caused by a block in vesicle fusion between stages controlled by rab5 and rab7. J. Biol. Chem. *272*, 13326–13331.

Wahl, L.M., Smith, P.D., Wahl, L.M., and Smith, P.D. (2001). Isolation of monocyte/macrophage populations. Curr. Protoc. Immunol. https://doi.org/10.1002/0471142735.im0706s16.

Wang, D.-K., Liu, Y., Myers, E.J., Guo, Y.-M., Xie, Z.-D., Jiang, D.-Z., Li, J.-M., Yang, J., Liu, M., Parker, M.D., et al. (2015a). Effects of Nt-truncation and

coexpression of isolated Nt domains on the membrane trafficking of electroneutral Na^+/HCO_3^- cotransporters. Sci. Rep. *5*, 12241.

Wang, S., Tsun, Z.-Y., Wolfson, R.L., Shen, K., Wyant, G.A., Plovanich, M.E., Yuan, E.D., Jones, T.D., Chantranupong, L., Comb, W., et al. (2015b). Lysosomal amino acid transporter SLC38A9 signals arginine sufficiency to mTORC1. Science *347*, 188–194.

Wieland, H., Goetz, F., and Neumeister, B. (2004). Phagosomal acidification is not a prerequisite for intracellular multiplication of *Legionella pneumophila* in human monocytes. J. Infect. Dis. *189*, 1610–1614.

Yang, J., Yan, R., Roy, A., Xu, D., Poisson, J., and Zhang, Y. (2015). The I-TASSER Suite: protein structure and function prediction. Nat. Methods *12*, 7–8.

STAR★METHODS

KEY RESOURCES TABLE

REAGENT or RESOURCE	SOURCE	IDENTIFIER
Antibodies		
Anti-SLC4A7, rabbit polyclonal	Abcam	Cat#82335; RRID: AB_10672662
Anti-SLC4A7, serum from rabbit immunized with the SLC4A7 N-terminal peptide MEADGAGEQMRPLLTRGPDE	Gift from Prof. J. Praetorius (Aarhus University, Denmark)	(Damkier et al., 2005)
Anti-HA, rabbit monoclonal	Cell signaling	Cat#3724; RRID: AB_1549585
Anti-pan actin, rabbit polyclonal	Cytoskeleton	Cat#AAN01; RRID: AB_10708070
Anti-LAMP1, mouse monoclonal	Abcam	Cat#25630; RRID: AB_470708
Goat anti-mouse IgG, Alexa-Fluor 488 coupled	Life Technologies	Cat#A-11001; RRID: AB_2534069
Donkey anti-rabbit IgG, Cy5 coupled	Jackson ImmunoResearch	Cat#711-175-152; RRID: AB_2340607
Goat anti-rabbit IgG, Peroxidase-conjugated	Jackson ImmunoResearch	Cat#111-035-003; RRID: AB_2313567
Goat anti-mouse IgG, Peroxidase-conjugated	Jackson ImmunoResearch	Cat#115-035-003; RRID: AB_10015289
Bacterial and Virus Strains		
Escherichia coli DH5-alpha	New England Biolabs	Cat#C2987
Streptococcus pyogenes ⊿SLO	N/A	(Gratz et al., 2008)
Staphylococcus carnosus Schleifer and Fischer	DSMZ	Cat# 20501
Staphylococcus aureus Newman	Gift from Arsanis Biosciences GmbH to PK	N/A
Staphylococcus aureus USA300	Gift from Prof. S. Knapp (CeMM, Vienna, Austria)	N/A
Chemicals, Peptides, and Recombinant Proteins		
Fluoresbrite YG Carboxylate Microspheres 1.75μm	Polyscience	Cat#17687-5
pHrodo Red, succinimidyl ester (pHrodo Red, SE)	Thermo Fisher Scientific	Cat#P36600
PMA, Phorbol 12-myristate 13-acetate	Sigma-Aldrich	Cat#P8139
Restriction enzyme BsmBI	New England Biolabs	Cat#R0580
BCECF AM	Thermo Fisher Scientific	Cat# B1170
Experimental Models: Cell Lines		
THP-1	ATCC	TIB-202
U937	Gift from Prof. P. Valent, (Medical University Vienna, Austria)	N/A
HEK293T	DSMZ	ACC 635
Oligonucleotides		
See Table S1 for oligonucleotides used to clone sgRNAs	This paper, Sigma	N/A
Recombinant DNA		
lentiCRISPR v2	Addgene	Cat#52961
psPAX2	Addgene	Cat#12260
pMD2.G	Addgene	Cat#12259
pDONR221	Thermo Fisher Scientific	12536017
Codon optimized SLC4A7 isoform 1 and 6 cDNA	GenScript	N/A
Software and Algorithms		
R (3.4.0)	https://www.r-project.org	N/A
Rstudio (1.0.143)	https://www.rstudio.com	N/A
Bioconductor (3.5)	https://bioconductor.org/	N/A
DESeq2 (1.16.1)	https://bioconductor.org/	N/A
Fgsea (1.2.1)	https://bioconductor.org/	N/A

(*Continued on next page*)

Continued		
REAGENT or RESOURCE	SOURCE	IDENTIFIER
ggplot2 (2.2.1)	https://cran.r-project.org/	N/A
Drc	https://CRAN.R-project.org/package=drc	N/A
Other		
RPMI Medium 1640 (1x)	Gibco	Cat#21875-034
DMEM Medium (1x)	Gibco	Cat# 11965-084
DPBS (1x)	Gibco	Cat#14190-094
Fetal Bovine Serum	Gibco	Cat#10270
Pen Strep	Gibco	Cat#15140-122
IC Fixation buffer	eBioscience	Cat#00-8222-49
ProLong Gold Antifade Mountant	Thermo Fisher	Cat#P10144
cOmplete Protease Inhibitor Tablets	Roche	Cat#04693159001
Protein Assay Dye Reagent Concentrate	Biorad	Cat#5000006
Nitrocellulose membranes	Amersham	Cat#10600002
Pierce ECL Western Blotting Substrate	Thermo Scientific	Cat#32106
PolyFect	Qiagen	Cat#301105
QuikChange II Site Directed Mutagenesis Kit	Agilent	Cat# 200523

CONTACT FOR REAGENT AND RESOURCE SHARING

Further information and requests for reagents may be directed to and will be fulfilled by the Lead Contact, Giulio Superti-Furga (gsuperti@cemm.oeaw.ac.at).

EXPERIMENTAL MODEL AND SUBJECT DETAILS

Cell Culture

U937 cells were a gift from Prof. Peter Valent of the Medical University of Vienna, THP-1 cells were purchased from ATCC. Cell lines were tested for mycoplasma with regular intervals. STR profiling was performed for all cell lines to confirm identity.

Cells were cultured in RPMI 1640 supplemented with 10% fetal bovine serum and penicillin/streptomycin with 5% CO_2 at 37°C. U937 cells were maintained at a density of $0.1x10^6$ – $1x10^6$ cells/ml; THP-1 cells were maintained at $0.5x10^6$ – $2x10^6$ cells/ml.

Primary Cells and Monocyte to Macrophage Differentiation

Human monocytes were isolated from healthy donor peripheral blood buffy coats (obtained from the Austrian Red Cross) by adherence to plastic for 3 h in serum-free RPMI medium (Wahl et al., 2001). Monocytes were then differentiated to macrophages for 7 days in RPMI supplemented with 100 ng/ml M-CSF, 10% fetal bovine serum and penicillin/streptomycin. Macrophage polarization was achieved by incubating cells for 18 h in medium with IFNγ (20 ng/ml) and LPS (100 ng/ml) for induction of M1 phenotype or IL-4 (20 ng/ml) for induction of M2 phenotype (Martinez et al., 2006).

Monocyte to macrophage differentiation of THP-1 and U937 cells was performed with 10 nM PMA (Sigma) at a cellular density of $1x10^6$ cells/ml for 48 h followed by washing and an additional 24 h resting period.

Culture and Preparation of Bacteria

Escherichia coli (K12) were inoculated from overnight culture into fresh LB media and grown till mid-log phase (OD_{600} = 0.5). Bacteria were washed in PBS and resuspended to the concentration of $1x10^9$ cfu/ml.

Staphylococcus carnosus (Schleifer and Fisher), *Staphylococcus aureus* (USA300, Newman) were plated on trypcase soy agar with 5% sheep blood from cryo stock and grown for 16 h at 37°C. Single colonies were inoculated in 30 ml of brain heart infusion media (BHI) and grown till reaching the stationary phase (16 h). Overnight cultures were diluted in 50 ml of BHI and grown till mid-log phase. Bacteria were washed 2 times in PBS and resuspended at a concentration of $1x10^9$ cfu/ml.

Streptococcus pyogenes was inoculated in 5 ml of Todd Hewitt Broth with 0.5% yeast (THY) extract and grown at 37°C in atmosphere with 5% CO_2 for 16 h. Overnight cultures were diluted in 30 ml of THY and grown till reaching mid-log phase. Bacteria were washed 2 times in PBS and resuspended at the concentration of $1x10^9$ cfu/ml.

METHOD DETAILS

SLC-Focused CRISPR/Cas9 Screen

The SLC KO CRISPR/Cas9 library used will be described in detail in Girardi et al. (in preparation). Briefly, a CRISPR/Cas9 library targeting 391 SLC genes with six sgRNAs per gene, together with a set of 120 sgRNAs targeting 20 genes essential in KBM7 and HAP1 cells (Blomen et al., 2015) and a set of 120 non-targeting sgRNAs was cloned by Gibson cloning in the lentiCRISPRv2 lentiviral vector. Viral particles were generated by transient transfection of low passage, subconfluent HEK293T cells with the SLC-targeting library and the packaging plasmids psPAX2 and pMD2.G using PolyFect. After 24 h the media was changed to fresh RPMI media supplemented with 10% FCS and antibiotics. The viral supernatant was collected after 48 h, filtered and stored at -80°C until further use. The supernatant dilution necessary to infect U937 cells at a MOI (multiplicity of infection) of 0.2 – 0.3 was determined by puromycin survival after transduction as described previously (Sanjana et al., 2014). U937 cells were infected in triplicates with the SLC KO library at high coverage (1000x) and after selection for 7 days with puromycin (2 μg/ml) an initial sample was collected to control for library composition. Cells were differentiated with PMA (10 nM) to macrophage-like phenotype. Phagocytosis assays were performed with dual-color opsonized latex beads as described in the "Phagocytosis assay" section. Phagocytosis positive (PhagoLate) and phagocytosis negative (PhagoNeg) populations were sorted using BD FACS Aria II, with at least 3 million cells per replicate and population. Genomic DNA was extracted using the DNAeasy kit (QIAGEN) and the cassettes containing the sgRNA sequence were amplified with one round of PCR following the procedure described in Joung et al. (2017). The amplified samples were sequenced on a HiSeq2000 (Illumina) at the Biomedical Sequencing Facility (BSF at CeMM, https://biomedical-sequencing.at), followed by processing with a custom analysis pipeline (see next section).

Analysis of CRISPR Screens

Sequences of sgRNAs were extracted from RNA-Seq reads, matched against the original sgRNA library index and counted using an in-house Python script. To compensate for the noise and off-target action of sgRNAs inherent to CRISPR screening approaches, we used a two-step differential abundance analysis. Differential abundance of sgRNAs was estimated with DESeq2 (Love et al., 2014). Subsequenly, sgRNAs were sorted by adjusted p-values and aggregated to genes using Gene Set Enrichment Algorithm (Sergushichev, 2016; Subramanian et al., 2005).

Phagocytosis Assay

Phagocytosis assays were performed as previously described (Colas et al., 2014). Fluoresbrite carboxylated 1.75 μM microspheres (YG: 441 nm excitation, 486 nm emission) were opsonized in 20% human male AB serum in PBS for 16 h at 4°C with constant rotation. Subsequently beads were washed twice with PBS and stained with 2 μg/ml pHrodo-Red, SE for 30 min at room temperature with agitation. After washing, beads were resuspended to a final concentration of $1x10^9$ beads/ml.

PMA-differentiated cells (U937 or THP-1) were seeded on 12-well cell culture coated dishes ($1x10^6$ cells/well). Stained beads were added to cells at the indicated MOIs. Dishes were centrifuged at 150 g for 10 min with break set to off. After 30 min incubation, cells were washed three times with warm PBS. Cells were further incubated for the indicated times and then detached by scraping with soft rubber policeman and analyzed by flow cytometry.

Flow Cytometry

All data acquisition was performed using the LSR Fortessa II cytometer interfaced with FACSDiva (BD). FlowJo X software (Tree Star) was used for data analysis and graphical representation.

Live-Cell Measurements of Cytosolic and Phagosomal pH

THP-1 and U937 cells were seeded on imaging dishes (ibidi 35 mm dishes with glass bottom) and differentiated with PMA (10 nM) for 48 h. Differentiated cells were washed twice in HBSS and subsequently loaded with BCECF-AM (5 μM) in HBSS with sodium bicarbonate and 10 mM HEPES for 30 min at 37°C. After washing three times in HBSS, the cells were supplemented with HBSS with 10% FBS. Dual-colored beads (pHrodo and bright blue) or pHrodo-coupled heat-killed S.aureus were added to the cells at an MOI of 10. After spinning at 1000 rpm for 2 min, the cells were further incubated in humidified atmosphere at 37°C and 5% CO_2. Live cell microscopy was performed on a Zeiss Axio Oberver Z1 widefield microscope (at 37°C and in 5% CO_2) at 1 and 6 h after loading the phagosomal cargo. pHrodo and bright blue signal was acquired in the respective channels (RFP/DAPI). BCECF emission at 525 nm was acquired after both excitation at 440 nm and 490 nm respectively. 5 independent z-stacks were acquired per dish, and three independent replicate dishes imaged per condition.

An *in situ* calibration curve was constructed by incubating cells in potassium buffers with 10 μM valinomycin and 10 μM nigericin with ranging pH (4.0 – 10.0).

For image analysis, maximum-projections of z-stacks were generated, background signal was subtracted and signal intensity in respective channels was measured in the respective regions of interest (cytoplasm of cells having undergone phagocytosis; acidified phagosomal particles).

Immunofluorescence

For immunofluorescence, THP-1 cells or U937 cells were seeded on glass coverslips and differentiated with PMA for 48 h. For staining of endogenous SLC4A7, PMA-differentiated control (sgRen) and SLC4A7 knockout (sg1) THP-1 cells were washed in PBS. Fixation buffer was added for 10 min at RT (room temperature), cells were washed in PBS again and ice-cold methanol was added for 10 min at 4°C. Subsequently, cells were blocked in IF buffer (2.5% BSA, 0.5% Tween in PBS) for 30 min and next incubated with anti-SLC4A7 (rabbit) primary antibody (at 1:200 dilution) in IF buffer over night. After washing 3 times, Alexa Fluor 488-coupled anti-rabbit (Life Technologies) was added at a dilution of 1:1000. DAPI was used to counterstain DNA and slides were mounted with ProLong Gold Antifade Mountant.

For localization of SLC4A7 isoform 1, isoform 6, and the respective SLC4A7 mutants, U937 cells expressing Strep-HA-tagged forms of SLC4A7 were subjected to the same fixation procedure and incubated with anti-HA (rabbit) and anti-Lamp1 (mouse) primary antibodies (at a 1:1000 and 1:200 dilution in IF buffer respectively), and Alexa Fluor 488-coupled anti-mouse (Life Technologies) and Cy5-coupled anti-rabbit (Jackson ImmunoResearch) secondary antibodies respectively.

Images were taken using a laser-scanning confocal microscope LSM700 (Zeiss).

For live-cell microscopy of GFP-SLC4A7 expressing THP-1 cells, these cells were seeded on chambered coverslips (ibidi) and differentiated with PMA (10 nM) for 48 h. Media was replaced by HBSS with 10 mM of HEPES and 10% of FBS, and dual-colored beads (pHrodo and bright blue) or pHrodo-coupled heat-killed S.aureus were added to the cells at an MOI of 10. After spinning at 1000 rpm for 2 min, the cells were further incubated in humidified atmosphere at 37°C and 5% CO_2. Live cell microscopy including time-lapse series was performed on a laser-scanning confocal microscope LSM780 (Zeiss) at 37°C and in 5% CO_2.

Cell Lysis and Immunoblotting

Cell samples were lysed in lysis buffer (NaCl 150 mM, Tris-HCl 50 mM, $MgCl_2$ 5 mM, EDTA 1 mM, NP-40 0.5 %, Glycerol 5 %) to which cOmplete Protease Inhibitor Tablets were added. After lysis in appropriate volumes and 20 min incubation on ice, cellular lysates were centrifuged at 14000 rpm and 4°C for 15 min to separate from cellular debris, protein concentration was measured according to the Bradford method using Protein Assay Dye Reagent Concentrate, and Laemmli buffer was added. The lysates were separated by SDS-PAGE and blotted onto nitrocellulose membranes. After blocking unspecific binding in 5% milk in TBS-T, membranes were incubated with primary antibodies diluted in 5% milk or 5% BSA (bovine serum albumin) in TBS-T. After addition of peroxidase coupled secondary antibodies, immunoblot membranes were developed using the ECL (enhanced chemoluminescence) method.

DNA Plasmids and Cloning

Codon-optimized cDNA for SLC4A7 isoform 1 and isoform 6 was synthesized by GenScript. After sequence verification, both cDNAs were first cloned into the pDONR221 plasmid and then shuttled into a modified pRRL-based lentiviral expression plasmid generated in our lab, which contains an N-terminal Strep-HA tag and a blasticidin resistance cassette. The cDNA of isoform 6 was additionally shuttled into another modified pRRL-based lentiviral expression plasmid generated in our lab, which contains an N-terminal GFP tag and a hygromycin resistance cassette.

The C-terminal deletion mutant of SLC4A7 isoform 6, lacking amino acids 1008-1131, was generated by PCR with respective primers and cloned as described above. For generation of the two SLC4A7 point mutants T549I and D811A, mutagenesis primers were designed using the QuikChange Primer Design tool from Agilent. Mutagenesis was performed using the QuikChange II Site-Directed Mutagenesis Kit (Agilent), following the instructions of the manufacturer. After sequence verification, the cDNAs were shuttled into the pRRL plasmid described above.

sgRNAs were cloned into Bsm BI sites of lentiCRISPR v2.

Lentivirus-Mediated DNA Transfer

For lentivirus production, HEK 293T cells were transfected with the sgRNA or expression plasmid, the envelope plasmid pMD2.G and the packaging plasmid psPAX2 using PolyFect. 48 h after transfection, the virus-containing medium was collected and filtered. For infection, THP-1 and U937 cells were plated in 6 well plates, in 2 ml of fresh medium,1 ml of harvested virus and 8 μg/ml protamine sulphate, spin infected at 2000 rpm for 45 min and incubated with the virus-containing supernatant for 24 h. Next day, medium was exchanged. Three days after infection, selection was started by addition of blasticidin (30 μg/ml) or puromycin (2 μg/ml) respectively.

Gentamicin Protection Assay

Gentamycin protection assays were performed as previously described (Elsinghorst, 1994; Richter et al., 2016). Briefly, PMA-differentiated THP-1 cells ($0.75x10^6$ cells per well on 24-well plates) were inoculated with bacteria at an MOI of 10. Plates were centrifuged at 150 g for 5 min with break set to off. After 30 min, cells were washed with PBS 3 times and supplemented with fresh medium containing 100 μg/ml gentamicin to remove or kill extracellular bacteria. After 30 min, cells were washed and supplemented with medium containing 5 μg/ml gentamycin. At consecutive time points, SLC4A7 knock-out and control THP-1 cells were lysed and plated on agar to allow for outgrowth of surviving intracellular bacteria.

QUANTIFICATION AND STATISTICAL ANALYSIS

Exploratory data analysis, visualization, and statistical testing were performed with R-project (http://www.R-project.org) using Rstudio IDE. Pair-wise differences in central tendencies were tested using Welch's t-test or Wilcoxon-Mann-Whitney-Test as indicated in figure legends. Error bars represent 95% confidence intervals, unless indicated otherwise in the figure legends.

DATA AND SOFTWARE AVAILABILITY

sgRNA count data are provided in Data S1.

3.3 Interlude

The previous results from section 3.2 show, that the transporter protein SLC4A7 is involved in the acidification of the phagolysosome. Since this electroneutral sodium bicarbonate co-transporter is located not directly on the phagolysosome but rather on the outer membrane it was clear that additional regulatory mechanisms must act between the regulation of SCL4A7 and the phagolysosome. To find these machinery and pathways we deploy in this part of the thesis a similar genetic screening approach on a genome-wide scale. Therefore, we switch to the monocytic cell model THP-1 and engineer a genome-wide screening approach with the phagocytosis reporter that was already used in the previous study.

With this genome-wide CRISPRko FACS screen we could identify 716 genes as phagocytic regulators. Since phagocytosis is a complex process that starts with the engulfment of material by the cell and continued by a route with multiple stops through the cell until reaching as final destination the phagolysosome we were wondering if our dataset could reconstruct this route. Therefore, we arrange these hits in a network connected based on the hit's interactions on the protein-protein level. Indeed, we can see, that when the genetic hits are arranged according to functional cellular processes, they reconstruct known routes of cellular transport through the cell. This approach also allows to prioritize genetic hits by retrieving protein complexes that were covered multiple times by the hits of the CRISPRko screen. What we find are not only known machineries such as the Arp2/3 complex, the Wave-2, or the vacuolar-ATPase-Rag machinery but also multiple new types of machinery that were previously not linked to phagocytosis such as the oligosaccharyltransferase complex or the hypusine pathway. Additionally, we believe that our approach of integrating protein-protein interaction data will be an attractive way to functionally interpret many other genome-wide screens.

3.4 Manuscript #2

Results section 3.4 contains the full reprint of the manuscript listed below. The author of this thesis is an author of the article. The article is published by Life Science Alliance under the Creative Commons Attribution CC-BY 4.0 License.

Essletzbichler P, Sedlyarov V, Frommelt F, Soulat D, Heinz LX, Stefanovic A, Neumayer B, Superti Furga G[#] (2023) A genome-wide CRISPR functional survey of the human phagocytosis molecular machinery. Life Science Alliance vol. 6 no.4 e202201715

[#]: corresponding author

Detailed information on the contribution of all authors is listed on page 15 under “Author Contributions” of the article.

Research Article

TRANSPARENT PROCESS OPEN ACCESS Life Science Alliance

A genome-wide CRISPR functional survey of the human phagocytosis molecular machinery

Patrick Essletzbichler[1], Vitaly Sedlyarov[1], Fabian Frommelt[1], Didier Soulat[2], Leonhard X Heinz[1], Adrijana Stefanovic[1], Benedikt Neumayer[1], Giulio Superti-Furga[1,3]

Phagocytosis, the process by which cells engulf large particles, plays a vital role in driving tissue clearance and host defense. Its dysregulation is connected to autoimmunity, toxic accumulation of proteins, and increased risks for infections. Despite its importance, we lack full understanding of all molecular components involved in the process. To create a functional map in human cells, we performed a genome-wide CRISPRko FACS screen that identified 716 genes. Mapping those hits to a comprehensive protein–protein interaction network annotated for functional cellular processes allowed retrieval of protein complexes identified multiple times and detection of missing phagocytosis regulators. In addition to known components, such as the Arp2/3 complex, the vacuolar-ATPase-Rag machinery, and the Wave-2 complex, we identified and validated new phagocytosis-relevant functions, including the oligosaccharyltransferase complex (MAGT1/SLC58A1, DDOST, STT3B, and RPN2) and the hypusine pathway (eIF5A, DHPS, and DOHH). Overall, our phagocytosis network comprises elements of cargo uptake, shuffling, and biotransformation through the cell, providing a resource for the identification of potential novel drivers for diseases of the endo-lysosomal system. Our approach of integrating protein–protein interaction offers a broadly applicable way to functionally interpret genome-wide screens.

DOI 10.26508/lsa.202201715 | Received 7 September 2022 | Revised 18 January 2023 | Accepted 19 January 2023 | Published online 1 February 2023

Introduction

Phagocytosis is a multifaceted, integrated biological process, that involves the engulfment of large (≥0.5 μm) particles under strict coordination over time and space, with an immunological and homeostatic purpose (Flannagan et al, 2012; Underhill & Goodridge, 2012; Gordon, 2016). It is a key defense and neutralization mechanism against pathogens and at the same time, it is involved in the clearance of apoptotic cells (Arandjelovic & Ravichandran, 2015), in the processes of wound healing (Giulian et al, 1989), in tumor cell phagocytosis (Feng et al, 2019; Kamber et al, 2021), microglial phagocytosis (Podleśny-Drabiniok et al, 2020), and in the resolution of tissue injury (Gerlach et al, 2021). Among other phenomena, dysregulated phagocytosis or aberrant phagosome maturation can promote Alzheimer's disease, allow pathogens such as bacteria or viruses and cancer cells to escape destruction, or promote autoimmunity through incomplete degradation of cell debris and DNA (Arandjelovic & Ravichandran, 2015; Podleśny-Drabiniok et al, 2020).

The material taken up by a cell is contained in a membrane-bound vacuole called phagosome that matures through a series of highly organized membrane fusion and fission events, altering its composition and gradually acidifying its pH (Flannagan et al, 2012). A freshly formed phagosome (pH ~7.4) fuses first with an early endosome acquiring, among others, the GTPase Rab5. Then it undergoes a series of maturation steps, yielding the late phagosome marked by the exchange of Rab5 to Rab7 and the acquisition of additional vacuolar ATPase proton pumps, which acidify the phagosome to pH 5.5–6.0, forming the ideal degradative environment (Flannagan et al, 2012).

Systematic searches for phagocytosis regulators have been widely undertaken with RNAi-based screens in cultured *Drosophila* cell models (Rämet et al, 2002; Kocks et al, 2005; Philips et al, 2005). Until recently, such genetic screens have been lacking mammalian cell systems (Haney et al, 2018; Sedlyarov et al, 2018; Yeung et al, 2019; Lindner et al, 2021). The advancement of gene-editing tools, in particular the discovery of CRISPR/Cas9 systems (Cong et al, 2013; Jinek et al, 2013; Mali et al, 2013) and increasingly sophisticated read-out systems, now allows conducting large genome-wide knock-out screens in mammalian cells at high precision (Cong et al, 2013; Sanjana et al, 2014; Shalem et al, 2015).

Once it is established that a reporter system faithfully represents the biology under investigation and once validation and calibration of the system allow it to display the necessary signal-to-noise ratio, pooled FACS-based genetic screens offer a powerful method to

[1]CeMM Research Center for Molecular Medicine of the Austrian Academy of Sciences, Vienna, Austria [2]Institute of Clinical Microbiology, Immunology and Hygiene, Universitätsklinikum Erlangen and Friedrich-Alexander-Universität Erlangen-Nürnberg, Erlangen, Germany [3]Center for Physiology and Pharmacology, Medical University of Vienna, Vienna, Austria

Correspondence: gsuperti@cemm.oeaw.ac.at
Vitaly Sedlyarov's present address is Boehringer Ingelheim RCV GmbH & Co KG, Vienna, Austria
Leonhard X Heinz's present address is Division of Rheumatology, Department of Internal Medicine III, Medical University of Vienna, Vienna, Austria

genetically map a large variety of biological processes (Doench, 2018; Bock et al, 2022).

Here, we present a FACS-based genome-wide CRISPR/Cas9 knock-out screen for phagocytosis using a reporter assay (Colas et al, 2014) that we previously employed for focused genetic screening (Sedlyarov et al, 2018) and for measuring the maturation of the phagolysosome (Heinz et al, 2020). As in vitro macrophage cell model, we chose PMA-differentiated human THP-1 cells, a classical cell model, to study phagocytosis and immune modulation (Fleit & Kobasiuk, 1991; Chanput et al, 2014).

The study reported here represents a comprehensive genetic assessment of cellular functionalities involved in phagocytosis, including its regulation, dynamic phagosomal maturation processes, and movement by the complex cell cargo transport machinery. Additionally, the study highlights the power of combining the information from functional genetic screening and publicly available protein–protein interaction (PPI) data, representing the physical base for concerted cellular activities. We present the efficient guiding of validation and rationalization of the genetic results in light of the annotated cellular machinery and its individual components.

Results

A FACS reporter-based screen for modulators of phagocytosis

Phagocytosis proceeds through defined key steps, including the uptake of cargo, the systematic coordinated transport to the lysosome, and proper acidification. We set out to identify genes potentially involved in the entire process by making use of pooled CRISPR/Cas9 knock-out screening in combination with reporter-based flow cytometry-assisted cell sorting. For this, we chose the myeloid cell line THP-1 (Chanput et al, 2014) and a PMA-based differentiation protocol that induces in these cells a macrophage-like phenotype (Fleit & Kobasiuk, 1991). To validate the experimental setup, we tested actin polymerization using Cytochalasin D (Carter, 1967) and lysosome-dependent acidification using Bafilomycin A1 (Fig 1B and C) (Dröse et al, 1993). Next, we introduced a genome-wide CRISPR/Cas9 knock-out library, targeting all protein-coding human genes with 70,948 sgRNAs and 142 control sgRNAs (Hart et al, 2017). We used the lentiCRISPRv2 single vector driving the expression of a sgRNA-cassette and Cas9 developed by Sanjana and colleagues (Sanjana et al, 2014).

To measure the phagocytic uptake of cargo as well as the transport and acidification of the resulting phagolysosome, we employed a flow cytometry readout based on opsonized 1.75-μm latex beads coated with the pH-sensitive dye pHrodo (Colas et al, 2014) and successfully adopted for genetic screening (Sedlyarov et al, 2018). Whereas cells that were fully functional in phagocytosis and acidification appeared in the PhagoLate fraction, cells still capable of phagocytosis, but deficient in acidification, emerged in the PhagoEarly fraction (Fig 1A). In contrast, cells that were completely deficient in phagocytosis appeared in the PhagoNeg fraction. Since the cytoskeleton has a key role in the formation of the phagocytic cup, and for material uptake, we employed the cytoskeletal inhibitor Cytochalasin D to show the efficient blockage of reporter uptake. Cytochalasin D–treated cells emerged predominantly in the PhagoNeg fraction, indicating that their phagocytic defect stemmed from an uptake issue (Fig 1B and C). We treated cells with a vacuolar-ATPase inhibitor Bafilomycin A1 to show that acidification of the lysosome was required for cells to emerge in the PhagoLate gate. The uptake of the reporter itself remained unaffected, which led to a rise of cells in the PhagoEarly gate (Fig 1B and C).

A genome-wide screen identifies known and novel modulators of phagocytosis

After setting up the phenotypic assay to measure phagocytosis in THP-1 cells, we next performed a genome-wide screen for modulators of phagocytosis in quadruplicates following the workflow portrayed in Figs 1A and S1. We first introduced a genome-wide CRISPR knock-out library into THP-1 cells and selected cells with puromycin before we induced a macrophage-like phenotype *via* PMA differentiation. The period chosen for further cell incubation was the time point where further incubation did not lead to additional phagocytosis (3 h), whereas the bead-to-cell ratio was optimized to yield ~one-third of cells in the PhagoNeg fraction and two-thirds of the cells in the phagocytosis- and acidification-positive fractions (PhagoEarly and PhagoLate) (Fig S2A). The stability of the assay was confirmed by storing cells for 24 h at 4°C which led to no significant change in the reported phagocytosis rate, compared to our standard 3-h condition (Fig S2B). Cell fractions were gated and FACS sorted and processed separately allowing for comparison of sgRNA abundance within each population and replicate (Fig S3A and B).

By comparing sgRNAs that were depleted in PhagoLate compared to PhagoNeg, we identified in total 716 genes to be involved either in phagocytosis itself or in phagosome acidification (Fig 1D and Table S1). Gene Ontology (GO) enrichment analysis for "Cellular components" GO terms yielded among others as strongly enriched compartments the lytic vacuole membrane, lysosome, and late endosome (adj. P-value < 1.08×10^{-6}). These components are all part of cellular processes and pathways which are well-known to be involved in phagocytosis (Fig 1E). Enriched biological processes included the dolichol-linked oligosaccharide biosynthetic process, TOR signaling, starvation response, and actin nucleation (adjusted P-value < 5.30×10^{-6}) (Fig 1E). RNA-sequencing of THP-1 cells treated with the reporter was further used to confirm that genes identified as phagocytic regulators were expressed in THP-1 cells across a wide range of expressions (Fig S4A and B and Table S3). By comparing sgRNAs that were depleted in cells right before differentiation (day 21 after infection) with the CRISPR library plasmid stock, we identified genes that led to a general reduction in growth in our screen (Table S2). We highlighted those genes as "essential genes" in Fig 1D and showed that this set of hits compares well with genes that have a gene effect score <−1 in the DepMap CRISPR dataset (DepMap, 2022) (Fig S5A). In addition, our essential genes show large overlaps (723 of 1041) with the "core essentialome," a list of 1,736 shared essential genes we have previously derived from HAP1 and KBM7 cell lines (Blomen et al, 2015) (Fig S5B). Although our screen could still identify several phagocytosis regulators that were essential, the majority of the 716 genes depleted in PhagoLate versus PhagoNeg did not have a gene effect score <−1 in

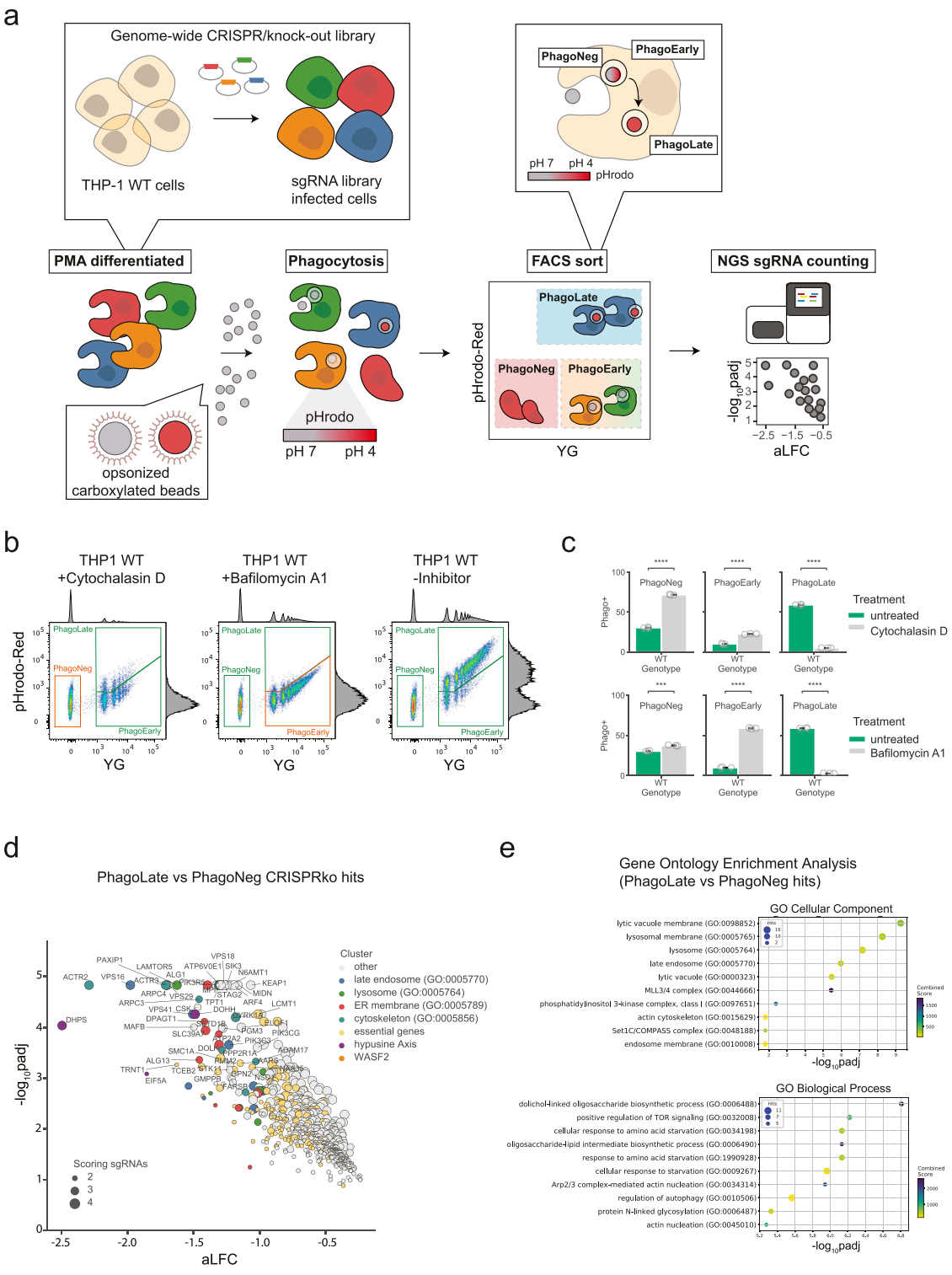

Figure 1. Genome-wide CRISPR/knock-out approach identifies regulators of phagocytosis.
(A) Schematic overview of the FACS-based genome-wide CRISPR/Cas9 knock-out screen to identify modulators of phagocytosis. **(B)** Representative flow cytometry scatterplots of phagocytosis assays. PMA-differentiated THP-1 cells were either treated with the control drugs Cytochalasin D or Bafilomycin A1 or were left untreated and then incubated with opsonized, dual-colored reporter beads. Each dot corresponds to one measured cell: The intensity of the pH-insensitive dye is represented on the x-axis (YG, striped pattern originates from the number of beads within the individual cell), and the signal of the pH-sensitive dye, which increases signal with decreased pH is displayed on the y-axis (pHrodo-Red). Double-negative cells were sorted as phagocytosis-negative (PhagoNeg), single-positive cells (YG high signal but low pHrodo-Red signal) were grouped as early stages of phagocytosis and double-positive cells (YG high signal and high pHrodo-Red signal) were classified as cells that underwent phagocytosis and phagosome acidification (PhagoLate). Cells treated with the control drug Cytochalasin D remained mostly in the PhagoNeg gate and cells treated with

DepMap (Fig S5C). For all the downstream analyses, we, therefore, worked with the complete set of 716 genes.

Mapping the identified phagocytosis genes to the cellular machinery

The virtually compiled assembly of human cellular protein complexes inferred from collective PPI studies is sufficiently advanced to represent a useful framework for modeling the molecular machinery of a cell. If our functionally determined genes were indeed representing important elements in the machinery involved in phagocytosis, they should converge on a limited number of protein complexes. Moreover, these protein complexes should in turn be involved in linked cellular processes and pathways. To test this hypothesis and to probe for physical interactions between the 716 genetic hits, we created a PPI network, derived from interactions recorded in the BioPlex 3.0, a high-quality dataset featured by the consistency of scoring across different baits (Huttlin et al, 2021). For 69% of the 716 hits, we could obtain a fairly coherent network with only a few small, isolated subnetworks. For a better interpretation of the network, the color of the circle represents the average $\log_2$-fold change (aLFC) of each gene (Fig 2). To map the proteins linked in the protein network to known molecular machines, we scored the membership to the well-characterized human protein complexes of the CORUM-core (Giurgiu et al, 2019), light brown shaded in Fig 2 (see also Table S4). This allowed us to map about a third of the identified phagocytosis modulators onto known biological complexes representing molecular machines (Fig 2). Additionally, the completeness of protein-complexes annotated in the CORUM-core was analyzed and indicated in percentages with either a blue (percent of the complex covered by all the genetic hits scoring in the screen) or a yellow pie chart (percent of the complex covered by all the genetic hits which have interactions reported in the Bioplex 3.0 dataset), whereas the diameter of the circle indicates the total size of the reported complex (Table S5).

Actin cytoskeleton nucleation plays an important role in phagocytosis

To ratify our dataset of phagocytic modulators, we decided to pick genes for an arrayed validation that displayed the largest aLFC from the identified complexes with the highest completeness, underlaid with light orange ellipses in the network (Fig 2). Among these was the Arp2/3 complex (Goley & Welch, 2006). This actin-nucleating machinery has been described to be highly essential for phagocytic cup formation and is also the mechanistic target of our chemical assay control, Cytochalasin D (May et al, 2000). Our genetic screen picked up all subunits of the Arp2/3 complex (ARPC1B, ARPC2, ARPC3, ARPC5, ARPC4, ACTR3, and ACTR2), highlighting the high degree of coverage of our experimental set-up. Assessing the reporter uptake of individual *ARPC2* KO cell lines showed significantly decreased phagocytosis (Fig 3A and B), validating the findings of the genome-wide pooled screen. Moreover, our screen identified 80% of the members of the Wave-2 complex as hits (WASF2, CYFIP1, ABI1, BRK1, and NCKAP1) and most of these had recorded interactors in the BioPlex 3.0 dataset. WASF2 is a scaffolding protein that employs the Arp2/3 complex and has been reported to be essential for the formation of lamellipodia (Oikawa et al, 2004), indicating that our reporter enters macrophages through these structures. Since WASF2 is a central actin-nucleator and scaffolding protein for Arp2/3, without being essential for diverse processes within the cell unrelated to phagocytosis as the Arp2/3 complex, we picked it as the first in-detail validation target (Fig 3C). Thus, we derived *WASF2* KO clones from the human monocyte cell line U937 (Liu & Wu, 1992), which is competent for phagocytosis and amenable to single clone isolation. We used 4 different sgRNAs targeting different exons of *WASF2* (Fig 3G). After confirming by immunoblotting, the successful knock-out of *WASF2* in these clones (Fig 3D), we rescued them either with a *WASF2* cDNA (designed to be resistant against sgRNAs 1, 2, and 4 but not against sgRNA 3, cutting control that can cut the *WASF2* cDNA, Fig 3G) or with mock cDNA as control. WASF2 is proposed to be a key effector in the life cycle of *Listeria monocytogenes* (Bierne et al, 2005). We took advantage of this to validate our cellular clones. We infected them with *Listeria* and quantified the total amount of bacteria phagocytosed after 3 h, as exemplified in Fig 3E. Effectively, the *WASF2* knock-out cell lines that only express the mock control cDNA, harbored lower levels of total phagocytosed bacteria (Fig 3F). The phagocytic activity of those cells was then evaluated using the reporter uptake assay. Indeed, cells knocked out for *WASF2*, only expressing the mock control cDNA, showed significant ablation for the PhagoLate fraction with a concurrent increase of the PhagoNeg fraction, indicating a decrease in total phagocytosis (Fig 3H). At the same time, this defect could be rescued by expressing a *WASF2* cDNA, confirming that the impairment of phagocytosis was caused by the knock-out of *WASF2* (Fig 3G and H).

Our physical interaction map of genetic hits offers the opportunity to streamline validation by navigating neighboring cellular complexes as a functional framework, instead of choosing randomly among the 716 genes (Fig 2). The underlying assumption is that proximity to a validated node will increase the validation efficiency of the next one, while allowing to derive a functional relationship between the two.

In our network, the Wave-2 complex is connected via BRK1 to the WASH complex (KIAA0196, CCDC53), an endosomal hub responsible for the activation of Arp2/3 (Jia et al, 2010) (Fig 2). Knock-out of *KIAA0196* indeed led to a phenotype (significant reduction of reporter uptake) comparable to *WASF2*, confirming the functional connection suggested by the protein network (Figs 2 and 3A).

Bafilomycin A1 stayed in the PhagoEarly gate. The marginal intensity distributions are illustrated on the side of the plot. **(B, C)** Barplot showing the quantification of the different fractions of cells gated in (B). Data are mean ± 95% confidence interval from 3 technical replicates, representative for two independent experiments. ***$P \leq 0.001$, ****$P \leq 0.0001$; by Welch's *t* test. **(D)** Volcano plot showing the 716 genes depleted in the PhagoLate population versus the PhagoNeg population. The x-axis shows the average $\log_2$-fold change calculated for all sgRNAs per gene against the y-axis, representing the statistical significance as $-\log_{10}$Padj. The size of the dot indicates the amount of sgRNAs changing significantly for the particular gene. **(D, E)** Gene Ontology (GO) enrichment analysis (two-sided Fisher's exact test, *P*-value adjusted for multiple testing) for genes depleted in the PhagoLate population seen in (D) for GO cellular components and GO biological processes. The x-axis shows the significance of enrichment ($-\log_{10}$-transformed *P*-value adjusted for multiple testing) against the y-axis showing the top 10 enriched terms, sorted by adjusted *P*-value.

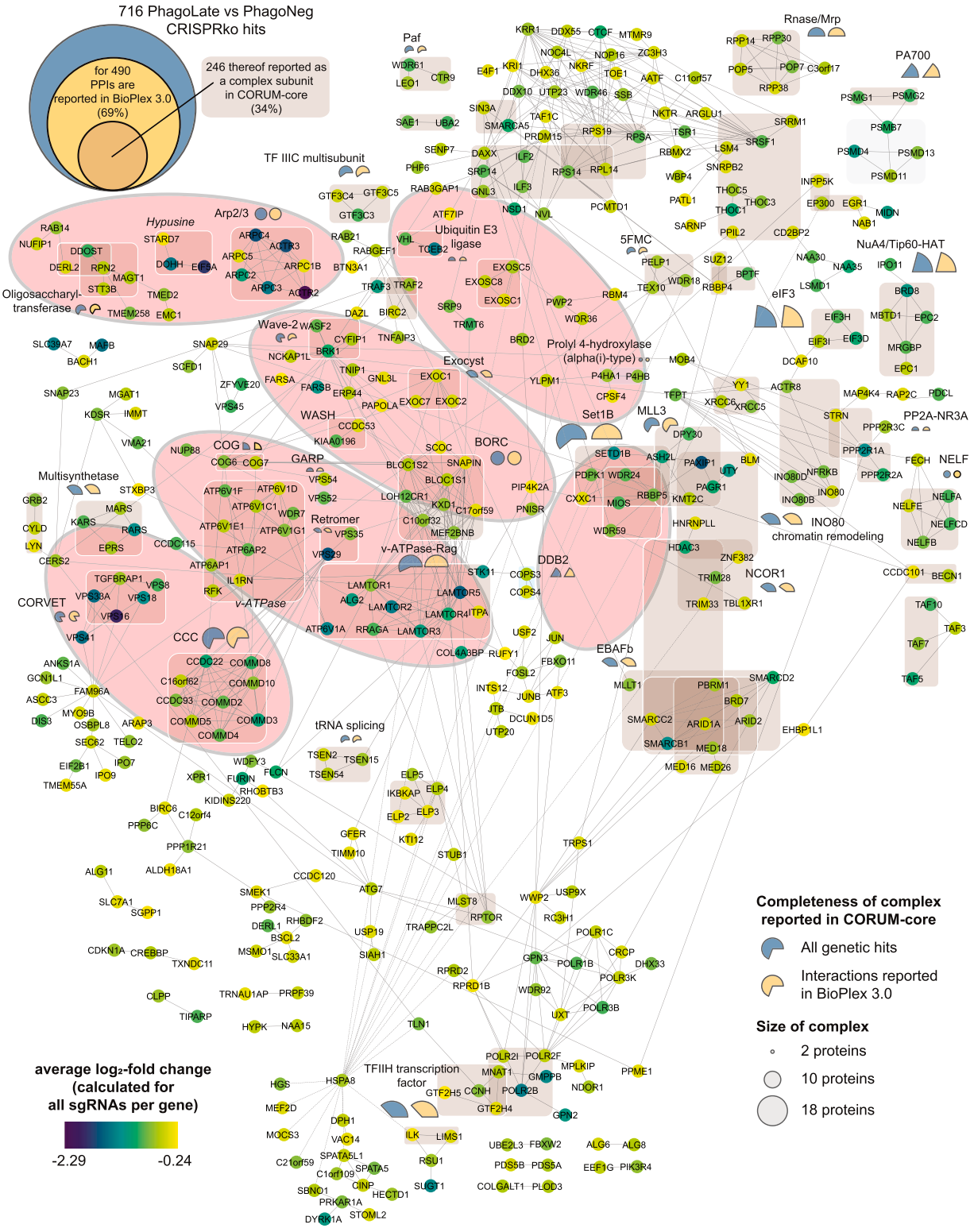

Figure 2. Physical interaction map of genetic hits yields the molecular network regulating phagocytosis.
Network of 490 genes that are depleted in the PhagoLate population (Fig 1D) and have reported protein–protein interactions in BioPlex 3.0. Each circle represents a gene, and the lines represent the reported protein–protein interactions. The color of the circle represents the average $\log_2$-fold change. 246 of the genes are reported as a complex subunit in the CORUM-core database and are highlighted with light brown boxes. The percent completeness of these complexes is indicated either with a blue (percent of respective complex covered by all the genetic hits scoring in the screen) or a yellow (percent of respective complex covered by all the genetic hits which

Lysosomal regulation modulates acidification of the lysosome and affects phagocytosis

Continuing along our "validation path" we observed that the WASH complex is connected multiple times to the BORC complex (BLOC1S1, BLOC1S2, SNAPIN, LOH12CR1, KXD1, C10orf32, C17orf59, and MEF2BNB) (Pu et al, 2015), which we identified in our genetic screen with a remarkable 100% completeness, underlining its importance for phagocytosis. Since the BORC complex in our network displays further connections to the vacuolar–ATPase–Rag complex (LAMTOR1, LAMTOR2, LAMTOR3, LAMTOR4, LAMTOR5, ALG2, ATP6V1A, and STK11) and is through these further connected to the vacuolar-ATPase protein machinery (ATP6V1F, ATP6V1D, ATP6V1C1, ATP6V1E1, ATP6V1G1, ATP6AP1, ATP6AP2, WDR7, and IL1RN) (Kissing et al, 2015), we believe that this subnetwork of hits delineates important lysosome-regulating functions. ARL8B is another prominent regulator of lysosomal trafficking that scored in our screen and is part of this subnetwork, but is not represented in our network as it lacks within BioPlex 3.0 any direct connection with hits identified within our screen (Garg et al, 2011; Pu et al, 2015). We validated this neighborhood by knocking out *LAMTOR5* as a member of the vacuolar–ATPase–Rag complex and *KXD1*, a member of the BORC complex. Whereas *LAMTOR5* loss of function cell lines showed asignificant reduction in phagocytosis, knock-out of *KXD1* led to less or no significant effects in the individual phagocytosis assays. This result correlates with the obtained aLFC for *LAMTOR5* (aLFC = −1.62, $-\log_{10}$Padj = 4.83) versus *KXD1* (aLFC = −0.696, $-\log_{10}$Padj = 2.29) in the genetic screen. We believe that this case demonstrates that single-cell line validation experiments often struggle to significantly validate small effects on a biological process, whereas on the other hand, pooled genetic screening that uses hundreds of millions of individual cells has the experimental and statistical power to detect the entire BORC complex as a regulator for phagocytosis (Fig 3A). Interestingly, the target of Bafilomycin A1, vacuolar-ATPase, is also a hit in this subnetwork. In contrast to long-lasting genetic ablation, as shown with *ATP6AP2* knock-out cell lines (Fig 3A), acute drug treatment allows revealing the importance of the acidification process of phagocytosis without affecting uptake or cargo shuffling (Fig 1B).

Involvement of the vesicle-trafficking machinery in phagocytosis

In our network of functional hits, the BORC complex was also connected to the conserved structural Golgi protein COG6 (Ungar et al, 2002) and through this, to four complexes responsible for vesicle trafficking within the cell, such as the exocyst complex (EXOC1, EXOC2, and EXOC7) (Katoh et al, 2015), the GARP complex (VPS52 and VPS54) (Pérez-Victoria et al, 2010), the retromer complex (VPS29 and VPS35) (Haft et al, 2000), and the CORVET complex (VPS16, VPS18, VPS33A, VPS8, and TGFBRAP1) (van der Kant et al, 2015). To continue our validation campaign, we generated knock-out cell lines for several subunits of the abovementioned complexes including *COG6*, *EXOC1*, *VPS52*, *VPS35*, and *VPS16*. We observed a significant reduction in phagocytosis in all these knock-out cell lines (Fig 3A).

The knock-out of *VPS35*, a subunit of the retromer complex, significantly reduced the PhagoNeg and interestingly increased the PhagoEarly fraction. This indicates that in a functional assessment of the different phagocytosis steps, absence of *VPS35* increases the uptake of the reporter, while leaving the rate of acidification of material unchanged. This could represent the equivalent of a "traffic jam" in the early endosome (PhagoEarly). Knock-out of *COG6* seems to affect the uptake of beads less, but rather the transport to the phagolysosome (Fig 3A).

In our network, we could then observe interactions between the retromer complex and all of the subunits of the CCC complex (also known as the Commander Complex). Within our genetic screen, we covered all 10 in CORUM-reported subunits of the CCC complex (COMMD2, COMMD3, COMMD4, COMMD5, COMMD8, COMMD10, CCDC22, CCDC93, VPS29, and C16orf62/VPS35L) as single individual hits. The CCC complex is a poorly studied protein assembly that seems to play a role in endosomal cargo retrieval, recycling, and regulation of NF-κB and hypoxia-induced transcription (Cullen & Steinberg, 2018; Laulumaa & Varjosalo, 2021). Through the strong interconnection with the retromer complex within the network presented in this work (Fig 2), we speculate to ascribe a biological role in phagocytosis to the CCC/Commander complex, likely to be related to the vesicular sorting function of the retromer complex (Figs 2 and 3A). Assessing uptake of the reporter in individual *COMMD3* KO cell lines showed variations between replicates of the phagocytosis assay. This may reflect a potentially more pleiotropic effect of the CCC complex on phagocytosis (Fig 3A), as one might expect based on the above-reported features of the CCC complex.

The oligosaccharyltransferase complex (OST) is a strong modulator of phagocytosis

Although the OST (RPN2, DDOST, STT3B, and MAGT1) forms an independent subnetwork on our map, we decided to further assess its role due to its high completeness in our screen. The OST complex is a core-member of the central machinery for N-linked protein glycosylation. We chose to knock out the magnesium transporter *MAGT1*/*SLC58A1*, known to be mutated in patients with a disorder called X-linked immunodeficiency with magnesium defect, EBV infection, and neoplasia (XMEN) (Ravell et al, 2020). A further hint that SLC58A1 is involved in phagocytosis is that *SLC58A1*-deficient cells manifested a very strong defect in phagocytosis (Fig 3A).

We chose to validate six additional hits from the screen that were not part of large molecular complexes but had not been previously associated with phagocytosis. Of these hits, three showed a less robust effect in the validation process, manifested by variations between individual replicates of phagocytosis assays (*COPS3*, *P4HA1*, and *PSMD13*). Knock-out of *STK11* mainly negatively affected the uptake of the material, revealed by decreased PhagoNeg fractions but fewer effects on the PhagoEarly and PhagoLate

have interactions reported in the Bioplex 3.0 dataset) pie chart, whereas the size of the circle indicates the total size of the reported complex. Identified complexes with the highest completeness are underlaid with light orange ellipses.

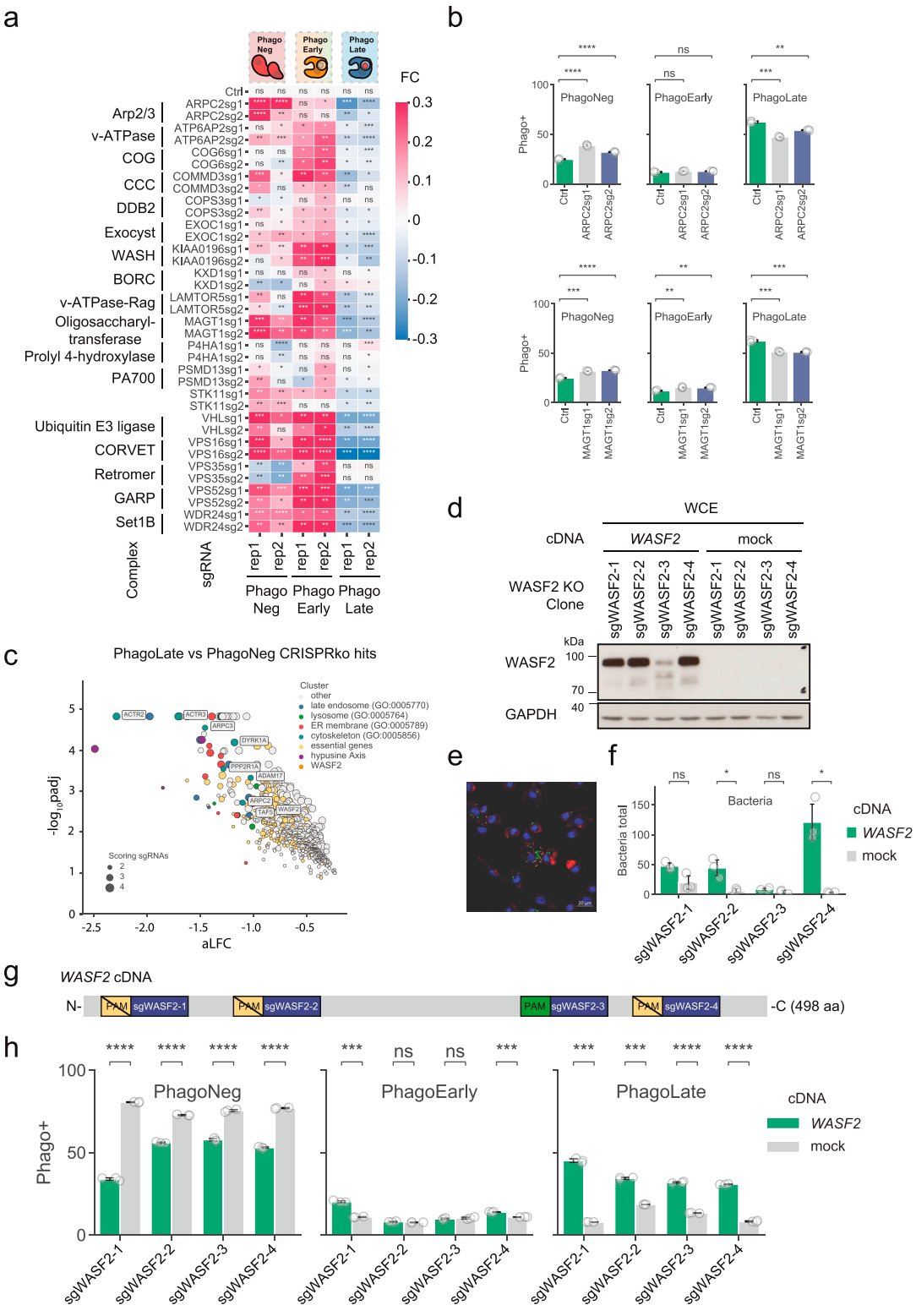

Figure 3. Systematic validation of phagocytosis hits.
(A, B) Heatmap showing the fold change (FC) of fractions recorded in phagocytosis assays in the respective knock-out cell lines listed on the y-axis compared to control cell lines (Ctrl), as shown in an example in (B). Blue color indicates negative FC, white color no FC, and red color positive FC. For each sgRNA phagocytosis assays were performed in two biological replicates (indicated as rep1 and rep2 on the x-axis), consisting of three technical replicates each, as indicated on the x-axis. Each cell represents the mean ± 95% confidence interval from three technical replicates. ns $P > 0.05$, *$P \leq 0.05$, **$P \leq 0.01$, ***$P \leq 0.001$, and ****$P \leq 0.0001$; by Welch's *t* test.
(B) Barplot showing the quantification of the PhagoNeg, PhagoEarly, and PhagoLate fractions as examples for validation of the Arp2/3 complex on *ARPC2* KO cell lines and

fractions and Ubiquitin E3 ligase *VHL*, and *WDR24*, led to a general defect in phagocytosis (Fig 3A).

In summary, of the genes that we assessed individually in phagocytosis assays tracking three different stages, more than three quarters validated effectively. This suggests that overall, the dataset encompassing 716 genes represents a valuable resource for the molecular characterization of the cellular machinery in the complex phagocytosis process.

Depletion of the unique post-translational modification hypusine on eIF5A reduces phagocytosis

Interestingly, the gene with the highest significant depletion in genome-wide phagocytosis screen was Deoxyhypusinesynthase (*DHPS*), scoring together with two other genes (*DOHH* and *eIF5A*) that are all involved in forming the unique post-translational modification hypusine (Park et al, 1981) (Figs 1D and 4G). eIF5A is a small ~17-kD conserved protein, the mammalian ortholog of the bacterial translation factor EFP (Doerfel et al, 2013), and the only known target of the post-translational modification hypusine, which is incorporated by an interplay of the two enzymes DHPS and DOHH from the polyamine precursor—spermidine (Wolff et al, 2007). Since not only *eIF5A* but also *DHPS* and *DOHH* scored as hits in the screen, we concluded that the absence of hypusine must be causative of a phagocytosis defect (Fig 4A). To check this, we generated an inducible THP-1 knock-out model for *DHPS* using an inducible CRISPR-Cas9 knockout backbone (TLCV2) (Barger et al, 2019). Furthermore, since there was no commercial antibody available for hypusine, we generated a recombinant hypusine-specific antibody based on a sequence published by Zhai and colleagues (Zhai et al, 2016). We validated the antibody by transiently expressing *DHPS*, *DOHH*, and *eIF5A* (either *eIF5A*-WT or mutated for the hypusine-modification site lysine 50) in HEK293T cells. The antibody successfully detected hypusinated eIF5A, whereas there was no signal detected in cells overexpressing the eIF5A-K50 variant (Fig 4B). To further validate the binder, we tested it on lysates of THP-1 cells treated with the DHPS-inhibitor GC7 (Melis et al, 2017) and observed down-regulation of hypusine after 24–72 h (Fig 4C). As GC7 could also act indirectly, we used the inducible *DHPS* knock-out cell models to show that the down-regulation of DHPS is sufficient to down-regulate hypusine (Fig 4F). Having validated our experimental set-up, we measured phagocytosis in both settings. Treating THP-1 cells with GC7 led to a significant drop of the PhagoLate fraction with a parallel rise of the PhagoNeg fraction, suggesting an effect of hypusine on the total rate of phagocytosis (Fig 4D). We observed the same effect when we measured phagocytosis after *DHPS* knock-out (Fig 4H). Introducing a *DHPS* WT cDNA, designed to be resistant against the sgRNA, could rescue the defect, demonstrating the specific dependency on *DHPS* (Fig 4E, F, and H). As an additional control of our cell model, we then rescued our *DHPS* knock-out model with *DHPS* cDNAs mutated to strongly reduce spermidine binding (D243A) (Lee et al, 2001). Interestingly, when we rescued our cell model with the D243A mutant *DHPS* cDNA, the cell seemed to compensate for the reduced function of the D243A *DHPS* variant by higher expression levels of D243A compared to other DHPS protein levels (Fig 4F). Nevertheless, despite higher expressed levels of the mutant DHPS, we observed less phagocytosis compared to cells rescued with *DHPS* WT cDNA (Fig 4H). A clinical study on patients with severe neurodevelopmental disorders reported recessive rare variants in the *DHPS* gene (Ganapathi et al, 2019). Therefore, we wondered if the expression of these mutant DHPS variants would also lead to a defect in our phagocytosis assay. Indeed, when we expressed either the N173S or the ΔY305–I306 patient *DHPS* variants in our *DHPS* knock-out model, we could observe a clear defect in phagocytosis (Fig 4H). The expression levels of the mutant DHPS proteins were comparable to the WT (Fig 4F). Thus, *DHPS*, *DOHH*, and *eIF5A* can be regarded as genes validated for their involvement in phagocytosis.

Discussion

The FACS-based genome-wide CRISPR/Cas9 knock-out screen allowed us to identify a large number of genes involved in the regulation and execution of the phagocytosis process. The high number of genes scoring positive in the assay represented a challenge for further validation. We designed a strategy that used integration with existing PPI networks to prioritize which genes to validate. We reasoned that focusing on those molecular machines of the cell, whose components were "genetically hit" multiple times in the screen, would be an expedient to increase the statistical significance of the various cellular functions associated with phagocytosis and thus ensure a higher validation rate. Recently, Haney and colleagues undertook a systematic search for phagocytic regulators with a pooled CRISPR screen approach (Haney et al, 2018). They used macrophage-differentiated U937 cells and incubated them

for the oligosaccharyltransferase complex on *MAGT1* KO cell lines. Data are mean ± 95% confidence interval from three technical replicates, representative for two independent experiments. ns $P > 0.05$, $^{**}P \le 0.01$, $^{***}P \le 0.001$, and $^{****}P \le 0.0001$; by Welch's *t* test. **(C)** Volcano plot highlighting *WASF2* and genes of the Arp2/3 complex scoring within the 716 genes depleted in the PhagoLate population. The x-axis shows the average $\log_2$-fold change calculated for all sgRNAs per gene against the y-axis, representing the statistical significance as $-\log_{10}$(Padj). The size of the dot indicates the amount of sgRNAs changing significantly for the particular gene. **(D, G)** Western blot showing the expression of WASF2 in U937 *WASF2* knock-out cell clones, overexpressing either a mock cDNA or a *WASF2* cDNA, designed to be resistant to cleavage by sgWASF2-1, 2, and 4 but not sgWASF2-3, as depicted in (G). **(E)** Representative image showing the readout used for quantification of the listeria assay. The green color highlights *Listeria monocytogenes*, the red color highlights actin, and blue highlights the DAPI staining. **(D, F)** Barplot showing the quantification of the total amount of *Listeria monocytogenes* of cell lines validated in (D). The green color highlights the clonal U937 *WASF2* KO cell lines expressing WASF2 and the grey color shows the same cell lines expressing a mock cDNA as control. Data are mean ± 95% confidence interval from three technical replicates. ns > 0.05, $^{*}P \le 0.05$ by Welch's *t* test. **(D, G)** Schematic representation of the *WASF2* cDNA overexpressed in cell lines validated in (D). PAM indicates the protospacer-adjacent motif compatible with Cas9 detection of each *WASF2* sgRNA, indicated by the blue boxes. **(D, H)** Barplot showing the quantification of the PhagoNeg, PhagoEarly, and PhagoLate fraction of cell lines validated in (D). The green color highlights the clonal U937 *WASF2* KO cell lines expressing WASF2, and the grey color represents the same cell lines expressing a mock cDNA as control. Data are mean ± 95% confidence interval from three technical replicates, representative for two independent experiments. ns $P > 0.05$, $^{***}P \le 0.001$, and $^{****}P \le 0.0001$; by Welch's *t* test.

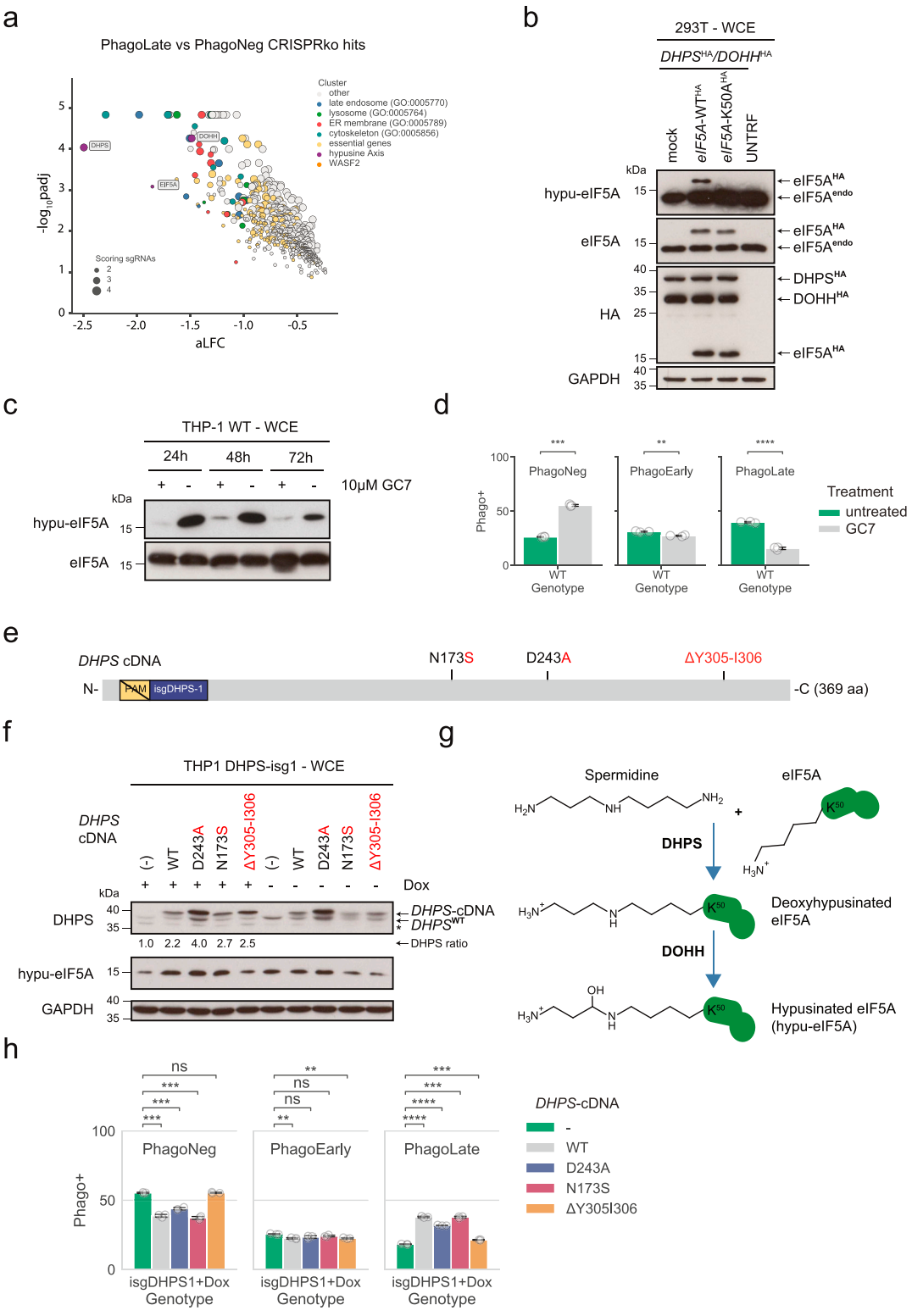

Figure 4. Absence of hypusine abrogates phagocytosis.
(A) Volcano plot highlighting the genes of the hypusine axis within the 716 genes depleted in the PhagoLate population. The x-axis shows the average $\log_2$-fold change calculated for all sgRNAs per gene against the y-axis, representing the statistical significance as $-\log_{10}$(Padj). The size of the dot indicates the amount of sgRNAs changing significantly for the particular gene. **(B, C)** Western blot analysis of hypusine (hypu-eIF5A) in HEK293T cells overexpressing either a mock or C-terminal HA-tagged eIF5A-WT (*eIF5A*-WT^{HA}) or eIF5A-K50A mutant cDNA (*eIF5A*-K50A^{HA}) and a C-terminal HA-tagged DHPS cDNA (*DHPS*^{HA}) and DOHH cDNA (*DOHH*^{HA}) (C). Western blot analysis of hypusine levels (hpu-eIF5A) in THP-1 WT cells treated with or without 10 μM GC7 at the respective time point (24–72 h). **(D)** Barplot showing the quantification of the

with magnetic beads conjugated to a series of different substrates such as myelin, zymosan, and sheep red blood cells. In our study, we use the human monocytic cell line THP-1 differentiated into macrophages and an FACS-sorting-based separation approach. We confirmed and expanded their identified regulators as to the importance of the Arp2/3 machinery, Wave-2 complex, and the mTOR-associated Ragulator complex. This was demonstrated by the high genetic coverage of these protein complexes in our dataset. As already shown by Haney and team in U937 cells, loss of subunits of the actin polymerization machinery is detrimental to phagocytosis in THP-1 cells. Several datasets collected in screening efforts for host regulators in the context of *Salmonella* (Yeung et al, 2019), *Legionella pneumophila* (Jeng et al, 2019), and *Staphylococcus aureus* (Lindner et al, 2021) pathogeneses confirmed the importance of the actin polymerization machinery. This indicates that our pathogen-agnostic reporter approach used in this screen successfully mapped the cellular routes taken by pathogens. Furthermore, we identified several members of the exocyst complex to be required for phagocytosis. Previous studies on the interaction of Cdc42 with the exocyst complex, which was found to be essential for promoting phagocytosis (Mohammadi & Isberg, 2013), helped us to interpret the scoring of the exocyst complex in our screen. As Cdc42 is a Rho GTPase central for actin dynamic (Bonfim-Melo et al, 2018), we can now position the exocyst complex close to the family of actin regulators in our hit-reconstructed protein-interaction network (Fig 2).

Our study also confirmed the importance of the positive regulation of mTOR signaling for phagocytosis (Haney et al, 2018), a finding that was also revealed by the identification of RagA (*RRAGA*) as a regulator of microglial phagocytic flux in a zebrafish screen (Shen et al, 2016). Remarkably, our screen identified all five members of the Ragulator complex (LAMTOR1, LAMTOR2, LAMTOR3, LAMTOR4, and LAMTOR5) as well as *RRAGA*. In addition, we found the full BORC complex, the machinery responsible for positioning lysosomes. The BORC complex is reported to interact with the Ragulator, a complex that negatively regulates the activity of BORC in response to amino acid starvation sensed by SLC38A9, a critical regulator of the lysosomal function that we had previously identified (Rebsamen et al, 2015; Filipek et al, 2017; Wyant et al, 2017). The role of BORC in phagocytosis can potentially be explained by a recent preprint showing the importance of TORC1, BORC, ARL-8, and kinesin-1 for vesiculation of the phagolysosome and especially the role of BORC as a promoter for phagolysosomal degradation (Fazeli et al, 2022 *Preprint*).

Our screen also highlighted the importance of coordinated cargo transport through the cell for phagocytosis. This requires the trafficking and fusion of endosomes, controlled by Rab-GTPases, SNARE proteins, and multi-subunit–tethering complexes (Bröcker et al, 2010). Using our dataset to identify the parts of this canonical vesicle-trafficking machinery of most relevance for phagocytosis, we observed that large parts of the CORVET and HOPS complexes, machinery that coordinate together with Rab5 and Rab7 (*RAB5C* and *RAB7A* are hits as well) the fusion of the endosome with the lysosome, score as strong phagocytic regulators. Notably, in VPS16, the shared subunit of both the CORVET and HOPS complex, showed the strongest depletion in our screen among the aforementioned regulators (van der Kant et al, 2015). Likewise, we identified large parts of the GARP complex, which, together with the COG complex, forms the Golgi machinery associated with phagocytosis (Pérez-Victoria et al, 2010), and large parts of the retromer complex, an apparatus responsible for the recycling of organelles in the cell (Haft et al, 2000).

MAGT1/*SLC58A1*, a gene whose loss-of-function mutations cause X-linked immunodeficiency with magnesium defects (XMEN; OMIM: 300853) (Watson et al, 2022), significantly scored together with other parts of the OST complex as phagocytosis regulators in our screen and was previously found as host cell regulators of *Legionella pneumophilia* (Jeng et al, 2019). Either MAGT1/SLC58A1 or its paralog TUSC3/SLC58A2 can assist the STT3B–OST complex during post-translational N-glycosylation in the endoplasmic reticulum (Harada et al, 2019; Ravell et al, 2020). However, since *TUSC3* is not expressed in immune cells, THP-1 cells rely only on *MAGT1* (Watson et al, 2022) and indeed, our screen scored only *MAGT1* but not *TUSC3* as a phagocytic regulator. As noted, MAGT1/SLC58A1 is also a transporter of magnesium ions (Mg^{2+}), a metal that is recognized recently as being crucial for the regulation of immune response (Maier et al, 2021). Therefore, both functions of SLC58A1, its facilitating role in the STT3B–OST complex, and the magnesium transport function, could play a crucial role in phagocytosis. Since we additionally identified the accessory proteins (DDOST and RPN2) and the catalytic subunits (STT3A and STT3B) of the OST complex as hits, we conclude that N-linked glycosylation plays an important general role in phagocytosis and consequently speculate that dysregulated phagocytosis might be a factor in XMEN disease (Ravell et al, 2020). How exactly N-linked glycosylation affects phagocytosis will require dedicated investigations.

Beyond the hits described so far, numerous uncharacterized genes that had never been previously linked to phagocytosis were scored in our screen. This valuable resource is included in the dataset associated with this study (Table S1). A detailed validation of the identified genes will undoubtedly represent a worthwhile follow-up of the work presented here.

PhagoNeg, PhagoEarly, and PhagoLate of a phagocytosis assay performed with cells treated with or without 10 μM GC7. Data are mean ± 95% confidence interval from three technical replicates, representative for two independent experiments. ***P* ≤ 0.01, ****P* ≤ 0.001, and *****P* ≤ 0.0001; by Welch's *t* test. **(E, F)** Schematic representation of the cDNA of *DHPS* overexpressed in cell lines validated in (F). PAM indicates the protospacer-adjacent motif compatible with Cas9 detection, isgDHPS-1 marks the binding site of the respective sgRNA, and N173S, D243A, and ΔY305-I306 indicate mutations introduced in the corresponding DHPS cDNAs. **(F)** Western blot analysis of the expression of endogenous DHPS ($DHPS^{WT}$), overexpressed WT or mutated DHPS (*DHPS*-cDNA) and hypusine levels (hypu-eIF5A) in doxycycline-inducible THP-1 knock-out cells grown either with or without doxycycline. The ratio of expression of the respective *DHPS*-cDNA compared to the expression of the reference ($DHPS\text{-cDNA}^{[-]}$, lane 1) is indicated below the DHPS blot. Asterisk denotes a non-specific band. **(G)** Schematic showing the key steps and enzymes involved in the hypusine axis. K50 highlights the lysine on eIF5A that undergoes the hypusine modification. **(F, H)** Barplot showing the quantification of the PhagoNeg, PhagoEarly, and PhagoLate of phagocytosis assays performed with the cell lines described in (F). Data are mean ± 95% confidence interval from three technical replicates, representative for two independent experiments. ns > 0.05, ***P* ≤ 0.01, ****P* ≤ 0.001, and *****P* ≤ 0.0001; by Welch's *t* test.

To our surprise, however, the top depleted gene in our screen was *DHPS*, along with its two interacting proteins DOHH and eIF5A, which both scored with very high significance. eIF5A is one of the 20 most abundant proteins in proliferating cells (Hukelmann et al, 2016) and therefore, it is not unexpected that it has been implicated in many cellular functions such as translational elongation (Saini et al, 2009), nucleoplasmic transport (Rosorius et al, 1999), cell proliferation, and as a modulator for mRNA decay (Valentini et al, 2002). DHPS generates the post-translational modification deoxyhypusine by conjugation of the aminobutyl moiety of spermidine on the lysine of eIF5A which is then matured to hypusine by DOHH (Park et al, 1981). Over the years, elegant work has led to the structure of the nuclear shuttle for hypusinated eIF5A (Xpo4) (Aksu et al, 2016), the description of RNA-binding properties for hypusinated eIF5A (Xu et al, 2004), and reports on patients with mutations in *eIF5A* (Faundes et al, 2021), *DHPS* (Ganapathi et al, 2019), or *DOHH* (Ziegler et al, 2022) that all showed neurodevelopmental phenotypes. Although until recently (Lindner et al, 2021), the hypusine axis was never identified in the context of phagocytosis, several previous studies suggested its implication in vesicular trafficking, cytoskeleton organization, and immune cell regulation; all processes highly relevant for phagocytosis. Already in 1952, spermine was found as an anti-mycobacterial natural agent (Hirsch & Dubos, 1952) and later, as an inhibitor for cytokine synthesis in human mononuclear cells (Zhang et al, 1997). Yeast studies found a synthetic lethal interaction between *eIF5A* and *YPT1* (the yeast ortholog of mammalian rab genes, coordinators of endocytosis) (Clague, 1998; Frigieri et al, 2008) and the regulators for yeast cell polarity and actin nucleation (*PKC1*, *ZDS1*, *GIC1* [human ortholog *CDC42*], as well as *PCL1* and *BNI1*) as suppressors for eIF5A depletion (Zanelli & Valentini, 2005). Like the bacterial ortholog EFP (Doerfel et al, 2013), eIF5A was found to assist the translation of polyproline stretches in mammalian proteins (Gutierrez et al, 2013; Ude et al, 2013; Barba-Aliaga et al, 2021) that are especially enriched in proteins of the actin/cytoskeleton, RNA splicing/turnover, DNA binding/transcription, cell signaling (Mandal et al, 2014), and in collagen. Furthermore, whereas the DOHH homolog nero and eIF5A showed to be required for autophagy in drosophila (Patel et al, 2009), eIF5A was found in human cells to regulate the translation of TFEB and therefore also regulate autophagy (Zhang et al, 2019). In addition, eIF5A was shown to assist with the co-translational translocation of proteins in the ER (Rossi et al, 2014), and ablation of eIF5A triggers ER stress in mammalian cells (Mandal et al, 2016). Recently, the hypusine axis was described in the context of macrophage respiration (Puleston et al, 2019), and as the effector of the macrophage inflammatory state in adipose tissue (Anderson-Baucum et al, 2021). Finally, mice lacking hypusine are more susceptible to *Heliobacter pylori* and *Citrobacter rodentium* infections (Gobert et al, 2020).

Since we identified the whole hypusine axis and eIF5A as the unique carriers of hypusine, we hypothesized that the hypusinated form of eIF5A must play a significant role in phagocytosis. Our experiments confirmed that the absence of hypusine, either by blocking DHPS, the key enzyme for hypusination, pharmacologically with GC7 or by a knock-down of *DHPS* with Cas9 indeed led to reduced phagocytosis. Remarkably, we could further show that this defect in phagocytosis also occurred when we replaced the endogenous version of DHPS in THP-1 cells with recessive rare variants of mutated DHPS found in patients (N173S and ΔY305-I306) with neurodevelopmental disorders or with a DHPS variant mutated in the predicted binding site of spermidine (D243A).

In summary, our screen functionally outlined the basic phagocytic machinery to involve several hundred gene products organized in at least two dozen protein complexes. Phagocytosis as a long and complex process functionally requires the contribution of several subprocesses, such as cytoskeletal mechanical and membrane-uptake machinery involved in engulfing and internalizing the foreign material in the phagosome, trafficking of the phagosome, fusion with the lysosome followed by acidification and clearance, and recycling to the plasma membrane. Here, publicly available PPI data and complex annotation allowed us to assign genes to cellular functions, at least in those instances where the annotation of cellular protein complexes was unequivocal. Our work offers an improved understanding of how cargo travels through the endo-lysosomal system and we anticipate that this could in turn direct therapeutics better to their proposed site within the cell, such as antibody–drug conjugates (Tsui et al, 2019) or Cas9 (Lino et al, 2018). In addition, it might help identify new targets for interventions in diseases caused by dysfunctional autophagy or endo-lysosomal systems such as the neurodegenerative diseases Alzheimer's disease, Parkinson's disease, or Huntington's disease. Because the screen presented in this work is based on a single reporter, further similar screens with different substrates will help to further refine the network of phagocytosis regulators. Ultimately, we believe that mining and integrating publicly available PPI data with reporter-based genome-wide genetic screens showcased in this study offers a powerful and widely applicable approach for genetically mapping complex biological processes.

Materials and Methods

Cell lines

THP-1, U937, and HEK293T cells were purchased from ATCC. THP-1 and U937 were maintained in RPMI1640. HEK293T was maintained in DMEM. All media were supplemented with 10% FBS and antibiotics (100 U/ml penicillin, 100 mg/ml streptomycin), all either from Gibco or Sigma-Aldrich. Cell lines were grown at 37°C in 5% CO_2.

Phagocytosis assay

Phagocytosis assay was conducted as previously described (Colas et al, 2014). Reporter beads were generated by opsonization of dual-colored 1.75-μm latex beads (Fluoresbrite carboxylated 1.75 μm microspheres [yellow-green: 441-nm excitation, 486-nm emission, cat no. 17687-5; Polyscience]) in 50% human male AB serum in PBS for 16 h at 4°C under permanent rotation. Then beads were washed twice with PBS and labeled with 2 μg/ml pHrodo-Red SE in PBS (cat no. P36600; Thermo Fisher Scientific) for 30 min at room temperature under constant agitation. Reporter beads were then washed with PBS and adjusted to a final concentration of 1×10^9 beads per ml in PBS.

For phagocytosis assays that were performed on individual cell lines, PMA-differentiated cells (THP-1 or U937) were seeded on 12-well cell culture-coated dishes (1 × 10^6 cells per well). Reporter beads were then added to the cells at an MOI of 10 for 3 h. Cells were then transferred onto ice, washed three times with ice-cold PBS, detached by scraping with a soft-rubber cell scraper, and analyzed on an LSR Fortessa II cytometer controlled with FACSDiva (BD), analyzed with FlowJo software (v.10), and visualized with Python project version 3.8.8 (Python Software Foundation. Available at http://www.python.org) with pandas (Reback et al, 2021) (1.2.4), numpy (1.20.1), matplotlib (Hunter, 2007) (3.3.4), seaborn (Waskom, 2021) (0.11.1), and statannotations (0.4.4). Live cells were gated based on FSC-A and SSC-A, followed by FSC-A and FSC-H, and then SSC-A and SSC-H gating to select single cells. The number of pre-gated cells was equal across samples (30,000 pre-gated cells were collected in each sample).

For the Cytochalasin D (cat no. BML-T109-0001; Enzo) and Bafilomycin A1 (cat no. BML-CM110-0100; Enzo) control assays, cell media were supplemented with the compound 30 min before the addition of the reporter beads and added during the whole assay at final concentrations of 8 μM and 200 nM, respectively.

For the GC7 (cat no. 259545; EMD Millipore)-treated phagocytosis assays, cell media were supplemented during the entire differentiation and seeding period with 10 μM of the compound.

Genome-wide CRISPR-Cas9/KO screening and cell sorting

For screening, the genome-wide CRISPR-Cas9/KO Toronto Knockout version 3 library from Hart and team (Hart et al, 2017) (Addgene no. 90294), cloned into the one-vector system (lentiCRISPRv2 carrying Cas9 and sgRNA expression on the same vector), was used. The library consists of 70,948 guides, targeting 18,053 protein-coding genes with four sgRNAs each and 142 control sgRNAs. Viral particles were produced by transient transfection of HEK293T cells with the library and packaging plasmids pMD2.G (Addgene no. 12259) and psPAX2 (Addgene no. 12260) using PEI (Sigma-Aldrich). 8 h post-transfection, the medium was exchanged to RPMI1640 supplemented with 10% FBS. 72 h after transfection, the viral supernatant was collected, filtered (0.45 μm), and stored at −80°C until further use. THP-1 cells were infected in quadruplicates with this viral supernatant (supplemented with 8 μg/ml protamine sulfate) at library coverage of 3000× and a MOI of around 0.3, allowing a single-viral integration event per cell. Infected cells were then selected with 2 μg/ml puromycin for 8 d, followed by 9 d of growth in puromycin-free medium. Afterward, per replicate 750 × 10^6 infected and recovered THP-1 cells were differentiated on 15 cm cell culture-coated dishes (20 × 10^6 cells per dish). For differentiation, the cells were kept 48 h in RPMI1640 supplemented with 10% FBS and 10 nM PMA (Sigma-Aldrich), followed by 24 h of growth in RPMI1640 supplemented with 10% FBS without PMA (Fig S1). Phagocytosis assay was performed as described in the section "Phagocytosis assay" using dual-colored opsonized latex beads. ~300 million cells (>3,000× coverage) were used as the input for each phagocytosis assay. All cells were then sorted on a BD FACS Aria II, collecting phagocytosis-positive (PhagoLate) and phagocytosis-negative (PhagoNeg) populations. Genomic DNA was extracted using the QIAamp DNA Mini Kit (QIAGEN) and the sgRNA-containing cassettes were amplified with a one-round PCR approach following the method of Joung and team (Joung et al, 2017). Amplified samples were then sequenced on a HiSeq2000 (Illumina) at the Biomedical Sequencing Facility (BSF at CeMM, https://biomedical-sequencing.at) and analyzed by a custom analysis pipeline (see below).

Analysis of CRISPR screens

Sequences of sgRNAs were extracted from NGS reads, matched versus the original sgRNA library index, counted using an in-house Python script, and their abundance assessed using a two-step differential approach. First, differential abundance of individual sgRNAs was calculated using DESeq2 (Love et al, 2014). Afterward, sgRNAs were sorted by adjusted *P*-value and aggregated using the gene set enrichment algorithm (Subramanian et al, 2005; Korotkevich et al, 2016 *Preprint*; Kuleshov et al, 2016). Essential genes were evaluated by using the same two-step differential approach, comparing sgRNA abundance in undifferentiated cells collected on the day of differentiation to the plasmid stock of the sgRNA library used for virus generation (Fig S1).

Protein–protein interaction mapping of genetic hits

To probe for physical interactions between the 716 top hits of the genetic screen, a PPI network was generated. The protein interactions were extracted from BioPlex 3.0 (for HEK293T and HCT116, downloaded on 20.04.2022) (Huttlin et al, 2021), whereas only the protein interactions between the genes identified as high scoring within the genetic screen were considered. For the extraction of protein interactions, all bait–prey interactions reported in BioPlex 3.0 were considered, resulting in a PPI network with 490 proteins (69% of all genetic hits) with 726 interactions. The network was further organized into protein complexes and modules by annotating all proteins within the network with complexes reported in the CORUM-core (the comprehensive resource of mammalian protein complexes, CORUM September 2018 release) (Giurgiu et al, 2019). Within CORUM, homo dimers were removed. 246 proteins (50% of all) in the interaction network were reported as a subunit in protein complexes. Network visualization and ordering were conducted in Cytoscape (v.3.8.0). As a first step, all duplicated edges were removed as the directionality obtained by reciprocal AP-MS is not of relevance for the visualization of protein complexes within the network. The interactions were grouped into functional modules by following the association to protein complexes, whereas if a protein is mapped to multiple complexes, which is often the case as the CORUM-core contains complex identifiers with partially overlapping subunits, the complex with the highest completeness was considered. The selection of interactions and mapping of complexes were prepared with the statistical software R (v.4.1.3).

Plasmids and cloning

Knock-out cell lines were generated using the lentiCRISPRv2 CRISPR-Cas9 knock-out vector (Addgene no. 52961). Inducible knock-out cell lines were produced with the TLCV2 CRISPR-Cas9 backbone (Addgene no. 87360) that includes a doxycycline-inducible Cas9-2A-eGFP cassette. In short, for each gene, sgRNAs were designed using the CHOPCHOP prediction tool (Labun et al, 2019) unless indicated otherwise. Oligos, containing BsmBI-compatible overhangs were annealed and cloned into lentiCRISPRv2 using Golden Gate assembly.

Cloned oligonucleotides were as follows (5′ to 3′ orientation).

sgWASF2-1	caccgTAACGAGGAACATCGAGCCA	
sgWASF2-2	caccgTCGGTCGACCCTCTCAGCAA	
sgWASF2-3	caccgTTGGTGGTATCAGAAAGCGG	
sgWASF2-4	caccgAATGCGACGAGACAAGATGG	
sgiDHPS-1	caccgGTGCGCGGTAATTCACACCG	From TKOv3 library
sgiDHPS-4	caccgTAAGTGCGGGACTAAACACA	From TKOv3 library
EXOC1sg1	caccgCTACCACAGCAAGATCTCGA	From TKOv3 library
EXOC1sg2	caccgGATATGCCAAGCTGATGGAG	From TKOv3 library
COG6sg1	caccgGATGAAATGAGTCTTCTCCG	From TKOv3 library
COG6sg2	caccgTGTGACACTGAAGGCTGCAA	From TKOv3 library
MAGT1sg1	caccgATAACGGAGTAATTTCTCGG	From TKOv3 library
MAGT1sg2	caccgCAGCTGAGCAGATTGCCCGG	From TKOv3 library
ARPC2sg1	caccgGGTGAACAACCGCATCATCG	From TKOv3 library
ARPC2sg2	caccgGAAAGACACAGACGCCGCTG	From TKOv3 library
COMMD3sg1	caccgCTTGAAACATATCGACCCAG	From TKOv3 library
COMMD3sg2	caccgGAGGAGAAGCGTGAAGGCGT	From TKOv3 library
COPS3sg1	caccgCATGATATGACTGACCGCCA	From TKOv3 library
COPS3sg2	caccgGATGGGATAAGTTCTTCGCA	From TKOv3 library
LAMTOR5sg1	caccgGCTCATCTGACAGGGTCCCG	From TKOv3 library
LAMTOR5sg2	caccgGAAACACGATGGCATCACGG	From TKOv3 library
STK11sg1	caccgTGTATAACACATCCACCAGC	From TKOv3 library
STK11sg2	caccgGGCACTGCACCCGTTCGCGG	From TKOv3 library
VPS52sg1	caccgTTGTGACCTGTACTTCAGCA	From TKOv3 library
VPS52sg2	caccgGAAATCGCCAGGCAGTTCGG	From TKOv3 library
KXD1sg1	caccgTGAGCACCCACCTGATACGG	From TKOv3 library
KXD1sg2	caccgGCGGCCGCAGAAGACCCTCG	From TKOv3 library
VPS35sg1	caccgTAGACAAGACATGCCTTCAG	From TKOv3 library
VPS35sg2	caccgATTCTGGTGTAACTCAGCAC	From TKOv3 library
P4HA1sg1	caccgGGATACAGATACCATCTCAA	From TKOv3 library
P4HA1sg2	caccgTGTGGATGGAACAAGCCCTA	From TKOv3 library
VHLsg1	caccgGCGATTGCAGAAGATGACCT	From TKOv3 library
VHLsg2	caccgTGTCCGTCAACATTGAGAGA	From TKOv3 library
VPS16sg1	caccgGAAATATGAGCTGTACAGCA	From TKOv3 library
VPS16sg2	caccgGCAGTGGAAGAGTGGACCCG	From TKOv3 library
PSMD13sg1	caccgGAACCGATGTCACACCAGGA	From TKOv3 library
PSMD13sg2	caccgGCAGGAGAGAGCCTTCACGC	From TKOv3 library
KIAA0196sg1	caccgGTAGAGAATCACGTACAGCA	From TKOv3 library
KIAA0196sg2	caccgACTGCAATGTTGCCATCCGA	From TKOv3 library
FAM96Asg1	caccgAGAGTCGCCAAAGAGCAATG	From TKOv3 library
FAM96Asg2	caccgGATAAATGACAAAGAGCGAG	From TKOv3 library
ATP6AP2sg1	caccgAGGAGAGCGGATCCCAGACG	From TKOv3 library
ATP6AP2sg2	caccgGAGCACGACAAACACAGCCA	From TKOv3 library
WDR24sg1	caccgGTGGCGCCAGGCAATTCCCG	From TKOv3 library
WDR24sg2	caccgGTTCTCAAAGGTGGAGGCGA	From TKOv3 library

Non-codon–optimized cDNA for *WASF2* was synthesized and cloned into the ENTR–Twist–Kozak vector by Twist. Mutations in the PAM site of *WASF2*-sgRNA1, *WASF2*-sgRNA2, and *WASF2*-sgRNA4 were introduced to make the cDNA resistant against those sgRNAs, using NEB Q5 site-directed mutagenesis kit. After sequence verification, the cDNA was cloned into pRRL-based lentiviral expression plasmids generated in our laboratory (Bigenzahn et al, 2018), which contain a STOP codon and a BlastR-resistance cassette, using the Gateway cloning system (Thermo Fisher Scientific).

DHPS (HsCD00295718, Harvard Medical School plasmid repository), eIF5A (HsCD00041224, Harvard Medical School plasmid repository), and DOHH (HsCD00372432, Harvard Medical School plasmid repository) plasmids were received, and point mutations to make the cDNA resistant against sgRNAs or patient variant mutations were introduced using the NEB Q5 site-directed mutagenesis kit. They were cloned into the same pRRL-based lentiviral expression plasmids as mentioned above, which contained this time, however, either an HA-tag or a STOP codon on the C-terminus and again a BlastR resistance cassette, using the Gateway cloning system (Thermo Fisher Scientific). Rescue experiments were conducted by using the cDNAs resistant to the sgRNAs targeting the endogenous genes.

Lentiviral transduction

Knock-out cell lines and cDNA-overexpression cell lines were generated by lentiviral transduction. Therefore, HEK293T was transfected with the respective lentiviral vectors and packaging plasmids pMD2.G (Addgene no. 12259), and psPAX2 (Addgene no. 12260) using PEI (Sigma-Aldrich). 16 h post-transfection, the medium was exchanged to RPMI1640 supplemented with 10% FBS. 72 h after transfection, the viral supernatant was collected, filtered through 0.45 μm polyethersulfone filters (GE Healthcare), supplemented with 8 μg/ml protamine sulfate, and directly added to the respective cells. 24 h after infection, the medium was exchanged, and 48 h after infection, cells were selected with the respective antibiotics.

Listeria infection assay

Listeria monocytogenes strain 10403S (PMID: 3114382) was grown in Brain–Heart infusion medium overnight at 37°C. The infection assay was performed on individual PMA-differentiated U937 cell clones, knocked out for *WASF2,* and rescued either with a *WASF2*-cDNA (depicted in Fig 3G) or with a mock cDNA as control. A day before infection, 3.0×10^5 cells were seeded on sterile glass coverslips laid at the bottom of the wells of a 24-well plate in the RPMI1640 medium supplemented with 10% FCS and containing no antibiotics. On the day of the infection, bacteria were washed with PBS and incubated at a concentration of 8.0×10^9 b/ml with 50 μM of the green fluorophore CFSE for 20 min at 37°C under shaking. Bacteria were then washed with PBS and used to infect the U937 cells at an MOI of 10. After one hour of infection, the cells were gently washed twice with a warm cell culture medium. For the next two remaining hours, the cells were incubated in the cell culture medium containing 20 μg/ml of gentamycin to kill the remaining extracellular

bacteria. The infection was terminated by washing the cells with PBS and fixing them with 4% paraformaldehyde (Alfa Aesar) for 15 min. Cells were then washed with PBS and permeabilized with 0.1% of Triton X-100 (Roth) in PBS for 5 min. After another washing step with PBS, cells were blocked with 2% FCS in PBS for 30 min. Actin was then stained by incubating the cells with Phalloidin coupled to the fluorophore Alexa647 (Life Technology). Finally, the cells were washed with PBS and mounted in Prolong Diamond containing DAPI (Molecular Probe) to stain genomic DNA. All staining steps were carried out at room temperature in the dark. Infected cells were imaged with the confocal microscope LSM 700 (ZEISS) using 405, 488, or 639 nm laser lines. Images were processed by the ZEN Software 2009 (ZEISS). A minimum of 200 cells were counted for each technical replicate. Then, a representative image of each technical replicate was chosen, and the total amount of bacteria quantified without further normalization. Cells were seeded at equal density. Thanks to the gentamycin protection assay, all bacteria detected were considered as phagocytosed. Green bacteria were considered still enclosed inside the phagolysosome, whereas yellow bacteria (CFSE and actin colocalized) had successfully escaped the phagolysosome. Quantified bacteria were analyzed and visualized with Python project version 3.8.8 (Python Software Foundation available at http://www.python.org) with pandas (Reback et al, 2021) (1.2.4), numpy (1.20.1), matplotlib (Hunter, 2007) (3.3.4), seaborn (Waskom, 2021), (0.11.1), and statannotations (0.4.4).

Gene set enrichment analysis

GO enrichment analysis for "Cellular components" GO terms and biological processes GO terms was performed via GSEA (Subramanian et al, 2005) and Enrichr (Kuleshov et al, 2016) using the Python package GSEApy (version 0.10.8, https://github.com/zqfang/GSEApy). Gene sets are described in the corresponding figure legends.

Cell lysis and immunoblotting

Cell pellets were lyzed in RIPA-lysis buffer (20 mM TRIS–HCl, pH 7.5, 150 mM NaCl, 1 mM EDTA, 1 mM EGTA, 1% NP40, 1% sodium deoxycholate, 10 mM NaF, and 0.1% SDS), supplemented with EDTA-free protease inhibitor (Roche) for 15 min on ice, followed by 20,600*g* at 4°C for 15 min to separate from cellular debris. Protein concentration was then measured with BCA (Pierce) or Bradford (Bio-Rad), Laemmli buffer was added, and samples were separated by SDS–PAGE and transferred to nitrocellulose membranes (GE Healthcare). Then, the membranes were blocked for unspecific binding in 5% milk in TBS-T followed by incubation with indicated antibodies. After incubating in peroxidase-coupled secondary antibodies, the membranes were developed using the ECL Western blot system (Thermo Fisher Scientific).

Bands in Fig 4F were quantified using Image Lab 6.1 (Bio-Rad). First, the intensity of the *DHPS*-cDNA band and GAPDH band was quantified in each lane. A normalization factor was calculated by dividing the GAPDH band intensity of each lane with the GAPDH band intensity of the first lane (reference). The intensity of the *DHPS*-cDNA band was then multiplied by this normalization factor. Normalized *DHPS*-cDNA expression levels were then compared to normalized *DHPS*-cDNA expression levels in each lane and indicated as ratio (*DHPS*-cDNA/*DHPS*-cDNA$^{(-)}$). All calculated intensities were background-subtracted.

Antibodies list

The primary antibodies used for Western blot were hypusine (generation see below, 1:20,000), eIF5A (611976, 1:20,000; BD Biosciences), DHPS/DHS (ab190266, 1:1,000; Abcam), DOHH (376929, B-12, 1:500; SantaCruz), HA (3724, C29F4, 1:500), for WASF2 the WAVE-2 (3659, D2C8, 1:1,000; CellSignaling), and GAPDH (47724, 0411, 1:2,000; SantaCruz).

The secondary antibodies used were anti-rabbit HRP (111-035-144, dilution 1:10,000; Jackson ImmunoResearch), anti-mouse HRP (115-035-003, dilution 1:10,000; Jackson ImmunoResearch).

A custom rabbit anti-hypusine antibody was designed based on a 2016-published sequence of context-independent anti-hypusine antibodies (Zhai et al, 2016) (Fig S6A), synthesized, expressed, and purified with Genscript (Fig S6B). In short, the synthesized sequence was cloned into pcDNA3.4 and plasmid DNA prepared. Expi293F cells, grown in a serum-free Expi293F Expression Medium (Thermo Fisher Scientific), at 37°C, 8% CO_2 on an orbital shaker, were then transfected according to the manual. On day six, post-transfection cell culture supernatant was collected and used for purification. Therefore, the supernatant was centrifuged, filtered, and then loaded and purified on Monofinity A Resin Prepacked Columns. Eluted antibody was then puffer exchanged, sterilized via a 0.22-μm filter, and stored in PBS pH 7.2 at −80°C. The concentration was determined with A280 as 4.74 mg/ml. Specificity was validated by Western blot in HEK293T cells overexpressing DHPS/DOHH and either an eIF5A-WT sequence or an eIF5A-K50 variant (Fig 4B), and in THP-1 cells treated with 10 μM of the DHPS inhibitor GC7 (Fig 4C).

Gene expression analysis

Libraries compatible with Illumina sequencing were prepared using the QuantSeq 3′ mRNA-seq Library prep kit (Lexogen) according to the manufacturer's instructions. Samples were multiplexed and then sequenced on HiSeq 4000 (Illumina) at the BSF at CeMM. Raw-sequencing reads were de-multiplexed and barcode, adaptor, and quality trimming were performed with cutadapt (https://cutadapt.readthedocs.io/en/stable/). Quality control was then performed using FastQC (http://www.bioinformatics.babraham.ac.uk/projects/fastqc/). The remaining reads were mapped to the GRCh38/h38 human genome assembly using genomic short-read RNA-seq aligner STAR v.2.5. More than 98% of the mapped reads in each sample could be obtained with 70–80% of reads mapping to a unique genomic location. End Sequence Analysis Toolkit was used to quantify the transcripts. We carried out a differential expression analysis using independent triplicates with DESeq2 (v.1.24.0) on the basis of read counts. Exploratory data analysis and visualizations were performed in R-project v.3.4.2 (Foundation for Statistical Computing, https://www.R-project.org/) with Rstudio IDE v.1.2.1578, ggplot2 (v.3.3.0), dplyr (v.0.8.5), readr (v.1.3.1), and gplots (v.3.0.1).

DepMap comparison

Growth effects induced by knock-out of individual genes recorded for THP-1 cells in our screen were compared with the growth effects recorded in the DepMap CRISPR dataset. Preprocessed CRISPR dependency scores (DepMap 22Q2 Public+Score, Chronos) (DepMap, 2022) were mined for all recorded genes in the cell line THP-1 from DepMap and extracted for essential genes (genes depleted on day 21, $P \leq 0.05$, Table S2) and the 716 CRISPRko hits depleted in PhagoLate versus PhagoNeg. For 1,040 out of 1,041 essential genes and 671 out of 716 CRISPRko hits a matching Chronos score could be identified. For comparing essential genes, Chronos scores of essential genes were compared to all CRISPR-derived dependency scores recorded for THP1 in the DepMap project in a density plot. Likewise, the distribution of growth effects caused across the 716 CRISPRko hits were compared to all other genes recorded in the DepMap dataset (17,384 genes) in a density plot. Data were visualized with Python project version 3.8.8 (Python Software Foundation available at http://www.python.org) with pandas (Reback et al, 2021) (1.2.4), numpy (1.20.1), matplotlib (Hunter, 2007) (3.3.4), and seaborn (Waskom, 2021) (0.11.1).

"Core essentialome" comparison

Our list of essential genes (genes depleted on day 21, $P \leq 0.05$, Table S2) was compared to the "core essentialome," a list of 1,736 shared essential genes that have been derived from HAP1 and KBM7 cells (Blomen et al, 2015) in a Venn diagram. Data were visualized with Python project version 3.8.8 (Python Software Foundation available at http://www.python.org) with pandas (Reback et al, 2021) (1.2.4), numpy (1.20.1), matplotlib (Hunter, 2007) (3.3.4), and matplotlib_venn (0.11.6).

Data Availability

Genomics datasets are provided in Tables S1 and S2. The transcriptomics dataset is attached in Table S3. PPI data mined from BioPlex 3.0 and CORUM-core specifically for this study are provided in Tables S4 and S5. DepMap cell line CRISPR scores were obtained from DepMap 22Q2 (https://depmap.org/portal/download/all/).

Supplementary Information

Supplementary Information is available at https://doi.org/10.26508/lsa.202201715.

Acknowledgements

We thank all members of the Superti-Furga laboratory for feedback, discussions, and reagents; the Max Perutz Labs FACS Facility for sorting; and the Biomedical Sequencing Facility (CeMM/Medical University of Vienna) for next-generation sequencing. In particular, we thank Andrea Garofoli for advice on statistics. We also thank thesis advisor Thijn Brummelkamp for helpful suggestions throughout the project. We thank Kai-Chun Li, Ann-Katrin Hopp, and Andreas Angermayr for scientific discussions and critical reading. CeMM and the Superti-Furga laboratory are supported by the Austrian Academy of Sciences. We further acknowledge the receipt of third-party funds from the European Research Council (ERC) Advanced Grant 695214 GameofGates (P Essletzbichler, V Sedlyarov, G Superti-Furga).

Author Contributions

P Essletzbichler: conceptualization, data curation, software, formal analysis, supervision, validation, investigation, visualization, methodology, writing—original draft, review, and editing.
V Sedlyarov: data curation, software, formal analysis, investigation, visualization, and methodology.
F Frommelt: data curation, software, formal analysis, investigation, visualization, and methodology.
D Soulat: formal analysis and investigation.
LX Heinz: investigation.
A Stefanovic: investigation.
B Neumayer: investigation.
G Superti-Furga: conceptualization, supervision, funding acquisition, project administration, writing—original draft, review, and editing.

Conflict of Interest Statement

G Superti-Furga and P Essletzbichler have filed patents based on this work that may lead to commercialization efforts in the future.

References

Aksu M, Trakhanov S, Görlich D (2016) Structure of the exportin Xpo4 in complex with RanGTP and the hypusine-containing translation factor eIF5A. *Nat Commun* 7: 11952. doi:10.1038/ncomms11952

Anderson-Baucum E, Piñeros AR, Kulkarni A, Webb-Robertson B-J, Maier B, Anderson RM, Wu W, Tersey SA, Mastracci TL, Casimiro I, et al (2021) Deoxyhypusine synthase promotes a pro-inflammatory macrophage phenotype. *Cell Metab* 33: 1883–1893.e7. doi:10.1016/j.cmet.2021.08.003

Arandjelovic S, Ravichandran KS (2015) Phagocytosis of apoptotic cells in homeostasis. *Nat Immunol* 16: 907–917. doi:10.1038/ni.3253

Barba-Aliaga M, Mena A, Espinoza V, Apostolova N, Costell M, Alepuz P (2021) Hypusinated eIF5A is required for the translation of collagen. *J Cell Sci* 134: jcs258643. doi:10.1242/jcs.258643

Barger CJ, Branick C, Chee L, Karpf AR (2019) Pan-cancer analyses reveal genomic features of FOXM1 overexpression in cancer. *Cancers (Basel)* 11: 251. doi:10.3390/cancers11020251

Bierne H, Miki H, Innocenti M, Scita G, Gertler FB, Takenawa T, Cossart P (2005) WASP-related proteins, Abi1 and Ena/VASP are required for Listeria invasion induced by the Met receptor. *J Cell Sci* 118: 1537–1547. doi:10.1242/jcs.02285

Bigenzahn JW, Collu GM, Kartnig F, Pieraks M, Vladimer GI, Heinz LX, Sedlyarov V, Schischlik F, Fauster A, Rebsamen M, et al (2018) LZTR1 is a regulator of RAS ubiquitination and signaling. *Science* 362: 1171–1177. doi:10.1126/science.aap8210

Blomen VA, Májek P, Jae LT, Bigenzahn JW, Nieuwenhuis J, Staring J, Sacco R, van Diemen FR, Olk N, Stukalov A, et al (2015) Gene essentiality and synthetic lethality in haploid human cells. *Science* 350: 1092–1096. doi:10.1126/science.aac7557

Bock C, Datlinger P, Chardon F, Coelho MA, Dong MB, Lawson KA, Lu T, Maroc L, Norman TM, Song B, et al (2022) High-content CRISPR screening. *Nat Rev Methods Primers* 2: 8. doi:10.1038/s43586-021-00093-4

Bonfim-Melo A, Ferreira ÉR, Mortara RA (2018) Rac1/WAVE2 and Cdc42/N-WASP participation in actin-dependent host cell invasion by extracellular amastigotes of trypanosoma cruzi. *Front Microbiol* 9: 360. doi:10.3389/fmicb.2018.00360

Bröcker C, Engelbrecht-Vandré S, Ungermann C (2010) Multisubunit tethering complexes and their role in membrane fusion. *Curr Biol* 20: R943–R952. doi:10.1016/j.cub.2010.09.015

Carter SB (1967) Effects of cytochalasins on mammalian cells. *Nature* 213: 261–264. doi:10.1038/213261a0

Chanput W, Mes JJ, Wichers HJ (2014) THP-1 cell line: An in vitro cell model for immune modulation approach. *Int Immunopharmacol* 23: 37–45. doi:10.1016/j.intimp.2014.08.002

Clague MJ (1998) Molecular aspects of the endocytic pathway. *Biochem J* 336: 271–282. doi:10.1042/bj3360271

Colas C, Menezes S, Gutiérrez-Martínez E, Péan CB, Dionne MS, Guermonprez P (2014) An improved flow cytometry assay to monitor phagosome acidification. *J Immunol Methods* 412: 1–13. doi:10.1016/j.jim.2014.06.008

Cong L, Ran FA, Cox D, Lin S, Barretto R, Habib N, Hsu PD, Wu X, Jiang W, Marraffini LA, et al (2013) Multiplex genome engineering using CRISPR/Cas systems. *Science* 339: 819–823. doi:10.1126/science.1231143

Cullen PJ, Steinberg F (2018) To degrade or not to degrade: Mechanisms and significance of endocytic recycling. *Nat Rev Mol Cell Biol* 19: 679–696. doi:10.1038/s41580-018-0053-7

DepMap B (2022) DepMap 22Q2 public. *figshare*. Dataset. doi:10.6084/m9.figshare.19700056.v2

Doench JG (2018) Am I ready for CRISPR? A user's guide to genetic screens. *Nat Rev Genet* 19: 67–80. doi:10.1038/nrg.2017.97

Doerfel LK, Wohlgemuth I, Kothe C, Peske F, Urlaub H, Rodnina MV (2013) EF-P is essential for rapid synthesis of proteins containing consecutive proline residues. *Science* 339: 85–88. doi:10.1126/science.1229017

Droese S, Bindseil KU, Bowman EJ, Siebers A, Zeeck A, Altendorf K (1993) Inhibitory effect of modified bafilomycins and concanamycins on P- and V-type adenosinetriphosphatases. *Biochemistry* 32: 3902–3906. doi:10.1021/bi00066a008

Faundes V, Jennings MD, Crilly S, Legraie S, Withers SE, Cuvertino S, Davies SJ, Douglas AGL, Fry AE, Harrison V, et al (2021) Impaired eIF5A function causes a Mendelian disorder that is partially rescued in model systems by spermidine. *Nat Commun* 12: 833. doi:10.1038/s41467-021-21053-2

Fazeli G, Levin-Konigsberg R, Bassik MC, Stigloher C, Wehman AM (2022) TORC1, BORC, ARL-8 cycling, and kinesin-1 drive vesiculation of cell corpse phagolysosomes. *BioRxiv*. doi:10.1101/2022.02.09.479694 (Preprint posted June 19, 2022).

Feng M, Jiang W, Kim BYS, Zhang CC, Fu Y-X, Weissman IL (2019) Phagocytosis checkpoints as new targets for cancer immunotherapy. *Nat Rev Cancer* 19: 568–586. doi:10.1038/s41568-019-0183-z

Filipek PA, de Araujo MEG, Vogel GF, De Smet CH, Eberharter D, Rebsamen M, Rudashevskaya EL, Kremser L, Yordanov T, Tschaikner P, et al (2017) LAMTOR/Ragulator is a negative regulator of Arl8b- and BORC-dependent late endosomal positioning. *J Cell Biol* 216: 4199–4215. doi:10.1083/jcb.201703061

Flannagan RS, Jaumouillé V, Grinstein S (2012) The cell biology of phagocytosis. *Annu Rev Pathol Mech Dis* 7: 61–98. doi:10.1146/annurev-pathol-011811-132445

Fleit HB, Kobasiuk CD (1991) The human monocyte-like cell line THP-1 expresses Fc gamma RI and Fc gamma RII. *J Leukoc Biol* 49: 556–565. doi:10.1002/jlb.49.6.556

Frigieri MC, João Luiz MVS, Apponi LH, Zanelli CF, Valentini SR (2008) Synthetic lethality between eIF5A and Ypt1 reveals a connection between translation and the secretory pathway in yeast. *Mol Genet Genomics* 280: 211–221. doi:10.1007/s00438-008-0357-y

Ganapathi M, Padgett LR, Yamada K, Devinsky O, Willaert R, Person R, Au P-YB, Tagoe J, McDonald M, Karlowicz D, et al (2019) Recessive rare variants in deoxyhypusine synthase, an enzyme involved in the synthesis of hypusine, are associated with a neurodevelopmental disorder. *Am J Hum Genet* 104: 287–298. doi:10.1016/j.ajhg.2018.12.017

Garg S, Sharma M, Ung C, Tuli A, Barral DC, Hava DL, Veerapen N, Besra GS, Hacohen N, Brenner MB (2011) Lysosomal trafficking, antigen presentation, and microbial killing are controlled by the Arf-like GTPase Arl8b. *Immunity* 35: 182–193. doi:10.1016/j.immuni.2011.06.009

Gerlach BD, Ampomah PB, Yurdagul A, Liu C, Lauring MC, Wang X, Kasikara C, Kong N, Shi J, Tao W, et al (2021) Efferocytosis induces macrophage proliferation to help resolve tissue injury. *Cell Metab* 33: 2445–2463.e8. doi:10.1016/j.cmet.2021.10.015

Giulian D, Chen J, Ingeman JE, George JK, Noponen M (1989) The role of mononuclear phagocytes in wound healing after traumatic injury to adult mammalian brain. *J Neurosci* 9: 4416–4429. doi:10.1523/jneurosci.09-12-04416.1989

Giurgiu M, Reinhard J, Brauner B, Dunger-Kaltenbach I, Fobo G, Frishman G, Montrone C, Ruepp A (2019) CORUM: The comprehensive resource of mammalian protein complexes-2019. *Nucleic Acids Res* 47: D559–D563. doi:10.1093/nar/gky973

Gobert AP, Finley JL, Latour YL, Asim M, Smith TM, Verriere TG, Barry DP, Allaman MM, Delagado AG, Rose KL, et al (2020) Hypusination orchestrates the antimicrobial response of macrophages. *Cell Rep* 33: 108510. doi:10.1016/j.celrep.2020.108510

Goley ED, Welch MD (2006) The ARP2/3 complex: An actin nucleator comes of age. *Nat Rev Mol Cell Biol* 7: 713–726. doi:10.1038/nrm2026

Gordon S (2016) Phagocytosis: An immunobiologic process. *Immunity* 44: 463–475. doi:10.1016/j.immuni.2016.02.026

Gutierrez E, Shin B-S, Woolstenhulme CJ, Kim J-R, Saini P, Buskirk AR, Dever TE (2013) eIF5A promotes translation of polyproline motifs. *Mol Cell* 51: 35–45. doi:10.1016/j.molcel.2013.04.021

Haft CR, Sierra MdlL, Bafford R, Lesniak MA, Barr VA, Taylor SI (2000) Human orthologs of yeast vacuolar protein sorting proteins Vps26, 29, and 35: Assembly into multimeric complexes. *Mol Biol Cell* 11: 4105–4116. doi:10.1091/mbc.11.12.4105

Haney MS, Bohlen CJ, Morgens DW, Ousey JA, Barkal AA, Tsui CK, Ego BK, Levin R, Kamber RA, Collins H, et al (2018) Identification of phagocytosis regulators using magnetic genome-wide CRISPR screens. *Nat Genet* 50: 1716–1727. doi:10.1038/s41588-018-0254-1

Harada Y, Ohkawa Y, Kizuka Y, Taniguchi N (2019) Oligosaccharyltransferase: A gatekeeper of health and tumor progression. *Int J Mol Sci* 20: 6074. doi:10.3390/ijms20236074

Hart T, Tong AHY, Chan K, Van Leeuwen J, Seetharaman A, Aregger M, Chandrashekhar M, Hustedt N, Seth S, Noonan A, et al (2017) Evaluation and design of genome-wide CRISPR/SpCas9 knockout screens. *G3 (Bethesda)* 7: 2719–2727. doi:10.1534/g3.117.041277

Heinz LX, Lee J, Kapoor U, Kartnig F, Sedlyarov V, Papakostas K, César-Razquin A, Essletzbichler P, Goldmann U, Stefanovic A, et al (2020) TASL is the SLC15A4-associated adaptor for IRF5 activation by TLR7-9. *Nature* 581: 316–322. doi:10.1038/s41586-020-2282-0

Hirsch JG, Dubos RJ (1952) The effect of spermine on tubercle bacilli. *J Exp Med* 95: 191–208. doi:10.1084/jem.95.2.191

Hukelmann JL, Anderson KE, Sinclair LV, Grzes KM, Murillo AB, Hawkins PT, Stephens LR, Lamond AI, Cantrell DA (2016) The cytotoxic T cell proteome and its shaping by the kinase mTOR. *Nat Immunol* 17: 104–112. doi:10.1038/ni.3314

Hunter JD (2007) Matplotlib: A 2D graphics environment. *Comput Sci Eng* 9: 90–95. doi:10.1109/mcse.2007.55

Huttlin EL, Bruckner RJ, Navarrete-Perea J, Cannon JR, Baltier K, Gebreab F, Gygi MP, Thornock A, Zarraga G, Tam S, et al (2021) Dual proteome-

scale networks reveal cell-specific remodeling of the human interactome. *Cell* 184: 3022–3040.e28. doi:10.1016/j.cell.2021.04.011

Jeng EE, Bhadkamkar V, Ibe NU, Gause H, Jiang L, Chan J, Jian R, Jimenez-Morales D, Stevenson E, Krogan NJ, et al (2019) Systematic identification of host cell regulators of Legionella pneumophila pathogenesis using a genome-wide CRISPR screen. *Cell Host Microbe* 26: 551–563.e6. doi:10.1016/j.chom.2019.08.017

Jia D, Gomez TS, Metlagel Z, Umetani J, Otwinowski Z, Rosen MK, Billadeau DD (2010) WASH and WAVE actin regulators of the Wiskott-Aldrich syndrome protein (WASP) family are controlled by analogous structurally related complexes. *Proc Natl Acad Sci U S A* 107: 10442–10447. doi:10.1073/pnas.0913293107

Jinek M, East A, Cheng A, Lin S, Ma E, Doudna J (2013) RNA-programmed genome editing in human cells. *Elife* 2: e00471. doi:10.7554/elife.00471

Joung J, Konermann S, Gootenberg JS, Abudayyeh OO, Platt RJ, Brigham MD, Sanjana NE, Zhang F (2017) Genome-scale CRISPR-Cas9 knockout and transcriptional activation screening. *Nat Protoc* 12: 828–863. doi:10.1038/nprot.2017.016

Kamber RA, Nishiga Y, Morton B, Banuelos AM, Barkal AA, Vences-Catalán F, Gu M, Fernandez D, Seoane JA, Yao D, et al (2021) Inter-cellular CRISPR screens reveal regulators of cancer cell phagocytosis. *Nature* 597: 549–554. doi:10.1038/s41586-021-03879-4

Katoh Y, Nozaki S, Hartanto D, Miyano R, Nakayama K (2015) Architectures of multisubunit complexes revealed by a visible immunoprecipitation assay using fluorescent fusion proteins. *J Cell Sci* 128: 2351–2362. doi:10.1242/jcs.168740

Kissing S, Hermsen C, Repnik U, Nesset CK, von Bargen K, Griffiths G, Ichihara A, Lee BS, Schwake M, De Brabander J, et al (2015) Vacuolar ATPase in phagosome-lysosome fusion. *J Biol Chem* 290: 14166–14180. doi:10.1074/jbc.m114.628891

Kocks C, Cho JH, Nehme N, Ulvila J, Pearson AM, Meister M, Strom C, Conto SL, Hetru C, Stuart LM, et al (2005) Eater, a transmembrane protein mediating phagocytosis of bacterial pathogens in Drosophila. *Cell* 123: 335–346. doi:10.1016/j.cell.2005.08.034

Korotkevich G, Sukhov V, Budin N, Shpak B, Artyomov MN, Sergushichev A (2016) Fast gene set enrichment analysis. *BioRxiv*. doi:10.1101/060012 (Preprint posted February 01, 2021).

Kuleshov MV, Jones MR, Rouillard AD, Fernandez NF, Duan Q, Wang Z, Koplev S, Jenkins SL, Jagodnik KM, Lachmann A, et al (2016) Enrichr: A comprehensive gene set enrichment analysis web server 2016 update. *Nucleic Acids Res* 44: W90–W97. doi:10.1093/nar/gkw377

Labun K, Montague TG, Krause M, Torres Cleuren YN, Tjeldnes H, Valen E (2019) CHOPCHOP v3: Expanding the CRISPR web toolbox beyond genome editing. *Nucleic Acids Res* 47: W171–W174. doi:10.1093/nar/gkz365

Laulumaa S, Varjosalo M (2021) Commander complex-A multifaceted operator in intracellular signaling and cargo. *Cells* 10: 3447. doi:10.3390/cells10123447

Lee CH, Um PY, Park MH (2001) Structure-function studies of human deoxyhypusine synthase: Identification of amino acid residues critical for the binding of spermidine and NAD. *Biochem J* 355: 841–849. doi:10.1042/bj3550841

Lindner B, Martin E, Steininger M, Bundalo A, Lenter M, Zuber J, Schuler M (2021) A genome-wide CRISPR/Cas9 screen to identify phagocytosis modulators in monocytic THP-1 cells. *Sci Rep* 11: 12973. doi:10.1038/s41598-021-92332-7

Lino CA, Harper JC, Carney JP, Timlin JA (2018) Delivering CRISPR: A review of the challenges and approaches. *Drug Deliv* 25: 1234–1257. doi:10.1080/10717544.2018.1474964

Liu MY, Wu MC (1992) Induction of human monocyte cell line U937 differentiation and CSF-1 production by phorbol ester. *Exp Hematol* 20: 974–979.

Love MI, Huber W, Anders S (2014) Moderated estimation of fold change and dispersion for RNA-seq data with DESeq2. *Genome Biol* 15: 550. doi:10.1186/s13059-014-0550-8

Maier JA, Castiglioni S, Locatelli L, Zocchi M, Mazur A (2021) Magnesium and inflammation: Advances and perspectives. *Semin Cell Dev Biol* 115: 37–44. doi:10.1016/j.semcdb.2020.11.002

Mali P, Yang L, Esvelt KM, Aach J, Guell M, DiCarlo JE, Norville JE, Church GM (2013) RNA-guided human genome engineering via Cas9. *Science* 339: 823–826. doi:10.1126/science.1232033

Mandal A, Mandal S, Park MH (2014) Genome-wide analyses and functional classification of proline repeat-rich proteins: Potential role of eIF5A in eukaryotic evolution. *PLoS One* 9: e111800. doi:10.1371/journal.pone.0111800

Mandal A, Mandal S, Park MH (2016) Global quantitative proteomics reveal up-regulation of endoplasmic reticulum stress response proteins upon depletion of eIF5A in HeLa cells. *Sci Rep* 6: 25795. doi:10.1038/srep25795

May RC, Caron E, Hall A, Machesky LM (2000) Involvement of the Arp2/3 complex in phagocytosis mediated by FcγR or CR3. *Nat Cell Biol* 2: 246–248. doi:10.1038/35008673

Melis N, Rubera I, Cougnon M, Giraud S, Mograbi B, Belaid A, Pisani DF, Huber SM, Lacas-Gervais S, Fragaki K, et al (2017) Targeting eIF5A hypusination prevents anoxic cell death through mitochondrial silencing and improves kidney transplant outcome. *J Am Soc Nephrol* 28: 811–822. doi:10.1681/asn.2016010012

Mohammadi S, Isberg RR (2013) Cdc42 interacts with the exocyst complex to promote phagocytosis. *J Cell Biol* 200: 81–93. doi:10.1083/jcb.201204090

Oikawa T, Yamaguchi H, Itoh T, Kato M, Ijuin T, Yamazaki D, Suetsugu S, Takenawa T (2004) PtdIns(3,4,5)P3 binding is necessary for WAVE2-induced formation of lamellipodia. *Nat Cell Biol* 6: 420–426. doi:10.1038/ncb1125

Park MH, Cooper HL, Folk JE (1981) Identification of hypusine, an unusual amino acid, in a protein from human lymphocytes and of spermidine as its biosynthetic precursor. *Proc Natl Acad Sci U S A* 78: 2869–2873. doi:10.1073/pnas.78.5.2869

Patel PH, Costa-Mattioli M, Schulze KL, Bellen HJ (2009) The Drosophila deoxyhypusine hydroxylase homologue nero and its target eIF5A are required for cell growth and the regulation of autophagy. *J Cell Biol* 185: 1181–1194. doi:10.1083/jcb.200904161

Pérez-Victoria FJ, Schindler C, Magadán JG, Mardones GA, Delevoye C, Romao M, Raposo G, Bonifacino JS (2010) Ang2/fat-free is a conserved subunit of the Golgi-associated retrograde protein complex. *Mol Biol Cell* 21: 3386–3395. doi:10.1091/mbc.e10-05-0392

Philips JA, Rubin EJ, Perrimon N (2005) Drosophila RNAi screen reveals CD36 family member required for mycobacterial infection. *Science* 309: 1251–1253. doi:10.1126/science.1116006

Podleśny-Drabiniok A, Marcora E, Goate AM (2020) Microglial phagocytosis: A disease-associated process emerging from Alzheimer's disease genetics. *Trends Neurosci* 43: 965–979. doi:10.1016/j.tins.2020.10.002

Pu J, Schindler C, Jia R, Jarnik M, Backlund P, Bonifacino JS (2015) BORC, a multisubunit complex that regulates lysosome positioning. *Dev Cell* 33: 176–188. doi:10.1016/j.devcel.2015.02.011

Puleston DJ, Buck MD, Klein Geltink RI, Kyle RL, Caputa G, O'Sullivan D, Cameron AM, Castoldi A, Musa Y, Kabat AM, et al (2019) Polyamines and eIF5A hypusination modulate mitochondrial respiration and macrophage activation. *Cell Metab* 30: 352–363.e8. doi:10.1016/j.cmet.2019.05.003

Rämet M, Manfruelli P, Pearson A, Mathey-Prevot B, Ezekowitz RAB (2002) Functional genomic analysis of phagocytosis and identification of a Drosophila receptor for E. coli. *Nature* 416: 644–648. doi:10.1038/nature735

Ravell JC, Chauvin SD, He T, Lenardo M (2020) An update on XMEN disease. *J Clin Immunol* 40: 671–681. doi:10.1007/s10875-020-00790-x

Reback J, McKinney W, jbrockmendel, Van Den Bossche J, Augspurger T, Cloud P, Hawkins S, gfyoung, Sinhrks, Roeschke M, et al (2021) pandas-dev/pandas: Pandas 1.2.4 (v1.2.4). *Zenodo* doi:10.5281/zenodo.4681666

Rebsamen M, Pochini L, Stasyk T, de Araújo MEG, Galluccio M, Kandasamy RK, Snijder B, Fauster A, Rudashevskaya EL, Bruckner M, et al (2015) SLC38A9 is a component of the lysosomal amino acid sensing machinery that controls mTORC1. *Nature* 519: 477–481. doi:10.1038/nature14107

Rosorius O, Reichart B, Krätzer F, Heger P, Dabauvalle MC, Hauber J (1999) Nuclear pore localization and nucleocytoplasmic transport of eIF-5A: Evidence for direct interaction with the export receptor CRM1. *J Cell Sci* 112: 2369–2380. doi:10.1242/jcs.112.14.2369

Rossi D, Galvão FC, Bellato HM, Boldrin PEG, Andrews BJ, Valentini SR, Zanelli CF (2014) eIF5A has a function in the cotranslational translocation of proteins into the ER. *Amino Acids* 46: 645–653. doi:10.1007/s00726-013-1618-6

Saini P, Eyler DE, Green R, Dever TE (2009) Hypusine-containing protein eIF5A promotes translation elongation. *Nature* 459: 118–121. doi:10.1038/nature08034

Sanjana NE, Shalem O, Zhang F (2014) Improved vectors and genome-wide libraries for CRISPR screening. *Nat Methods* 11: 783–784. doi:10.1038/nmeth.3047

Sedlyarov V, Eichner R, Girardi E, Essletzbichler P, Goldmann U, Nunes-Hasler P, Srndic I, Moskovskich A, Heinz LX, Kartnig F, et al (2018) The bicarbonate transporter SLC4A7 plays a key role in macrophage phagosome acidification. *Cell Host Microbe* 23: 766–774.e5. doi:10.1016/j.chom.2018.04.013

Shalem O, Sanjana NE, Zhang F (2015) High-throughput functional genomics using CRISPR-Cas9. *Nat Rev Genet* 16: 299–311. doi:10.1038/nrg3899

Shen K, Sidik H, Talbot WS (2016) The rag-ragulator complex regulates lysosome function and phagocytic flux in microglia. *Cell Rep* 14: 547–559. doi:10.1016/j.celrep.2015.12.055

Subramanian A, Tamayo P, Mootha VK, Mukherjee S, Ebert BL, Gillette MA, Paulovich A, Pomeroy SL, Golub TR, Lander ES, et al (2005) Gene set enrichment analysis: A knowledge-based approach for interpreting genome-wide expression profiles. *Proc Natl Acad Sci U S A* 102: 15545–15550. doi:10.1073/pnas.0506580102

Tsui CK, Barfield RM, Fischer CR, Morgens DW, Li A, Smith BAH, Gray MA, Bertozzi CR, Rabuka D, Bassik MC (2019) CRISPR-Cas9 screens identify regulators of antibody-drug conjugate toxicity. *Nat Chem Biol* 15: 949–958. doi:10.1038/s41589-019-0342-2

Ude S, Lassak J, Starosta AL, Kraxenberger T, Wilson DN, Jung K (2013) Translation elongation factor EF-P alleviates ribosome stalling at polyproline stretches. *Science* 339: 82–85. doi:10.1126/science.1228985

Underhill DM, Goodridge HS (2012) Information processing during phagocytosis. *Nat Rev Immunol* 12: 492–502. doi:10.1038/nri3244

Ungar D, Oka T, Brittle EE, Vasile E, Lupashin VV, Chatterton JE, Heuser JE, Krieger M, Waters MG (2002) Characterization of a mammalian Golgi-localized protein complex, COG, that is required for normal Golgi morphology and function. *J Cell Biol* 157: 405–415. doi:10.1083/jcb.200202016

Valentini SR, Casolari JM, Oliveira CC, Silver PA, McBride AE (2002) Genetic interactions of yeast eukaryotic translation initiation factor 5A (eIF5A) reveal connections to poly(A)-binding protein and protein kinase C signaling. *Genetics* 160: 393–405. doi:10.1093/genetics/160.2.393

van der Kant R, Jonker CTH, Wijdeven RH, Bakker J, Janssen L, Klumperman J, Neefjes J (2015) Characterization of the mammalian CORVET and HOPS complexes and their modular restructuring for endosome specificity. *J Biol Chem* 290: 30280–30290. doi:10.1074/jbc.m115.688440

Waskom M (2021) Seaborn: statistical data visualization. *JOSS* 6: 3021. doi:10.21105/joss.03021

Watson CM, Nadat F, Ahmed S, Crinnion LA, O'Riordan S, Carter C, Savic S (2022) Identification of a novel MAGT1 mutation supports a diagnosis of XMEN disease. *Genes Immun* 23: 66–72. doi:10.1038/s41435-022-00166-8

Wolff EC, Kang KR, Kim YS, Park MH (2007) Posttranslational synthesis of hypusine: Evolutionary progression and specificity of the hypusine modification. *Amino Acids* 33: 341–350. doi:10.1007/s00726-007-0525-0

Wyant GA, Abu-Remaileh M, Wolfson RL, Chen WW, Freinkman E, Danai LV, Vander Heiden MG, Sabatini DM (2017) mTORC1 activator SLC38A9 is required to efflux essential amino acids from lysosomes and use protein as a nutrient. *Cell* 171: 642–654.e12. doi:10.1016/j.cell.2017.09.046

Xu A, Jao DE, Chen KY (2004) Identification of mRNA that binds to eukaryotic initiation factor 5A by affinity co-purification and differential display. *Biochem J* 384: 585–590. doi:10.1042/bj20041232

Yeung ATY, Choi YH, Lee AHY, Hale C, Ponstingl H, Pickard D, Goulding D, Thomas M, Gill E, Kim JK, et al (2019) A genome-wide knockout screen in human macrophages identified host factors modulating Salmonella infection. *MBio* 10: e02169-19. doi:10.1128/mbio.02169-19

Zanelli CF, Valentini SR (2005) Pkc1 acts through Zds1 and Gic1 to suppress growth and cell polarity defects of a yeast eIF5A mutant. *Genetics* 171: 1571–1581. doi:10.1534/genetics.105.048082

Zhai Q, He M, Song A, Deshayes K, Dixit VM, Carter PJ (2016) Structural analysis and optimization of context-independent anti-hypusine antibodies. *J Mol Biol* 428: 603–617. doi:10.1016/j.jmb.2016.01.006

Zhang M, Caragine T, Wang H, Cohen PS, Botchkina G, Soda K, Bianchi M, Ulrich P, Cerami A, Sherry B, et al (1997) Spermine inhibits proinflammatory cytokine synthesis in human mononuclear cells: A counterregulatory mechanism that restrains the immune response. *J Exp Med* 185: 1759–1768. doi:10.1084/jem.185.10.1759

Zhang H, Alsaleh G, Feltham J, Sun Y, Napolitano G, Riffelmacher T, Charles P, Frau L, Hublitz P, Yu Z, et al (2019) Polyamines control eIF5A hypusination, TFEB translation, and autophagy to reverse B cell senescence. *Mol Cell* 76: 110–125.e9. doi:10.1016/j.molcel.2019.08.005

Ziegler A, Steindl K, Hanner AS, Kumar Kar R, Prouteau C, Boland A, Deleuze JF, Coubes C, Bézieau S, Küry S, et al (2022) Bi-allelic variants in DOHH, catalyzing the last step of hypusine biosynthesis, are associated with a neurodevelopmental disorder. *Am J Hum Genet* 109: 1549–1558. doi:10.1016/j.ajhg.2022.06.010

3.5 Interlude

The genome-wide survey for phagocytosis regulators in section 3.4 led to a global overview of what kind of molecular machinery is involved in the process of phagocytosis. One process that we could not easily explain with existing knowledge was the hypusine axis. It stood out to us because it scored entirely and with high significance. The fact that both enzymes (DHPS and DOHH) that are responsible for the formation of hypusine on eIF5A scored as hits, indicated that hypusine, a unique modification on eIF5A is important for the process (Wolff *et al.*, 1995, 2007, Kim *et al.*, 2006*b*). Due to the little knowledge about how hypusination is regulated and how it could thereby talk back to phagocytosis, we decided to focus the rest of our work entirely on the exploration of the hypusine axis.

In the following results part, we are making use of our hypusine antibody in a genome-wide exploration of regulators of hypusine levels. This genetic approach allows us to observe a novel direct crosstalk between oxidative phosphorylation and hypusine levels. We observe that among many other pathways, any perturbations to the oxidative phosphorylation pathway within the cell lead to an upregulation of hypusine levels in the cell. As eIF5A is in the meanwhile known as a translational elongation factor, we make use of expression proteomics to measure effects caused by inhibition of hypusination. Interestingly, we observe again an effect of hypusine on oxidative respiration. This time, blocking hypusination leads to a decrease in OXPHOS-related proteins and additionally to an upregulation of ATF4-related proteins. We test these findings with a set of mitochondria-targeted pharmacological perturbations and could confirm that blocking mitochondrial translation leads to an increase in hypusine levels. Finally, we investigate also a second modification on eIF5A, which is acetylation on lysine 47. Opposing to hypusine, this modification is reversible, and our experiments showed that it correlates positively with cells performing glycolysis, while cells requiring more OXPHOS show lower levels of acetylation on eIF5A.

3.6 Multi-omics Characterization of the Hypusine Axis

Chapter 3.6 is intended for publication. The author of this thesis designed and conducted most of the experiments analyzed and interpreted the data and made the figures. Nicolaas Boon from the Brummelkamp lab, that has extensive experience in using haploid genetics to study posttranslational modifications, performed genetic haploid screening, Katja Parapatics (Proteomics Facility, CeMM) performed TMT proteomics, Fabian Frommelt contributed experimental advice and performed data analysis for TMT proteomics data, Sohani Da Sharma at the Jovanovic lab performed ribosome profiling and Evandro Ferrada performed analysis of ribosome profiling. Thijn Brummelkamp, Marko Jovanovic, Gaia Novarino, and Ann-Katrin Hopp gave experimental advice. Experimental designs were jointly determined by the author of this thesis and Giulio Superti-Furga.

3.6.1 A genome-wide hypusine abundance screen

Hypusination is a process that introduces a unique posttranslational modification on the protein eIF5A with the help of the two enzymes DHPS and DOHH. Despite being understood as an essential modification for eIF5A already over 40 years ago, systematic studies in mammalian cells characterizing regulators of the highly conserved hypusination process are still lacking (Park *et al.*, 1981). To study hypusination we generated a hypusine-specific antibody based on a published sequence, that we described and characterized in the previous study of this section (Zhai *et al.*, 2016; Essletzbichler *et al.*, 2023). Using haploid genetics to study posttranslational modifications, we performed haploid screens to systematically screen for regulators of hypusination (Brockmann *et al.*, 2017; Haahr *et al.*, 2022) (Figure 21a).

HAP1 cells were mutagenized and stained with a hypusine antibody, and cell populations with low and high antibody staining were isolated using a FACS separation approach (Brockmann *et al.*, 2017) (Figure 21a). By looking for genes enriched for disruptive gene-trap mutations in the cell fractions with high and low hypusine staining we identified negative and positive regulators of hypusination respectively (Figure 21a-d). Gene Ontology (GO) enrichment analysis on the identified negative regulators for “Biological processes” GO terms yielded out of the top ten terms eight terms related to oxidative phosphorylation, including mitochondrial (mt) gene expression and mt translation (adj. p-value < 1.43 x 10-80) as well as aerobic electron transport chain, mt ATP synthesis, oxidative phosphorylation, regulation of mt translation, cellular respiration, mt respiration chain assembly (adj. p-value < 4.11 x 10-14) (Figure 21c). Similarly, seven out of the top ten GO terms enriched for negative regulators in the category “Cellular components” were related to mitochondria, involving mt inner membrane and mt membrane (adj. p-value < 3.56 x 10-80) as well as mt matrix, mt ribosome,

mt respiration chain complex III, and mt envelop (adj. p-value < 1.99 x 10-6) (Figure 21c). Additionally, in the GO enrichment analysis on negative regulators for hypusination for “Molecular function” the cluster RNA binding (adj. p-value < 3.60 x 10-30) stood out (Figure 21c).

GO enrichment analysis on the identified positive regulators for “Biological processes” yielded as the top GO term the amide biosynthetic process (adj. p-value < 5.66 x 10-4) containing six positive regulators identified in our hypusine abundance screen (*SPTLC1*, *SPTLC2*, *SGMS1*, *VAPA*, *DMD*, *SPTSSA*) (Figure 21d). Interestingly, three of these genes (*SPTLC1*, *SPTLC2*, and *SPTSSA*) also led to the top GO term for positive regulators in the category “Cellular component”, which is the serine C-palmitoyltransferase complex (adj. p-value < 6.96 x 10-4) (Figure 21d). Importantly, as expected we could also identify the hypusine axis (*DHPS*, *DOHH*, and *eIF5A*), as well as *Xpo4*, the nuclear shuttle protein for eIF5A as part of the positive regulators of the hypusine abundance screen (Figure 21b,d).

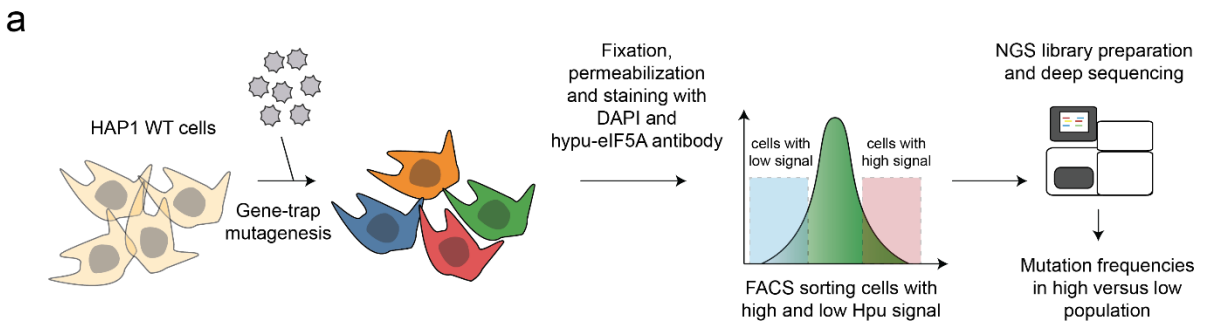
a
HAP1 WT cells
Gene-trap mutagenesis
Fixation, permeabilization and staining with DAPI and hypu-eIF5A antibody
cells with low signal
cells with high signal
FACS sorting cells with high and low Hpu signal
NGS library preparation and deep sequencing
Mutation frequencies in high versus low population

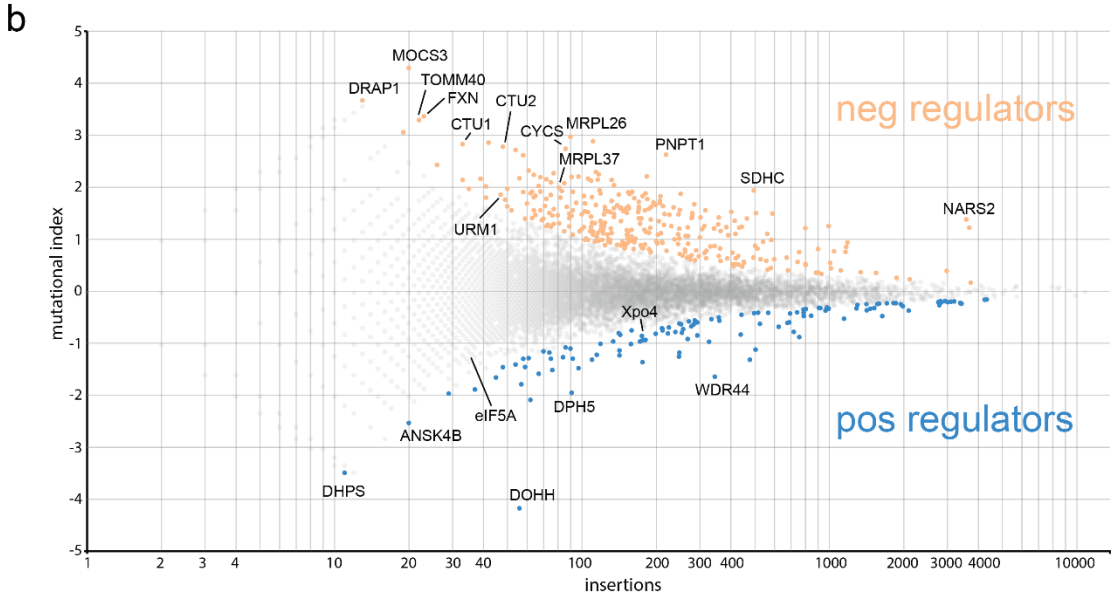
b
mutational index
insertions
neg regulators
pos regulators
MOCS3
DRAP1
TOMM40
FXN
CTU2
CTU1
CYCS
MRPL26
MRPL37
PNPT1
SDHC
NARS2
URM1
Xpo4
WDR44
eIF5A
DPH5
ANSK4B
DHPS
DOHH


c
neg regulators
Gene Ontology Enrichment Analysis
GO Biological Process
Mitochondrial Gene Expression (GO:0140053)
Mitochondrial Translation (GO:0032543)
Translation (GO:0006412)
Aerobic Electron Transport Chain (GO:0019646)
Mitochondrial ATP Synthesis Coupled Electron Transport (GO:0042775)
Oxidative Phosphorylation (GO:0006119)
Regulation Of Mitochondrial Translation (GO:0070129)
Cellular Respiration (GO:0045333)
Mitochondrial Respiratory Chain Complex Assembly (GO:0033108)
Macromolecule Biosynthetic Process (GO:0009059)
-log10padj
GO Cellular Component
Mitochondrial Inner Membrane (GO:0005743)
Organelle Inner Membrane (GO:0019866)
Mitochondrial Membrane (GO:0031966)
Mitochondrial Matrix (GO:0005759)
Mitochondrial Ribosome (GO:0005761)
Intracellular Organelle Lumen (GO:0070013)
Mitochondrial Respiratory Chain Complex III (GO:0005750)
Respiratory Chain Complex III (GO:0045275)
Mitochondrial Envelope (GO:0005740)
Organelle Envelope Lumen (GO:0031970)
-log10padj
GO Molecular Function
RNA Binding (GO:0003723)
aminoacyl-tRNA Ligase Activity (GO:0004812)
tRNA Binding (GO:0000049)
Oxidoreduction-Driven Active Transmembrane Transporter Activity (GO:0015453)
rRNA Binding (GO:0019843)
NADH Dehydrogenase (Ubiquinone) Activity (GO:0008137)
NADH Dehydrogenase (Quinone) Activity (GO:0050136)
Carbon-Nitrogen Ligase Activity, With Glutamine As amido-N-donor (GO:0016884)
Prenyltransferase Activity (GO:0004659)
Four-Way Junction DNA Binding (GO:0000400)
-log10padj
d
pos regulators
Gene Ontology Enrichment Analysis
GO Biological Process
Amide Biosynthetic Process (GO:0043604)
Positive Regulation Of Cell Junction Assembly (GO:1901890)
Retinal Ganglion Cell Axon Guidance (GO:0031290)
Regulation Of Axonogenesis (GO:0050770)
Protein-Containing Complex Organization (GO:0043933)
Regulation Of Synapse Assembly (GO:0051963)
Reg. Of Intracellular Estrogen Receptor Signaling Pathway (GO:0033146)
Cellular Nitrogen Compound Biosynthetic Process (GO:0044271)
Positive Regulation Of Synapse Assembly (GO:0051965)
Sphingoid Biosynthetic Process (GO:0046520)
-log10padj
GO Cellular Component
Serine C-palmitoyltransferase Complex (GO:0017059)
-log10padj

Figure 21: Genome-wide haploid genetic screening identifies regulators of hypusine levels.

a. Schematic overview of hypusine-antibody and FACS-based haploid genetic screen to identify modulators of hypusine levels in cells. **b.** Plot highlighting negative (highlighted in orange) and positive regulators (highlighted in blue) of hypusination (two-sided Fisher's exact test, false discovery rate-corrected $p \leq 0.05$). Per gene (dots), the x axis shows the total number of mutations assigned to each gene. The y-axis shows the mutational index calculated by dividing the frequency of mutations in the "high" channel through the frequency of mutations in the "low" channel. Selected regulators are labeled. **c.** Gene Ontology (GO) enrichment analysis (two-sided Fisher's exact test, p value adjusted for multiple testing) for negative regulators (highlighted in orange in (b)) for GO Biological Process, GO Cellular Component, and GO Molecular Function. The x-axis indicates the significance of enrichment ($-\log_{10}$-transformed p value adjusted for multiple testing) against the y-axis showing the top 10 enriched terms, sorted by adjusted p value. **d.** Gene Ontology (GO) enrichment analysis (two-sided Fisher's exact test, p value adjusted for multiple testing) for positive regulators (highlighted in blue in (b)) for GO Biological Process, GO Cellular Component. The x-axis indicates the significance of enrichment ($-\log_{10}$-transformed p value adjusted for multiple testing) against the y-axis showing the top 10 enriched terms for GO Biological Process and the enriched term for GO Cellular Component, sorted by adjusted p value.

3.6.2 Expression proteomics in cells depleted for hypusine

Since one of the main roles of eIF5A, the target protein of hypusination, is to act as a translational elongation factor, we decided to additionally explore the regulatory roles of hypusine by quantifying changes in protein abundances upon inhibition of hypusination. For this we chose the cell model THP-1 and the DHPS inhibitor GC7 combined with a TMT proteomics approach. THP-1 cells were treated with 30 µM GC7 or DMSO as control, harvested after 24, 48, 55, and 60 hours, and protein abundances were subsequently analyzed with TMT proteomics in these samples (Figure 22a).

In total, we could quantify 9603 unique protein groups and identified 193 significantly changed protein groups (max. delta log2 differences < -0.5, -log10padj > 2 and max. log2 differences > 0.5, -log10padj > 2 respectively) (Figure 22b). Using the Fuzzy-C means soft clustering method, perturbed proteins were assigned to three different clusters based on their standard normalized abundance over time (Figure 22c,e,g). Downregulated proteins were grouped in one cluster that contains proteins that are lowered in abundance over a longer time (48 hours) and are then stable ("gradually down") (Figure 22c) and one cluster containing proteins that have lower abundance 24 hours after inhibition of hypusination and then stay at the same abundance level ("fast down") (Figure 22e). GO enrichment analysis on proteins of the "gradually down" cluster for "Biological processes" GO terms yielded as top terms mitochondrial translation, termination, and elongation terms (adj. p-value < 2.45 x 10-6), all processes that are required to synthesize proteins encoded on the mitochondrial DNA, which encodes 13 proteins all involved in the oxidative phosphorylation process (Kummer and Ban, 2021) (Figure 22d). Similarly, GO enrichment analysis on proteins of the "fast down" cluster for "Biological processes" GO terms yielded as top ten terms, four terms related

to mitochondria: mt translation, mt translational elongation, mt translational termination, mt gene expression (adj. p-value < 1.48 x 10-26) as well as terms related to general protein translation: translational termination, translational elongation and translation (adj. p-value < 3.12 x 10-32) (Figure 22f).

The third cluster contains proteins that are upregulated in the absence of hypusine (Figure 22g). Eight out of the top ten terms enriched in GO enrichment analysis for “Biological processes” for proteins of the “up” cluster are related to ER stress response, integrated stress response, or general stress response (adj. p-value < 7.03 x 10-3) (Figure 22h).

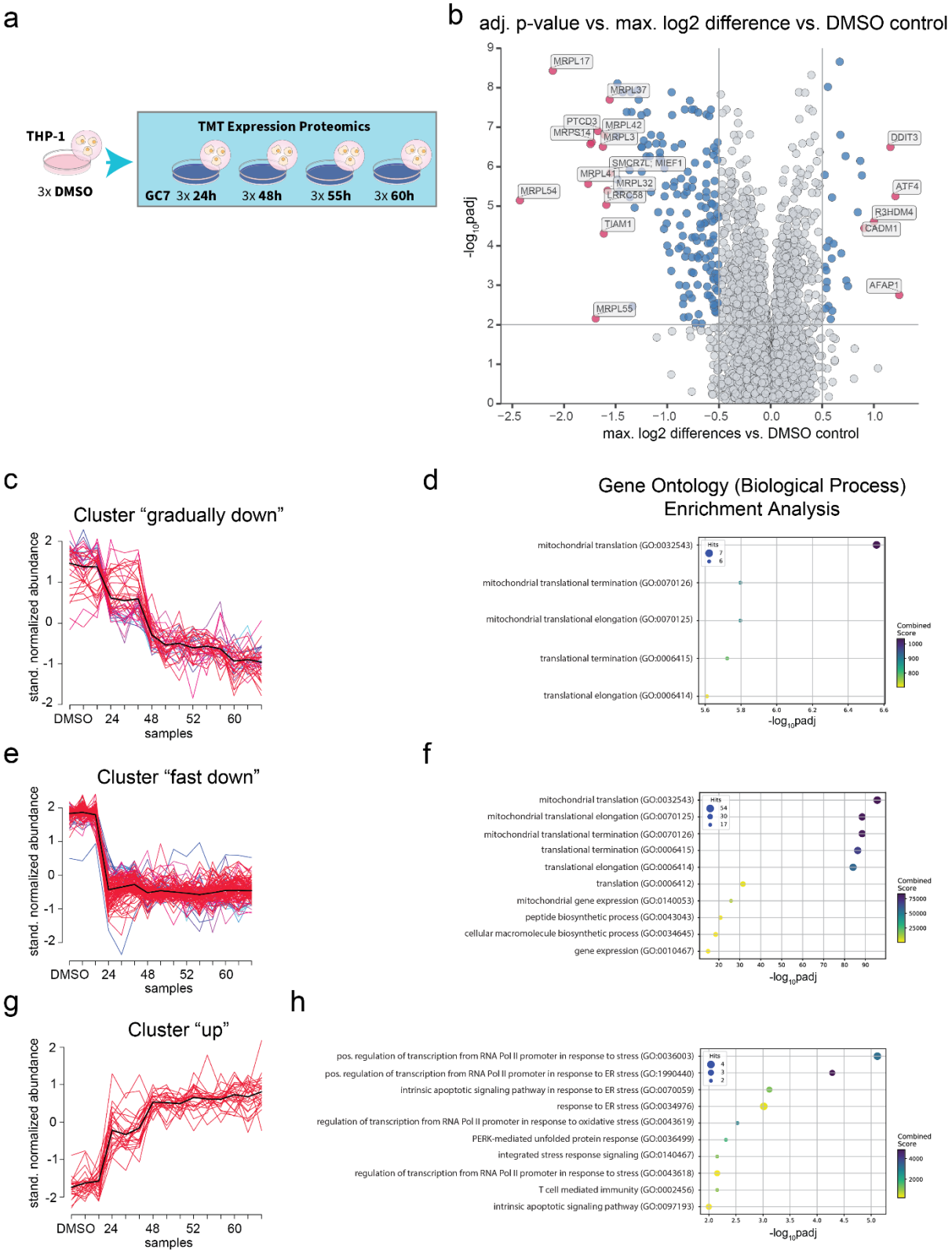

Figure 22: TMT expression proteomics identifies proteins affected by inhibition of hypusination.

a. Schematic overview of the experimental design for the hypusine time course indicating cell sample collection time points. **b.** Volcano plot showing the significantly down or up-regulated protein groups (max. delta log2 differences < -0.5, $-\log_{10}$padj > 2 and max. log2 differences > 0.5, $-\log_{10}$padj > 2 respectively) in THP-1 cells inhibited for hypusination with GC7. The x-axis shows the maximum log2 difference of the treated samples versus the

control samples for protein abundances, against the y-axis, representing the statistical significance as -$\log_{10}$padj. Each dot represents a quantified protein. Dots in red represent the top downregulated (max. log2 difference < -1.5) and top upregulated proteins (max. log2 difference > 0.9). Data collected from 4 replicates. **c.** Line plot representing a cluster of proteins that are lowered in abundance over a longer time (48 hours) and are then stable (gradually downregulated), extracted by dividing proteins from (b) in three clusters using the Fuzzy-C means clustering method. Each line represents an individual protein and its abundance in the different samples indicated in (a). The black line represents the mean of the cluster. Red lines represent proteins more similar to the mean and blue lines proteins less similar to the mean of each cluster. The x-axis indicates the different samples, collected at different time points after inhibiting hypusination or treated with DMSO as a control sample. The y-axis shows the standard normalized abundance of proteins. **d.** Gene Ontology (GO) enrichment analysis (two-sided Fisher's exact test, p value adjusted for multiple testing) for proteins contained in the cluster (c) for GO Biological Process. The x-axis indicates the significance of enrichment (-$\log_{10}$-transformed p value adjusted for multiple testing) against the y-axis showing the top enriched terms, sorted by adjusted p value. **e.** Line plot representing a cluster of proteins that have lower abundance after 24 hours and then stay at the same abundance level (fast downregulated), extracted by dividing proteins from (b) into three clusters using the Fuzzy-C means clustering method. Each line represents an individual protein and its abundance in the different samples indicated in (a). The black line represents the mean of the cluster. Red lines represent proteins more similar to the media and blue lines proteins less similar to the mean of the cluster. The x-axis indicates the different samples, collected at different time points after inhibiting hypusination or treated with DMSO as a control sample. The y-axis shows the standard normalized abundance of proteins. **f.** Gene Ontology (GO) enrichment analysis (two-sided Fisher's exact test, p value adjusted for multiple testing) for proteins contained in cluster (e) for GO Biological Process. The x-axis indicates the significance of enrichment (-$\log_{10}$-transformed p value adjusted for multiple testing) against the y-axis showing the top 10 enriched terms, sorted by adjusted p value. **g.** Line plot representing a cluster of proteins that have higher abundance compared to control samples treated with DMSO at later time points (upregulated), extracted by dividing proteins from (b) into three clusters using the Fuzzy-C means clustering method. Each line represents an individual protein and its abundance in the different samples indicated in (a). The black line represents the mean of the cluster. Red lines represent proteins more similar to the media and blue lines proteins less similar to the mean of the cluster. The x-axis indicates the different samples, collected at different time points after inhibiting hypusination or treated with DMSO as a control sample. The y-axis shows the standard normalized abundance of proteins. **h.** Gene Ontology (GO) enrichment analysis (two-sided Fisher's exact test, p value adjusted for multiple testing) for proteins contained in cluster (g) for GO Biological Process. The x-axis indicates the significance of enrichment (-$\log_{10}$-transformed p value adjusted for multiple testing) against the y-axis showing the top 10 enriched terms, sorted by adjusted p value.

3.6.3 Ribosome profiling in cells depleted of hypusine

While eIF5A is known as a translational elongation factor, early work on the bacterial orthologue EF-P, but also on eIF5A in yeast, showed that this protein is among other things specifically involved in assisting translation by resolving ribosome pausing on polyproline stretches (Doerfel *et al.*, 2013; Ude *et al.*, 2013, Li *et al.*, 2014*b*). Absence of hypusine should therefore increase the frequency of ribosome pausing across translated transcripts. Ribosome profiling informs about the position of ribosomes on these translated transcripts and should therefore allow for identification of positions sensitive to absence of hypusine (Woolstenhulme *et al.*, 2015). Therefore, we decided to additionally

investigate the global effects of hypusine inhibition with ribosome profiling (Woolstenhulme *et al.*, 2015). For this purpose, we collected additional replicate material from the 24-hour time point from the same experiment used for the expression proteomics analysis performed in the last chapter (Figure 23a). In short, the material was derived from THP-1 cells treated for 24 hours either with 30 µM of the hypusination inhibitor GC7 or a control treated with DMSO. Therefore, ribosomal footprints and total RNA was recovered from cells, analyzed using next generation sequencing and then analyzed via ribosome profiling (Figure 23a). By mapping these ribosomal footprints subsequently to the human genome, the abundance of ribosomes at the moment of harvesting can be assessed. We then analyzed the average abundance of ribosomes for each gene as exemplified in Figure 23b. By comparing the average abundance for each genomic position in cells inhibited for hypusination with untreated cells, we identified regions with higher ribosome abundances when hypusine is absent (indicated in red "significant difference") (Figure 23b). Our analyses suggest that these regions, or the amino acid motifs immediately upstream of these regions, require hypusine for efficient translation. We performed these analyses genome-wide, which will allow us to identify amino acids amino acids that require hypusine for their efficient translation, or that require hypusine to reduce interactions of N-terminal peptide domains in the ribosome exit tunnel. Additionally, the plot includes details on the hydrophobicity and the relative synonymous codon usage, which compares the frequency of the codon at the respective genomic coordinate with the codon usage across the whole genome (Figure 23b).

In summary, our analyses intend to identify locations in genes that require hypusine for efficient translation. We are currently deriving a list of hypusine target genes ranked by strength of pausing based on the "significant difference" score. After extracting the sequences localized to these pausing-zones we plan to derive amino acid motifs and other features enriched in them, that therefore should have a specific dependence on hypusine. To identify lowly expressed genes, such as transcription factors, we are currently sequencing the libraries deeper. Our goal is to derive global maps of ribosome-pausing.

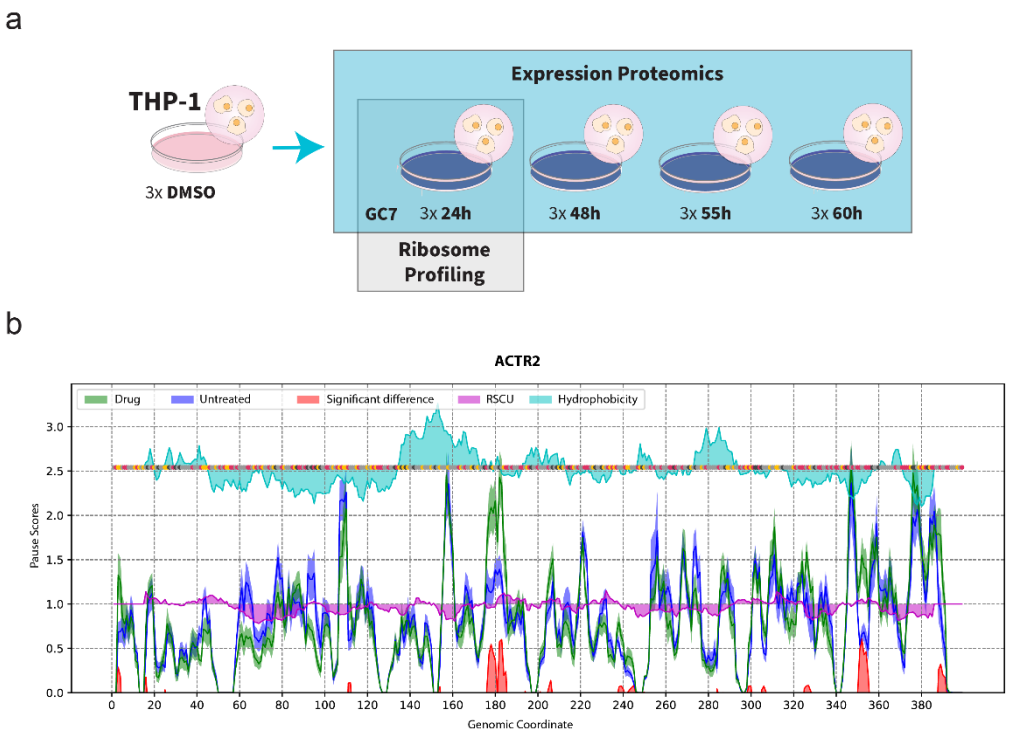

Figure 23 Ribosome profiling identifies ribosomal stalling specific to cells inhibited for hypusination.

a. Schematic overview of the time course of cell sample collection for ribosome profiling. **b.** Representative plot as an example for genome-wide analysis of the ribosome profiling data performed for the single gene ACTR2. Green and blue lines represent the normalized NGS read counts in cells treated for 24 hours with the hypusination inhibitor GC7 (green line) and treated with DMSO (blue line). Read counts were normalized by dividing the abundance of NGS reads on each position of the gene by the mean NGS read abundance across the whole gene. The blue line represents the normalized NGS read counts in cells treated with DMSO as control calculated by dividing the abundance of NGS reads on each position of the gene by the mean NGS read abundance across the whole gene. The red line represents the significant difference score, calculated as the difference in standard error between the normalized NGS read counts of the drug-treated (green) and the untreated (blue) samples. The lilac line represents the relative synonymous codon usage (RSCU) which compares the frequency of the codon at the respective genomic coordinate with the codon usage across the whole genome. The turquoise line represents the hydrophobicity of the amino acid at the genomic coordinate with a negative score meaning hydrophilic, and a positive score meaning hydrophobic amino acid stretches. Data are mean ± 95% confidence interval from 5-6 replicates.

3.6.4 Validation of ATF4 induction and hypusine increase with immunoblot and FACS

To validate the findings of the genetic hypusine abundance screen and expression proteomics dataset we perturbed mammalian cells with a set of small molecules targeting mitochondria or translation as well as with shRNAs knocking down *CTU2*, a prominent genetic hit in the screen and monitored hypusine levels with our hypusine antibody conjugated directly to a fluorophore and ATF4 levels using a reporter cell line as well as immunoblots (Figure 24).

In a first experiment, we used immunoblotting to assess ATF4 levels in THP-1 cells treated with the hypusination inhibitor GC7 and as control with Torin 1, a drug that targets mTORC1 and thereby should lead to a general reduction in protein translation after 4, 8, 24 and 48 hours (Figure 24a). 8 hours after hypusination inhibition the first visible expression of ATF4, which then increases over the next two days, can be observed (Figure 24a). Since ATF4 is a key transcription factor induced by ER stress and integrated stress response as well as by mitochondrial stress, this upregulation confirms the cluster of upregulated proteins identified in the expression proteomics experiment above (Quirós *et al.*, 2017; Costa-Mattioli and Walter, 2020; Guo *et al.*, 2020) (Figure 22). Interestingly, inhibition of hypusination also leads to the upregulation of acetylated eIF5A, a phenomenon that will be closer investigated in the next chapter below (Figure 24a).

Using our hypusine antibody directly coupled to a 594 nm fluorophore we next looked at hypusine levels in cells treated with the hypusination inhibitor GC7, with the mitochondrial translation inhibitor chloramphenicol as well as with Torin 1 as control (Figure 24b). As expected, treatment with GC7 and Torin 1 led to reduced hypusine levels (Figure 24b). Additionally, cells blocked for mitochondrial translation indeed showed an increase in hypusine levels, strengthening and validating the finding of our genetic screening results, where mitochondrial translation scored among the strongest types of machinery as negative regulators of hypusination (Figure 21b,c).

As an alternative method for measuring *ATF4* response, we generated HAP1 reporter cells employing an *ATF4* reporter construct developed by Guo *et al.* and read out ATF4 induction upon inhibition of hypusination with increasing doses of GC7 (Figure 24c) (Guo *et al.*, 2020). The correct function of the reporter was successfully tested with the control drug oligomycin A, a drug known to induce ATF4 expression through the mitochondrial stress pathway (Fessler *et al.*, 2020; Guo *et al.*, 2020). Indeed, *ATF4* reporter expression is induced by the inhibition of hypusination and responds dose-dependently to increasing concentrations of the inhibitor GC7 (Figure 24c).

One prominent genetic negative regulator of the genetic hypusine abundance screen was the *Translocase Of Outer Mitochondrial Membrane 40* (*TOMM40*), a protein involved in the import of protein precursors into mitochondria (Humphries *et al.*, 2005). To validate this finding, we blocked mitochondrial protein import with the novel drug Mitoblock-6 at increasing doses for 24 hours (Figure 24d). Indeed, we could see again *ATF4* induction at doses of Mitoblock-6 larger than 50 µM (Figure 24d). If hypusine levels are increased as well in this situation, will soon be tested with the more sensitive method presented in Figure 24b. As before in Figure 24b, we treated cells with increasing doses of chloramphenicol and this time assessed ATF4 levels after 24 hours by immunoblotting (Figure 24e). Again, we could observe *ATF4* induction with chloramphenicol doses ≥ 5 mM (Figure 24e). Lastly,

we validated the machinery responsible for 2-thiolation of mcm_5S_2U at the wobble position of certain tRNAs, that scored entirely (*Cytoplasmic tRNA 2-thiolation protein 2* (*CTU2*), *Cytoplasmic tRNA 2-thiolation protein 1* (*CTU1*), *Molybdenum Cofactor Synthesis 3* (*MOCS3*) and *Ubiquitin-Related Modifier 1* (*URM1*)) and highly significant as a negative regulator for hypusination in the genetic screen (Figure 21b) (Schlieker *et al.*, 2008). Being the most significant hit of this machinery, *CTU2* was picked for validation of this machinery, and we generated inducible *CTU2* knock-down cell lines in HAP1 using two different shRNA constructs (Figure 24f). Again, we observed clear *ATF4* expression on immunoblot, 72 hours after induction of the *CTU2* shRNAs (Figure 24f). Effects of *CTU2* knock-down on hypusine levels will be assessed as well with the method presented in Figure 24b.

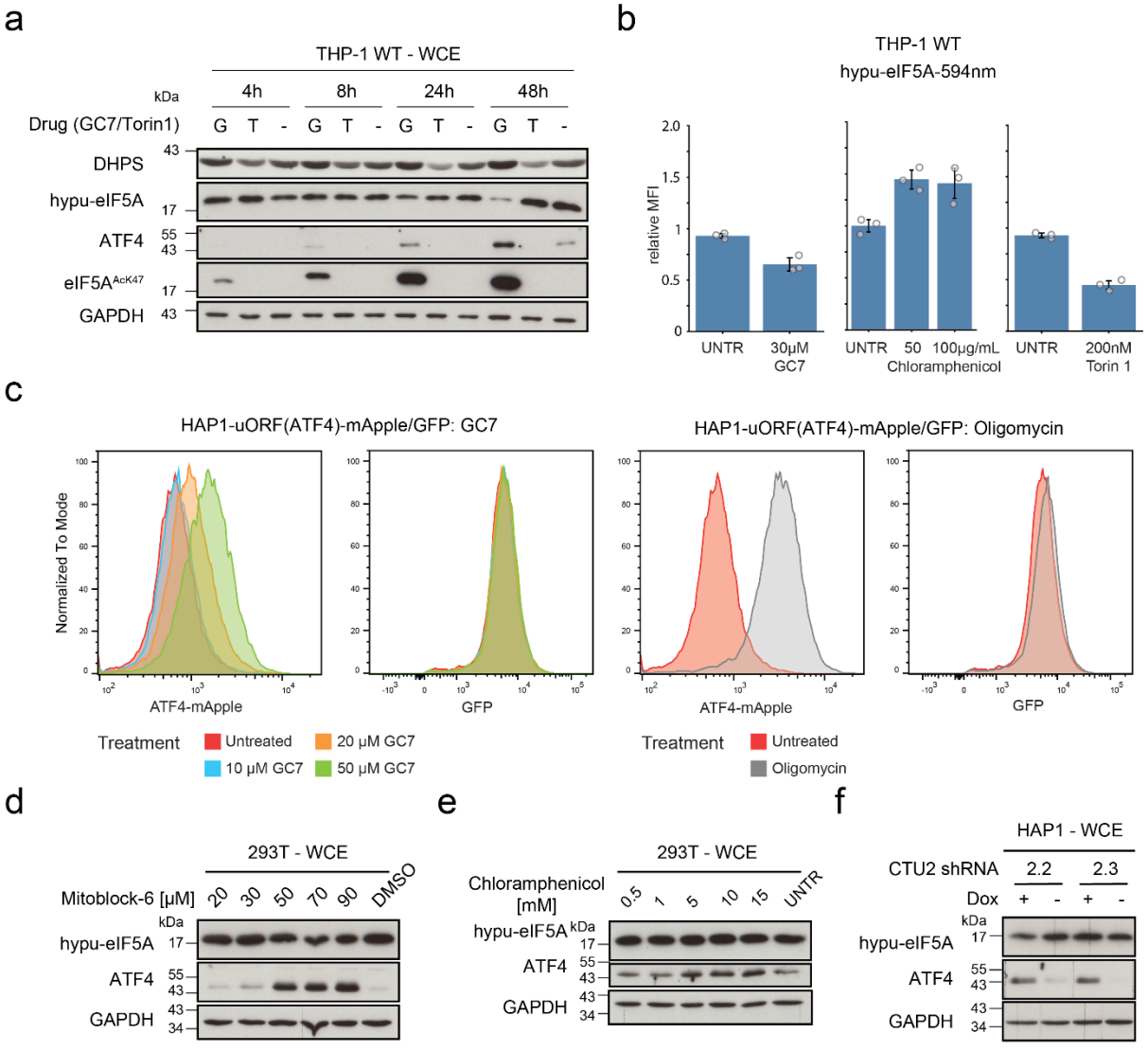

Figure 24: Inhibition of hypusination leads to expression of ATF4 and inhibition of mitochondrial translation increases hypusine levels.

a. Western blot analysis of DHPS, hypusine (hypu-eIF5A), ATF4, acetylation of eIF5A at lysine 47 ($eIF5A^{AcK47}$) in THP-1 cells treated with either 30 µM GC7 or as control with 200 nM Torin 1 at the respective time point (4-48 hours). **b.** Barplot showing the ratio of the amount of hypusine quantified in THP-1 cells treated with the respective drug (30 µM GC7; 50-100 µg/mL

chloramphenicol, 200 nM Torin 1) compared hypusine amounts in untreated cells (UNTR) quantified with a hypusine-antibody directly conjugated to a fluorophore (hypu-eIF5A-594 nm). Data are mean ± 95% confidence interval from 3 technical replicates. **c.** Histogram summarizing signal intensity for HAP1 reporter cells expressing the uORF(ATF4)-mApple/GFP reporter constructs reporting on *ATF4* activation (ATF4-mApple) and general expression as control with GFP. Cells are either untreated or treated with increasing amounts of GC7 (10-50 μM) or with the control drug oligomycin A as indicated. **d.** Western blot analysis of hypusine (hypu-eIF5A) and ATF4 in HEK293T treated with increasing levels of Mitoblock-6 (20-90 μM) or treated with DMSO as a control for 24 hours. **e.** Western blot analysis of hypusine (hypu-eIF5A) and ATF4 in HEK293T treated with increasing levels of chloramphenicol (0.5-15 mM) or treated with DMSO as a control for 24 hours. **f.** Western blot analysis of hypusine (hypu-eIF5A) and ATF4 in HAP1 cells stable expressing two different doxycycline-inducible shRNA constructs (2.2, 2.3) targeting *CTU2* induced or uninduced with doxycycline for 72 hours.

3.6.5 Acetylation of eIF5A

To validate the eIF5A^{AcK47} antibody we transiently expressed *DHPS*, *DOHH*, and *eIF5A* (either *eIF5A*-WT or mutated for the acetylation site lysine 47) in HEK293T cells. The antibody successfully detected acetylation on *eIF5A*-WT, while no signal was detected in cells overexpressing the *eIF5A*-K47 variants (Figure 25e).

As already described in the last chapter, blocking hypusination leads to rapid upregulation of eIF5A acetylated at the lysine 47 position (eIF5A^{AcK47}) and can already be seen by immunoblotting in the first (4-hour) timepoint after blocking hypusination (Figure 24a). This potentially indicates that unhypusinated eIF5A has a high tendency to get acetylated at lysine 47 (Figure 24a). Looking at the eIF5A^{AcK47} levels with immunoblot in HEK293T cells growing in increasing amounts of glucose revealed a gradual increase in acetylation dependent on levels of glucose, suggesting a link between acetylation status and carbon source or type of respiration (Figure 25a). In another experiment, immunoblotting was used to compare the eIF5A^{AcK47} status of cells grown in glucose versus cells grown in galactose over a period of four to 24 hours (Figure 25b). Interestingly, eIF5A^{AcK47} levels were decreased in cells grown in galactose compared to cells grown in glucose (Figure 25b). Since the switch of carbon source from glucose to galactose in cell culture medium, forces cells to perform more oxidative phosphorylation, this data suggests that eIF5A^{AcK47} levels negatively correlate with the need to perform oxidative phosphorylation (Figure 25b) (Warburg, 1925; Frey, 1996). However, when we treated cells with oligomycin A, an inhibitor for ATP synthase, we observe again a drop in the eIF5A^{AcK47} levels in cells analyzed via immunoblot, possibly suggesting that the need to generate more functional mitochondria or more functional oxidative phosphorylation machinery leads to a decrease in eIF5A^{AcK47} levels (Figure 25c) (Smith *et al.*, 1954). Motivated by the possible link of eIF5A^{AcK47} status to the respiration type performed in cells, we surveyed the eIF5A^{AcK47} levels with immunoblotting in a panel of different cell types known to perform to a different degree either glycolysis or oxidative

phosphorylation for their energy generation (Figure 25d). Interestingly, when looking at MDA-MB231, a cell model known to highly rely on glycolysis for energy generation, and comparing it to MCF7, cells known to use more oxidative phosphorylation for ATP generation one can clearly see again the higher eIF5A^{AcK47} levels in MDA-MB231 cells (Figure 25d) (Zare *et al.*, 2021).

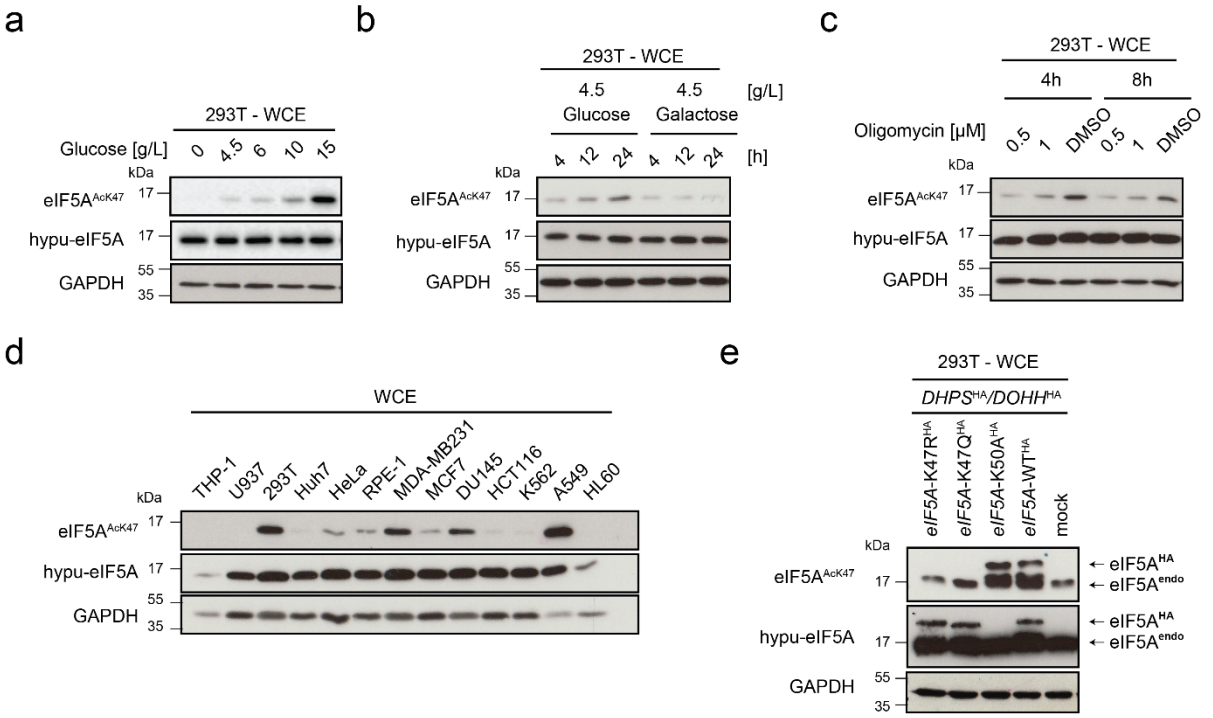

Figure 25: Acetylation of eIF5A.

a. Western blot analysis of acetylation of eIF5A at lysine 47 (eIF5A^{AcK47}) and hypusine (hypu-eIF5A) in HEK293T cells grown in increasing amounts of glucose. **b.** Western blot analysis of acetylation of eIF5A at lysine 47 (eIF5A^{AcK47}) and hypusine (hypu-eIF5A) in HEK293T cells grown either in medium containing 4.5 g/L glucose or in medium instead with 4.5 g/L galactose at the respective time point (4-24 hours). **c.** Western blot analysis of acetylation of eIF5A at lysine 47 (eIF5A^{AcK47}) and hypusine (hypu-eIF5A) in HEK293T cells treated with oligomycin A at 0.5 or 1 µM or treated with DMSO as control at the respective timepoint (4 or 8 hours). **d.** Western blot analysis of eIF5A at lysine 47 (eIF5A^{AcK47}) and hypusine (hypu-eIF5A) in a panel of different cells. **e.** Western blot analysis of acetylation of eIF5A at lysine 47 (eIF5A^{AcK47}) and hypusine (hypu-eIF5A) in HEK293T cells overexpressing either a mock or C-terminal HA-tagged eIF5A-WT (*eIF5A*-WT^{HA}) or eIF5A-K47R mutant cDNA (*eIF5A*-K47R^{HA}) or eIF5A-K47Q mutant cDNA (*eIF5A*-K47Q^{HA}) or eIF5A-K50A mutant cDNA (*eIF5A*-K50A^{HA}) as well as a C-terminal HA-tagged DHPS cDNA (*DHPS*^{HA}) and DOHH cDNA (*DOHH*^{HA}).

3.6.6 Validation with endogenously tagged hit proteins

Next, we wanted to validate proteins identified as downregulated upon inhibition of hypusination in our TMT expression proteomics experiment described above (Figure 22). Due to the absence of commercially available antibodies for many of the identified mitochondrial proteins, we surveyed vpCells, a collection of endogenously tagged lines established at CeMM, and found available

cell lines tagged for the proteomics hits *ATP Synthase Membrane Subunit G* (*ATP5MG*), *Mitochondrial ribosomal protein L42* (*MRPL42*), *ATP Synthase Peripheral Stalk-Membrane Subunit B* (*ATP5PB*), *NADH:Ubiquinone Oxidoreductase Subunit AB1* (*NDUFAB1*) and *Oxidase Assembly 1-Like protein* (*OXA1L*) (Reicher *et al.*, 2020). Since those cell lines have a GFP inserted endogenously in their protein sequence, we decided to monitor GFP levels upon hypusination inhibition with GC7 for 24 hours (Figure 26a). Changes are illustrated as percent changes in mean fluorescent intensity quantified with FACS and are in the range of -14 to -30 percent compared to untreated samples (Figure 26a). These results confirm the finding of the expression proteomics experiment and show that indeed mitochondrial proteins are downregulated when hypusination is inhibited (Figure 22, Figure 26a). WT HAP1 cells were included to confirm no general reduction of GFP signal upon treatment with GC7 unrelated to the tagged target protein and showed indeed no reduction in GFP signal upon inhibition of hypusination (Figure 26a). Next, we took the cell line endogenously tagged with GFP in *MRPL42* ($HAP1^{MRPL42:GFP}$) and assessed if the reduction in protein level is affected dose-dependently upon increasing GC7 inhibitor concentrations (2.5-30 µM) and could indeed observe a dose-dependent reduction in GFP levels (Figure 26b).

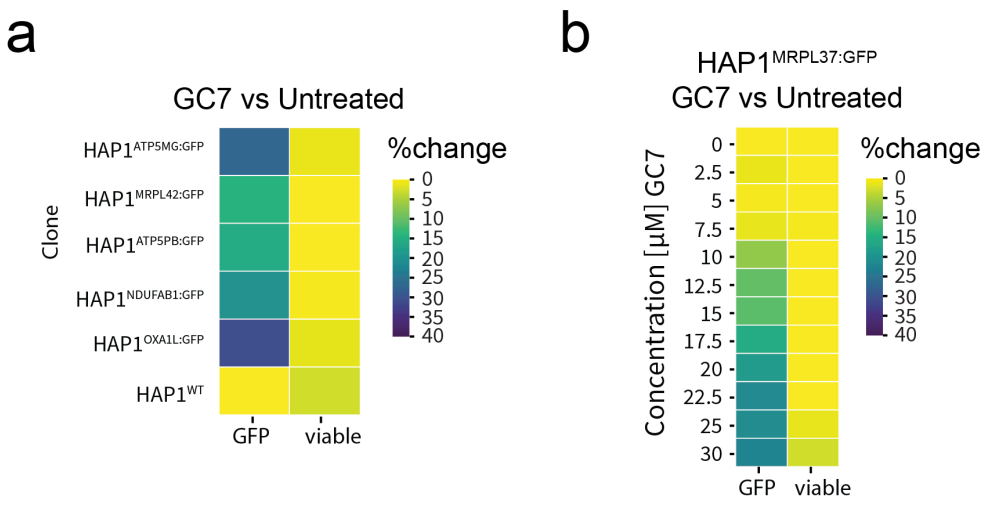

Figure 26: Endogenous tagged proteins in HAP1 confirm sensitivity to hypusine inhibition.

a. Heatmap illustrating quantification of GFP levels and viability in HAP1 cells endogenously tagged with GFP in *ATP5MG*, *MRPL42*, *ATP5PB*, *NDUFAB1*, and *OXA1L* and treated with 30 µM GC7 for 24 hours as percentage change compared to untreated cells. Data are mean from 3 technical replicates. **b.** Heatmap illustrating quantification of GFP levels and viability in HAP1 cells endogenously tagged with GFP in *MRPL42* and treated with increasing doses of GC7 (2.5-30 µM) for 24 hours as a percentage change compared to untreated cells. Data are mean from 3 technical replicates.

The dose-dependent response of the endogenous tagged cell lines to hypusine inhibition opens the possibility to use them as a reporter system for follow-up genetic screens that look for example for genes that can overcome defects caused by inhibition of the hypusine axis. To be able to use a haploid genetic screening approach similar to the one presented in Figure 21 we had to generate the

presented reporter cell lines in Figure 26 in a haploid state. For this, we endogenously intron-tagged mitochondrial proteins, isolated clonal cell lines, and used Hoechst 33342 to assess the ploidy of the different clonal cell lines as exemplified by one clone tagged with GFP in *NDUFAB1* (Figure 27a-b). Finally, we used confocal imaging to assess the localization of the tagged proteins (Figure 27c). In summary, haploid clonal cell lines, tagged endogenously with GFP were generated for *ATP5MG*, *NDUFAB1*, and *OXA1L* and are now in use for genetics screens that will be reported in the future.

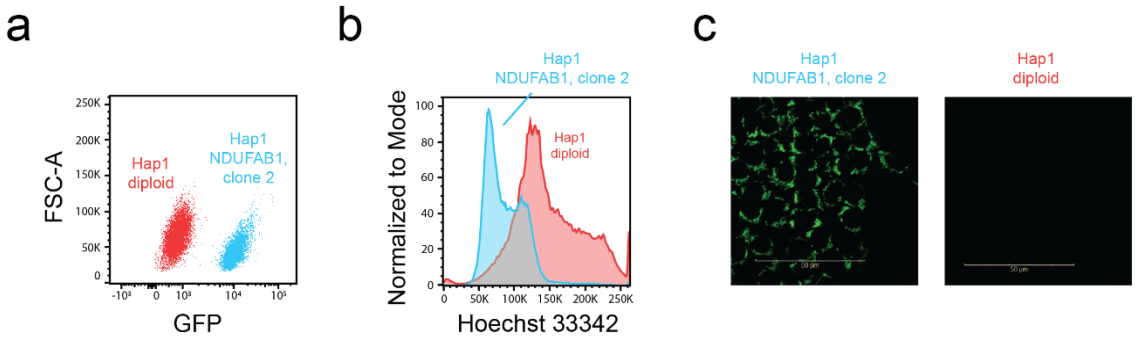

Figure 27: Generation of haploid HAP1 reporter cell lines endogenously tagged in mitochondrial proteins.

a. Representative flow cytometry scatterplots as an example for validation of tagging and expression of isolated HAP1 cell lines endogenously tagged in the mitochondrial protein *NDUFAB1*. Isolated cell lines (blue) were compared to a non-modified WT HAP1 pool of cells that are mostly diploid (red) and don't express GFP as control. Each dot corresponds to one measured cell: the intensity of the GFP signal is represented on the x-axis and serves as confirmation for successful tagging and expression of the target protein, and the forward scatter of the cell on the y-axis. **b.** Representative flow cytometry histogram as an example for validation of ploidy of isolated HAP1 cell lines endogenously tagged in the mitochondrial protein *NDUFAB1*. Isolated cell lines (blue) were compared to a non-modified WT HAP1 pool of cells that are mostly diploid (red) as control. Each dot corresponds to one measured cell: the intensity of the Hoechst 33342 signal is represented on the x-axis and serves as a readout for the ploidy of the cell lines genome. **c.** Representative image showing the localization of the tagged protein in green.

4 Discussion

Huge advances in functional genomics, matured this area of research in the last few decades into a scalable and powerful instrument for generating unbiased hypothesis-generating research. At the same time, innovations in the field of liquid chromatography, electrospray ionization (ESI), and the development of TMT labels now allow us to assess whole proteomes of cells in different conditions within days. The combination of genetics and proteomics became therefore a powerful approach to discover and characterize novel molecular pathways. The addition of more targeted systematic techniques such as ribosome profiling can then help to understand yet more additional layers of regulation. Furthermore, a growing number of publicly shared large-scale datasets such as protein-protein interaction data or gene expression datasets are becoming available, can be mined, and then assist with the interpretation of new large-scale studies.

This thesis aimed to engineer tools and optimize their use in genetic screens and thereby allowing to map the genetic regulation landscape of molecular pathways. The first such study led to a map of regulators of phagocytosis derived from a genome-wide genetic screen and interpreted with the aid of publicly available protein-protein interaction data. This unbiased search of regulators led to the discovery of the enigmatic hypusine axis as the top enriched and most unknown gene family in the context of phagocytosis. Therefore, the second part of the thesis focused on the complete molecular characterization of the hypusine pathway, using further genetic screening, expression proteomics, ribosome profiling as well as endogenous protein tagging as validation tools. Specific findings obtained from the different studies will be discussed in the following sections.

4.1 Functional Genomics applied in a Phagocytosis Screen

Phagocytosis is a lengthy and complex multistep process that involves a whole spectrum of machineries within cells. By setting up and conducting a reporter-based FACS-based genome-wide CRISPR/Cas9 knock-out screen we could identify modulators of phagocytosis. Due to the large number of modulators that we identified, we had to come up with an approach to prioritize genes for validation and found a solution in publicly available protein-protein interaction data from BioPlex 3.0 and protein complex data from CORUM-core (Giurgiu *et al.*, 2019; Huttlin *et al.*, 2021). This information allowed us to group genetic hits in molecular complexes and to orient them in defined proximity to each other in a protein-protein interaction network. Since phagocytosis is a lengthy and complex process it requires the orchestration of several steps such as the mechanical cytoskeleton machinery, membrane uptake processes involved in the internalization of external material into the

phagosome, trafficking of the phagosome, fusion of the phagosome with lysosome followed by its acidification, and clearance and recycling to the plasma membrane.

Compared to the systematic search for phagocytic regulators performed by Haney *et al.* using a genetic screen and magnetic bead separation in the U937 cell line (Haney *et al.*, 2018), we instead used a more sensitive FACS-sorting approach in the cell line THP-1. We could confirm and expand their identified hits such as the Wave-2 complex, the Arp2/3 machinery, the mTOR-associated Ragulator complex, and many genes known to be part of coordinated vesicle trafficking and cargo transport. In addition, we could identify regulators previously not linked to phagocytosis such as the oligosaccharyltransferase complex (MAGT1/SLC58A1, STT3B, DDOST, RPN2) as well as a whole set of uncharacterized genes, that are published within the study described above (see chapter 3.4). To our surprise, the top-scoring gene family was the hypusine axis, a discovery that led our focus in the second part of this thesis entirely on this pathway. Even though spermidine was already associated in 1952 as being an anti-mycobacterial natural compound and later also as an inhibitor for cytokine synthesis in human mononuclear cells, the first mechanistic link of hypusination to phagocytosis was only discovered recently (Hirsch and Dubos, 1952; Zhang *et al.*, 1997; Lindner *et al.*, 2021). In addition, mice lacking hypusine have recently been found to be more susceptible to infections by *Heliobacter pylori* and *Citrobacter rodentium*, while hypusine plays a role in translating a set of antimicrobial factors in these mice (Gobert *et al.*, 2020). In yeast, part of the hypusine axis could be additionally linked to processes related to phagocytosis, such as vesicular transport and cytoskeleton arrangement. One such example is the synthetic lethal interaction between *eIF5A* and *YPT1* (*the yeast ortholog of mammalian rab genes*, coordinators of endocytosis) (Clague, 1998; Frigieri *et al.*, 2008). Another example in yeast are regulators for cell polarity and actin nucleation (*PKC1*, *ZDS1*, *GIC1* (human ortholog *CDC42*) as well as *PCL1* and *BNI1*) that were identified as suppressors for *eIF5A* depletion (Zanelli and Valentini, 2005). In *Drosophila* the *DOHH* homolog *nero* and *eIF5A* were shown to be required for autophagy (Patel *et al.*, 2009). Furthermore, in human cells, *eIF5A* was shown to regulate the translation of the transcription factor *TFEB*, a master regulator of lysosomal biogenesis (Zhang *et al.*, 2019). Recently, the hypusine axis has also been shown to be involved in the context of macrophage respiration (Puleston *et al.*, 2019) and in addition as an effector of macrophage inflammatory state in adipose tissue (Anderson-Baucum *et al.*, 2021). Indeed, in our work, we could show experimentally that inactivation or knock-out of the hypusine axis manifests in the cell with a reduction of phagocytosis. Despite all the above potential links of hypusination to phagocytosis, summarized in Figure 28 it remains to be shown how hypusinated eIF5A mechanistically influences immune cells.

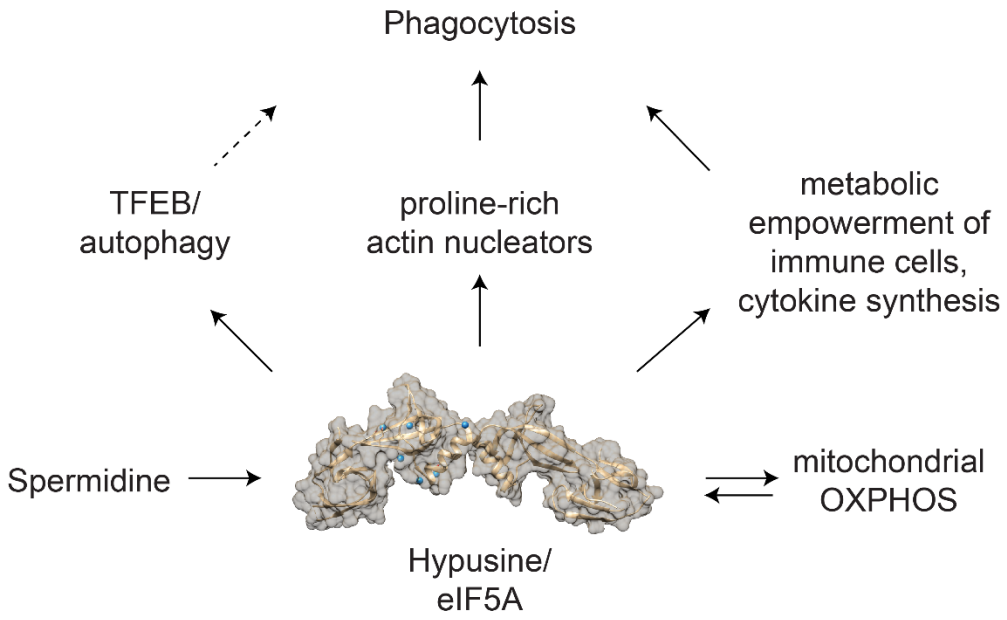

Figure 28: Summary of hypothetical interaction between eIF5A and phagocytosis.

Adapted from PDB: 3CPF, Proteins, 75(4):1040-5, Tong, Y., Park, I., Hong, B-S., Nedyalkova, L., Tempel, W., Park, H-W., Crystal structure of human eIF5A1: insight into functional similarity of human eIF5A1 and eIF5A2, 2009, with permission form John Wiley and Sons; created with UCSF Chimera, J Comput Chem, 25(13):1605-12, Petterson, EF., Goddard, TD., Huang, CC., Couch, GS., Greenblatt, DM., Meng, EC., Ferrin, TE., UCSF Chimera--a visualization system for exploratory research and analysis, 2004

Even though a pathogen agnostic reporter was used for our genetic screen, we could identify the key genes and regulators taken also by pathogen as found by studies with *Legionella pneumophilia*, *Staphylococcus aureus*, and *Salmonella* such as the actin polymerization machinery (Jeng *et al.*, 2019; Yeung *et al.*, 2019; Lindner *et al.*, 2021). Our work updates the current view of how cargo is trafficked through the cell and might be useful to pinpoint new targets for directing therapeutics, such as RNA therapeutics, Cas9, or antibody-drug conjugates, better to their intended side of action (Lino *et al.*, 2018; Tsui *et al.*, 2019; Dowdy *et al.*, 2022). Our dataset could in addition be a useful resource for the community to identify new targets in diseases related to dysfunctions in the endo-lysosomal system or non-functional autophagy such as the neurodegenerative diseases Parkinson's disease, Alzheimer's disease, or Huntington's disease (Malik *et al.*, 2019). The relevance of this dataset is also highlighted by the association of the hypusine axis with phagocytosis, which was a rather new association at the time of discovery and now proved to become an important pathway in the context of immune cell activity, respiration, and specification (Puleston *et al.*, 2019, 2021; Gobert *et al.*, 2020). Furthermore, we demonstrated the power of interpreting reporter-based genome-wide genetic screens with the help of publicly available protein-protein interaction data, an approach that we think can be applied to the interpretation of any genome-wide genetic screen. In

addition, other publicly available datasets such as DepMap can be helpful to separate phenotypes induced by general fitness effects of the deactivated genes or by specific phenotypes in the cell model of choice (Meyers *et al.*, 2017).

While being a very precise technique for cell separation, FACS sorting comes with the disadvantage of lengthy processing times which makes the technique time-consuming for the experimenter. Additionally, the complexity of the screen varies with the chosen reporter readout. While simpler readouts, such as antibody staining of protein levels in fixed cells are easier to scale, multi-stage readouts that require processing of live cells are more difficult to handle. The phagocytosis assay used in this study requires the differentiation of cells as well as the incubation of the reporter with live cells to allow for phagocytosis. Therefore, in total three billion cells (750 million per replicate) had to be handled and processed in parallel, which forced us to perform the phagocytosis experiments only with a single substrate. Clearly, it would be interesting in the future to screen for a whole array of different phagocytosis substrates using the precise FACS sorting technique. In addition to different substrates, it would also be interesting to run phagocytosis screens in a whole selection of different phagocytic cell models. The CRISPR/Cas9 knock-out technique, used for this screen, induces full knock-out of genes and thereby total ablation of the respective protein (Cong *et al.*, 2013; Mali *et al.*, 2013). While phenotypes observed in knock-out screens can be specifically linked to the respective gene, they come with the drawback of potentially missing some essential genes as being involved in phagocytosis, which could be discovered with alternative screening techniques that only reduce protein levels or act shorter, such as RNAi, CRISPR interference or inducible Cas9 versions (Boutros and Ahringer, 2008; Gilbert *et al.*, 2014; de Almeida *et al.*, 2021). For screens where Cas9 is only induced for a shorter time, it is however highly recommendable to test and generate clonal cell lines with inducible Cas9 expressed at defined levels. While the generation of clonal cells lines for THP-1 is possible, as demonstrated in our study above for inducible DHPS knock-out clones, it has been proven to be a lengthy process for THP-1 and involves the survival of only a comparable small fraction of the original cell pool, raising the question of how representative these clonal cell lines would be in a genome-wide screen. However, for other cell lines that tolerate clonal cell selection well, an inducible Cas9 system might be a good alternative knock-out platform.

Even though the long processing times for FACS sorting make this technique harder to scale, constant improvements in the sorting speed of machines and software as well as other ways to automate these FACS procedures will make this technique quicker in the future. Additionally, new features of FACS sorters, such as image-enabled cell sorting (Schraivogel *et al.*, 2022) or the development of totally new cell separation techniques will increase the possibility of phenotypic readouts for genetic screens tremendously. This could then allow screening in multiple cellular

systems with a variety of different reporters in parallel, which will drive improved precision of understanding of molecular processes. In the case of phagocytosis, it would be great in the future to perform phagocytosis assays with different natural substrates in phagocytic cells isolated from all different locations in the body, making the prioritization of targets for therapy even more precise. Additionally, it will be beneficial to supplement the genetic data generated with gene knock-out or gene interference techniques with complementary CRISPR activation screens (Tian *et al.*, 2021). This is helpful for the interpretation because the downregulation of single members of protein complexes via knock-out and gene interference can trigger downregulation of the entire complex, upregulation of single members of a complex however has usually no effect (Tian *et al.*, 2021). In our phagocytosis screen, we can indeed see, that our genome-wide knock-out screen identifies entire protein complexes such as the Arp2/3 or Wave-2 complex with different guide RNAs that induce comparable phenotypes. A CRISPR activation screen could potentially enhance this knowledge by informing on which exact subunit of this complex is most essential for the right function of this complex. Additionally, CRISPR activation can upregulate genes that are naturally not expressed at all. Lastly, the increasing amount of publicly available datasets, such as protein-protein interaction data, gene expression, and gene fitness data (GTEx Consortium, 2013; Meyers *et al.*, 2017; Huttlin *et al.*, 2021), which proved to be useful for the interpretation of our genome-wide screen, will make it worth to constantly re-analyze past genetic screening datasets to derive new insights. Therefore, sharing these datasets in public databases that make it easy to cross-compare studies will be of great benefit in the future.

4.2 Hypusine Omics

The highly significant and complete discovery of the enigmatic hypusine axis in the first part of this thesis motivated us to dissect the regulation of this pathway in greater detail in the second part of this work. Therefore, we applied a whole spectrum of functional genomics techniques ranging from haploid genetics to assigning gene function and studying the effect of the translation elongation factor eIF5A on translation using expression proteomics as well as ribosome profiling. Together, the genetic survey of hypusine regulation and the effects observed in the proteome upon hypusine inhibition suggest that there is a crosstalk between respiration or specifically OXPHOS and hypusine levels. In summary, we observe, that the absence of hypusine leads to a reduction of OXPHOS, and at the same time genetic or pharmacological inhibition of OXPHOS leads to an increase in hypusine levels in the cell.

This crosstalk can be seen for example in the haploid genetic survey that we used to screen genome-wide for genes affecting hypusination levels. As described above many of the identified

negative regulators, that led to an increase in hypusine levels when knocked out, are directly involved in OXPHOS, or involved in mitochondrial gene expression. Mitochondrial transcription and translation are responsible for the expression of the mitochondrial genome, which encodes not more than 13 mitochondrial proteins (Kummer and Ban, 2021). Since all of these proteins are key proteins of the OXPHOS machinery, it is fair to say that also these genetic hits are also indirectly linked to OXPHOS (Kummer and Ban, 2021). While previous studies established a regulatory function of polyamine or hypusine on OXPHOS, like the observation that supplementation of spermidine to aged *Drosophila* increases levels of OXPHOS proteins or that inhibition of hypusination triggers macrophages to switch their respiration towards glycolysis (Puleston *et al.*, 2019; Liang *et al.*, 2021), we are to our knowledge the first to show the inverse crosstalk of OXPHOS to the hypusine axis in an unbiased genetic screen. A possible link between hypusine and mitochondrial biogenesis is that inhibition of hypusination with GC7 was frequently observed to lead to the upregulation of PGC-1a a key regulator of energy metabolism (Giraud *et al.*, 2020). Inversely, one could speculate that the reduction of OXPHOS leads to more availability of molecular oxygen in the cell, which is essential for forming the DOHH intermediate that is responsible for the final step in hypusine synthesis (Wolff *et al.*, 2007). It remains however to be experimentally tested how the crosstalk is mechanistically happening. It is furthermore worth mentioning, that also in yeast there exists a connection between *eIF5A* and respiration status. While one *eIF5A* isoform (*TIF51A*) promotes respiration, the other one (*TIF51B*) promotes aerobic glycolysis (Barba-Aliaga and Alepuz, 2022*b*). Interestingly, the human *eIF5A-2* isoform is also frequently expressed in cancer cells, which are known to often have glycolytic enzymes expressed at higher levels (Meng *et al.*, 2015; Cao *et al.*, 2017). Despite these clear showcases of *eIF5A* isoforms correlating with the metabolic state of cells, it remains to be investigated if this differential expression is triggered by the metabolic state or is in fact causing it. Using expression proteomics, we furthermore tracked the changes in the proteome upon inhibition of hypusination. Interestingly, we could again observe a clear link to OXPHOS with many proteins involved in mitochondrial gene expression being downregulated. This data confirms the crosstalk identified in the genetic screen now from a different angle. Inhibition of OXPHOS increases hypusine levels and inhibition of hypusination decreases OXPHOS. Due to the lack of available antibodies for many of the downregulated proteins, we endogenously tagged some OXPHOS-related proteins with the fluorescent protein GFP and could indeed observe a downregulation of these proteins when hypusination was inhibited. The exact same samples used for expression proteomics were then also studied using ribosome profiling and that allows us to generate a global map of changes in ribosome speed upon inhibition of hypusination. Since previous studies have shown, that eIF5A acts as a translation elongation factor, assisting with the translation of specific amino acid motifs, we currently try to extract global motifs of amino acids

whose translation is dependent on eIF5A. This, in combination with our expression proteomics and genetic data, will help us to understand the global impact of hypusinated eIF5A in the cell. In addition, expression proteomics also allowed for the identification of upregulated proteins within the cells and exposed a clear cluster of *ATF4*-related proteins as being upregulated in hypusine-inhibited cells (Quirós *et al.*, 2017; Costa-Mattioli and Walter, 2020). With validation experiments, we could indeed prove that inhibition of hypusination leads to induction of *ATF4* expression, an observation that has also been made when *eIF5A* is depleted altogether by another group (Mandal *et al.*, 2016). Interestingly, all further validations involving pharmacological and genetic inactivation of negative hypusination regulators also revealed an upregulation of ATF4 protein. Since, *ATF4* is also known as a sensor that is activated during the mitochondrial stress response, this means that our observed ATF4 response could also be an indirect effect triggered by downregulated OXPHOS (Quirós *et al.*, 2017). Lastly, the relationship could also be vice versa. The induction of *ATF4* has also been linked to a blockage of mitochondrial protein import, which could trigger a downregulation of OXPHOS (Schäfer *et al.*, 2022). Indeed, one of the most significant negative regulators that was identified with genetics is *TOMM40*, a key protein for importing mitochondrial protein precursors (Humphries *et al.*, 2005). But also when we knocked down *CTU2*, another negative regulator of hypusine, which is part of the 2-thiolation of mcm_5S_2U pathway we observed again an *ATF4* induction (Schlieker *et al.*, 2008). Since cysteine, the substrate for thiolation is believed to derive from mitochondria (Zhang *et al.*, 2021), one could hypothesize that inhibition of thiolation could increase mitochondrial cysteine synthesis as a compensatory reaction and thereby again trigger mitochondrial stress . Since all the so-far described validations led to an induction of *ATF4*, it opens yet another possibility, which is that *ATF4* itself is responsible for the upregulation of hypusine levels. To test this possibility, we created clonal *ATF4* reporter cell lines and will use them to test if the upregulation of ATF4 correlates with increased hypusine levels. Finally, inhibition of mitochondrial translation with the inhibitor chloramphenicol could show that hypusine levels are indeed increased in settings where mitochondrial gene expression is inhibited. In summary, this data suggests that any perturbation along the OXPHOS pathway leads to upregulation of hypusine, while any perturbation of hypusine leads to downregulation of the OXPHOS machinery and both perturbations in the OXPHOS pathway but also inhibition of hypusination lead to upregulation of ATF4.

The crosstalk of respiration and hypusination got us interested in the enigmatic reversible acetylation modification of eIF5A which is introduced by PCAF, in an acetyl-CoA consuming process, and can be removed by SIRT2 or HDAC6 (Ishfaq *et al.*, 2012). Indeed, when looking at $eIF5A^{AcK47}$ levels in cells grown in the alternative carbon source galactose, which forces cells to rely on OXPHOS, we observed a differential regulation of $eIF5A^{AcK47}$ (Warburg, 1925; Frey, 1996). At the same time

inhibition of OXPHOS, as tested with the ATP synthase inhibitor oligomycin A, lowers eIF5A^{AcK47} levels indicating that the requirement to generate more OXPHOS-related proteins leads to lower eIF5A^{AcK47} status in cells (Smith *et al.*, 1954). Furthermore, looking across cell lines with different known dependencies for glycolysis or OXPHOS suggests that more glycolytic cell lines such as MD-MB231 have higher levels of eIF5A^{AcK47} (Zare *et al.*, 2021). Although the understanding of how acetylation of eIF5A is precisely regulated and even more of what role acetylated eIF5A plays in the cell, is still in its infancy, our data suggest that a strong acetylation state of eIF5A is associated with cells performing glycolysis while requiring more OXPHOS correlates with lower acetylation levels of eIF5A.

In terms of genetically identified positive regulators for hypusination, it was interesting to find also *Xpo4*, the nuclear shuttle protein for eIF5A (Aksu *et al.*, 2016). This proves genetically that absence of *Xpo4* leads to lower levels of hypusinated eIF5A in the cell, potentially by failing to export it out of the nucleus and thereby making it less available for hypusination in the cytosol.

It is well known that there is a discrepancy between RNA transcripts and actual protein levels within the cell, especially for proteins that perform basic cellular functions (Jovanovic *et al.*, 2015). Traditionally, RNA regulation is better studied because nucleic acid sequencing is easier to scale and handle than for example proteomics. Nevertheless, the actual functional unit in the cell is the protein. Our work tries to explore a corner of this underexplored area of translational regulation, by studying the translational modulations triggered by the translational elongation factor eIF5A. Our combination of genetics, expression proteomics, and ribosome profiling allowed us to generate a dataset that gives a global idea of how hypusination is regulated and how it is implicated in protein production. The dataset will be useful for finding new pathways that can be targeted to treat hypusine-related disease summarized in Chapter 1.3.7. In addition, our study will offer a useful resource for the community to check if certain proteins are potentially dependent on eIF5A for their expression. We think this is important because due to its high abundance in the cell eIF5A has been linked over the last decades to a whole array of different molecular processes. Many of these initial observations around *eIF5A* were made before the discovery that *eIF5A* acts as a translational elongation factor, precisely as crucial helper for the translation of certain amino acid combinations. It is therefore not unthinkable that many of these early ascribed roles for *eIF5A* could be secondary to its role in protein translation. In the light that eIF5A is nowadays more understood as an essential part of translational elongation, it also might make more sense to look in addition at global effects triggered by the absence of hypusination. Therefore, we think that our unbiased genetic exploration, focused on levels of hypusinated eIF5A in the cell, combined with monitoring effects of hypusination on protein translation can help to dissect the primary and secondary effects of this important pathway. Additionally, it might help to identify new pathways and targets that crosstalk with the hypusine axis and will thereby aid

the molecular characterization of this highly conserved pathway. Finally, we identified an interesting crosstalk of hypusination and respiration that we will hopefully fully mechanistically understand with future studies and that could become a powerful new avenue for modulating respiration in the cell. Furthermore, progress in research is often hindered by the lack of tools that allow us to measure specific proteins or their modifications. In our work, we generated and validated endogenously tagged haploid cell lines for mitochondrial proteins for which previously no reliable tools for quantification of their protein levels were available. We believe that these cell lines and the information of the position within the protein that can be endogenously tagged without perturbing the natural protein function will allow us to finally investigate these proteins in the future in greater detail.

Due to the myriad of functions associated with *eIF5A*, reports on its role can sometimes seem contradictory. This could stem from the fact that eIF5A is a very conserved and a highly abundant protein that could have acquired tissue-specific roles. It is therefore important to note that our studies were made mostly in the two cell lines THP-1 and HAP1. Doing similar systematic explorations in different cellular systems such as neuronal cell lines, a cell type that seems to be especially affected in the absence of hypusine, will be highly interesting (Kar *et al.*, 2021; Liang *et al.*, 2021). In addition, the way and method of perturbing eIF5A can have different effects on the cell. In our study, we mostly used the DHPS inhibitor GC7, which leads to inhibition of the first step of hypusination, and as a side effect increases drastically the amount of acetylated eIF5A in the cell. As already mentioned above it is currently only poorly understood what role acetylated eIF5A has in the cell. Alternative methods to inactivate *eIF5A* would be to knock out *DHPS*, which we used in one of our studies above. The knock-out of *DHPS* led to similar effects, but requires more time and therefore doesn't allow us to study acute effects of inhibition of eIF5A. Additionally, studies found that when eIF5A was overexpressed it led to induction of apoptosis (Sun *et al.*, 2010; Tan *et al.*, 2010). This illustrates, that unmodified eIF5A has an additional effect on the cell and it could therefore be interesting in the future to also perform experiments where *eIF5A* is knocked down altogether. Furthermore, the often envisioned "one gene, one protein" theory does not always hold true. Especially, highly abundant and very conserved proteins like eIF5A could potentially be so-called moonlight proteins that have multiple functions in different locations in the cell (Jeffery, 1999). In our study, we made use of expression proteomics, a technique that routinely quantified >8,000 proteins per sample. While these are impressive numbers it is still hard to quantify very low abundant proteins with standard protocols, such as some transcription factors, that could however be very interesting targets of hypusination due to their amplifying power within cells. With ribosome profiling, it should be easier to look at an even larger number of targets, but it suffers from similar limitations as expression proteomics. The technique requires total RNA sequencing, which makes the analysis of low-expressed genes again expensive.

Currently, we can therefore not analyze very low expressed genes in our dataset, a situation that we are currently trying to improve by increasing sequencing depth even further. Lastly, we observed an interesting regulation of acetylation of eIF5A in our study. However, we are clearly only scratching the surface of its regulation and it would be therefore needed to perform a similar systematic study for acetylation of eIF5A as we performed here for hypusine, which requires the development of more specific binders and inhibitors for this pathway first.

4.3 Conclusions and Recommendations for Future

Functional genomics offers nowadays a powerful toolbox to decipher the role of genes in the context of different cellular settings. The ease of sharing genome-wide CRISPR libraries and the associated good economics of genome-wide genetic CRISPR screens democratized functional genomics and allowed many new labs to functionalize their cellular readouts in genome-wide campaigns for dissecting molecular processes. It is clear, that we are only at the beginning of this trend and the development of new readouts or the use of single-cell omics with gradually decreasing costs, will lead in the future to many more variants of CRISPR screens. In addition, the design of progressively more integrative systematic studies that investigate several aspects of gene expression by making use of omics techniques such as proteomics, transcriptomics, ribosome profiling, and metabolomics will help to accelerate the annotation of gene functions.

The hypusine pathway and eIF5A are part of the translational control in a cell, a field that is still in its infancy with plenty of opportunities for discoveries in the future. Basic questions, like how the cell prioritizes the translation of certain mRNAs, are still largely unanswered. For the hypusine axis specifically, it will be interesting to understand how the eIF5A-DHPS-DOHH pathway cross-talks with the metabolic state of a cell and in response reprograms the cellular translatome. Current inhibitors for hypusination such as GC7 could already offer innovative ways to prevent hypoxic-ischemia induced damage, as showcased in rat and pig kidney transplantation models (Melis *et al.*, 2017). A key challenge here is that *eIF5A* exists in different isoforms and can be modified by hypusination, acetylation, and phosphorylation (Park *et al.*, 1981; Kang *et al.*, 1993; Klier *et al.*, 1995). To dissect all the individual roles of the hypusine pathway it will therefore be necessary to develop specific inhibitors for each individual modification and isoform or the respective enzyme and have specific binders that allow to measure and study the different modification states of eIF5A. These new tools will empower specific campaigns similar to the work presented in this thesis and allow to separate effects caused by individual isoforms and modification states of eIF5A. In addition, such specific inhibitors will also be therapeutically very interesting. This is because for example, the second isoform of *eIF5A* (*eIF5A-2*) is expressed in many different types of tumors, which could make it an interesting

target in cancer cell therapy (Caraglia *et al.*, 2013; Mathews and Hershey, 2015). Additionally, the involvement of hypusine in a large variety of diseases, as described earlier, but also its metabolic role, makes the hypusine axis an attractive target for drug development programs that will be aided in the future by the recent release of high-resolution structures for DHPS (Liao *et al.*, 1998; Umland *et al.*, 2004; Wątor *et al.*, 2023), DOHH (Han *et al.*, 2015), and eIF5A (Schmidt *et al.*, 2016). It would also be useful to address another interesting future question: deciphering the role of eIF5A in the nucleus, which positively correlates with $eIF5A^{AcK47}$. Due to the nucleic acid binding properties of eIF5A, it is frequently speculated that eIF5A could serve as a mechanism that shuttles RNA out of the nucleus and some studies suggest that this is indeed the case (Liu *et al.*, 1997; Xu and Chen, 2001; Xu *et al.*, 2004; Balukoff *et al.*, 2020). The nuclear transport receptor Xpo4, that is responsible for eIF5A export, acts additionally like a chaperone that shields most conserved positively charged RNA interacting residues of eIF5A (Aksu *et al.*, 2016). Combined with the fact that eIF5A enters the nucleus via passive diffusion, this speaks against a prominent role of eIF5A as an RNA shuttle system (Lipowsky *et al.*, 2000). Rather it would mean that the cell evolved a mechanism to export eIF5A from the nucleus in order to keep it clean and to prevent detrimental interactions in the nucleus. On the other hand, acetylated eIF5A binds around 35 times weaker to Xpo4 and remains as a result much longer in the nucleus (Lipowsky *et al.*, 2000). Therefore, the acetylated form of eIF5A would have more time to bind RNA. Additionally, it has been found that the absence of Xpo4 leads to an accumulation of eIF5A in the nucleoli, the location where ribosomes are assembled which suggests that nuclear eIF5A could interfere with ribosome biogenesis and thereby general protein production. In summary, it will be interesting to see in the future what the nuclear role of eIF5A is. Lastly, the high importance of *eIF5A* comes with the consequence that disruption of the hypusine-pathway leads to a whole array of secondary and collateral effects in the cell. In the future it will be key to perform even earlier and tighter time-course experiments that will allow us to identify the pathways that are most upstream and stand under the direct regulation of the hypusine axis.

5 Material and Methods

Methods and experimental procedures used in the presented manuscript have been extensively described in the respective manuscripts. The remaining methods are presented in this chapter below.

Cell lines

THP-1, HEK293T, and RPE-1 cells were purchased from ATCC. HAP1 cells were obtained from Horizon Genomics (Vienna, Austria). THP-1, U937, MCF7, DU145, HCT116, and K562 were grown in RPMI1640. HEK293T, Huh7, HeLa, and A549 were maintained in Dulbecco's modified Eagle's medium (DMEM). HAP1 and HL-60 were grown in Iscove's Modified Dulbecco's Medium (IMDM). RPE-1 were maintained in DMEM:F12 (1:1) medium. All media were supplemented with 10% fetal bovine serum (FBS) and antibiotics (100 U/mL penicillin, 100 mg/mL streptomycin), all either from Gibco or Sigma and FBS from biowest. Cell lines were grown at 37 °C in 5% CO_2. Transient transfection of HEK293T was done using PEI (Sigma). Viral particles were produced by transient transfection of HEK293T cells with the library and packaging plasmids pMD2.G (Addgene no. 12259) as well as psPAX2 (Addgene no. 12260) using PEI (Sigma).

Cells grown in alternative carbon sources or with extra glucose were maintained in media supplemented with either D-(+)-Glucose monohydrate (16301, Sigma) or D-(+)-Galactose (G5388, Sigma).

Lentiviral transduction

Stable HAP1 expression cell lines were generated by lentiviral transduction. Therefore, HEK293T were transfected with the packaging plasmids pMD2.G (Addgene no. 12259) and psPAX2 (Addgene no. 12260) as well as with the individual lentiviral vector, using PEI (Sigma). 16 hours post-transfection the medium was exchanged to IMDM supplemented with 10% FBS. Virus supernatant was collected 72 hours after transfection, filtered through 0.45 µm polyethersulfone filters (GE Healthcare), supplemented with 8 µg/mL protamine sulfate, and added directly to the respective cells. 24 hours after infection, the medium was exchanged, and 48 hours after infection cells were checked for expression of the respective insert.

ATF4 reporter cell lines

ATF4 reporter cell lines were generated as described in a previous study (Guo *et al.*, 2020). Reporter cells were generated in the human cancer cell line HAP1 by first stably integrating a translational reporter construct, which reports on *ATF4* induction via expression of the fluorescent

protein mApple (pXG237, Addgene no. 141281). Second a *EGFP* expressing construct (pXG260, Addgene no. 141282) was stable introduced to the same cell pool, serving as a general protein expression control in the cell. Both constructs were delivered via lentivirus. Next, clonal cell lines were isolated and validated by treating them with 1.25 ng/mL of the control drug oligomycin A (495455, EMD Millipore) and measuring their mApple (ATF4-mApple) and GFP levels on an LSR Fortessa II cytometer controlled with FACSDiva (BD), analyzed, and illustrated with FlowJo software (v.10) (Figure 24c).

For GC7, the reporter cells were treated with increasing doses (10-50 µM) of GC7 (259545, EMD Millipore) and measured with the same LSR Fortessa II set-up as described above.

Cell lysis and immunoblotting

Cell pellets were processed and analyzed via immunoblotting as described in the methods part of our paper attached in chapter 3.4.

Antibodies list

The primary antibodies used for western blot were: Hypusine (generation see chapter 3.4 (Zhai *et al.*, 2016; Essletzbichler *et al.*, 2023), 1:20,000), eIF5A^{AcK47} (P01727, Boster Bio, 1:500), eIF5A (611976, BD Biosciences, 1:20,000), DHPS/DHS (ab190266, abcam, 1:1,000), DOHH (376929, B-12, SantaCruz, 1:500), HA (3724, C29F4, 1:500), for ATF4/ATF-4 (11815, D4B8, Cell Signaling, 1:500), GAPDH (47724, 0411, SantaCruz, 1:2,000).

The secondary antibodies used were: anti-rabbit HRP (111-035-144, Jackson ImmunoResearch, dilution 1:10,000), anti-mouse HRP (115-035-003, Jackson ImmunoResearch, dilution 1:10,000).

For directly coupling hypusine antibody to a 594 nm fluorophore our hypusine antibody was dilute to 1 mg/mL in PBS and subsequently labeled using the Mix-n-Stain CF 594 antibody labeling kit (MX594S20, Sigma).

Drugs

The small molecules used for the study were: GC7 (259545, EMD Millipore), chloramphenicol (3886, Roth), oligomycin A (495455, EMD Millipore), Torin-1 (4247, Tocris), and Mitoblock-6 (505759, EMD Millipore)

Ribosome profiling

6 million THP1 WT cells each were seeded in 10 cm plates and treated with 30 µM GC7 (259545, EMD Millipore) or with DMSO as a control in triplicates and harvested after 24 hours as indicated in

Figure 23a. For harvesting cells were pelleted at 400 g for minutes at 4 °C and afterwards supernatant was removed and pellets placed on ice. Next, cells were rinsed with 10 mL of ice-cold PBS, either supplemented with 100 µL of cycloheximide (Sigma) at 10 mg/mL or without cycloheximide, and then pelleted at 400 g for 2 min at 4 °C and then supernatant was aspirated. Next, 800 µL of ice-cold polysome lysis buffer (20 mM Tris (pH 7.4) (Sigma), 250 mM NaCl (Sigma), 15 mM $MgCl_2$ (EMSURE), 1000x protease inhibitor (P8340, Sigma), RNAsin (N2515, Promega), TurboDNAse (AM2238, Invitrogen)), supplemented either with or without cycloheximide at the same final concentration as above was added to the samples and they were mixed by pipetting the sample up and down and the whole time kept on ice. To homogenize, the lysate was then passed five time through a 23G needle (Braun). Lysates were then clarified by centrifugation at 20,000 g for 10 min at 4 °C. Next, the supernatants were transferred into fresh tubes and 10% of the sample was stored in a separate tube for subsequent RNA isolation for RNA-Seq library construction (see below). Lastly, all samples were snap frozen in liquid nitrogen and then shipped on dry ice to our collaboration lab in Columbia.

RNA-Seq Library Construction

Total RNA was isolated from cell lysates using a RNeasy kit (74104, Qiagen), and ribosomal RNA was depleted using the rRNA removal kit (E7405X, NEB), following the manufacturer's instructions. Strand-specific RNASeq libraries were prepared using the NEBNext® Ultra Directional RNA Library Prep Kit (E7760L, NEB). Each sample condition had three biological replicates. RNA-Seq libraries were quantified using a Qubit fluorometer (ThermoFisher), and the library size was measured using an Agilent Bioanalyzer. Sequencing was performed on an Illumina NextSeq 500/550 desktop sequencer with a read length of 75 bases. Approximately 25 million demultiplexed, pass-filtered, single-end reads were obtained for each sample.

Ribosome-Profiling Study

A ligation-free library preparation approach was employed (Hornstein *et al.*, 2016; Das Sharma *et al.*, 2019) to generate RiboSeq libraries. In summary, cell lysates were subjected to RNAse I digestion. Monosomes were collected using a 50% sucrose cushion supplemented with Cycloheximide (C1988, Sigma) and subsequently purified using Trizol (Sigma). Footprints were size-selected using gel electrophoresis as described in (Hornstein *et al.*, 2016; Das Sharma *et al.*, 2019) and dephosphorylation of the size-selected footprints were performed using T4 Polynucleotide kinase (NEB). The RNA footprints were polyadenylated and then subjected to reverse transcription using an RT enzyme with template switching activity using SMARTer small RNA-Seq Library Preparation Kit (635029, Takara). During this process, a low complexity sequence was added to the 3' end of the cDNA through the terminal transferase activity of the template switching enzyme, along with a second

universal sequence adapter that hybridizes to the added tail. This resulted in the RT-switched templates, with the second adapter copied onto the 3' end of the cDNA. The libraries were further depleted of rRNA (Hornstein *et al.*, 2016; Das Sharma *et al.*, 2019). Depleted libraries were amplified, and full-length Illumina adapters are added via PCR. Sequencing was performed on an Illumina NextSeq 500/550 desktop sequencer with a read length of 50 bases. Approximately 60 million demultiplexed, pass-filtered, single-end reads were obtained for each sample.

Ribosome-Profiling Study Analysis

Bioinformatics analysis was carried out following the protocol previously described (Das Sharma *et al.*, 2019). In short, RiboSeq libraries underwent processing, which involved removal of the first 4 and last 10 bases of each sequence read, using the following command in FASTX-Toolkit (Hannon 2010): fastx_trimmer -f 4 -l 40 -Q33 -i INFILE -o OUTLFILE. The subsequent step involved trimming the residual poly(A) sequences from the 3' end and considering only reads with a length of more than 25 nucleotides. Subsequently, ribosomal RNA depletion was performed by aligning the libraries to an rRNA reference sequence derived from hg38, utilizing bowtie2, and allowing for a single alignment error. Unaligned reads were then aligned to the hg38 human genome assembly using STAR (Dobin *et al.*, 2013). Alignments to exons and coding sequences (CDS) were quantified using the featureCounts program (Liao *et al.*, 2014) from the subread suite. This approach yielded aligned count files for uniquely aligned Exon and CDS reads. On average, individual RiboSeq samples contained approximately 6 to 10 million unique reads.

Alignment files in BAM format were processed using samtools (Danecek *et al.*, 2021). We filtered reads of lengths ranging from 27 to 31 nucleotides. Chromosome coordinates of reads were used to assign codons and amino acids previously filtered from coding sequences from the human reference genome, hg38. Reads were counted at each codon position, along coding sequences, and a pause score (P) per codon (i), was calculated as normalized count relative to the total number of reads per gene, or with C_i the total counts at codon *i* and *L*, the length of the gene in number of codons. A mean, standard deviation, and confidence intervals for the pause score were calculated from the replicates of each condition. Significance of a pause score was estimated by comparing conditions of treatment versus non-treatment. Pauses were defined at regions with a difference between treatment versus control conditions larger than the 95% confidence interval. For ease of visualization, we plot pause scores using a window average of 5 codons. To better understand the origins of pauses, we calculated sequence hydrophobicity of amino acids (Kyte and Doolittle, 1982), a classification of amino acid polarity (Nelson and Cox, 2012), codon usage as the codon adaption index (Sharp and Li, 1987); protein and mRNA secondary structure. Protein secondary structures were calculated for each

human gene using their respective AlphaFold model (Jumper *et al.*, 2021), using the DSSP algorithm (Kabsch and Sander, 1983). Similarly, mRNA secondary structures were estimated using ViennaRNA software (Hofacker, 2004). Stability of secondary structure motifs were calculated for segments of 100 nucleotides long starting at each position along the sequence.

Gene set enrichment analysis

Gene Ontology (GO) enrichment analysis for "Biological process", "Cellular component", and "Molecular function" GO terms was performed via GSEA (Subramanian *et al.*, 2005) and Enrichr (Kuleshov *et al.*, 2016) using the Python package GSEApy (version 0.10.8, https://github.com/zqfang/GSEApy). Gene sets are described in the corresponding figure legends.

Generation of haploid intron tagged cell lines

Intron tagged cell line generation was conducted as previously described (Reicher *et al.*, 2020). Oligos, targeting the intron of the gene of choice, containing BsmBI compatible overhangs were annealed and cloned into pX330 (Addgene no. 42230) using Golden Gate assembly.

Cloned oligonucleotides were as follows (5' to 3' orientation):

sgATP5MG	caccgTAGATAGGATGGCTATAGGA	from vpCells (CeMM)
sgNDUFAB1	caccgTTGAAGGAATAAGCCCCAGG	from vpCells (CeMM)
sgOXA1L	caccgTTATCGCAGACCCACATCGG	from vpCells (CeMM)

For intron tagged cell line generation that was conducted separately for each construct, 5 million haploid HAP1 cells each were seeded on 10 cm cell-culture coated plates. Cells were then transfected with the respective CRISPR sgRNA specifically targeting the intron of choice cloned in pX330 as described above, a vector expressing Cas9 in combination with a sgRNA that excises GFP (Intron-Tagging-pX330-Cas9-Blast, Addgene no. 159741), and a GFP expressing vector (Intron-Tagging-EGFP-Donor, Addgene no. 159740) using PEI (Sigma). 24 hours post transfection media was replaced to IMDM supplemented with 10% FBS and cells continuously expanded. 4 days later, cells were sorted on a Sony SH800S cell sorter and enriched for GFP expressing cells and afterwards grown in culture. 7 days post sorting clonal cell lines were derived by limiting dilutions. Clonal cell lines were then expanded and validated for haploidy using Hoechst 33342 (Thermo Fisher Scientific) staining as well as validated for successful integration of GFP via measuring GFP signal on a LSR Fortessa II cytometer controlled with FACSDiva (BD), analyzed, and illustrated with FlowJo software (v.10) as illustrated in Figure 27a-b. Additionally, the localization of the tagged proteins was assessed using an Opera Phenix

High-Content Screening System (Perkin Elmer), looking for localization of GFP signal as exemplified in Figure 27c.

Generation of shRNA expressing cell lines

CTU2 shRNA vectors were generated following the principle of a previous study (Sigl *et al.*, 2014). shRNA sequences containing the 5'-, loop, and 3'- sequence were cloned into pENTR-THT (Addgene no. 55790), via restriction site cloning. Then the sequences were cloned from pENTR-THT via gateway cloning into the all-in-one inducible lentiviral shRNA pGLTR-X-PURO expression plasmid (Addgene no. 58246). Lentivirus production and stable cell line production in HAP1 was conducted as described above.

Cloned sequences were as follows (5', loop, and 3' sequence):

	5' end	sense	loop sequence	antisense	3' end incl HindIII
CTU2.2	GATCCCC	GTTCCTTCTGTCTTCACACCA	TTCAAGAGA	TGGTGTGAAGACAGAAGGAAC	TTTTTGGAAAAGCTT
CTU2.3	GATCCCC	CTATCAAGCTCATGACCAA	TTCAAGAGA	TTGGTCATGAGCTTGATAG	TTTTTGGAAAAGCTT

Hypusine antibody staining for FACS

HAP1 cells were dissociated by trypsinization, resuspended in Phosphate buffered saline (PBS) (Sigma) and pelleted at 500g for 3 minutes. Cells were then resuspended and fixed in BD Fix buffer I (BD) at 37°C for 10 minutes. Next, cells were pelleted at 1300g for 5 minutes and washed once with PBS. Cells were next permeabilized with BD Perm Buffer III (BD) on ice for 30 minutes and afterwards pelleted at 500g for 3 minutes. Next, they were resuspended in blocking buffer (PBS supplemented with 10% fetal bovine serum (FBS) (biowest)) and incubated for 20 minutes at room temperature. Cells were then pelleted at 1300g for 5 minutes and afterwards incubated in primary hypusine antibody (described above) diluted 1:500 in blocking buffer for 1 hour at room temperature under light agitation. Next, cells were pelleted at 1300g and washed twice in blocking buffer. Cells stained with primary antibody were then stained with an Alexa Fluor-coupled fluorescently labeled goat anti-rabbit secondary antibody (Thermo Fisher Scientific) diluted 1:100 in blocking buffer for 1 hour at room temperature under permanent rotation in the dark. Cells were then pelleted at 1300g and washed twice with blocking buffer. Lastly, cells were resuspended in blocking buffer and filtered for subsequent FACS processing. For cell sorting cell were processed with a FACSAria Fusion cell sorter (BD Biosciences), using DAPI to gate for haploid G1 cells. For analysis cells were measured on a LSR Fortessa II cytometer controlled with FACSDiva (BD), analyzed, and illustrated with FlowJo software (v.10).

For staining with the conjugated hypusine antibody, described above, the staining with the secondary antibody was skipped and the remaining steps remained identical.

Hypusine Abundance Screen

Haploid genetic screens were conducted as previously reported (Brockmann *et al.*, 2017). Viral particles were produced by transient transfection of HEK293T cells with GT-GFP, VSVG, ΔVPR, and pAdvantage. Virus supernatant was collected 48 hours post transfection, filtered through 0.40 µm filter and concentrated with Amicon filters (Merck) following manufacturer's instructions. Fresh media was re-applied to the transfected HEK293T cells and viral harvest repeated. The concentrated virus was immediately added to HAP1 cells, supplemented with 8 µg/mL protamine sulfate. 24 hours after infection, the media was exchanged, and the cells were cultivated for 8-10 days, as described above, before use in the genetic screen.

To perform haploid genetic screens, the infected HAP1 cells were grown in T175 flasks to a total number of 3 x 10^9 cells. Cells were then detached by trypsinization and stained with primary hypusine antibody, fluorescently labeled secondary antibody, and with DAPI, as described in the methods section above ("Hypusine antibody staining for FACS"). Cells were passed through a 40 µm cell strainer and then sorted on a FACSAria Fusion cell sorter (BD Biosciences). DAPI was used to gate for haploid G1 cells, and 10 million cells were collected for the 5% of cells with the highest and lowest fluorescent signal for hypusine. Genomic DNA was isolated, NGS sequencing libraries prepared and sequencing data analyzed as described before (Brockmann *et al.*, 2017). NGS reads were aligned to the GRCh38 reference genome, allowing for one mismatch. The sense insertions in the high and low populations were compared using a two-sided Fisher's exact test to calculate the significant differences (FDR corrected $p<0.05$). For analysis, data was processed with GraphPad Prism software and Adobe Illustrator to generate fishtail plots.

Expression Proteomics

For each replicate 13 million THP1 WT cells were seeded in 15 cm plates and treated with 30 µM GC7 (259545, EMD Millipore) or as a negative control with DMSO. All conditions were done in triplicates. Cells were harvested after (24-60 hours) as indicated in Figure 22a. For harvesting, cells were washed once with ice cold PBS and afterwards snap frozen in liquid nitrogen. For lysis cell pellets were thawed on ice and resuspended in freshly prepared lysis buffer containing 50 mM HEPES (pH 8.0) (Merck), 2 % SDS, 1 mM PMSF, and protease inhibitor cocktail (Sigma). Samples were incubated at room temperature (RT) for 20 min, then heated to 99 °C for 5 min and then cooled back to RT. Next, the DNA in the samples was sheared by sonication using a Covaris S2 high performance ultrasonicator.

Lysates were then cleared at 16,000 g for 10 min. The supernatants were then transferred to fresh Eppendorf tubes and protein concentration was quantified using the BCA Protein Assay kit (Pierce Biotechnology).

After checking that the pH of the lysates was in a range of pH 6-8 proteins were reduced by addition of DTT (Sigma) at a final concentration of 10 mM. Samples were then vortexed and afterwards incubated for 1 hour at 56°C in an incubator. After cooling the samples back to RT, proteins were then alkylated by addition of iodoacetamide (Sigma) to a final concentration of around 55 mM, briefly vortexed and incubated at RT for 30 min. Next, Sera-Mag beads (#45152105050250, GE Healthcare and #65152105050250, GE Healthcare) were mixed in a ratio of 1:1, placed on a magnetic rack, to remove the supernatant. Beads were washed twice with H_2O with short magnetization in-between each washing step to separate beads from the washing solution. After the last washing steps, the clarified lysates were added to the beads, the samples were then vortexed and incubated for 5 min. To precipitate proteins onto the beads, acetonitrile (Fisher Scientific) was added to the samples, reaching a final concentration of at least 70% (v/v). Samples were cautiously mixed with precipitation buffer by pipetting. Samples were then incubated until beads settled down at the bottom of the tube and then beads were immobilized on a magnetic rack for 2 min. The separated supernatants were discarded. Beads were then rinsed twice with 70% ethanol (Merck) in water, incubated for 30 seconds and then beads were immobilized on a magnetic rack to discard the supernatant. Then beads were rinsed with acetonitrile, incubated for 30 seconds, and again immobilized on a magnetic rack to discard the supernatant. Now, the cleaned protein was eluted from the beads by addition of NH_4HCO_3 at a final concentration of 50 mM, incubated for several minutes and then vortexed. After checking the pH to be around pH 8, the protein was next digested by addition of trypsin, shaking the samples at 600 rpm for 1 min and incubating them for 14-18 hours at 37 °C. To clean up the samples, they were next acidified with 30% trifluoroacetic acid, vortexed and their pH confirmed to be pH ≤ 2. Samples were then centrifuged and immobilized on a magnetic rack. All digested samples were then desalted using C18 solid phase extraction (SPE) spin columns (The Nest Group). Next the concentrations of the peptides were quantified using the CPA assay (#23275, Thermo).

The desalted peptides were then labeled with the TMT 16plex reagents according to the manufacturer (Pierce, Rockford, IL; LOT: WA314599). The labeling reaction was next quenched, samples containing the labeled peptide were pooled and the organic solvent removed in a vacuum concentrator. Labeled peptides were cleaned again via C18 SPE (see above).

The labeled peptides were then buffered in 20 mM ammonium formiate buffer (pH 10) and separated by reverse phase liquid chromatography at pH 10 as described (Gilar *et al.*, 2005). In short,

the peptides were separated into 96 time-based fractions on a Phenomenex C18 RP column (150 x 2.0 mm Gemini-NX 3 µm C18 110Å, Phenomenex, Torrance, Ca, USA) with an Agilent 1200 series HPLC system fitted with a binary pump delivering solvent at 100 µL/min. Acidified fractions were then consolidated into 36 fractions following a concatenated strategy described (Wang *et al.*, 2011). Solvent was then removed using a vacuum concentrator and peptides were then reconstituted in 5% formic acid for subsequent LC-MS/MS analysis and kept at -80°C until further analysis.

For separation of peptides a reverse-phase chromatography using a nano-flow HPLC (Dionex Ultimate 3000, Thermo Fisher Scientific) was employed. Peptides were first loaded onto a trap column (Pepmap 100 5 µm, 5 × 0.3 mm, ThermoFisher Scientific) at a flow rate of 10 µL/min using 0.1% TFA as loading buffer. Then, the trap column was switched in-line with the analytical column (50 cm, 75 µm inner diameter analytical column packed in house with ReproSil-Pur 120 C18-AQ, 3µm). Mobile-phase A consisted of 0.4% formic acid in water and mobile-phase B of 0.4% formic acid in a mix of 90% acetonitrile in water. The flow rate was set to 300 nL/min and a 120 min gradient was used (6 to 30% solvent B within 82 min, 30 to 65% solvent B within 8 min and, 65 to 100% solvent B within 1 min, 100% solvent B for 6 min before equilibrating at 6% solvent B for 18 min prior to next injection). Eluted peptides were ionized in a positive mode (1.8 Kv) using a Nanospray Flex™ Ion Source.

Mass spectrometry was performed on a Orbitrap Fusion Lumos mass spectrometer (ThermoFisher Scientific). Tandem Mass spectrometry (MS/MS) analysis was performed in a data-dependent acquisition mode. Full MS scans were acquired across a precursor mass range of 400-1600 m/z at a resolution of 120,000 (at 445.120024 m/z). Automatic gain control (AGC) was set to a target of 4e6 with a maximum injection time of 50 ms. MS2 fragment spectra were acquired in the Orbitrap at a resolution of 50,000, a fixed first mass of 100 m/z, a maximum injection time of 86 ms and an AGC of 1e6.

To achieve maximum proteome coverage, classical tandem MS was employed (TMT reporter ion intensities extracted from MS2-scans) instead of the available synchronous precursor selection (SPS)-MS3 approach. While the latter provides on average better TMT ratio accuracies, it suffers from prolonged duty cycles and reduced identification rates. An extended fractionation scheme was applied (36 fractions, see above). The monoisotopic peak determination was set to peptides with inclusion of charge states between 2 and 5. The intensity threshold for MS2 selection was set to 5×10^4. Higher energy collision induced dissociation (HCD) was applied with a normalized collision energy (NCE) of 34%. Dynamic exclusion for selected ions was 60 s.

Expression Proteomics Data Analysis

Raw files were processed using ProteomeDiscoverer (2.4). The peptide identification search was performed against the human swissprot database containing isoforms (Version 052020, 42‘289 protein sequences) supplemented with common lab contaminants (298 protein sequences). Decoys were generated by reversing protein sequences. The spectrum search was performed with Sequest HT with enabled Spectrum Selector (precursor mass of 350 Da to 5000 Da and a minimum peak count of 1), against fully tryptic peptides with up to two missed cleavages. Further the peptide length was set to a minimum of 6 aminoacids and 144 maximum length. The search was performed with a 10 ppm precursor mass tolerance and a 0.025 Da fragment mass tolerance respectively. As variable modifications oxidation of Methionine residues, deamidation of Asparagine and Glutamine residues, acetylation of the N-terminus and N-terminal loss of initial Methionine group or combinations of the latter were set. Up to 3 variable modifications were allowed per peptide. As static modification carbamidomethylation on Cysteine residues and the TMTpro-reporter modification at the N-terminus and Lysine residues was set. The evaluation of the search was performed with Percolator with the concatenated mode enabled (only the best scoring PSM target or decoy is used for the evaluation). The FDR was controlled on PSM, peptide and protein level at 1%. For protein grouping a strict parsimony principle was applied, and all protein groups were excluded which are not strictly necessary to explain the identified peptides. The final output was filtered to contain only high-confidence identification and all contaminants were filtered.

The peptide level intensities for all PeptideGroups were exported from ProteomeDiscoverer and further analyzed in R (R-4.3.1). To remove noisy signal, the Coefficient of Variation (CV) across replicates per time point (see Formula 1) per peptide was calculated.

$$Forumla\ 1: CV\ = \frac{\sigma}{\mu}$$

If the CV of a peptide was for more than two timepoints greater than or equal to 0.3 across time points replicates, the peptide was removed from the dataset. Peptide intensities of the entire dataset were log2 transformed and median normalized. Missing peptides were imputed by taking 80% of the lowest measured value for each sample. Protein intensities were inferred by summing the peptides per protein group. The normalized and imputed protein abundances served as input for the Analysis of Variance (ANOVA) test. Obtained p-values were corrected for multiple comparisons using Benjamini-Hochberg. A maximal difference of +0.5 and -0.5 log2 from the overall mean across all conditions and an adjusted p-value of 0.01 were set as thresholds to identify significantly changed proteins across the timecourse experiment. Fuzzy clustering was performed with the Mfuzz R-package (Kumar and E

Futschik, 2007) for the significantly regulated proteins. First the 193 significantly variable proteins were standardized (average expression of protein to zero with a standard deviation of one). For the fuzzy c-means clustering first the number of clusters was estimated employing repeated soft clustering for a range of cluster numbers to identify the minimum centroid distance. The minimum cluster membership value threshold for a protein was set to 0.5. Fuzzy clustering identified 3 clusters for 184 protein groups, 9 proteins were not clustered.

6 References

Abudayyeh OO, Gootenberg JS, Essletzbichler P, Han S, Joung J, Belanto JJ, et al. RNA targeting with CRISPR-Cas13. Nature 2017; 550: 280–4.

Abudayyeh OO, Gootenberg JS, Konermann S, Joung J, Slaymaker IM, Cox DBT, et al. C2c2 is a single-component programmable RNA-guided RNA-targeting CRISPR effector. Science 2016; 353: aaf5573.

Acevedo-Arozena A, Wells S, Potter P, Kelly M, Cox RD, Brown SDM. ENU mutagenesis, a way forward to understand gene function. Annu Rev Genomics Hum Genet 2008; 9: 49–69.

Adams R, Cristol SJ, Anderson AA, Albert AA. The structure of leucenol. I. J Am Chem Soc 1945; 67: 89–92.

Adli M. The CRISPR tool kit for genome editing and beyond. Nat Commun 2018; 9: 1911.

Aebersold R, Mann M. Mass-spectrometric exploration of proteome structure and function. Nature 2016; 537: 347–55.

Aksu M, Trakhanov S, Görlich D. Structure of the exportin Xpo4 in complex with RanGTP and the hypusine-containing translation factor eIF5A. Nat Commun 2016; 7: 11952.

Alberts B. The cell as a collection of protein machines: preparing the next generation of molecular biologists. Cell 1998; 92: 291–4.

de Almeida M, Hinterndorfer M, Brunner H, Grishkovskaya I, Singh K, Schleiffer A, et al. AKIRIN2 controls the nuclear import of proteasomes in vertebrates. Nature 2021; 599: 491–6.

Alsaleh G, Panse I, Swadling L, Zhang H, Richter FC, Meyer A, et al. Autophagy in T cells from aged donors is maintained by spermidine and correlates with function and vaccine responses. eLife 2020; 9

Anderson-Baucum E, Piñeros AR, Kulkarni A, Webb-Robertson B-J, Maier B, Anderson RM, et al. Deoxyhypusine synthase promotes a pro-inflammatory macrophage phenotype. Cell Metab 2021; 33: 1883-1893.e7.

Andrade MA, Petosa C, O'Donoghue SI, Müller CW, Bork P. Comparison of ARM and HEAT protein repeats. J Mol Biol 2001; 309: 1–18.

Andrus L, Szabo P, Grady RW, Hanauske AR, Huima-Byron T, Slowinska B, et al. Antiretroviral effects of deoxyhypusyl hydroxylase inhibitors: a hypusine-dependent host cell mechanism for replication of human immunodeficiency virus type 1 (HIV-1). Biochem Pharmacol 1998; 55: 1807–18.

Ardrey RE. Liquid Chromatography - Mass Spectrometry: An Introduction. 1st ed. New York: Wiley; 2003

Artyomov MN, Sergushichev A, Schilling JD. Integrating immunometabolism and macrophage diversity. Semin Immunol 2016; 28: 417–24.

Aviner R, Lee T-T, Masto VB, Gestaut D, Li KH, Andino R, et al. Ribotoxic collisions on CAG expansions disrupt proteostasis and stress responses in Huntington's Disease. BioRxiv 2022

Baltz AG, Munschauer M, Schwanhäusser B, Vasile A, Murakawa Y, Schueler M, et al. The mRNA-bound proteome and its global occupancy profile on protein-coding transcripts. Mol Cell 2012; 46: 674–90.

Balukoff NC, Ho JJD, Theodoridis PR, Wang M, Bokros M, Llanio LM, et al. A translational program that suppresses metabolism to shield the genome. Nat Commun 2020; 11: 5755.

Barba-Aliaga M, Alepuz P. Role of eIF5A in Mitochondrial Function. Int J Mol Sci 2022; 23

Barba-Aliaga M, Alepuz P. The activator/repressor Hap1 binds to the yeast eIF5A-encoding gene TIF51A to adapt its expression to the mitochondrial functional status. FEBS Lett 2022

Barrangou R, Fremaux C, Deveau H, Richards M, Boyaval P, Moineau S, et al. CRISPR provides acquired resistance against viruses in prokaryotes. Science 2007; 315: 1709–12.

Bartig D, Lemkemeier K, Frank J, Lottspeich F, Klink F. The archaebacterial hypusine-containing protein. Structural features suggest common ancestry with eukaryotic translation initiation factor 5A. Eur J Biochem 1992; 204: 751–8.

Baudin A, Ozier-Kalogeropoulos O, Denouel A, Lacroute F, Cullin C. A simple and efficient method for direct gene deletion in Saccharomyces cerevisiae. Nucleic Acids Res 1993; 21: 3329–30.

Bauer NC, Doetsch PW, Corbett AH. Mechanisms regulating protein localization. Traffic 2015; 16: 1039–61.

Bayraktar EC, La K, Karpman K, Unlu G, Ozerdem C, Ritter DJ, et al. Metabolic coessentiality mapping identifies C12orf49 as a regulator of SREBP processing and cholesterol metabolism. Nat Metab 2020; 2: 487–98.

Bekker-Jensen DB, Kelstrup CD, Batth TS, Larsen SC, Haldrup C, Bramsen JB, et al. An optimized shotgun strategy for the rapid generation of comprehensive human proteomes. Cell Syst 2017; 4: 587-599.e4.

Belew AT, Meskauskas A, Musalgaonkar S, Advani VM, Sulima SO, Kasprzak WK, et al. Ribosomal frameshifting in the CCR5 mRNA is regulated by miRNAs and the NMD pathway. Nature 2014; 512: 265–9.

Ben-Shem A, Garreau de Loubresse N, Melnikov S, Jenner L, Yusupova G, Yusupov M. The structure of the eukaryotic ribosome at 3.0 Å resolution. Science 2011; 334: 1524–9.

Bennett HM, Stephenson W, Rose CM, Darmanis S. Single-cell proteomics enabled by next-generation sequencing or mass spectrometry. Nat Methods 2023; 20: 363–74.

Benne R, Brown-Luedi ML, Hershey JW. Purification and characterization of protein synthesis initiation factors eIF-1, eIF-4C, eIF-4D, and eIF-5 from rabbit reticulocytes. J Biol Chem 1978; 253: 3070–7.

Bernards R, Brummelkamp TR, Beijersbergen RL. shRNA libraries and their use in cancer genetics. Nat Methods 2006; 3: 701–6.

Beusch CM, Sabatier P, Zubarev RA. Ion-Based Proteome-Integrated Solubility Alteration Assays for Systemwide Profiling of Protein-Molecule Interactions. Anal Chem 2022; 94: 7066–74.

Bevec D, Jaksche H, Oft M, Wöhl T, Himmelspach M, Pacher A, et al. Inhibition of HIV-1 replication in lymphocytes by mutants of the Rev cofactor eIF-5A. Science 1996; 271: 1858–60.

Bianchi M, Ulrich P, Bloom O, Meistrell M, Zimmerman GA, Schmidtmayerova H, et al. An inhibitor of macrophage arginine transport and nitric oxide production (CNI-1493) prevents acute inflammation and endotoxin lethality. Mol Med 1995; 1: 254–66.

Bigenzahn JW, Collu GM, Kartnig F, Pieraks M, Vladimer GI, Heinz LX, et al. LZTR1 is a regulator of RAS ubiquitination and signaling. Science 2018; 362: 1171–7.

Birsoy K, Wang T, Chen WW, Freinkman E, Abu-Remaileh M, Sabatini DM. An essential role of the mitochondrial electron transport chain in cell proliferation is to enable aspartate synthesis. Cell 2015; 162: 540–51.

Birsoy K, Wang T, Possemato R, Yilmaz OH, Koch CE, Chen WW, et al. MCT1-mediated transport of a toxic molecule is an effective strategy for targeting glycolytic tumors. Nat Genet 2013; 45: 104–8.

Blomen VA, Májek P, Jae LT, Bigenzahn JW, Nieuwenhuis J, Staring J, et al. Gene essentiality and synthetic lethality in haploid human cells. Science 2015; 350: 1092–6.

Boch J, Scholze H, Schornack S, Landgraf A, Hahn S, Kay S, et al. Breaking the code of DNA binding specificity of TAL-type III effectors. Science 2009; 326: 1509–12.

Bock C, Datlinger P, Chardon F, Coelho MA, Dong MB, Lawson KA, et al. High-content CRISPR screening. Nat Rev Methods Primers 2022; 2

Boettcher M, McManus MT. Choosing the right tool for the job: rnai, TALEN, or CRISPR. Mol Cell 2015; 58: 575–85.

Bolotin A, Quinquis B, Sorokin A, Ehrlich SD. Clustered regularly interspaced short palindrome repeats (CRISPRs) have spacers of extrachromosomal origin. Microbiology (Reading, Engl) 2005; 151: 2551–61.

Bourourou M, Gouix E, Melis N, Friard J, Heurteaux C, Tauc M, et al. Inhibition of eIF5A hypusination pathway as a new pharmacological target for stroke therapy. J Cereb Blood Flow Metab 2021; 41: 1080–90.

Boutros M, Ahringer J. The art and design of genetic screens: RNA interference. Nat Rev Genet 2008; 9: 554–66.

Brar GA, Weissman JS. Ribosome profiling reveals the what, when, where and how of protein synthesis. Nat Rev Mol Cell Biol 2015; 16: 651–64.

Brenes A, Hukelmann J, Bensaddek D, Lamond AI. Multibatch TMT reveals false positives, batch effects and missing values. Mol Cell Proteomics 2019; 18: 1967–80.

Brent MR. Genome annotation past, present, and future: how to define an ORF at each locus. Genome Res 2005; 15: 1777–86.

Brockmann M, Blomen VA, Nieuwenhuis J, Stickel E, Raaben M, Bleijerveld OB, et al. Genetic wiring maps of single-cell protein states reveal an off-switch for GPCR signalling. Nature 2017; 546: 307–11.

Brouns SJJ, Jore MM, Lundgren M, Westra ER, Slijkhuis RJH, Snijders APL, et al. Small CRISPR RNAs guide antiviral defense in prokaryotes. Science 2008; 321: 960–4.

Browne GJ, Proud CG. A novel mTOR-regulated phosphorylation site in elongation factor 2 kinase modulates the activity of the kinase and its binding to calmodulin. Mol Cell Biol 2004; 24: 2986–97.

Budkevich TV, Giesebrecht J, Behrmann E, Loerke J, Ramrath DJF, Mielke T, et al. Regulation of the mammalian elongation cycle by subunit rolling: a eukaryotic-specific ribosome rearrangement. Cell 2014; 158: 121–31.

Bukhari H, Müller T. Endogenous fluorescence tagging by CRISPR. Trends Cell Biol 2019; 29: 912–28.

Bullwinkle TJ, Zou SB, Rajkovic A, Hersch SJ, Elgamal S, Robinson N, et al. (R)-β-lysine-modified elongation factor P functions in translation elongation. J Biol Chem 2013; 288: 4416–23.

Bürckstümmer T, Banning C, Hainzl P, Schobesberger R, Kerzendorfer C, Pauler FM, et al. A reversible gene trap collection empowers haploid genetics in human cells. Nat Methods 2013; 10: 965–71.

Cano VSP, Jeon GA, Johansson HE, Henderson CA, Park J-H, Valentini SR, et al. Mutational analyses of human eIF5A-1--identification of amino acid residues critical for eIF5A activity and hypusine modification. FEBS J 2008; 275: 44–58.

Cao T-T, Lin S-H, Fu L, Tang Z, Che C-M, Zhang L-Y, et al. Eukaryotic translation initiation factor 5A2 promotes metabolic reprogramming in hepatocellular carcinoma cells. Carcinogenesis 2017; 38: 94–104.

Caraglia M, Park MH, Wolff EC, Marra M, Abbruzzese A. eIF5A isoforms and cancer: two brothers for two functions? Amino Acids 2013; 44: 103–9.

Carette JE, Guimaraes CP, Varadarajan M, Park AS, Wuethrich I, Godarova A, et al. Haploid genetic screens in human cells identify host factors used by pathogens. Science 2009; 326: 1231–5.

Carette JE, Guimaraes CP, Wuethrich I, Blomen VA, Varadarajan M, Sun C, et al. Global gene disruption in human cells to assign genes to phenotypes by deep sequencing. Nat Biotechnol 2011; 29: 542–6.

Carette JE, Pruszak J, Varadarajan M, Blomen VA, Gokhale S, Camargo FD, et al. Generation of iPSCs from cultured human malignant cells. Blood 2010; 115: 4039–42.

Carette JE, Raaben M, Wong AC, Herbert AS, Obernosterer G, Mulherkar N, et al. Ebola virus entry requires the cholesterol transporter Niemann-Pick C1. Nature 2011; 477: 340–3.

Carlberg U, Nilsson A, Nygård O. Functional properties of phosphorylated elongation factor 2. Eur J Biochem 1990; 191: 639–45.

Carroll D. Genome engineering with zinc-finger nucleases. Genetics 2011; 188: 773–82.

Carthew RW, Sontheimer EJ. Origins and Mechanisms of miRNAs and siRNAs. Cell 2009; 136: 642–55.

Castello A, Fischer B, Eichelbaum K, Horos R, Beckmann BM, Strein C, et al. Insights into RNA biology from an atlas of mammalian mRNA-binding proteins. Cell 2012; 149: 1393–406.

Castresana J, Saraste M. Evolution of energetic metabolism: the respiration-early hypothesis. Trends Biochem Sci 1995; 20: 443–8.

César-Razquin A, Snijder B, Frappier-Brinton T, Isserlin R, Gyimesi G, Bai X, et al. A call for systematic research on solute carriers. Cell 2015; 162: 478–87.

Chan JCW, Chim C-S, Ooi CGC, Cheung B, Liang R, Chan T-K, et al. Use of the oral chelator deferiprone in the treatment of iron overload in patients with Hb H disease. Br J Haematol 2006; 133: 198–205.

Chartron JW, Hunt KCL, Frydman J. Cotranslational signal-independent SRP preloading during membrane targeting. Nature 2016; 536: 224–8.

Chen KY, Dou QP. NAD+ stimulated the spermidine-dependent hypusine formation on the 18 kDa protein in cytosolic lysates derived from NB-15 mouse neuroblastoma cells. FEBS Lett 1988; 229: 325–8.

Chen S, Francioli LC, Goodrich JK, Collins RL, Kanai M, Wang Q, et al. A genome-wide mutational constraint map quantified from variation in 76,156 human genomes. BioRxiv 2022

Cho NH, Cheveralls KC, Brunner A-D, Kim K, Michaelis AC, Raghavan P, et al. OpenCell: Endogenous tagging for the cartography of human cellular organization. Science 2022; 375: eabi6983.

Chu J, Hong NA, Masuda CA, Jenkins BV, Nelms KA, Goodnow CC, et al. A mouse forward genetics screen identifies LISTERIN as an E3 ubiquitin ligase involved in neurodegeneration. Proc Natl Acad Sci USA 2009; 106: 2097–103.

Clague MJ. Molecular aspects of the endocytic pathway. Biochem J 1998; 336 (Pt 2): 271–82.

Clement PMJ, Hanauske-Abel HM, Wolff EC, Kleinman HK, Park MH. The antifungal drug ciclopirox inhibits deoxyhypusine and proline hydroxylation, endothelial cell growth and angiogenesis in vitro. Int J Cancer 2002; 100: 491–8.

Clement PMJ, Henderson CA, Jenkins ZA, Smit-McBride Z, Wolff EC, Hershey JWB, et al. Identification and characterization of eukaryotic initiation factor 5A-2. Eur J Biochem 2003; 270: 4254–63.

Clement PMJ, Johansson HE, Wolff EC, Park MH. Differential expression of eIF5A-1 and eIF5A-2 in human cancer cells. FEBS J 2006; 273: 1102–14.

Colas C, Menezes S, Gutiérrez-Martínez E, Péan CB, Dionne MS, Guermonprez P. An improved flow cytometry assay to monitor phagosome acidification. J Immunol Methods 2014; 412: 1–13.

Cong L, Ran FA, Cox D, Lin S, Barretto R, Habib N, et al. Multiplex genome engineering using CRISPR/Cas systems. Science 2013; 339: 819–23.

Cooper HL, Park MH, Folk JE, Safer B, Braverman R. Identification of the hypusine-containing protein hy+ as translation initiation factor eIF-4D. Proc Natl Acad Sci USA 1983; 80: 1854–7.

Costa-Mattioli M, Walter P. The integrated stress response: From mechanism to disease. Science 2020; 368

Cougnon M, Carcy R, Melis N, Rubera I, Duranton C, Dumas K, et al. Inhibition of eIF5A hypusination reprogrammes metabolism and glucose handling in mouse kidney. Cell Death Dis 2021; 12: 283.

Csonga R, Ettmayer P, Auer M, Eckerskorn C, Eder J, Klier H. Evaluation of the metal ion requirement of the human deoxyhypusine hydroxylase from HeLa cells using a novel enzyme assay. FEBS Lett 1996; 380: 209–14.

Ctortecka C, Krššáková G, Stejskal K, Penninger JM, Mendjan S, Mechtler K, et al. Comparative Proteome Signatures of Trace Samples by Multiplexed Data-Independent Acquisition. Mol Cell Proteomics 2022; 21: 100177.

Ctortecka C, Stejskal K, Krššáková G, Mendjan S, Mechtler K. Quantitative Accuracy and Precision in Multiplexed Single-Cell Proteomics. Anal Chem 2022; 94: 2434–43.

Cui Y, Cheng X, Chen Q, Song B, Chiu A, Gao Y, et al. CRISP-view: a database of functional genetic screens spanning multiple phenotypes. Nucleic Acids Res 2021; 49: D848–54.

Danecek P, Bonfield JK, Liddle J, Marshall J, Ohan V, Pollard MO, et al. Twelve years of SAMtools and BCFtools. Gigascience 2021; 10

Das Sharma S, Metz JB, Li H, Hobson BD, Hornstein N, Sulzer D, et al. Widespread alterations in translation elongation in the brain of juvenile fmr1 knockout mice. Cell Rep 2019; 26: 3313-3322.e5.

Deltcheva E, Chylinski K, Sharma CM, Gonzales K, Chao Y, Pirzada ZA, et al. CRISPR RNA maturation by trans-encoded small RNA and host factor RNase III. Nature 2011; 471: 602–7.

DepMap B. DepMap 22Q2 Public. Figshare 2022

Dever TE, Dinman JD, Green R. Translation elongation and recoding in eukaryotes. Cold Spring Harb Perspect Biol 2018; 10

Dever TE, Gutierrez E, Shin B-S. The hypusine-containing translation factor eIF5A. Crit Rev Biochem Mol Biol 2014; 49: 413–25.

Dixon AS, Schwinn MK, Hall MP, Zimmerman K, Otto P, Lubben TH, et al. Nanoluc complementation reporter optimized for accurate measurement of protein interactions in cells. ACS Chem Biol 2016; 11: 400–8.

Dobin A, Davis CA, Schlesinger F, Drenkow J, Zaleski C, Jha S, et al. STAR: ultrafast universal RNA-seq aligner. Bioinformatics 2013; 29: 15–21.

Dobson CM. Protein folding and misfolding. Nature 2003; 426: 884–90.

Doench JG. Am I ready for CRISPR? A user's guide to genetic screens. Nat Rev Genet 2018; 19: 67–80.

Doerfel LK, Wohlgemuth I, Kothe C, Peske F, Urlaub H, Rodnina MV. EF-P is essential for rapid synthesis of proteins containing consecutive proline residues. Science 2013; 339: 85–8.

Dong MB, Tang K, Zhou X, Zhou JJ, Chen S. Tumor immunology CRISPR screening: present, past, and future. Trends Cancer 2022; 8: 210–25.

Dong X, Biswas A, Süel KE, Jackson LK, Martinez R, Gu H, et al. Structural basis for leucine-rich nuclear export signal recognition by CRM1. Nature 2009; 458: 1136–41.

Doron-Mandel E, Bokor BJ, Ma Y, Street LA, Tang LC, Abdou AA, et al. SEC-TMT facilitates quantitative differential analysis of protein interaction networks. BioRxiv 2023

Doudna JA, Charpentier E. Genome editing. The new frontier of genome engineering with CRISPR-Cas9. Science 2014; 346: 1258096.

Dowdy SF, Setten RL, Cui X-S, Jadhav SG. Delivery of RNA therapeutics: the great endosomal escape! Nucleic Acid Ther 2022; 32: 361–8.

Duncan RF, Hershey JW. Changes in eIF-4D hypusine modification or abundance are not correlated with translational repression in HeLa cells. J Biol Chem 1986; 261: 12903–6.

Dunkley TPJ, Watson R, Griffin JL, Dupree P, Lilley KS. Localization of organelle proteins by isotope tagging (LOPIT). Mol Cell Proteomics 2004; 3: 1128–34.

Eagle H. Amino acid metabolism in mammalian cell cultures. Science 1959; 130: 432–7.

Eisenberg T, Knauer H, Schauer A, Büttner S, Ruckenstuhl C, Carmona-Gutierrez D, et al. Induction of autophagy by spermidine promotes longevity. Nat Cell Biol 2009; 11: 1305–14.

Elling U, Taubenschmid J, Wirnsberger G, O'Malley R, Demers S-P, Vanhaelen Q, et al. Forward and reverse genetics through derivation of haploid mouse embryonic stem cells. Cell Stem Cell 2011; 9: 563–74.

Essletzbichler P, Konopka T, Santoro F, Chen D, Gapp BV, Kralovics R, et al. Megabase-scale deletion using CRISPR/Cas9 to generate a fully haploid human cell line. Genome Res 2014; 24: 2059–65.

Essletzbichler P, Sedlyarov V, Frommelt F, Soulat D, Heinz LX, Stefanovic A, et al. A genome-wide CRISPR functional survey of the human phagocytosis molecular machinery. Life Sci Alliance 2023; 6

Faundes V, Jennings MD, Crilly S, Legraie S, Withers SE, Cuvertino S, et al. Impaired eIF5A function causes a Mendelian disorder that is partially rescued in model systems by spermidine. Nat Commun 2021; 12: 833.

Feng S, Sekine S, Pessino V, Li H, Leonetti MD, Huang B. Improved split fluorescent proteins for endogenous protein labeling. Nat Commun 2017; 8: 370.

Fenn JB, Mann M, Meng CK, Wong SF, Whitehouse CM. Electrospray ionization for mass spectrometry of large biomolecules. Science 1989; 246: 64–71.

Ferreira da Silva J, Salic S, Wiedner M, Datlinger P, Essletzbichler P, Hanzl A, et al. Genome-scale CRISPR screens are efficient in non-homologous end-joining deficient cells. Sci Rep 2019; 9: 15751.

Fessler E, Eckl E-M, Schmitt S, Mancilla IA, Meyer-Bender MF, Hanf M, et al. A pathway coordinated by DELE1 relays mitochondrial stress to the cytosol. Nature 2020; 579: 433–7.

Folk JE, Park MH, Chung SI, Schrode J, Lester EP, Cooper HL. Polyamines as physiological substrates for transglutaminases. J Biol Chem 1980; 255: 3695–700.

Forsburg SL. The art and design of genetic screens: yeast. Nat Rev Genet 2001; 2: 659–68.

Franken H, Mathieson T, Childs D, Sweetman GMA, Werner T, Tögel I, et al. Thermal proteome profiling for unbiased identification of direct and indirect drug targets using multiplexed quantitative mass spectrometry. Nat Protoc 2015; 10: 1567–93.

Frey PA. The Leloir pathway: a mechanistic imperative for three enzymes to change the stereochemical configuration of a single carbon in galactose. FASEB J 1996; 10: 461–70.

Frigieri MC, João Luiz MVS, Apponi LH, Zanelli CF, Valentini SR. Synthetic lethality between eIF5A and Ypt1 reveals a connection between translation and the secretory pathway in yeast. Mol Genet Genomics 2008; 280: 211–21.

Fromont-Racine M, Senger B, Saveanu C, Fasiolo F. Ribosome assembly in eukaryotes. Gene 2003; 313: 17–42.

Gaetani M, Sabatier P, Saei AA, Beusch CM, Yang Z, Lundström SL, et al. Proteome Integral Solubility Alteration: A High-Throughput Proteomics Assay for Target Deconvolution. J Proteome Res 2019; 18: 4027–37.

Gaj T, Gersbach CA, Barbas CF. ZFN, TALEN, and CRISPR/Cas-based methods for genome engineering. Trends Biotechnol 2013; 31: 397–405.

Ganapathi M, Padgett LR, Yamada K, Devinsky O, Willaert R, Person R, et al. Recessive Rare Variants in Deoxyhypusine Synthase, an Enzyme Involved in the Synthesis of Hypusine, Are Associated with a Neurodevelopmental Disorder. Am J Hum Genet 2019; 104: 287–98.

Garneau JE, Dupuis M-È, Villion M, Romero DA, Barrangou R, Boyaval P, et al. The CRISPR/Cas bacterial immune system cleaves bacteriophage and plasmid DNA. Nature 2010; 468: 67–71.

Gasiunas G, Barrangou R, Horvath P, Siksnys V. Cas9-crRNA ribonucleoprotein complex mediates specific DNA cleavage for adaptive immunity in bacteria. Proc Natl Acad Sci USA 2012; 109: E2579-86.

Gavin A-C, Aloy P, Grandi P, Krause R, Boesche M, Marzioch M, et al. Proteome survey reveals modularity of the yeast cell machinery. Nature 2006; 440: 631–6.

Gavin A-C, Bösche M, Krause R, Grandi P, Marzioch M, Bauer A, et al. Functional organization of the yeast proteome by systematic analysis of protein complexes. Nature 2002; 415: 141–7.

Gesteland RF, Atkins JF. Recoding: dynamic reprogramming of translation. Annu Rev Biochem 1996; 65: 741–68.

Ghaemmaghami S, Huh W-K, Bower K, Howson RW, Belle A, Dephoure N, et al. Global analysis of protein expression in yeast. Nature 2003; 425: 737–41.

Giaever G, Chu AM, Ni L, Connelly C, Riles L, Véronneau S, et al. Functional profiling of the Saccharomyces cerevisiae genome. Nature 2002; 418: 387–91.

Gilar M, Olivova P, Daly AE, Gebler JC. Two-dimensional separation of peptides using RP-RP-HPLC system with different pH in first and second separation dimensions. J Sep Sci 2005; 28: 1694–703.

Gilbert LA, Horlbeck MA, Adamson B, Villalta JE, Chen Y, Whitehead EH, et al. Genome-scale CRISPR-mediated control of gene repression and activation. Cell 2014; 159: 647–61.

Gingold H, Pilpel Y. Determinants of translation efficiency and accuracy. Mol Syst Biol 2011; 7: 481.

Girardi E, César-Razquin A, Lindinger S, Papakostas K, Konecka J, Hemmerich J, et al. A widespread role for SLC transmembrane transporters in resistance to cytotoxic drugs. Nat Chem Biol 2020; 16: 469–78.

Giraud S, Kerforne T, Zely J, Ameteau V, Couturier P, Tauc M, et al. The inhibition of eIF5A hypusination by GC7, a preconditioning protocol to prevent brain death-induced renal injuries in a preclinical porcine kidney transplantation model. Am J Transplant 2020; 20: 3326–40.

Giurgiu M, Reinhard J, Brauner B, Dunger-Kaltenbach I, Fobo G, Frishman G, et al. CORUM: the comprehensive resource of mammalian protein complexes-2019. Nucleic Acids Res 2019; 47: D559–63.

Gobert AP, Finley JL, Latour YL, Asim M, Smith TM, Verriere TG, et al. Hypusination orchestrates the antimicrobial response of macrophages. Cell Rep 2020; 33: 108510.

Go CD, Knight JDR, Rajasekharan A, Rathod B, Hesketh GG, Abe KT, et al. A proximity-dependent biotinylation map of a human cell. Nature 2021; 595: 120–4.

Gonçalves E, Poulos RC, Cai Z, Barthorpe S, Manda SS, Lucas N, et al. Pan-cancer proteomic map of 949 human cell lines. Cancer Cell 2022; 40: 835-849.e8.

Gontan C, Güttler T, Engelen E, Demmers J, Fornerod M, Grosveld FG, et al. Exportin 4 mediates a novel nuclear import pathway for Sox family transcription factors. J Cell Biol 2009; 185: 27–34.

Goodwin S, McPherson JD, McCombie WR. Coming of age: ten years of next-generation sequencing technologies. Nat Rev Genet 2016; 17: 333–51.

Gordon ED, Mora R, Meredith SC, Lindquist SL. Hypusine formation in eukaryotic initiation factor 4D is not reversed when rates or specificity of protein synthesis is altered. J Biol Chem 1987; 262: 16590–5.

Gregio APB, Cano VPS, Avaca JS, Valentini SR, Zanelli CF. eIF5A has a function in the elongation step of translation in yeast. Biochem Biophys Res Commun 2009; 380: 785–90.

Grimm S. The art and design of genetic screens: mammalian culture cells. Nat Rev Genet 2004; 5: 179–89.

Gromadski KB, Schümmer T, Strømgaard A, Knudsen CR, Kinzy TG, Rodnina MV. Kinetics of the interactions between yeast elongation factors 1A and 1Balpha, guanine nucleotides, and aminoacyl-tRNA. J Biol Chem 2007; 282: 35629–37.

Gstaiger M, Aebersold R. Applying mass spectrometry-based proteomics to genetics, genomics and network biology. Nat Rev Genet 2009; 10: 617–27.

GTEx Consortium. The Genotype-Tissue Expression (GTEx) project. Nat Genet 2013; 45: 580–5.

Guerrero-Castillo S, Krisp C, Küchler K, Arnold S, Schlüter H, Gersting SW. Multiplexed complexome profiling using tandem mass tags. Biochim Biophys Acta Bioenerg 2021; 1862: 148448.

Guo X, Aviles G, Liu Y, Tian R, Unger BA, Lin Y-HT, et al. Mitochondrial stress is relayed to the cytosol by an OMA1-DELE1-HRI pathway. Nature 2020; 579: 427–32.

Gupta AK, Plott T. Ciclopirox: a broad-spectrum antifungal with antibacterial and anti-inflammatory properties. Int J Dermatol 2004; 43 Suppl 1: 3–8.

Gutierrez E, Shin B-S, Woolstenhulme CJ, Kim J-R, Saini P, Buskirk AR, et al. eIF5A promotes translation of polyproline motifs. Mol Cell 2013; 51: 35–45.

Haahr P, Galli RA, van den Hengel LG, Bleijerveld OB, Kazokaitė-Adomaitienė J, Song J-Y, et al. Actin maturation requires the ACTMAP/C19orf54 protease. Science 2022; 377: 1533–7.

Han Z, Sakai N, Böttger LH, Klinke S, Hauber J, Trautwein AX, et al. Crystal Structure of the Peroxo-diiron(III) Intermediate of Deoxyhypusine Hydroxylase, an Oxygenase Involved in Hypusination. Structure 2015; 23: 882–92.

Hanauske-Abel HM, Park MH, Hanauske AR, Popowicz AM, Lalande M, Folk JE. Inhibition of the G1-S transition of the cell cycle by inhibitors of deoxyhypusine hydroxylation. Biochim Biophys Acta 1994; 1221: 115–24.

Haney MS, Bohlen CJ, Morgens DW, Ousey JA, Barkal AA, Tsui CK, et al. Identification of phagocytosis regulators using magnetic genome-wide CRISPR screens. Nat Genet 2018; 50: 1716–27.

Hanson G, Coller J. Codon optimality, bias and usage in translation and mRNA decay. Nat Rev Mol Cell Biol 2018; 19: 20–30.

Hart T, Brown KR, Sircoulomb F, Rottapel R, Moffat J. Measuring error rates in genomic perturbation screens: gold standards for human functional genomics. Mol Syst Biol 2014; 10: 733.

Hart T, Chandrashekhar M, Aregger M, Steinhart Z, Brown KR, MacLeod G, et al. High-Resolution CRISPR Screens Reveal Fitness Genes and Genotype-Specific Cancer Liabilities. Cell 2015; 163: 1515–26.

Hart T, Tong AHY, Chan K, Van Leeuwen J, Seetharaman A, Aregger M, et al. Evaluation and Design of Genome-Wide CRISPR/SpCas9 Knockout Screens. G3 (Bethesda) 2017; 7: 2719–27.

Hauber I, Bevec D, Heukeshoven J, Krätzer F, Horn F, Choidas A, et al. Identification of cellular deoxyhypusine synthase as a novel target for antiretroviral therapy. J Clin Invest 2005; 115: 76–85.

Havugimana PC, Goel RK, Phanse S, Youssef A, Padhorny D, Kotelnikov S, et al. Scalable multiplex co-fractionation/mass spectrometry platform for accelerated protein interactome discovery. Nat Commun 2022; 13: 4043.

Havugimana PC, Hart GT, Nepusz T, Yang H, Turinsky AL, Li Z, et al. A census of human soluble protein complexes. Cell 2012; 150: 1068–81.

Hellen CUT. Translation termination and ribosome recycling in eukaryotes. Cold Spring Harb Perspect Biol 2018; 10

Heller JS, Canellakis ES. Cellular control of ornithine decarboxylase activity by its antizyme. J Cell Physiol 1981; 107: 209–17.

Henderson A, Hershey JW. Eukaryotic translation initiation factor (eIF) 5A stimulates protein synthesis in Saccharomyces cerevisiae. Proc Natl Acad Sci USA 2011; 108: 6415–9.

Henderson BR, Percipalle P. Interactions between HIV Rev and nuclear import and export factors: the Rev nuclear localisation signal mediates specific binding to human importin-beta. J Mol Biol 1997; 274: 693–707.

Hershey JW. Expression of initiation factor genes in mammalian cells. Biochimie 1994; 76: 847–52.

Hershey JWB, Sonenberg N, Mathews MB. Principles of translational control. Cold Spring Harb Perspect Biol 2019; 11

Heusel M, Bludau I, Rosenberger G, Hafen R, Frank M, Banaei-Esfahani A, et al. Complex-centric proteome profiling by SEC-SWATH-MS. Mol Syst Biol 2019; 15: e8438.

Hinnebusch AG, Ivanov IP, Sonenberg N. Translational control by 5’-untranslated regions of eukaryotic mRNAs. Science 2016; 352: 1413–6.

Hirsch JG, Dubos RJ. The effect of spermine on tubercle bacilli. J Exp Med 1952; 95: 191–208.

Hoban MD, Cost GJ, Mendel MC, Romero Z, Kaufman ML, Joglekar AV, et al. Correction of the sickle cell disease mutation in human hematopoietic stem/progenitor cells. Blood 2015; 125: 2597–604.

Hockemeyer D, Soldner F, Beard C, Gao Q, Mitalipova M, DeKelver RC, et al. Efficient targeting of expressed and silent genes in human ESCs and iPSCs using zinc-finger nucleases. Nat Biotechnol 2009; 27: 851–7.

Hockemeyer D, Wang H, Kiani S, Lai CS, Gao Q, Cassady JP, et al. Genetic engineering of human pluripotent cells using TALE nucleases. Nat Biotechnol 2011; 29: 731–4.

Hofacker IL. RNA secondary structure analysis using the Vienna RNA package. Curr Protoc Bioinformatics 2004; Chapter 12: Unit 12.2.

Hofer SJ, Simon AK, Bergmann M, Eisenberg T, Kroemer G, Madeo F. Mechanisms of spermidine-induced autophagy and geroprotection. Nat Aging 2022; 2: 1112–29.

Hommes D, van den Blink B, Plasse T, Bartelsman J, Xu C, Macpherson B, et al. Inhibition of stress-activated MAP kinases induces clinical improvement in moderate to severe Crohn's disease. Gastroenterology 2002; 122: 7–14.

Hood L, Rowen L. The Human Genome Project: big science transforms biology and medicine. Genome Med 2013; 5: 79.

Hoque M, Hanauske-Abel HM, Palumbo P, Saxena D, D'Alliessi Gandolfi D, Park MH, et al. Inhibition of HIV-1 gene expression by Ciclopirox and Deferiprone, drugs that prevent hypusination of eukaryotic initiation factor 5A. Retrovirology 2009; 6: 90.

Hornstein N, Torres D, Das Sharma S, Tang G, Canoll P, Sims PA. Ligation-free ribosome profiling of cell type-specific translation in the brain. Genome Biol 2016; 17: 149.

Hsu PD, Lander ES, Zhang F. Development and applications of CRISPR-Cas9 for genome engineering. Cell 2014; 157: 1262–78.

Huber KVM, Olek KM, Müller AC, Tan CSH, Bennett KL, Colinge J, et al. Proteome-wide drug and metabolite interaction mapping by thermal-stability profiling. Nat Methods 2015; 12: 1055–7.

Hukelmann JL, Anderson KE, Sinclair LV, Grzes KM, Murillo AB, Hawkins PT, et al. The cytotoxic T cell proteome and its shaping by the kinase mTOR. Nat Immunol 2016; 17: 104–12.

Humphries AD, Streimann IC, Stojanovski D, Johnston AJ, Yano M, Hoogenraad NJ, et al. Dissection of the mitochondrial import and assembly pathway for human Tom40. J Biol Chem 2005; 280: 11535–43.

Hussmann JA, Ling J, Ravisankar P, Yan J, Cirincione A, Xu A, et al. Mapping the genetic landscape of DNA double-strand break repair. Cell 2021; 184: 5653-5669.e25.

Huttlin EL, Bruckner RJ, Navarrete-Perea J, Cannon JR, Baltier K, Gebreab F, et al. Dual proteome-scale networks reveal cell-specific remodeling of the human interactome. Cell 2021; 184: 3022-3040.e28.

Huttlin EL, Bruckner RJ, Paulo JA, Cannon JR, Ting L, Baltier K, et al. Architecture of the human interactome defines protein communities and disease networks. Nature 2017; 545: 505–9.

Huttlin EL, Ting L, Bruckner RJ, Gebreab F, Gygi MP, Szpyt J, et al. The BioPlex Network: A Systematic Exploration of the Human Interactome. Cell 2015; 162: 425–40.

Imaoka N, Nakajima T. Hypusine, N6-(4-amino-2-hydroxybutyl)-2,6-diaminohexanoic acid, in tissue proteins of mammals. Biochimica et Biophysica Acta (BBA) - General Subjects 1973; 320: 97–103.

Ingolia NT, Brar GA, Rouskin S, McGeachy AM, Weissman JS. The ribosome profiling strategy for monitoring translation in vivo by deep sequencing of ribosome-protected mRNA fragments. Nat Protoc 2012; 7: 1534–50.

Ingolia NT, Brar GA, Stern-Ginossar N, Harris MS, Talhouarne GJS, Jackson SE, et al. Ribosome profiling reveals pervasive translation outside of annotated protein-coding genes. Cell Rep 2014; 8: 1365–79.

Ingolia NT, Ghaemmaghami S, Newman JRS, Weissman JS. Genome-wide analysis in vivo of translation with nucleotide resolution using ribosome profiling. Science 2009; 324: 218–23.

Ingolia NT, Hussmann JA, Weissman JS. Ribosome profiling: global views of translation. Cold Spring Harb Perspect Biol 2019; 11

Ingolia NT, Lareau LF, Weissman JS. Ribosome profiling of mouse embryonic stem cells reveals the complexity and dynamics of mammalian proteomes. Cell 2011; 147: 789–802.

Ingolia NT. Ribosome profiling: new views of translation, from single codons to genome scale. Nat Rev Genet 2014; 15: 205–13.

International Human Genome Sequencing Consortium, Whitehead Institute for Biomedical Research, Center for Genome Research:, Lander ES, Linton LM, Birren B, Nusbaum C, et al. Initial sequencing and analysis of the human genome. Nature 2001; 409: 860–921.

International Human Genome Sequencing Consortium. Finishing the euchromatic sequence of the human genome. Nature 2004; 431: 931–45.

Ishfaq M, Maeta K, Maeda S, Natsume T, Ito A, Yoshida M. Acetylation regulates subcellular localization of eukaryotic translation initiation factor 5A (eIF5A). FEBS Lett 2012; 586: 3236–41.

Ishino Y, Shinagawa H, Makino K, Amemura M, Nakata A. Nucleotide sequence of the iap gene, responsible for alkaline phosphatase isozyme conversion in Escherichia coli, and identification of the gene product. J Bacteriol 1987; 169: 5429–33.

Ivanov IP, Shin B-S, Loughran G, Tzani I, Young-Baird SK, Cao C, et al. Polyamine Control of Translation Elongation Regulates Start Site Selection on Antizyme Inhibitor mRNA via Ribosome Queuing. Mol Cell 2018; 70: 254-264.e6.

Jackson AL, Bartz SR, Schelter J, Kobayashi SV, Burchard J, Mao M, et al. Expression profiling reveals off-target gene regulation by RNAi. Nat Biotechnol 2003; 21: 635–7.

Jackson AL, Linsley PS. Recognizing and avoiding siRNA off-target effects for target identification and therapeutic application. Nat Rev Drug Discov 2010; 9: 57–67.

Jackson RJ, Hellen CUT, Pestova TV. The mechanism of eukaryotic translation initiation and principles of its regulation. Nat Rev Mol Cell Biol 2010; 11: 113–27.

Jae LT, Raaben M, Riemersma M, van Beusekom E, Blomen VA, Velds A, et al. Deciphering the glycosylome of dystroglycanopathies using haploid screens for lassa virus entry. Science 2013; 340: 479–83.

Jakus J, Wolff EC, Park MH, Folk JE. Features of the spermidine-binding site of deoxyhypusine synthase as derived from inhibition studies. Effective inhibition by bis- and mono-guanylated diamines and polyamines. J Biol Chem 1993; 268: 13151–9.

Jasin M, Haber JE. The democratization of gene editing: Insights from site-specific cleavage and double-strand break repair. DNA Repair (Amst) 2016; 44: 6–16.

Jazayeri A, Jackson SP. Screening the yeast genome for new DNA-repair genes. Genome Biol 2002; 3: REVIEWS1009.

Jeffery CJ. Moonlighting proteins. Trends Biochem Sci 1999; 24: 8–11.

Jeng EE, Bhadkamkar V, Ibe NU, Gause H, Jiang L, Chan J, et al. Systematic Identification of Host Cell Regulators of Legionella pneumophila Pathogenesis Using a Genome-wide CRISPR Screen. Cell Host Microbe 2019; 26: 551-563.e6.

Jinek M, Chylinski K, Fonfara I, Hauer M, Doudna JA, Charpentier E. A programmable dual-RNA-guided DNA endonuclease in adaptive bacterial immunity. Science 2012; 337: 816–21.

Joe YA, Park MH. Structural features of the eIF-5A precursor required for posttranslational synthesis of deoxyhypusine. J Biol Chem 1994; 269: 25916–21.

Joung JK, Sander JD. TALENs: a widely applicable technology for targeted genome editing. Nat Rev Mol Cell Biol 2013; 14: 49–55.

Jovanovic M, Rooney MS, Mertins P, Przybylski D, Chevrier N, Satija R, et al. Immunogenetics. Dynamic profiling of the protein life cycle in response to pathogens. Science 2015; 347: 1259038.

Jumper J, Evans R, Pritzel A, Green T, Figurnov M, Ronneberger O, et al. Highly accurate protein structure prediction with AlphaFold. Nature 2021; 596: 583–9.

Kabsch W, Sander C. Dictionary of protein secondary structure: pattern recognition of hydrogen-bonded and geometrical features. Biopolymers 1983; 22: 2577–637.

Kaiser A, Heiss K, Mueller A-K, Fimmers R, Matthes J, Njuguna JT. Inhibition of EIF-5A prevents apoptosis in human cardiomyocytes after malaria infection. Amino Acids 2020; 52: 693–710.

Kaiser A. Translational control of eIF5A in various diseases. Amino Acids 2012; 42: 679–84.

Kang HA, Schwelberger HG, Hershey JW. Translation initiation factor eIF-5A, the hypusine-containing protein, is phosphorylated on serine in Saccharomyces cerevisiae. J Biol Chem 1993; 268: 14750–6.

Kang KR, Kim YS, Wolff EC, Park MH. Specificity of the deoxyhypusine hydroxylase-eukaryotic translation initiation factor (eIF5A) interaction: identification of amino acid residues of the enzyme required for binding of its substrate, deoxyhypusine-containing eIF5A. J Biol Chem 2007; 282: 8300–8.

Kapur M, Ackerman SL. mRNA Translation Gone Awry: Translation Fidelity and Neurological Disease. Trends Genet 2018; 34: 218–31.

Karas M, Hillenkamp F. Laser desorption ionization of proteins with molecular masses exceeding 10,000 daltons. Anal Chem 1988; 60: 2299–301.

Kar RK, Hanner AS, Starost MF, Springer D, Mastracci TL, Mirmira RG, et al. Neuron-specific ablation of eIF5A or deoxyhypusine synthase leads to impairments in growth, viability, neurodevelopment, and cognitive functions in mice. J Biol Chem 2021; 297: 101333.

Karczewski KJ, Francioli LC, Tiao G, Cummings BB, Alföldi J, Wang Q, et al. The mutational constraint spectrum quantified from variation in 141,456 humans. Nature 2020; 581: 434–43.

Katti A, Diaz BJ, Caragine CM, Sanjana NE, Dow LE. CRISPR in cancer biology and therapy. Nat Rev Cancer 2022; 22: 259–79.

Kemper WM, Berry KW, Merrick WC. Purification and properties of rabbit reticulocyte protein synthesis initiation factors M2Balpha and M2Bbeta. J Biol Chem 1976; 251: 5551–7.

Keng VW, Villanueva A, Chiang DY, Dupuy AJ, Ryan BJ, Matise I, et al. A conditional transposon-based insertional mutagenesis screen for genes associated with mouse hepatocellular carcinoma. Nat Biotechnol 2009; 27: 264–74.

Keshishian H, Burgess MW, Specht H, Wallace L, Clauser KR, Gillette MA, et al. Quantitative, multiplexed workflow for deep analysis of human blood plasma and biomarker discovery by mass spectrometry. Nat Protoc 2017; 12: 1683–701.

Kiechl S, Pechlaner R, Willeit P, Notdurfter M, Paulweber B, Willeit K, et al. Higher spermidine intake is linked to lower mortality: a prospective population-based study. Am J Clin Nutr 2018; 108: 371–80.

Kiechl S, Willeit J. In a Nutshell: Findings from the Bruneck Study. Gerontology 2019; 65: 9–19.

Kim SC, Sprung R, Chen Y, Xu Y, Ball H, Pei J, et al. Substrate and functional diversity of lysine acetylation revealed by a proteomics survey. Mol Cell 2006; 23: 607–18.

Kim YG, Cha J, Chandrasegaran S. Hybrid restriction enzymes: zinc finger fusions to Fok I cleavage domain. Proc Natl Acad Sci USA 1996; 93: 1156–60.

Kim YS, Kang KR, Wolff EC, Bell JK, McPhie P, Park MH. Deoxyhypusine hydroxylase is a Fe(II)-dependent, HEAT-repeat enzyme. Identification of amino acid residues critical for Fe(II) binding and catalysis [corrected]. J Biol Chem 2006; 281: 13217–25.

Kirkwood KJ, Ahmad Y, Larance M, Lamond AI. Characterization of native protein complexes and protein isoform variation using size-fractionation-based quantitative proteomics. Mol Cell Proteomics 2013; 12: 3851–73.

Klier H, Csonga R, Joäo HC, Eckerskorn C, Auer M, Lottspeich F, et al. Isolation and structural characterization of different isoforms of the hypusine-containing protein eIF-5A from HeLa cells. Biochemistry 1995; 34: 14693–702.

Klier H, Wöhl T, Eckerskorn C, Magdolen V, Lottspeich F. Determination and mutational analysis of the phosphorylation site in the hypusine-containing protein Hyp2p. FEBS Lett 1993; 334: 360–4.

Klinge S, Voigts-Hoffmann F, Leibundgut M, Arpagaus S, Ban N. Crystal structure of the eukaryotic 60S ribosomal subunit in complex with initiation factor 6. Science 2011; 334: 941–8.

Koike-Yusa H, Li Y, Tan E-P, Velasco-Herrera MDC, Yusa K. Genome-wide recessive genetic screening in mammalian cells with a lentiviral CRISPR-guide RNA library. Nat Biotechnol 2014; 32: 267–73.

Kojic M, Abbassi NEH, Lin T-Y, Jones A, Wakeling EL, Clement E, et al. A novel ELP1 mutation impairs the function of the Elongator complex and causes a severe neurodevelopmental phenotype. J Hum Genet 2023

Komor AC, Badran AH, Liu DR. CRISPR-Based Technologies for the Manipulation of Eukaryotic Genomes. Cell 2017; 168: 20–36.

Konermann S, Brigham MD, Trevino A, Hsu PD, Heidenreich M, Cong L, et al. Optical control of mammalian endogenous transcription and epigenetic states. Nature 2013; 500: 472–6.

Ko SH, Nauta A, Morrison SD, Zhou H, Zimmermann A, Gurtner GC, et al. Antimycotic ciclopirox olamine in the diabetic environment promotes angiogenesis and enhances wound healing. PLoS ONE 2011; 6: e27844.

Koraïchi F, Gence R, Bouchenot C, Grosjean S, Lajoie-Mazenc I, Favre G, et al. High-content tripartite split-GFP cell-based assays to screen for modulators of small GTPase activation. J Cell Sci 2018; 131

Kotecki M, Reddy PS, Cochran BH. Isolation and characterization of a near-haploid human cell line. Exp Cell Res 1999; 252: 273–80.

Kristensen AR, Gsponer J, Foster LJ. A high-throughput approach for measuring temporal changes in the interactome. Nat Methods 2012; 9: 907–9.

Kulak NA, Pichler G, Paron I, Nagaraj N, Mann M. Minimal, encapsulated proteomic-sample processing applied to copy-number estimation in eukaryotic cells. Nat Methods 2014; 11: 319–24.

Kuleshov MV, Jones MR, Rouillard AD, Fernandez NF, Duan Q, Wang Z, et al. Enrichr: a comprehensive gene set enrichment analysis web server 2016 update. Nucleic Acids Res 2016; 44: W90-7.

Kumar A, Dhawan A, Kadam A, Shinde A. Autophagy and mitochondria: targets in neurodegenerative disorders. CNS Neurol Disord Drug Targets 2018; 17: 696–705.

Kumar L, E Futschik M. Mfuzz: a software package for soft clustering of microarray data. Bioinformation 2007; 2: 5–7.

Kummer E, Ban N. Mechanisms and regulation of protein synthesis in mitochondria. Nat Rev Mol Cell Biol 2021; 22: 307–25.

Kutay U, Bischoff FR, Kostka S, Kraft R, Görlich D. Export of importin alpha from the nucleus is mediated by a specific nuclear transport factor. Cell 1997; 90: 1061–71.

Kyrpides NC, Woese CR. Universally conserved translation initiation factors. Proc Natl Acad Sci USA 1998; 95: 224–8.

Kyte J, Doolittle RF. A simple method for displaying the hydropathic character of a protein. J Mol Biol 1982; 157: 105–32.

Lackner DH, Carré A, Guzzardo PM, Banning C, Mangena R, Henley T, et al. A generic strategy for CRISPR-Cas9-mediated gene tagging. Nat Commun 2015; 6: 10237.

Larance M, Lamond AI. Multidimensional proteomics for cell biology. Nat Rev Mol Cell Biol 2015; 16: 269–80.

Lassak J, Wilson DN, Jung K. Stall no more at polyproline stretches with the translation elongation factors EF-P and IF-5A. Mol Microbiol 2016; 99: 219–35.

Leeb M, Wutz A. Derivation of haploid embryonic stem cells from mouse embryos. Nature 2011; 479: 131–4.

Leesch F, Lorenzo-Orts L, Pribitzer C, Grishkovskaya I, Roehsner J, Chugunova A, et al. A molecular network of conserved factors keeps ribosomes dormant in the egg. Nature 2023; 613: 712–20.

Lee SB, Park JH, Folk JE, Deck JA, Pegg AE, Sokabe M, et al. Inactivation of eukaryotic initiation factor 5A (eIF5A) by specific acetylation of its hypusine residue by spermidine/spermine acetyltransferase 1 (SSAT1). Biochem J 2011; 433: 205–13.

Lee SB, Park JH, Kaevel J, Sramkova M, Weigert R, Park MH. The effect of hypusine modification on the intracellular localization of eIF5A. Biochem Biophys Res Commun 2009; 383: 497–502.

Lee YB, Joe YA, Wolff EC, Dimitriadis EK, Park MH. Complex formation between deoxyhypusine synthase and its protein substrate, the eukaryotic translation initiation factor 5A (eIF5A) precursor. Biochem J 1999; 340 (Pt 1): 273–81.

Levasseur EM, Yamada K, Piñeros AR, Wu W, Syed F, Orr KS, et al. Hypusine biosynthesis in β cells links polyamine metabolism to facultative cellular proliferation to maintain glucose homeostasis. Sci Signal 2019; 12

Lewinski MK, Yamashita M, Emerman M, Ciuffi A, Marshall H, Crawford G, et al. Retroviral DNA integration: viral and cellular determinants of target-site selection. PLoS Pathog 2006; 2: e60.

Li T, Belda-Palazón B, Ferrando A, Alepuz P. Fertility and polarized cell growth depends on eIF5A for translation of polyproline-rich formins in Saccharomyces cerevisiae. Genetics 2014; 197: 1191–200.

Liang Y, Piao C, Beuschel CB, Toppe D, Kollipara L, Bogdanow B, et al. eIF5A hypusination, boosted by dietary spermidine, protects from premature brain aging and mitochondrial dysfunction. Cell Rep 2021; 35: 108941.

Liao DI, Wolff EC, Park MH, Davies DR. Crystal structure of the NAD complex of human deoxyhypusine synthase: an enzyme with a ball-and-chain mechanism for blocking the active site. Structure 1998; 6: 23–32.

Liao Y, Smyth GK, Shi W. featureCounts: an efficient general purpose program for assigning sequence reads to genomic features. Bioinformatics 2014; 30: 923–30.

Lima T, Li TY, Mottis A, Auwerx J. Pleiotropic effects of mitochondria in aging. Nat Aging 2022

Lindner B, Martin E, Steininger M, Bundalo A, Lenter M, Zuber J, et al. A genome-wide CRISPR/Cas9 screen to identify phagocytosis modulators in monocytic THP-1 cells. Sci Rep 2021; 11: 12973.

Lindqvist LM, Tandoc K, Topisirovic I, Furic L. Cross-talk between protein synthesis, energy metabolism and autophagy in cancer. Curr Opin Genet Dev 2018; 48: 104–11.

Lino CA, Harper JC, Carney JP, Timlin JA. Delivering CRISPR: a review of the challenges and approaches. Drug Deliv 2018; 25: 1234–57.

Lin A, Giuliano CJ, Palladino A, John KM, Abramowicz C, Yuan ML, et al. Off-target toxicity is a common mechanism of action of cancer drugs undergoing clinical trials. Sci Transl Med 2019; 11

Lin H, Caroll KS. Introduction: posttranslational protein modification. Chem Rev 2018; 118: 887–8.

Lipowsky G, Bischoff FR, Schwarzmaier P, Kraft R, Kostka S, Hartmann E, et al. Exportin 4: a mediator of a novel nuclear export pathway in higher eukaryotes. EMBO J 2000; 19: 4362–71.

Liu K-L, Li X-Y, Wang D-P, Xue W-H, Qian X-H, Li Y-H, et al. Novel Allosteric Inhibitors of Deoxyhypusine Synthase against Malignant Melanoma: Design, Synthesis, and Biological Evaluation. J Med Chem 2021; 64: 13356–72.

Liu MY, Wu MC. Induction of human monocyte cell line U937 differentiation and CSF-1 production by phorbol ester. Exp Hematol 1992; 20: 974–9.

Liu S, Bachran C, Gupta P, Miller-Randolph S, Wang H, Crown D, et al. Diphthamide modification on eukaryotic elongation factor 2 is needed to assure fidelity of mRNA translation and mouse development. Proc Natl Acad Sci USA 2012; 109: 13817–22.

Liu Y, Beyer A, Aebersold R. On the Dependency of Cellular Protein Levels on mRNA Abundance. Cell 2016; 165: 535–50.

Liu YP, Nemeroff M, Yan YP, Chen KY. Interaction of eukaryotic initiation factor 5A with the human immunodeficiency virus type 1 Rev response element RNA and U6 snRNA requires deoxyhypusine or hypusine modification. Biol Signals 1997; 6: 166–74.

Li J, Van Vranken JG, Pontano Vaites L, Schweppe DK, Huttlin EL, Etienne C, et al. TMTpro reagents: a set of isobaric labeling mass tags enables simultaneous proteome-wide measurements across 16 samples. Nat Methods 2020; 17: 399–404.

Li JJ, Bickel PJ, Biggin MD. System wide analyses have underestimated protein abundances and the importance of transcription in mammals. PeerJ 2014; 2: e270.

Li JJ, Biggin MD. Gene expression. Statistics requantitates the central dogma. Science 2015; 347: 1066–7.

Li K-C, Girardi E, Kartnig F, Grosche S, Pemovska T, Bigenzahn JW, et al. Cell-surface SLC nucleoside transporters and purine levels modulate BRD4-dependent chromatin states. Nat Metab 2021; 3: 651–64.

Liu T, O'Rourke B. Enhancing mitochondrial Ca2+ uptake in myocytes from failing hearts restores energy supply and demand matching. Circ Res 2008; 103: 279–88.

Liu X, Salokas K, Tamene F, Jiu Y, Weldatsadik RG, Öhman T, et al. An AP-MS- and BioID-compatible MAC-tag enables comprehensive mapping of protein interactions and subcellular localizations. Nat Commun 2018; 9: 1188.

Lubas M, Harder LM, Kumsta C, Tiessen I, Hansen M, Andersen JS, et al. eIF5A is required for autophagy by mediating ATG3 translation. EMBO Rep 2018; 19

Lu J, Zhao H-W, Chen Y, Wei J-H, Chen Z-H, Feng Z-H, et al. Eukaryotic translation initiation factor 5A2 is highly expressed in prostate cancer and predicts poor prognosis. Exp Ther Med 2019; 17: 3741–7.

Lyons TW, Reinhard CT, Planavsky NJ. The rise of oxygen in Earth's early ocean and atmosphere. Nature 2014; 506: 307–15.

Mackmull M-T, Klaus B, Heinze I, Chokkalingam M, Beyer A, Russell RB, et al. Landscape of nuclear transport receptor cargo specificity. Mol Syst Biol 2017; 13: 962.

Maier B, Ogihara T, Trace AP, Tersey SA, Robbins RD, Chakrabarti SK, et al. The unique hypusine modification of eIF5A promotes islet beta cell inflammation and dysfunction in mice. J Clin Invest 2010; 120: 2156–70.

Mailloux RJ. An update on mitochondrial reactive oxygen species production. Antioxidants (Basel) 2020; 9

Malik BR, Maddison DC, Smith GA, Peters OM. Autophagic and endo-lysosomal dysfunction in neurodegenerative disease. Mol Brain 2019; 12: 100.

Mali P, Yang L, Esvelt KM, Aach J, Guell M, DiCarlo JE, et al. RNA-guided human genome engineering via Cas9. Science 2013; 339: 823–6.

Malyutin AG, Musalgaonkar S, Patchett S, Frank J, Johnson AW. Nmd3 is a structural mimic of eIF5A, and activates the cpGTPase Lsg1 during 60S ribosome biogenesis. EMBO J 2017; 36: 854–68.

Mandal A, Mandal S, Park MH. Genome-wide analyses and functional classification of proline repeat-rich proteins: potential role of eIF5A in eukaryotic evolution. PLoS ONE 2014; 9: e111800.

Mandal A, Mandal S, Park MH. Global quantitative proteomics reveal up-regulation of endoplasmic reticulum stress response proteins upon depletion of eIF5A in HeLa cells. Sci Rep 2016; 6: 25795.

Mandon EC, Trueman SF, Gilmore R. Protein translocation across the rough endoplasmic reticulum. Cold Spring Harb Perspect Biol 2013; 5

Manjunath H, Zhang H, Rehfeld F, Han J, Chang T-C, Mendell JT. Suppression of Ribosomal Pausing by eIF5A Is Necessary to Maintain the Fidelity of Start Codon Selection. Cell Rep 2019; 29: 3134-3146.e6.

Mann M. Origins of mass spectrometry-based proteomics. Nat Rev Mol Cell Biol 2016; 17: 678.

Mansueto G, Armani A, Viscomi C, D'Orsi L, De Cegli R, Polishchuk EV, et al. Transcription Factor EB Controls Metabolic Flexibility during Exercise. Cell Metab 2017; 25: 182–96.

Marraffini LA, Sontheimer EJ. CRISPR interference limits horizontal gene transfer in staphylococci by targeting DNA. Science 2008; 322: 1843–5.

Martinez Molina D, Jafari R, Ignatushchenko M, Seki T, Larsson EA, Dan C, et al. Monitoring drug target engagement in cells and tissues using the cellular thermal shift assay. Science 2013; 341: 84–7.

Martin PB, Kigoshi-Tansho Y, Sher RB, Ravenscroft G, Stauffer JE, Kumar R, et al. NEMF mutations that impair ribosome-associated quality control are associated with neuromuscular disease. Nat Commun 2020; 11: 4625.

Mast FD, Ratushny AV, Aitchison JD. Systems cell biology. J Cell Biol 2014; 206: 695–706.

Mateus A, Kurzawa N, Becher I, Sridharan S, Helm D, Stein F, et al. Thermal proteome profiling for interrogating protein interactions. Mol Syst Biol 2020; 16: e9232.

Mathews MB, Hershey JWB. The translation factor eIF5A and human cancer. Biochim Biophys Acta 2015; 1849: 836–44.

Mazouzi A, Moser SC, Abascal F, van den Broek B, Del Castillo Velasco-Herrera M, van der Heijden I, et al. FIRRM/C1orf112 mediates resolution of homologous recombination intermediates in response to DNA interstrand crosslinks. Sci Adv 2023; 9: eadf4409.

Ma D, Zheng B, Liu H-L, Zhao Y-B, Liu X, Zhang X-H, et al. Klf5 down-regulation induces vascular senescence through eIF5a depletion and mitochondrial fission. PLoS Biol 2020; 18: e3000808.

McAlister GC, Nusinow DP, Jedrychowski MP, Wühr M, Huttlin EL, Erickson BK, et al. MultiNotch MS3 enables accurate, sensitive, and multiplexed detection of differential expression across cancer cell line proteomes. Anal Chem 2014; 86: 7150–8.

McCaffrey TA, Pomerantz KB, Sanborn TA, Spokojny AM, Du B, Park MH, et al. Specific inhibition of eIF-5A and collagen hydroxylation by a single agent. Antiproliferative and fibrosuppressive effects on smooth muscle cells from human coronary arteries. J Clin Invest 1995; 95: 446–55.

McManus J, Cheng Z, Vogel C. Next-generation analysis of gene expression regulation--comparing the roles of synthesis and degradation. Mol Biosyst 2015; 11: 2680–9.

Melis N, Rubera I, Cougnon M, Giraud S, Mograbi B, Belaid A, et al. Targeting eIF5A Hypusination Prevents Anoxic Cell Death through Mitochondrial Silencing and Improves Kidney Transplant Outcome. J Am Soc Nephrol 2017; 28: 811–22.

Melnikov S, Mailliot J, Shin B-S, Rigger L, Yusupova G, Micura R, et al. Crystal Structure of Hypusine-Containing Translation Factor eIF5A Bound to a Rotated Eukaryotic Ribosome. J Mol Biol 2016; 428: 3570–6.

Meng Q-B, Kang W-M, Yu J-C, Liu Y-Q, Ma Z-Q, Zhou L, et al. Overexpression of eukaryotic translation initiation factor 5A2 (EIF5A2) correlates with cell aggressiveness and poor survival in gastric cancer. PLoS ONE 2015; 10: e0119229.

Merrick WC, Pavitt GD. Protein synthesis initiation in eukaryotic cells. Cold Spring Harb Perspect Biol 2018; 10

Meyers RM, Bryan JG, McFarland JM, Weir BA, Sizemore AE, Xu H, et al. Computational correction of copy number effect improves specificity of CRISPR-Cas9 essentiality screens in cancer cells. Nat Genet 2017; 49: 1779–84.

Michel AM, Fox G, M Kiran A, De Bo C, O'Connor PBF, Heaphy SM, et al. GWIPS-viz: development of a ribo-seq genome browser. Nucleic Acids Res 2014; 42: D859-64.

Miller-Fleming L, Olin-Sandoval V, Campbell K, Ralser M. Remaining mysteries of molecular biology: the role of polyamines in the cell. J Mol Biol 2015; 427: 3389–406.

Miyake T, Pradeep S, Wu SY, Rupaimoole R, Zand B, Wen Y, et al. XPO1/CRM1 Inhibition Causes Antitumor Effects by Mitochondrial Accumulation of eIF5A. Clin Cancer Res 2015; 21: 3286–97.

Moazed D, Noller HF. Intermediate states in the movement of transfer RNA in the ribosome. Nature 1989; 342: 142–8.

Mohr S, Bakal C, Perrimon N. Genomic screening with RNAi: results and challenges. Annu Rev Biochem 2010; 79: 37–64.

Mojica FJM, Díez-Villaseñor C, García-Martínez J, Soria E. Intervening sequences of regularly spaced prokaryotic repeats derive from foreign genetic elements. J Mol Evol 2005; 60: 174–82.

Monecke T, Güttler T, Neumann P, Dickmanns A, Görlich D, Ficner R. Crystal structure of the nuclear export receptor CRM1 in complex with Snurportin1 and RanGTP. Science 2009; 324: 1087–91.

Monzel AS, Enríquez JA, Picard M. Multifaceted mitochondria: moving mitochondrial science beyond function and dysfunction. Nat Metab 2023; 5: 546–62.

Moore CC, Martin EN, Lee G, Taylor C, Dondero R, Reznikov LL, et al. Eukaryotic translation initiation factor 5A small interference RNA-liposome complexes reduce inflammation and increase survival in murine models of severe sepsis and acute lung injury. J Infect Dis 2008; 198: 1407–14.

Morgens DW, Wainberg M, Boyle EA, Ursu O, Araya CL, Tsui CK, et al. Genome-scale measurement of off-target activity using Cas9 toxicity in high-throughput screens. Nat Commun 2017; 8: 15178.

Morris JA, Caragine C, Daniloski Z, Domingo J, Barry T, Lu L, et al. Discovery of target genes and pathways at GWAS loci by pooled single-cell CRISPR screens. Science 2023; 380: eadh7699.

Moscou MJ, Bogdanove AJ. A simple cipher governs DNA recognition by TAL effectors. Science 2009; 326: 1501.

Muller HJ. Artificial transmutation of the gene. Science 1927; 66: 84–7.

Mulvey CM, Breckels LM, Geladaki A, Britovšek NK, Nightingale DJH, Christoforou A, et al. Using hyperLOPIT to perform high-resolution mapping of the spatial proteome. Nat Protoc 2017; 12: 1110–35.

Murakami Y, Matsufuji S, Kameji T, Hayashi S, Igarashi K, Tamura T, et al. Ornithine decarboxylase is degraded by the 26S proteasome without ubiquitination. Nature 1992; 360: 597–9.

Murphey RJ, Gerner EW. Hypusine formation in protein by a two-step process in cell lysates. J Biol Chem 1987; 262: 15033–6.

Murphy JP, Stepanova E, Everley RA, Paulo JA, Gygi SP. Comprehensive Temporal Protein Dynamics during the Diauxic Shift in Saccharomyces cerevisiae. Mol Cell Proteomics 2015; 14: 2454–65.

Murphy MP. How mitochondria produce reactive oxygen species. Biochem J 2009; 417: 1–13.

Nakajima T, Matsubayashi T, Kakimoto Y, Sano I. Distribution of hypusione, N6(-4amino-2-hydroxybutyl)-2, 6-diaminohexanoic acid, in mammalian organs. Biochimica et Biophysica Acta (BBA) - General Subjects 1971; 252: 92–7.

Nakanishi S, Cleveland JL. Targeting the polyamine-hypusine circuit for the prevention and treatment of cancer. Amino Acids 2016; 48: 2353–62.

Namy O, Moran SJ, Stuart DI, Gilbert RJC, Brierley I. A mechanical explanation of RNA pseudoknot function in programmed ribosomal frameshifting. Nature 2006; 441: 244–7.

Navarre WW, Zou SB, Roy H, Xie JL, Savchenko A, Singer A, et al. PoxA, yjeK, and elongation factor P coordinately modulate virulence and drug resistance in Salmonella enterica. Mol Cell 2010; 39: 209–21.

Nelson DL, Cox MM. Lehninger Principles of Biochemistry. Sixth. New York: W.H. Freeman; 2012

Nishimura K, Lee SB, Park JH, Park MH. Essential role of eIF5A-1 and deoxyhypusine synthase in mouse embryonic development. Amino Acids 2012; 42: 703–10.

Nishimura K, Murozumi K, Shirahata A, Park MH, Kashiwagi K, Igarashi K. Independent roles of eIF5A and polyamines in cell proliferation. Biochem J 2005; 385: 779–85.

Nurk S, Koren S, Rhie A, Rautiainen M, Bzikadze AV, Mikheenko A, et al. The complete sequence of a human genome. Science 2022; 376: 44–53.

Nurse P, Hayles J. The cell in an era of systems biology. Cell 2011; 144: 850–4.

Nusinow DP, Szpyt J, Ghandi M, Rose CM, McDonald ER, Kalocsay M, et al. Quantitative proteomics of the cancer cell line encyclopedia. Cell 2020; 180: 387-402.e16.

Nüsslein-Volhard C, Wieschaus E. Mutations affecting segment number and polarity in Drosophila. Nature 1980; 287: 795–801.

O'Connell JD, Paulo JA, O'Brien JJ, Gygi SP. Proteome-Wide Evaluation of Two Common Protein Quantification Methods. J Proteome Res 2018; 17: 1934–42.

O'Neill LAJ, Pearce EJ. Immunometabolism governs dendritic cell and macrophage function. J Exp Med 2016; 213: 15–23.

Oliverio S, Corazzari M, Sestito C, Piredda L, Ippolito G, Piacentini M. The spermidine analogue GC7 (N1-guanyl-1,7-diamineoheptane) induces autophagy through a mechanism not involving the hypusination of eIF5A. Amino Acids 2014; 46: 2767–76.

Olokoba AB, Obateru OA, Olokoba LB. Type 2 diabetes mellitus: a review of current trends. Oman Med J 2012; 27: 269–73.

Olsen ME, Cressey TN, Mühlberger E, Connor JH. Differential Mechanisms for the Involvement of Polyamines and Hypusinated eIF5A in Ebola Virus Gene Expression. J Virol 2018; 92

Olsen ME, Filone CM, Rozelle D, Mire CE, Agans KN, Hensley L, et al. Polyamines and hypusination are required for ebolavirus gene expression and replication. MBio 2016; 7

Orre LM, Vesterlund M, Pan Y, Arslan T, Zhu Y, Fernandez Woodbridge A, et al. SubCellBarCode: Proteome-wide Mapping of Protein Localization and Relocalization. Mol Cell 2019; 73: 166-182.e7.

Oughtred R, Stark C, Breitkreutz B-J, Rust J, Boucher L, Chang C, et al. The BioGRID interaction database: 2019 update. Nucleic Acids Res 2019; 47: D529–41.

Padgett LR, Shinkle MR, Rosario S, Stewart TM, Foley JR, Casero RA, et al. Deoxyhypusine synthase mutations alter the post-translational modification of eukaryotic initiation factor 5A resulting in impaired human and mouse neural homeostasis. HGG Adv 2023; 4: 100206.

Pällmann N, Braig M, Sievert H, Preukschas M, Hermans-Borgmeyer I, Schweizer M, et al. Biological relevance and therapeutic potential of the hypusine modification system. J Biol Chem 2015; 290: 18343–60.

Palmiter RD. Quantitation of parameters that determine the rate of ovalbumin synthesis. Cell 1975; 4: 189.

Pappireddi N, Martin L, Wühr M. A review on quantitative multiplexed proteomics. Chembiochem 2019; 20: 1210–24.

Park J-H, Aravind L, Wolff EC, Kaevel J, Kim YS, Park MH. Molecular cloning, expression, and structural prediction of deoxyhypusine hydroxylase: a HEAT-repeat-containing metalloenzyme. Proc Natl Acad Sci USA 2006; 103: 51–6.

Park J-H, Johansson HE, Aoki H, Huang BX, Kim H-Y, Ganoza MC, et al. Post-translational modification by β-lysylation is required for activity of Escherichia coli elongation factor P (EF-P). J Biol Chem 2012; 287: 2579–90.

Park MH, Cooper HL, Folk JE. Identification of hypusine, an unusual amino acid, in a protein from human lymphocytes and of spermidine as its biosynthetic precursor. Proc Natl Acad Sci USA 1981; 78: 2869–73.

Park MH, Cooper HL, Folk JE. The biosynthesis of protein-bound hypusine (N epsilon -(4-amino-2-hydroxybutyl)lysine). Lysine as the amino acid precursor and the intermediate role of deoxyhypusine (N epsilon -(4-aminobutyl)lysine). J Biol Chem 1982; 257: 7217–22.

Park MH, Wolff EC, Folk JE. Is hypusine essential for eukaryotic cell proliferation? Trends Biochem Sci 1993; 18: 475–9.

Park MH, Wolff EC, Smit-McBride Z, Hershey JW, Folk JE. Comparison of the activities of variant forms of eIF-4D. The requirement for hypusine or deoxyhypusine. J Biol Chem 1991; 266: 7988–94.

Park MH, Wolff EC. Hypusine, a polyamine-derived amino acid critical for eukaryotic translation. J Biol Chem 2018; 293: 18710–8.

Park MH. Regulation of biosynthesis of hypusine in Chinese hamster ovary cells. Evidence for eIF-4D precursor polypeptides. J Biol Chem 1987; 262: 12730–4.

Park MH. The post-translational synthesis of a polyamine-derived amino acid, hypusine, in the eukaryotic translation initiation factor 5A (eIF5A). J Biochem 2006; 139: 161–9.

Parreiras-E-Silva LT, Gomes MD, Oliveira EB, Costa-Neto CM. The N-terminal region of eukaryotic translation initiation factor 5A signals to nuclear localization of the protein. Biochem Biophys Res Commun 2007; 362: 393–8.

Patel PH, Costa-Mattioli M, Schulze KL, Bellen HJ. The Drosophila deoxyhypusine hydroxylase homologue nero and its target eIF5A are required for cell growth and the regulation of autophagy. J Cell Biol 2009; 185: 1181–94.

Pavlov MY, Watts RE, Tan Z, Cornish VW, Ehrenberg M, Forster AC. Slow peptide bond formation by proline and other N-alkylamino acids in translation. Proc Natl Acad Sci USA 2009; 106: 50–4.

Pechmann S, Chartron JW, Frydman J. Local slowdown of translation by nonoptimal codons promotes nascent-chain recognition by SRP *in vivo*. Nat Struct Mol Biol 2014; 21: 1100–5.

Pechmann S, Frydman J. Evolutionary conservation of codon optimality reveals hidden signatures of cotranslational folding. Nat Struct Mol Biol 2013; 20: 237–43.

Pechmann S, Willmund F, Frydman J. The ribosome as a hub for protein quality control. Mol Cell 2013; 49: 411–21.

Pegg AE. Mammalian polyamine metabolism and function. IUBMB Life 2009; 61: 880–94.

Pelechano V, Alepuz P. eIF5A facilitates translation termination globally and promotes the elongation of many non polyproline-specific tripeptide sequences. Nucleic Acids Res 2017; 45: 7326–38.

Pereira KD, Tamborlin L, de Lima TI, Consonni SR, Silveira LR, Luchessi AD. Alternative human eIF5A protein isoform plays a critical role in mitochondria. J Cell Biochem 2021; 122: 549–61.

Pereira KD, Tamborlin L, Meneguello L, de Proença ARG, Almeida IC de PA, Lourenço RF, et al. Alternative Start Codon Connects eIF5A to Mitochondria. J Cell Physiol 2016; 231: 2682–9.

Pervez MT, Hasnain MJU, Abbas SH, Moustafa MF, Aslam N, Shah SSM. A Comprehensive Review of Performance of Next-Generation Sequencing Platforms. Biomed Res Int 2022; 2022: 3457806.

Pochopien AA, Beckert B, Kasvandik S, Berninghausen O, Beckmann R, Tenson T, et al. Structure of Gcn1 bound to stalled and colliding 80S ribosomes. Proc Natl Acad Sci USA 2021; 118

Pourcel C, Salvignol G, Vergnaud G. CRISPR elements in Yersinia pestis acquire new repeats by preferential uptake of bacteriophage DNA, and provide additional tools for evolutionary studies. Microbiology (Reading, Engl) 2005; 151: 653–63.

Proud CG. Regulation and roles of elongation factor 2 kinase. Biochem Soc Trans 2015; 43: 328–32.

Proud CG. Phosphorylation and signal transduction pathways in translational control. Cold Spring Harb Perspect Biol 2019; 11

Przybyla L, Gilbert LA. A new era in functional genomics screens. Nat Rev Genet 2022; 23: 89–103.

Puleston DJ, Baixauli F, Sanin DE, Edwards-Hicks J, Villa M, Kabat AM, et al. Polyamine metabolism is a central determinant of helper T cell lineage fidelity. Cell 2021; 184: 4186-4202.e20.

Puleston DJ, Buck MD, Klein Geltink RI, Kyle RL, Caputa G, O'Sullivan D, et al. Polyamines and eIF5A Hypusination Modulate Mitochondrial Respiration and Macrophage Activation. Cell Metab 2019; 30: 352-363.e8.

Puleston DJ. A metabolic vulnerability of pancreatic cancer. Nature 2023

Quirós PM, Prado MA, Zamboni N, D'Amico D, Williams RW, Finley D, et al. Multi-omics analysis identifies ATF4 as a key regulator of the mitochondrial stress response in mammals. J Cell Biol 2017; 216: 2027–45.

Ran FA, Hsu PD, Wright J, Agarwala V, Scott DA, Zhang F. Genome engineering using the CRISPR-Cas9 system. Nat Protoc 2013; 8: 2281–308.

Rauniyar N, Yates JR. Isobaric labeling-based relative quantification in shotgun proteomics. J Proteome Res 2014; 13: 5293–309.

Redpath NT, Foulstone EJ, Proud CG. Regulation of translation elongation factor-2 by insulin via a rapamycin-sensitive signalling pathway. EMBO J 1996; 15: 2291–7.

Reicher A, Koren A, Kubicek S. Pooled protein tagging, cellular imaging, and in situ sequencing for monitoring drug action in real time. Genome Res 2020; 30: 1846–55.

Robbins RD, Tersey SA, Ogihara T, Gupta D, Farb TB, Ficorilli J, et al. Inhibition of deoxyhypusine synthase enhances islet {beta} cell function and survival in the setting of endoplasmic reticulum stress and type 2 diabetes. J Biol Chem 2010; 285: 39943–52.

Roberts B, Haupt A, Tucker A, Grancharova T, Arakaki J, Fuqua MA, et al. Systematic gene tagging using CRISPR/Cas9 in human stem cells to illuminate cell organization. Mol Biol Cell 2017; 28: 2854–74.

Rolfe DF, Brown GC. Cellular energy utilization and molecular origin of standard metabolic rate in mammals. Physiol Rev 1997; 77: 731–58.

Romero MF, Chen A-P, Parker MD, Boron WF. The SLC4 family of bicarbonate (HCO_3^-) transporters. Mol Aspects Med 2013; 34: 159–82.

Ronaghi M, Uhlén M, Nyrén P. A sequencing method based on real-time pyrophosphate. Science 1998; 281: 363, 365.

Rose AJ, Broholm C, Kiillerich K, Finn SG, Proud CG, Rider MH, et al. Exercise rapidly increases eukaryotic elongation factor 2 phosphorylation in skeletal muscle of men. J Physiol (Lond) 2005; 569: 223–8.

Rossi D, Galvão FC, Bellato HM, Boldrin PEG, Andrews BJ, Valentini SR, et al. eIF5A has a function in the cotranslational translocation of proteins into the ER. Amino Acids 2014; 46: 645–53.

Rouet P, Smih F, Jasin M. Introduction of double-strand breaks into the genome of mouse cells by expression of a rare-cutting endonuclease. Mol Cell Biol 1994; 14: 8096–106.

Ruckhäberle E, Karn T, Hanker L, Schwarz J, Schulz-Knappe P, Kuhn K, et al. Breast Cancer Proteomics - Differences in Protein Expression between Estrogen Receptor-Positive and -Negative Tumors Identified by Tandem Mass Tag Technology. Breast Care (Basel) 2010; 5: 7–10.

Ruhl M, Himmelspach M, Bahr GM, Hammerschmid F, Jaksche H, Wolff B, et al. Eukaryotic initiation factor 5A is a cellular target of the human immunodeficiency virus type 1 Rev activation domain mediating trans-activation. J Cell Biol 1993; 123: 1309–20.

Russell JB, Cook GM. Energetics of bacterial growth: balance of anabolic and catabolic reactions. Microbiol Rev 1995; 59: 48–62.

Russell WL, Kelly EM, Hunsicker PR, Bangham JW, Maddux SC, Phipps EL. Specific-locus test shows ethylnitrosourea to be the most potent mutagen in the mouse. Proc Natl Acad Sci USA 1979; 76: 5818–9.

Ryazanov AG, Shestakova EA, Natapov PG. Phosphorylation of elongation factor 2 by EF-2 kinase affects rate of translation. Nature 1988; 334: 170–3.

Sagi I, Chia G, Golan-Lev T, Peretz M, Weissbein U, Sui L, et al. Derivation and differentiation of haploid human embryonic stem cells. Nature 2016; 532: 107–11.

Saini P, Eyler DE, Green R, Dever TE. Hypusine-containing protein eIF5A promotes translation elongation. Nature 2009; 459: 118–21.

Sakuma T, Nakade S, Sakane Y, Suzuki K-IT, Yamamoto T. MMEJ-assisted gene knock-in using TALENs and CRISPR-Cas9 with the PITCh systems. Nat Protoc 2016; 11: 118–33.

Sanger F, Air GM, Barrell BG, Brown NL, Coulson AR, Fiddes CA, et al. Nucleotide sequence of bacteriophage phi X174 DNA. Nature 1977; 265: 687–95.

Sanjana NE, Shalem O, Zhang F. Improved vectors and genome-wide libraries for CRISPR screening. Nat Methods 2014; 11: 783–4.

Sanson KR, Hanna RE, Hegde M, Donovan KF, Strand C, Sullender ME, et al. Optimized libraries for CRISPR-Cas9 genetic screens with multiple modalities. Nat Commun 2018; 9: 5416.

Sass F, Schlein C, Jaeckstein MY, Pertzborn P, Schweizer M, Schinke T, et al. TFEB deficiency attenuates mitochondrial degradation upon brown adipose tissue whitening at thermoneutrality. Mol Metab 2021; 47: 101173.

Savitski MM, Reinhard FBM, Franken H, Werner T, Savitski MF, Eberhard D, et al. Tracking cancer drugs in living cells by thermal profiling of the proteome. Science 2014; 346: 1255784.

Schäfer JA, Bozkurt S, Michaelis JB, Klann K, Münch C. Global mitochondrial protein import proteomics reveal distinct regulation by translation and translocation machinery. Mol Cell 2022; 82: 435-446.e7.

Schlieker CD, Van der Veen AG, Damon JR, Spooner E, Ploegh HL. A functional proteomics approach links the ubiquitin-related modifier Urm1 to a tRNA modification pathway. Proc Natl Acad Sci USA 2008; 105: 18255–60.

Schmid-Burgk JL, Höning K, Ebert TS, Hornung V. CRISPaint allows modular base-specific gene tagging using a ligase-4-dependent mechanism. Nat Commun 2016; 7: 12338.

Schmidt C, Becker T, Heuer A, Braunger K, Shanmuganathan V, Pech M, et al. Structure of the hypusinylated eukaryotic translation factor eIF-5A bound to the ribosome. Nucleic Acids Res 2016; 44: 1944–51.

Schmidt HB, Görlich D. Transport selectivity of nuclear pores, phase separation, and membraneless organelles. Trends Biochem Sci 2016; 41: 46–61.

Schmidt M, Schwarzwaelder K, Bartholomae C, Zaoui K, Ball C, Pilz I, et al. High-resolution insertion-site analysis by linear amplification-mediated PCR (LAM-PCR). Nat Methods 2007; 4: 1051–7.

Schnier J, Schwelberger HG, Smit-McBride Z, Kang HA, Hershey JW. Translation initiation factor 5A and its hypusine modification are essential for cell viability in the yeast Saccharomyces cerevisiae. Mol Cell Biol 1991; 11: 3105–14.

Schraivogel D, Kuhn TM, Rauscher B, Rodríguez-Martínez M, Paulsen M, Owsley K, et al. High-speed fluorescence image-enabled cell sorting. Science 2022; 375: 315–20.

Schreier MH, Erni B, Staehelin T. Initiation of mammalian protein synthesis. I. Purification and characterization of seven initiation factors. J Mol Biol 1977; 116: 727–53.

Schröder M, Kolodzik A, Windshügel B, Krepstakies M, Priyadarshini P, Hartjen P, et al. Linker-Region Modified Derivatives of the Deoxyhypusine Synthase Inhibitor CNI-1493 Suppress HIV-1 Replication. Arch Pharm (Weinheim) 2016; 349: 91–103.

Schroeder S, Hofer SJ, Zimmermann A, Pechlaner R, Dammbrueck C, Pendl T, et al. Dietary spermidine improves cognitive function. Cell Rep 2021; 35: 108985.

Schuller AP, Green R. Roadblocks and resolutions in eukaryotic translation. Nat Rev Mol Cell Biol 2018; 19: 526–41.

Schuller AP, Wu CC-C, Dever TE, Buskirk AR, Green R. eIF5A Functions Globally in Translation Elongation and Termination. Mol Cell 2017; 66: 194-205.e5.

Schultz CR, Sheldon RD, Xie H, Demireva EY, Uhl KL, Agnew DW, et al. New K50R mutant mouse models reveal impaired hypusination of eif5a2 with alterations in cell metabolite landscape. Biol Open 2023

Schwanhäusser B, Busse D, Li N, Dittmar G, Schuchhardt J, Wolf J, et al. Global quantification of mammalian gene expression control. Nature 2011; 473: 337–42.

Schwarz A, Beck M. The benefits of cotranslational assembly: A structural perspective. Trends Cell Biol 2019; 29: 791–803.

Scuoppo C, Miething C, Lindqvist L, Reyes J, Ruse C, Appelmann I, et al. A tumour suppressor network relying on the polyamine-hypusine axis. Nature 2012; 487: 244–8.

Sedlyarov V, Eichner R, Girardi E, Essletzbichler P, Goldmann U, Nunes-Hasler P, et al. The bicarbonate transporter SLC4A7 plays a key role in macrophage phagosome acidification. Cell Host Microbe 2018; 23: 766-774.e5.

Serebrenik YV, Sansbury SE, Kumar SS, Henao-Mejia J, Shalem O. Efficient and flexible tagging of endogenous genes by homology-independent intron targeting. Genome Res 2019; 29: 1322–8.

Shadel GS, Horvath TL. Mitochondrial ROS signaling in organismal homeostasis. Cell 2015; 163: 560–9.

Shah P, Ding Y, Niemczyk M, Kudla G, Plotkin JB. Rate-limiting steps in yeast protein translation. Cell 2013; 153: 1589–601.

Shalem O, Sanjana NE, Hartenian E, Shi X, Scott DA, Mikkelson T, et al. Genome-scale CRISPR-Cas9 knockout screening in human cells. Science 2014; 343: 84–7.

Shalem O, Sanjana NE, Zhang F. High-throughput functional genomics using CRISPR-Cas9. Nat Rev Genet 2015; 16: 299–311.

Sharp PM, Li WH. The codon Adaptation Index--a measure of directional synonymous codon usage bias, and its potential applications. Nucleic Acids Res 1987; 15: 1281–95.

Shiba T, Mizote H, Kaneko T, Nakajima T, Kakimoto Y. Hypusine, a new amino acid occurring in bovine brain. Isolation and structural determination. Biochim Biophys Acta 1971; 244: 523–31.

Shin B-S, Katoh T, Gutierrez E, Kim J-R, Suga H, Dever TE. Amino acid substrates impose polyamine, eIF5A, or hypusine requirement for peptide synthesis. Nucleic Acids Res 2017; 45: 8392–402.

Shi XP, Yin KC, Zimolo ZA, Stern AM, Waxman L. The subcellular distribution of eukaryotic translation initiation factor, eIF-5A, in cultured cells. Exp Cell Res 1996; 225: 348–56.

Sievert H, Pällmann N, Miller KK, Hermans-Borgmeyer I, Venz S, Sendoel A, et al. A novel mouse model for inhibition of DOHH-mediated hypusine modification reveals a crucial function in embryonic development, proliferation and oncogenic transformation. Dis Model Mech 2014; 7: 963–76.

Sigl R, Ploner C, Shivalingaiah G, Kofler R, Geley S. Development of a multipurpose GATEWAY-based lentiviral tetracycline-regulated conditional RNAi system (GLTR). PLoS ONE 2014; 9: e97764.

Slobodin B, Dikstein R. So close, no matter how far: multiple paths connecting transcription to mRNA translation in eukaryotes. EMBO Rep 2020; 21: e50799.

Smit-McBride Z, Dever TE, Hershey JW, Merrick WC. Sequence determination and cDNA cloning of eukaryotic initiation factor 4D, the hypusine-containing protein. J Biol Chem 1989; 264: 1578–83.

Smith RM, Peterson WH, McCOY E. Oligomycin, a new antifungal antibiotic. Antibiot Chemother (Northfield Ill) 1954; 4: 962–70.

Sommer M-N, Bevec D, Klebl B, Flicke B, Hölscher K, Freudenreich T, et al. Screening assay for the identification of deoxyhypusine synthase inhibitors. J Biomol Screen 2004; 9: 434–8.

Song J, Herrmann JM, Becker T. Quality control of the mitochondrial proteome. Nat Rev Mol Cell Biol 2021; 22: 54–70.

Sowa ME, Bennett EJ, Gygi SP, Harper JW. Defining the human deubiquitinating enzyme interaction landscape. Cell 2009; 138: 389–403.

Spellman PT, Sherlock G, Zhang MQ, Iyer VR, Anders K, Eisen MB, et al. Comprehensive identification of cell cycle-regulated genes of the yeast Saccharomyces cerevisiae by microarray hybridization. Mol Biol Cell 1998; 9: 3273–97.

Spinelli JB, Haigis MC. The multifaceted contributions of mitochondria to cellular metabolism. Nat Cell Biol 2018; 20: 745–54.

Spradling AC, Stern DM, Kiss I, Roote J, Laverty T, Rubin GM. Gene disruptions using P transposable elements: an integral component of the Drosophila genome project. Proc Natl Acad Sci USA 1995; 92: 10824–30.

Steitz JA. Polypeptide chain initiation: nucleotide sequences of the three ribosomal binding sites in bacteriophage R17 RNA. Nature 1969; 224: 957–64.

Subbaiah KCV, Wu J, Tang WHW, Yao P. Ciclopirox Inhibition of eIF5A Hypusination Attenuates Fibroblast Activation and Cardiac Fibrosis. J Cardiovasc Dev Dis 2023; 10

Subramanian A, Tamayo P, Mootha VK, Mukherjee S, Ebert BL, Gillette MA, et al. Gene set enrichment analysis: a knowledge-based approach for interpreting genome-wide expression profiles. Proc Natl Acad Sci USA 2005; 102: 15545–50.

Sugimoto A. High-throughput RNAi in Caenorhabditis elegans: genome-wide screens and functional genomics. Differentiation 2004; 72: 81–91.

Sun N, Youle RJ, Finkel T. The mitochondrial basis of aging. Mol Cell 2016; 61: 654–66.

Sun Z, Cheng Z, Taylor CA, McConkey BJ, Thompson JE. Apoptosis induction by eIF5A1 involves activation of the intrinsic mitochondrial pathway. J Cell Physiol 2010; 223: 798–809.

Su X, Lin Z, Lin H. The biosynthesis and biological function of diphthamide. Crit Rev Biochem Mol Biol 2013; 48: 515–21.

Tahmasebi S, Sonenberg N, Hershey JWB, Mathews MB. Protein synthesis and translational control: A historical perspective. Cold Spring Harb Perspect Biol 2019; 11

Takahashi K, Yamanaka S. Induction of pluripotent stem cells from mouse embryonic and adult fibroblast cultures by defined factors. Cell 2006; 126: 663–76.

Tamborlin L, Pereira KD, Guimarães DSPSF, Silveira LR, Luchessi AD. The first evidence of biological activity for free Hypusine, an enigmatic amino acid discovered in the ’70s. Amino Acids 2023

Tanaka Y, Kurasawa O, Yokota A, Klein MG, Ono K, Saito B, et al. Discovery of novel allosteric inhibitors of deoxyhypusine synthase. J Med Chem 2020; 63: 3215–26.

Tanaka Y, Kurasawa O, Yokota A, Klein MG, Saito B, Matsumoto S, et al. New series of potent allosteric inhibitors of deoxyhypusine synthase. ACS Med Chem Lett 2020; 11: 1645–52.

Tan TCJ, Kelly V, Zou X, Wright D, Ly T, Zamoyska R. Translation factor eIF5a is essential for IFNγ production and cell cycle regulation in primary CD8+ T lymphocytes. Nat Commun 2022; 13: 7796.

Tan X, Wang D-B, Lu X, Wei H, Zhu R, Zhu S-S, et al. Doxorubicin induces apoptosis in H9c2 cardiomyocytes: role of overexpressed eukaryotic translation initiation factor 5A. Biol Pharm Bull 2010; 33: 1666–72.

Tauc M, Cougnon M, Carcy R, Melis N, Hauet T, Pellerin L, et al. The eukaryotic initiation factor 5A (eIF5A1), the molecule, mechanisms and recent insights into the pathophysiological roles. Cell Biosci 2021; 11: 219.

Tebas P, Stein D, Tang WW, Frank I, Wang SQ, Lee G, et al. Gene editing of CCR5 in autologous CD4 T cells of persons infected with HIV. N Engl J Med 2014; 370: 901–10.

Teixeira FK, Lehmann R. Translational Control during Developmental Transitions. Cold Spring Harb Perspect Biol 2019; 11

Tersey SA, Colvin SC, Maier B, Mirmira RG. Protective effects of polyamine depletion in mouse models of type 1 diabetes: implications for therapy. Amino Acids 2014; 46: 633–42.

Tesina P, Ebine S, Buschauer R, Thoms M, Matsuo Y, Inada T, et al. Molecular basis of eIF5A-dependent CAT tailing in eukaryotic ribosome-associated quality control. Mol Cell 2023; 83: 607-621.e4.

Thompson A, Schäfer J, Kuhn K, Kienle S, Schwarz J, Schmidt G, et al. Tandem mass tags: a novel quantification strategy for comparative analysis of complex protein mixtures by MS/MS. Anal Chem 2003; 75: 1895–904.

Thompson A, Wölmer N, Koncarevic S, Selzer S, Böhm G, Legner H, et al. TMTpro: Design, Synthesis, and Initial Evaluation of a Proline-Based Isobaric 16-Plex Tandem Mass Tag Reagent Set. Anal Chem 2019; 91: 15941–50.

Thompson GM, Cano VSP, Valentini SR. Mapping eIF5A binding sites for Dys1 and Lia1: in vivo evidence for regulation of eIF5A hypusination. FEBS Lett 2003; 555: 464–8.

Thul PJ, Åkesson L, Wiking M, Mahdessian D, Geladaki A, Ait Blal H, et al. A subcellular map of the human proteome. Science 2017; 356

Tian R, Abarientos A, Hong J, Hashemi SH, Yan R, Dräger N, et al. Genome-wide CRISPRi/a screens in human neurons link lysosomal failure to ferroptosis. Nat Neurosci 2021; 24: 1020–34.

Ting L, Rad R, Gygi SP, Haas W. MS3 eliminates ratio distortion in isobaric multiplexed quantitative proteomics. Nat Methods 2011; 8: 937–40.

Tong Y, Park I, Hong B-S, Nedyalkova L, Tempel W, Park H-W. Crystal structure of human eIF5A1: insight into functional similarity of human eIF5A1 and eIF5A2. Proteins 2009; 75: 1040–5.

Torrelio BM, Paz MA, Gallop PM. The formation and stability of the hypusine containing protein in Chinese hamster ovary cells. Biochem Biophys Res Commun 1987; 145: 1335–41.

Tran JC, Zamdborg L, Ahlf DR, Lee JE, Catherman AD, Durbin KR, et al. Mapping intact protein isoforms in discovery mode using top-down proteomics. Nature 2011; 480: 254–8.

Trinh LA, Fraser SE. Enhancer and gene traps for molecular imaging and genetic analysis in zebrafish. Dev Growth Differ 2013; 55: 434–45.

Tsitsiridis G, Steinkamp R, Giurgiu M, Brauner B, Fobo G, Frishman G, et al. CORUM: the comprehensive resource of mammalian protein complexes-2022. Nucleic Acids Res 2023; 51: D539–45.

Tsui CK, Barfield RM, Fischer CR, Morgens DW, Li A, Smith BAH, et al. CRISPR-Cas9 screens identify regulators of antibody-drug conjugate toxicity. Nat Chem Biol 2019; 15: 949–58.

Turnbull C, Scott RH, Thomas E, Jones L, Murugaesu N, Pretty FB, et al. The 100 000 Genomes Project: bringing whole genome sequencing to the NHS. BMJ 2018; 361: k1687.

Turpaev KT. Translation Factor eIF5A, Modification with Hypusine and Role in Regulation of Gene Expression. eIF5A as a Target for Pharmacological Interventions. Biochemistry Mosc 2018; 83: 863–73.

Udagawa T, Seki M, Okuyama T, Adachi S, Natsume T, Noguchi T, et al. Failure to Degrade CAT-Tailed Proteins Disrupts Neuronal Morphogenesis and Cell Survival. Cell Rep 2021; 34: 108599.

Ude S, Lassak J, Starosta AL, Kraxenberger T, Wilson DN, Jung K. Translation elongation factor EF-P alleviates ribosome stalling at polyproline stretches. Science 2013; 339: 82–5.

Umland TC, Wolff EC, Park MH, Davies DR. A new crystal structure of deoxyhypusine synthase reveals the configuration of the active enzyme and of an enzyme.NAD.inhibitor ternary complex. J Biol Chem 2004; 279: 28697–705.

Urnov FD, Rebar EJ, Holmes MC, Zhang HS, Gregory PD. Genome editing with engineered zinc finger nucleases. Nat Rev Genet 2010; 11: 636–46.

Van Vranken JG, Li J, Mitchell DC, Navarrete-Perea J, Gygi SP. Assessing target engagement using proteome-wide solvent shift assays. eLife 2021; 10

Vaquerizas JM, Kummerfeld SK, Teichmann SA, Luscombe NM. A census of human transcription factors: function, expression and evolution. Nat Rev Genet 2009; 10: 252–63.

Varjosalo M, Sacco R, Stukalov A, van Drogen A, Planyavsky M, Hauri S, et al. Interlaboratory reproducibility of large-scale human protein-complex analysis by standardized AP-MS. Nat Methods 2013; 10: 307–14.

Venkataramanan S, Floor SN. The traffic jam: polyamine prevalence pauses protein production. Mol Cell 2018; 70: 191–2.

Venter JC, Adams MD, Myers EW, Li PW, Mural RJ, Sutton GG, et al. The sequence of the human genome. Science 2001; 291: 1304–51.

Vigne P, Frelin C. The role of polyamines in protein-dependent hypoxic tolerance of Drosophila. BMC Physiol 2008; 8: 22.

Vogel C, Marcotte EM. Insights into the regulation of protein abundance from proteomic and transcriptomic analyses. Nat Rev Genet 2012; 13: 227–32.

Wainberg M, Kamber RA, Balsubramani A, Meyers RM, Sinnott-Armstrong N, Hornburg D, et al. A genome-wide atlas of co-essential modules assigns function to uncharacterized genes. Nat Genet 2021; 53: 638–49.

Walsh CT, Tu BP, Tang Y. Eight Kinetically Stable but Thermodynamically Activated Molecules that Power Cell Metabolism. Chem Rev 2018; 118: 1460–94.

Wang JY, Doudna JA. CRISPR technology: A decade of genome editing is only the beginning. Science 2023; 379: eadd8643.

Wang R, Amoyel M. mRNA Translation Is Dynamically Regulated to Instruct Stem Cell Fate. Front Mol Biosci 2022; 9: 863885.

Wang S, Chen Y, Li X, Zhang W, Liu Z, Wu M, et al. Emerging role of transcription factor EB in mitochondrial quality control. Biomed Pharmacother 2020; 128: 110272.

Wang T, Birsoy K, Hughes NW, Krupczak KM, Post Y, Wei JJ, et al. Identification and characterization of essential genes in the human genome. Science 2015; 350: 1096–101.

Wang T, Wei JJ, Sabatini DM, Lander ES. Genetic screens in human cells using the CRISPR-Cas9 system. Science 2014; 343: 80–4.

Wang Y, Yang F, Gritsenko MA, Wang Y, Clauss T, Liu T, et al. Reversed-phase chromatography with multiple fraction concatenation strategy for proteome profiling of human MCF10A cells. Proteomics 2011; 11: 2019–26.

Warburg O. The metabolism of carcinoma cells. J Cancer Res 1925; 9: 148–63.

Warren HR, Evangelou E, Cabrera CP, Gao H, Ren M, Mifsud B, et al. Genome-wide association analysis identifies novel blood pressure loci and offers biological insights into cardiovascular risk. Nat Genet 2017; 49: 403–15.

Wątor E, Wilk P, Biela A, Rawski M, Zak KM, Steinchen W, et al. Cryo-EM structure of human eIF5A-DHS complex reveals the molecular basis of hypusination-associated neurodegenerative disorders. Nat Commun 2023; 14: 1698.

Wątor E, Wilk P, Grudnik P. Half Way to Hypusine-Structural Basis for Substrate Recognition by Human Deoxyhypusine Synthase. Biomolecules 2020; 10

Watson PA, Hanauske-Abel HH, Flint A, Lalande M. Mimosine reversibly arrests cell cycle progression at the G1-S phase border. Cytometry 1991; 12: 242–6.

Weinberg DE, Shah P, Eichhorn SW, Hussmann JA, Plotkin JB, Bartel DP. Improved Ribosome-Footprint and mRNA Measurements Provide Insights into Dynamics and Regulation of Yeast Translation. Cell Rep 2016; 14: 1787–99.

Weiner S, Sauer M, Visser PJ, Tijms BM, Vorontsov E, Blennow K, et al. Optimized sample preparation and data analysis for TMT proteomic analysis of cerebrospinal fluid applied to the identification of Alzheimer's disease biomarkers. Clin Proteomics 2022; 19: 13.

White R, Caskey CT. The human as an experimental system in molecular genetics. Science 1988; 240: 1483–8.

Wilson RC, Doudna JA. Molecular mechanisms of RNA interference. Annu Rev Biophys 2013; 42: 217–39.

Winter GE, Radic B, Mayor-Ruiz C, Blomen VA, Trefzer C, Kandasamy RK, et al. The solute carrier SLC35F2 enables YM155-mediated DNA damage toxicity. Nat Chem Biol 2014; 10: 768–73.

Winzeler EA, Shoemaker DD, Astromoff A, Liang H, Anderson K, Andre B, et al. Functional characterization of the S. cerevisiae genome by gene deletion and parallel analysis. Science 1999; 285: 901–6.

Wohlgemuth I, Brenner S, Beringer M, Rodnina MV. Modulation of the rate of peptidyl transfer on the ribosome by the nature of substrates. J Biol Chem 2008; 283: 32229–35.

Wolff EC, Folk JE, Park MH. Enzyme-substrate intermediate formation at lysine 329 of human deoxyhypusine synthase. J Biol Chem 1997; 272: 15865–71.

Wolff EC, Kang KR, Kim YS, Park MH. Posttranslational synthesis of hypusine: evolutionary progression and specificity of the hypusine modification. Amino Acids 2007; 33: 341–50.

Wolff EC, Lee YB, Chung SI, Folk JE, Park MH. Deoxyhypusine synthase from rat testis: purification and characterization. J Biol Chem 1995; 270: 8660–6.

Wolff EC, Park MH, Folk JE. Cleavage of spermidine as the first step in deoxyhypusine synthesis. The role of NAD. J Biol Chem 1990; 265: 4793–9.

Wolff EC, Wolff J, Park MH. Deoxyhypusine synthase generates and uses bound NADH in a transient hydride transfer mechanism. J Biol Chem 2000; 275: 9170–7.

Wolin SL, Walter P. Ribosome pausing and stacking during translation of a eukaryotic mRNA. EMBO J 1988; 7: 3559–69.

Woolstenhulme CJ, Guydosh NR, Green R, Buskirk AR. High-precision analysis of translational pausing by ribosome profiling in bacteria lacking EFP. Cell Rep 2015; 11: 13–21.

Wu G-Q, Xu Y-M, Lau ATY. Recent insights into eukaryotic translation initiation factors 5A1 and 5A2 and their roles in human health and disease. Cancer Cell Int 2020; 20: 142.

Xu A, Chen KY. Hypusine is required for a sequence-specific interaction of eukaryotic initiation factor 5A with postsystematic evolution of ligands by exponential enrichment RNA. J Biol Chem 2001; 276: 2555–61.

Xu A, Jao DL-E, Chen KY. Identification of mRNA that binds to eukaryotic initiation factor 5A by affinity co-purification and differential display. Biochem J 2004; 384: 585–90.

Yanagisawa T, Sumida T, Ishii R, Takemoto C, Yokoyama S. A paralog of lysyl-tRNA synthetase aminoacylates a conserved lysine residue in translation elongation factor P. Nat Struct Mol Biol 2010; 17: 1136–43.

Yeh CD, Richardson CD, Corn JE. Advances in genome editing through control of DNA repair pathways. Nat Cell Biol 2019; 21: 1468–78.

Yeung ATY, Choi YH, Lee AHY, Hale C, Ponstingl H, Pickard D, et al. A Genome-Wide Knockout Screen in Human Macrophages Identified Host Factors Modulating Salmonella Infection. MBio 2019; 10

Youle RJ, van der Bliek AM. Mitochondrial fission, fusion, and stress. Science 2012; 337: 1062–5.

Youle RJ, Narendra DP. Mechanisms of mitophagy. Nat Rev Mol Cell Biol 2011; 12: 9–14.

Yu C-H, Dang Y, Zhou Z, Wu C, Zhao F, Sachs MS, et al. Codon Usage Influences the Local Rate of Translation Elongation to Regulate Co-translational Protein Folding. Mol Cell 2015; 59: 744–54.

Zanelli CF, Valentini SR. Pkc1 acts through Zds1 and Gic1 to suppress growth and cell polarity defects of a yeast eIF5A mutant. Genetics 2005; 171: 1571–81.

Zare ME, Kansestani AN, Hemmati S, Mansouri K, Vaisi-Raygani A. The rate of aerobic glycolysis is a pivotal regulator of tumor progression. J Diabetes Metab Disord 2021; 20: 523–31.

Zetsche B, Volz SE, Zhang F. A split-Cas9 architecture for inducible genome editing and transcription modulation. Nat Biotechnol 2015; 33: 139–42.

Zhai Q, He M, Song A, Deshayes K, Dixit VM, Carter PJ. Structural Analysis and Optimization of Context-Independent Anti-Hypusine Antibodies. J Mol Biol 2016; 428: 603–17.

Zhang H, Alsaleh G, Feltham J, Sun Y, Napolitano G, Riffelmacher T, et al. Polyamines Control eIF5A Hypusination, TFEB Translation, and Autophagy to Reverse B Cell Senescence. Mol Cell 2019; 76: 110-125.e9.

Zhang M, Caragine T, Wang H, Cohen PS, Botchkina G, Soda K, et al. Spermine inhibits proinflammatory cytokine synthesis in human mononuclear cells: a counterregulatory mechanism that restrains the immune response. J Exp Med 1997; 185: 1759–68.

Zhang X, Lytovchenko O, Lundström SL, Zubarev RA, Gaetani M. Proteome Integral Solubility Alteration (PISA) Assay in Mammalian Cells for Deep, High-Confidence, and High-Throughput Target Deconvolution. Bio Protoc 2022; 12

Zhang X, Xin Y, Chen Z, Xia Y, Xun L, Liu H. Sulfide-quinone oxidoreductase is required for cysteine synthesis and indispensable to mitochondrial health. Redox Biol 2021; 47: 102169.

Zhou H, Shen T, Luo Y, Liu L, Chen W, Xu B, et al. The antitumor activity of the fungicide ciclopirox. Int J Cancer 2010; 127: 2467–77.

Ziegler A, Steindl K, Hanner AS, Kumar Kar R, Prouteau C, Boland A, et al. Bi-allelic variants in DOHH, catalyzing the last step of hypusine biosynthesis, are associated with a neurodevelopmental disorder. Am J Hum Genet 2022; 109: 1549–58.

Veritas Genetics Launches $999 Whole Genome And Sets New Standard For Genetic Testing [Internet]. [cited 2023 Jun 3] Available from: https://www.prnewswire.com/news-releases/veritas-genetics-launches-999-whole-genome-and-sets-new-standard-for-genetic-testing-300230258.html

7 Appendix

7.1 Curriculum Vitae

Personal Information

Name:	Patrick Essletzbichler
Date of birth:	September 12th, 1992
Citizenship:	Austrian
Current address:	Margaretenstraße 135/1/28, 1050, Vienna (AT)
Email:	pessletzbichler@cemm.at
Linkedin:	at.linkedin.com/in/pessletz

ORCID-ID

0000-0003-2237-0005

Education

2018-now	**PhD in Molecular Medicine** *CeMM Research Center for Molecular Medicine, Vienna (AT)* Supervisor: Univ.-Prof. Dr. Giulio Superti-Furga Title: "Dissection of the hypusine-eIF5A axis by CRISPR/Cas9-aided functional genomics"
2015-2017	**Master of Science in Biotechnology** *University of Natural Resources and Life Sciences, Vienna (AT)* Supervisor: Feng Zhang, PhD Title: "Characterization and Engineering of the RNA-targeting CRISPR enzyme Cas13a for nucleotide detection and mammalian applications" Pass with distinction (best possible overall rating); Thesis defense 1 (best 1, worst 5)
2011-2015	**Bachelor of Science in Biotechnology and Food Science** *University of Natural Resources and Life Sciences, Vienna (AT)* Supervisor: Dr. Tilmann Bürckstümmer Title: "Towards a CRISPR knockout collection for the entire human kinome" Pass with distinction (best possible overall rating)
2007	**High School** *Minneapolis, Minnesota (USA)*
2001-2010	**Gymnasium** *Melk (AT)* Specialization: Science Matura (General Qualification for University Entrance)

Fellowships and Grants

2022	Contribution to successful FWF Stand Alone Grant
2020	Contribution to successful FWF 1000 Ideas Program

Professional experience

2017-now	**Predoctoral Fellow, Giulio Superti-Furga Lab** *CeMM Research Center for Molecular Medicine, Vienna (AT)*
2015,2016	**Guest Scientist, Feng Zhang Lab** *Broad Institute of MIT and Harvard, Boston (USA)*
2014	**Practical Trainee, Veit Hornung Lab** *Institute of Molecular Medicine, University Hospital, Bonn (DE)*
2013	**Intern** *Haplogen Genomics GmbH, Vienna (AT)*
2011,2012	**Blue-collar worker** *Doka GmbH, Amstetten (AT)*
2010-2011	**Mandatory military service: Infantry and truck motorist, Austrian Army** *Amstetten, Dürnkrut (AT)*

Conferences and Meetings

2023	RESOLUTE Conference: Unlocking Transporters for Drug Discovery, Vienna (AT)
2023	GRC Polyamines in Cancer, Medical Genetics, Aging, Pathogens and Plants, Waterville Valley, NH (USA) *Poster presentation*
2022	CeMM Scientific Symposium, 60th birthday and 15 years of CeMM, Vienna (AT)
2022	EMBO Workshop: Molecular biology of mitochondrial gene maintenance and expression, Bro (SWE) *Poster presentation*
2021	EMBL Conference: Protein Synthesis and Translational Control (virtual)
2021	CSH Conference: Mechanisms of Metabolic Signaling (virtual)
2021	CRISPR 2021 (virtual)
2021	CeMM Scientific Advisory Board Meeting *Oral presentation*
2021	CeMM Science Day *Poster presentation*
2020	CeMM Scientific recess *Oral presentation*

2019	BioMedical Transporter Conference, NCCR TransCure, Bern (CH) *Poster presentation*
2019	The Onassis Foundation Science Lecture Series: Genome Editing, Heraklion, (GRC)
2019	CeMM Scientific Advisory Board Meeting *Oral presentation*
2018	ITTS Conference: The Transporter Transition, Vienna (AT)
2018	EMBO Workshop: Cell and developmental systems, Arolla (CH) *Poster presentation*
2018	CeMM Scientific recess *Oral presentation*

Peer review assistance

2022	*Peer review assistance with Nature Reviews Immunology*

Teaching

2023-now	**Yee Kwan Law – PhD student** *Experimental co-supervision*
2020-2021	**Benedikt Neumayer – Diploma student** Master thesis: "Investigating the functional relationship between hypusination and phagocytosis" *(Co-supervised with Prof. Giulio Superti-Furga)*

Awards and scholarships

2012/2013	Scholarship for academic excellence of University of Natural Resources and Life Sciences, Vienna (AT)
2011/2012	Scholarship for academic excellence of University of Natural Resources and Life Sciences, Vienna (AT)

Languages

German (Native), English (Fluent)

Driving Licenses

A, B, C

References

Available upon request

8 List of Publications

1. Essletzbichler P, Konopka T, Santoro F, Chen D, Gapp BV, Kralovics R, et al. **Megabase-scale deletion using CRISPR/Cas9 to generate a fully haploid human cell line.** *Genome Res* 2014; 24: 2059–65.
2. Zetsche B, Gootenberg JS, Abudayyeh OO, Slaymaker IM, Makarova KS, Essletzbichler P, et al. **Cpf1 is a single RNA-guided endonuclease of a class 2 CRISPR-Cas system.** *Cell* 2015; 163: 759–71.
3. Smargon AA, Cox DBT, Pyzocha NK, Zheng K, Slaymaker IM, Gootenberg JS, Abudayyeh OA, Essletzbichler P, et al. **Cas13b Is a Type VI-B CRISPR-Associated RNA-Guided RNase Differentially Regulated by Accessory Proteins Csx27 and Csx28.** *Mol Cell* 2017; 65: 618-630.e7.
4. Abudayyeh OO, Gootenberg JS, Essletzbichler P, Han S, Joung J, Belanto JJ, et al. **RNA targeting with CRISPR-Cas13.** *Nature* 2017; 550: 280–4.
5. Gootenberg JS, Abudayyeh OO, Lee JW, Essletzbichler P, Dy AJ, Joung J, et al. **Nucleic acid detection with CRISPR-Cas13a/C2c2.** *Science* 2017; 356: 438–42.
6. Sedlyarov V, Eichner R, Girardi E, Essletzbichler P, Goldmann U, Nunes-Hasler P, et al. The bicarbonate transporter **SLC4A7 plays a key role in macrophage phagosome acidification.** *Cell Host Microbe* 2018; 23: 766-774.e5.
7. Ferreira da Silva J, Salic S, Wiedner M, Datlinger P, Essletzbichler P, Hanzl A, et al. **Genome-scale CRISPR screens are efficient in non-homologous end-joining deficient cells.** *Sci Rep* 2019; 9: 15751.
8. Heinz LX, Lee J, Kapoor U, Kartnig F, Sedlyarov V, Papakostas K, Cesar-Razquin A, Essletzbichler P, et al. **TASL is the SLC15A4-associated adaptor for IRF5 activation by TLR7-9.** *Nature* 2020; 581: 316–22.
9. Bensimon A, Pizzagalli MD, Kartnig F, Dvorak V, Essletzbichler P, Winter GE, et al. **Targeted Degradation of SLC Transporters Reveals Amenability of Multi-Pass Transmembrane Proteins to Ligand-Induced Proteolysis.** *Cell Chem Biol* 2020; 27: 728-739.e9.
10. Essletzbichler P, Sedlyarov V, Frommelt F, Soulat D, Heinz LX, Stefanovic A, et al. **A genome-wide CRISPR functional survey of the human phagocytosis molecular machinery.** *Life Sci Alliance* 2023; 6
11. Gernot Wolf, Conner Craigon, Svenja Onstein, Patrick Essletzbichler, Vojtech Dvorak, et al. **Identification of a novel PROTAC efflux pump using transporter-focused genetic drug resistance screns.** *Manuscript in preparation.*